การพัฒนาเกราะกันกระสุนน้ำหนักเบาจากเบนซอกซาซีนอัลลอยโดยใช้เส้นใยเสริมแรง

นางสาวพรนภา เกษมศิริ

วิทยานิพนธ์นี้เป็นส่วนหนึ่งของการศึกษาตามหลักสูตรปริญญาวิศวกรรมศาสตรดุษฎีบัณฑิต
สาขาวิชาวิศวกรรมเคมี ภาควิชาวิศวกรรมเคมี
คณะวิศวกรรมศาสตร์ จุฬาลงกรณ์มหาวิทยาลัย
ปีการศึกษา 2554

DEVELOPMENT OF LIGHT WEIGHT BALLISTIC ARMOR FROM FIBERS-REINFORCED WITH BENZOXAZINE ALLOYS

Miss Pornnapa Kasemsiri

A Dissertation Submitted in Partial Fulfillment of the Requirements

for the Degree of Doctor of Doctoral of Engineering Program in Chemical Engineering

Department of Chemical Engineering

Faculty of Faculty of Engineering

Chulalongkorn University

Academic year 2011

Thesis Title	DEVELOPMENT OF LIGHT WEIGHT BALLISTIC ARMOR FROM FIBERS-REINFORCED WITH BENZOXAZINE ALLOYS
By	Ms. Pornnapa Kasemsiri
Field of Study	Chemical Engineering
Thesis Advisor	Associate Professor Sarawut Rimdusit, Ph.D
Thesis Co-advisor	Professor Salim Hiziroglu, Ph.D.

Accepted by the Faculty of Engineering, Chulalongkorn University in Partial Fulfillment of the Requirements for the Doctoral Degree

..... Dean of the Faculty of Engineering
(Associate Professor Boonsom Lerdhirunwong, D.Ing.)

THESIS COMMITTEE

..... Chairman
(Associate Professor Muenduen Phisalaphong, Ph.D.)

..... Thesis advisor
(Associate Professor Sarawut Rimdusit, Ph.D.)

..... Thesis Co-advisor
(Professor Salim Hiziroglu, Ph.D.)

..... Examiner
(Associate Professor Siriporn Damrongsakkul, Ph.D.)

Phiriyatorn Suwanmala ..... External Examiner
(Phiriyatorn Suwanmala, Ph.D.)

พรนภา เกษมศิริ : การพัฒนาเกราะกันกระสุนน้ำหนักเบาจากเบนซอกซาซีนอัลลอยโดยใช้เส้นใย เสริมแรง (DEVELOPMENT OF LIGHT WEIGHT BALLISTIC ARMOR FROM FIBERS-REINFORCED WITH BENZOXAZINE ALLOYS) อ. ที่ปรึกษาวิทยานิพนธ์หลัก: รศ. ดร. ศราวุธ ริมดุสิต, อ. ที่ปรึกษาวิทยานิพนธ์ร่วม: Prof. Salim Hiziroglu, Ph.D., 118 หน้า.

จุดมุ่งหมายของงานวิจัยนี้เพื่อศึกษาประสิทธิภาพของเกราะกันกระสุนจากเบนซอกซาซีนเสริมแรงด้วยเส้นใยแก้วและเบนซอกซาซีน-ยูรีเทน อัลลอยเสริมแรงด้วยเส้นใยเคฟลาร์ ในการต้านการเจาะทะลุของกระสุน 7.62 มม. โดยเบนซอกซาซีน (BA-a) เป็นพอลิเมอร์ในตระกูลฟีนอลิกที่มีคุณสมบัติเด่นหลายประการ ได้แก่ สังเคราะห์ได้ง่าย ความหนืดต่ำ ไม่มีผลพลอยได้จากการบ่ม ค่าการหดตัวจากการขึ้นรูปใกล้ศูนย์ เสถียรภาพทางความร้อนและสมบัติทางกลสูง นอกจากนี้สามารถทำอัลลอยร่วมกับเรซินอื่นได้หลายชนิดเนื่องจากมีหมู่ฟังก์ชันที่หลากหลาย งานวิจัยนี้ใช้ยูรีเทนอิลาสโตเมอร์ (PU) เพื่อเพิ่มความยืดหยุ่นของพอลิเบนซอกซาซีน และผลกระทบที่มีต่อลักษณะของเกราะกันกระสุน จากผลการทดลองพบว่าอุณหภูมิการเปลี่ยนสถานะคล้ายแก้วของเบนซอกซาซีนเสริมแรงด้วยเส้นใยแก้วเป็น 182 องศาเซลเซียส ในขณะที่เบนซอกซาซีน-ยูรีเทน อัลลอยเสริมแรงด้วยเส้นใยเคฟลาร์ มีอุณหภูมิการเปลี่ยนสถานะคล้ายแก้วเพิ่มขึ้นจาก 184 องศาเซลเซียส เป็น 247 องศาเซลเซียส เมื่อมีปริมาณยูรีเทน 0-40% โดยน้ำหนัก ค่าพลังงานก่อกัมมันต์ที่ได้จากอุณหภูมิการเปลี่ยนสถานะคล้ายแก้วของคอมพอสิทเพิ่มขึ้น เมื่อสัดส่วนของยูรีเทนเพิ่มขึ้น สำหรับคุณสมบัติทางกลพบว่า ค่าความแข็งแรงภายใต้แรงดัดโค้งของเบนซอกซาซีนเสริมแรงด้วยเส้นใยแก้วมีค่า 506 เมกะปาสคาล และมีค่า 74-153 เมกะปาสคาล สำหรับเบนซอกซาซีน-ยูรีเทนอัลลอยเสริมแรงด้วยเส้นใยเคฟลาร์ เมื่อมีปริมาณยูรีเทน 0-40% โดยน้ำหนัก จากผลการทดลอบการยิงพบว่าเกราะแข็งกันกระสุนที่ประกอบด้วยเบนซอกซาซีนเสริมแรงด้วยเส้นใยแก้วจำนวน 2 แผ่น ประกบกับเบนซอกซาซีน-ยูรีเทนอัลลอยเสริมแรงด้วยเส้นใยเคฟลาร์จำนวน 1 แผ่น (อัตราส่วนของเบนซอกซาซีน/ยูรีเทน 80/20) สามารถต้านทานการเจาะทะลุของกระสุน 7.62 มม. (ความเร็ว 838 ± 15 เมตรต่อวินาที) ซึ่งเทียบเท่ากับการต้านทานในระดับ III ตามมาตรฐาน NIJ

ภาควิชา วิศวกรรมเคมี ลายมือชื่อนิสิต พรนภา เกษมศิริ

สาขาวิชา วิศวกรรมเคมี ลายมือชื่อ อ.ที่ปรึกษาวิทยานิพนธ์หลัก

ปีการศึกษา 2554 ลายมือชื่อ อ.ที่ปรึกษาวิทยานิพนธ์ร่วม

5171848021 : MAJOR CHEMICAL ENGINEERING
KEYWORDS: POLYBENZOXAZINE/URETHANE/FIBERS-REINFORCED/COMPOSITE/ BALLISTIC ARMOR

PORNNAPA KASEMSIRI: DEVELOPMENT OF LIGHT WEIGHT BALLISTIC ARMOR FROM FIBERS-REINFORCED WITH BENZOXAZINE ALLOYS. ADVISOR: ASSOC. PROF. SARAWUT RIMDUSIT, Ph.D., CO-ADVISOR: PROF. SALIM HIZIROGLU, Ph.D., 118 pp.

Ballistic impact performance of glass fiber and Kevlar ™ fiber reinforced benzoxazine resin and benzoxazine-urethane alloy has been studied against 7.62 mm armor piercing projectiles. Benzoxazine resin which is one kind of phenolic resins was selected to apply as matrix for reinforced fiber due to its outstanding properties, no by-product during polymerization, high thermal stability, excellent mechanical properties, and ability to alloy with various types of resins. In this work, urethane elastomer (PU) is used to enhance toughness of the polybenzoxazine and its effects on the ballistic characteristics. The results reveal that the glass transition temperature (T_g) was found to be about 182°C for glass fiber reinforced benzoxazine resin whereas T_g of Kevlar™ fiber reinforced benzoxazine-urethane alloys increased from 184°C to 247°C with the increasing amount of the urethane from 0-40% by weight. The activation energy obtained from T_g of composites increased with increasing amount of urethane fraction. For mechanical properties, flexural strength of glass fiber reinforced benzoxazine resin was to be about 506 MPa for glass fiber composite and 74-153 MPa for Kevlar™ fiber reinforced benzoxazine-urethane alloys at urethane content from 0 to 40% by weight. The result of fire test presented that the hard ballistic armor consisted of 2 panels of glass fiber reinforced benzoxazine resin and 1 panel of Kevlar™ fiber reinforced benzoxazine urethane alloy (80/20 BA-a/PU) can resist the penetration 7.62 mm AP projectile (838 ± 15m/s) equivalent to level III of NIJ standard.

Department: Chemical Engineering ..... Student's Signature Pornnapa Kasemsiri
Field of Study: Chemical Engineering ..... Advisor's Signature .....
Academic Year : 2011 ..... Co-Advisor's Signature .....

ACKNOWLEDGEMENTS

I am sincerely grateful to my advisor, Assoc. Prof. Dr. Sarawut Rimdusit, for his invaluable guidance and valuable suggestions including constant encourage throughout this study. Furthermore, I deeply appreciate all things, I have learnt from him and for the opportunity to work in his group. I am also grateful to my co-advisor, Professor Dr. Salim Hiziroglu from Natural Resource Ecology and Management, Oklahoma State University, Stillwater, Oklahoma, US. He guided me through every difficulty in this thesis and taught me how to face the problems in my life intellectually. Thanks are extended to Prof. Dr. Shinji Ando Department of Chemistry & Material Science, Tokyo Institute of Technology, Ookayama, Japan for the valuable advices during my short term research program in Japan.

I am also grateful to my committee members, who provided constructive and scientific advices for the completion of this thesis. This includes, Assoc Prof. Dr.Muenduen Phisalaphong , Chairman, Assoc. Prof. Dr. Siriporn Damrongsakkul from the Department of Chemical Engineering, Faculty of Engineering, Chulalongkorn University, and Dr. Phiriyatorn Suwanmala from Thailand Institute of Nuclear Technology.

I also appreciate Mr. Akekapon Seelaphum and Miss Patcharaporn Prajaksurt for always being there through good and bad times. I am very thankful for every inspiration that they have made throughout my difficult years. They are more than my best friends. Thank are also extended to every polymer engineering research laboratory member for every constructive discussion they contributed and all their help.

Finally, my deepest regard to my beloved family and parents, who have always been the source of my support and encouragement. There is never a single day without them standing by me. It is why I can journey this far. I am lifetime beholden.

CONTENTS

PAGE

LIST OF TABLES

LIST OF FIGURES

FIGURE PAGE

FIGURE PAGE

CHAPTER I

INTRODUCTION

1.1 General introduction

Personal armor is worn or carried to provide an individual with protection from energy. In the military and law-enforcement environment, this energy is principally in the form of impact by penetrating missiles non-penetrating projectiles blows, or blast waves from explosions. Energy can be performed as work that act on the body as well as may produce contusion and laceration of tissues and fracture of bones. The interaction between the energy and body depends on impact form i.e. penetrating missiles deliver energy internally during their passage through tissues, but blast waves and non-penetrating impacts interact with the body wall. Moreover, energy may be transferred internally from the motion of the body wall by stress waves and shear which will disparate motion of components of tissues and of organs. Therefore, many types of personal armor have been designed for protection from penetrating and non-penetrating impacts [1].

The first known use of armor was by the Egyptians. Armors were a cloth, shirt like garment overlapped with bronze layers or plates sawn together. The armor was very heavy, causing this style of protection to be short-lived. To solve the weight limitations of armor, the light weight armor was created. For example, the aramid fabric body armor was used by U.S. army in 1973-1975, over 600 people have been saved from death or serious injury and police fatalities have shown a significant change in trend and numbers. Moreover, during the Vietnam War, soft armors were manufactured from fabrics of fiberglass and nylon and used for ballistic protection [2].

Generally, textile armors were used for fragmentation or low energy bullet defeat, usually are woven. The yarns applied in woven ballistic have a high specific strength and high modulus. These properties imply that the fibers are particularly difficult to

break. The high modulus allows the energy to be dissipated as a longitudinal stress wave, which is along the yarn. In case a high velocity bullet, only textile armor can not defeat the bullet. Therefore, a hard strike face is necessary to break up and distort the projectile before the composite backing spread the energy over a greater area.

Ceramic materials are commonly used as a strike face portion for containment blast fragments and bullet penetration. It is due to their very high hardness and compressive strength. The most common ceramic materials used are alumina, boron carbide, silicon carbide and titanium diboride. However, the ceramic materials also have some disadvantages i.e. ceramic armor is relatively heavy, and is configured for a fixed level of protection against a single ballistic threat.

Fiber based composites are widely used as armor backing because of their low weight and excellent energy absorption characteristics. Fiber glass, Kevlar and Spectra are also commonly used in conjunction with high strength adhesive to create effective composite backings [3].

1.1.1 High performance fibers

The selection of fibers for application depends on its mechanical property to absorb the projectiles kinetic energy locally and spread out the absorbed energy fast before local conditions for the failure are met. The factors must be considered i.e. (i) the ability to absorb energy per their unit mass (E_{sp}) is related to the fiber stress at rupture (σ_{rupt}), the elongation at rupture (ε_{rupt}), and the fiber density (ρ) as:

$$E_{sp} = \left(0.5\sigma_{rupt} * \varepsilon_{rupt}\right)/\rho \qquad \text{(Eq 1.1)}$$

(ii) the ability of fibers to spread out energy is governed by their speed of sound (V_{sound}) which is defined in terms of fiber modulus (E) and fiber density (ρ) as:

$$V_{sound} = \left(E/\rho\right)^{(1/2)} \qquad \text{(Eq 1.2)}$$

The high strength of fibers has been developed for armor structure. Fibers conventionally used include aramids (Kevlar™ or Twaron™), polyethylene fiber (Spectra™ or Dyneema™), nylon fiber and glass fiber [4]. The properties of high performance fibers are summarized in Table 1.1.

Table1.1: Typical mechanical properties of high performance fibers.

Fiber type	Failure strength Gpa	Failure Strain	Axiall modulus GPa	Density g/cm^3
Aramid	2.8-3.2	0.015-0.045	60-115	1390-1440
UHMWPE	2.8-4.0	0.029-0.038	90-140	970-980
LCP	2.7-2.9	0.033-0.035	64-66	1400-1420
PBO	5.4-5.6	0.024-0.026	270-290	1540-1560
PIPD	3.9-4.1	0.011-0.013	320-340	1690-1710
Nylon	0.06-0.08	1.5-2.5	1.0-1.5	1070-1170
S-glass	4.64-4.66	0.053-0.055	82-92	2470-2490

Poly-aramids (Kevlar®, Twaron®, Technora®); Highly oriented ultra-high molecular weight poly-ethylene, UHMWPE (Spectra®, Dyneema®); Poly-benzobis-oxazole, PBO (Zylon®), and Poly-pyridobisimi-dazole, PIPD (M5®).

Among various fibers, aramid fabrics are popularly selected to use in ballistic armor due to its high thermal stability which allows aramid fabrics to retain overall high tensile resistance and elongation of yield during ballistic event. Other types of fibers are also used for ballistic armor such as polyethylene fabric which has an enhanced ability over aramid fabrics to adsorb energy of a projectile and reduces the back face deformation generated by a stopped projectile. However, the high cost of these fibers is disadvantage. Therefore, searching of others fibers to cooperate with Kevlar fiber is one alternative to reduce cost of manufactured ballistic armor.

Recently, glass fiber and carbon fiber are also attractive material to be used in ballistic armors. Nunes et al. (2004) observed that bullet proof following NIJ standard for level-I was achieved by using 30 plies of glass fiber reinforced-epoxy matrix composites.

None of these laminate were perforated by any of the shots. Interestingly, this composite can deform the bullet after impact. Furthermore, the impedance layer by simply dividing physically the 30-ply laminate into an array of two 15-ply laminates can decrease the back side delamination area. This behavior decreases the probability of debris on the inside of a ballistic protected structure [5]. Larsson and Svensson (2002) investigated the properties of hybrid composite materials based on carbon fiber, organic fibers (polyethylene and PBO). Separation of fibers, with the carbon fibers at the front portion is advantage for ballistic velocity limit. For example, the laminate consisting of 75% quasi-isotropic carbon fiber epoxy at the front and 25% cross-ply polyethylene fibers at the back surface has 82% higher specific ballistic velocity limit [6].

1.1.2 Polymer matrix for ballistic composites

In general, the resins used as a binder in ballistic armor have an adhesive characteristic as well as increase ductility energy absorption. Various resins such as epoxy, polyester, vinyl ester, and phenolics have been applied for ballistic armor. Traditional phenolic resins have been widely used as matrices for composites in aircraft interiors because of its good heat resistance, flame retardant, dielectric properties, low smoke generation, and low cost. However, phenolic resins have serious shortcomings i.e. the brittleness, release of water and ammonia during the curing process and along with limited shelf life. Recently, benzoxazine resin which is one kind of phenolic resins was selected to apply as matrix for reinforced fiber due to its outstanding properties, no by-product during polymerization, high thermal stability, excellent mechanical properties, and ability to alloy with various types of resins [6-11].

Alloying benzoxazine resin (BA-a) with urethane prepolymer (PU) can improve the flexibility of the more rigid polybenzoxazine. Moreover, the synergism in glass transition temperature (T_g) revealed and that the T_gs of the alloys are significantly greater than those of the parent polymers [7]. The research about effect of urethane prepolymer based on various type of isocyanate also reported that toluene-diisocyanate (TDI)

resulted in provided the highest T_g, flexural modulus, and flexural strength of the alloys. The BA-a/PU based on TDI alloys were used as matrices for reinforced carbon fiber at 80wt% in cross-ply orientation. The flexural strength of composites had relatively high values of about 490 MPa [8]. Because of desirable properties of this polymer alloys, they were used in the ballistic armor applications. The ballistic composite that contained Kevlar™ and benzoxazine-urethane alloys as reinforcing fiber and matrix, respectively was developed and under patent pending. The ballistic testing was reported that the thickness of Kevlar™-reinforced 80/20 BA-a/PU composite panel was 30 plies and 50 plies in order to resist the penetration from the ballistic impact of levels II-A and III-A, respectively [9].

The development of composite technology has improved properties of the final product of armor structure. Fibers and matrix are important factors to obtain high performance ballistic armor. In this work, the resistant of the armor composite penetration using benzoxazine resin and benzoxazine-urethane as matrix reinforced with Kevlar™ and other fibers including carbon fiber, and glass fiber are investigated by observing possibility incorporate with Kevlar™ in order to reduce cost of Kevlar™. The effect on other physical, mechanical and thermal properties of the matrices and their fibers-reinforced composites are also be evaluated within the scope of the study.

1.2 Objectives

1. To develop a light weight ballistic armor based on benzoxazine alloys as matrices i.e. benzoxazine-urethane
2. To study suitable composition ratios of the polymeric alloys and a number of layers of the Kevlar cloth to produce ballistic composites of level III-A or higher.
3. To investigate possibility of using other reinforced-fibers such as carbon fiber and glass fiber in order to cooperate with Kevlar™ fiber i.e. the glass fiber or carbon fiber composite will be designed as strike face whereas Kevlar composite will be armor backing.

4. To evaluate the physical, mechanical and thermal properties of the resulting composites to be used as ballistic armor.

1.3 Scopes of research

1. Synthesis of benzoxazine resin by solventless synthesis technology.
2. Synthesis of urethane prepolymer by diol (MW = 2000) and toluene diisocyanate (TDI).
3. Preparation of polymeric alloys between the benzoxazine resin/urethane prepolymers (BA-a/PU) at various weight ratios i.e. 100/0, 90/10, 80/20, 70/30 and 60/40.
4. Characterizations of benzoxazine resin, urethane prepolymer and benzoxazine/urethane alloys.
    4.1 Examination of the puritites of monomer and prepolymer.
        - Nuclear magnetic resonance spectrometer (^{1}H NMR)
    4.2 Evaluation of the curing condition or crosslinking process of the alloys
        - Fourier transform infrared spectroscopy (FTIR)
        - Differential scanning calorimeter (DSC)
5. Evaluation suitable composition ratios of the polymeric alloys and a number of layers of the fabric to produce ballistic composites of level III-A or higher.
    5.1 Fabricate the fibers-reinforced composite armor from carbon fiber, glass fiber and Kevlar fiber using suitable resin mixtures at 20% by weight of the alloy matrices.
    5.2 Investigation of thermal properties of the fibers-reinforced composites.
        - Thermogravimetric analyzer (TGA).
    5.3 Evaluation of mechanical properties of the fiber composites based on the above alloys.
        - Dynamic mechanical analyzer (DMA).
        - Universal testing machine (flexural mode) .
6. Evaluate the interfacial bonding between the resin alloys and the fibers by the analysis of fracture surface using scanning electron microscope (SEM).
7. Fire test using NIJ standard of Level III-A or higher.

8. Analyze of the data drawing conclusions.
9. Prepare the final report.

1.4 Chemicals and equipments

1. Kevlar fiber, glass fiber and carbon fiber
2. Chemicals
    - Bisphenol
    - Para-formaldehyde
    - Aniline
    - Toluene Diisocyanates (TDI)
    - Polyhydric compound (propylene glycol)
3. Hot press
4. Hot plate
5. Oven
6. Nuclear magnetic resonance spectrometer (^{1}H NMR)
7. Fourier Transform Infrared Spectroscopy (FTIR Spectroscopy)
8. Differential Scanning Calorimeter (DSC)
9. Dynamic Mechanic Analyzer (DMA)
10. Instron 5567 Testing Machine.
11. Fire test lead projectiles with 44 Magnum Lead SWC Gas Checked 9 mm FMJ for level III-A and 7.62 mm 308 Winchester FMJ for level III.

CHAPTER II

THEORY

2.1 Composite Materials

Composite materials consist of two major components which are the matrix and reinforcing agent as depicted in Figure 2.1. The matrix acts as a binder and in most cases a distinct region (inter phase) between reinforcement and matrix may also be observed.

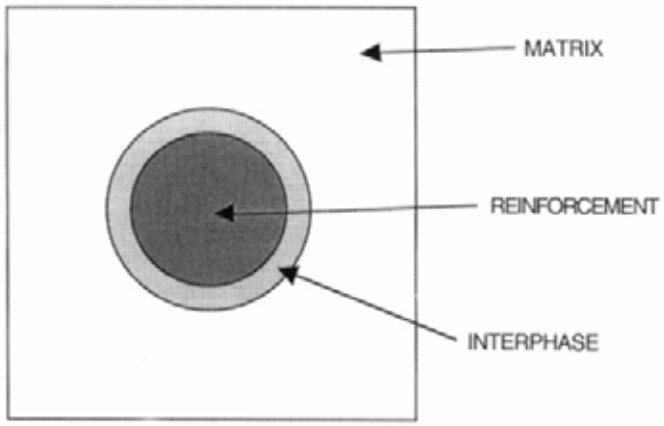

Figure 2.1 Schematic representation of the principal composite constituents.

The polymer based composites can be classified into many types as exhibited in Figure 2.2. There are three major types of polymer composites: those where the matrix is non-polymeric (although wood, clearly polymeric, plays a matrix role here), those with the polymer as the matrix, usually being reinforced or filled with another material, such as fibers, plates, or particulates and those where some degree of dual-phase continuity prevails, as in laminates foams [10].

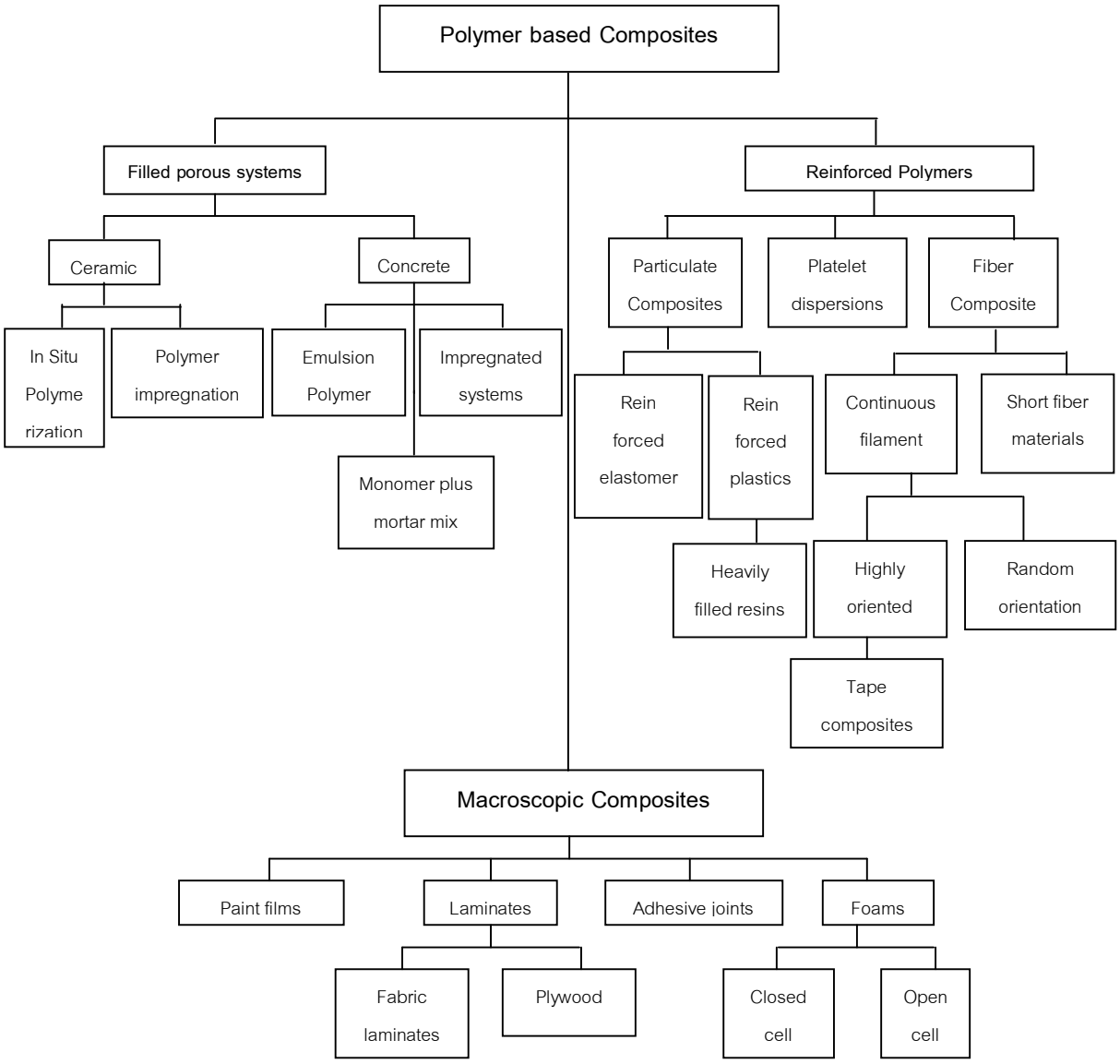

Figure 2.2 Classifications of polymer based composites [13].

2.1.1 Matrices

The matrix in fiber-reinforced composite plays important roles in composite material i.e. (1) to transfer stress between the fibers, (2) to provide a barrier against an adverse environment and (3) to protect the surface of the fibers from mechanical abrasion. Therefore, selection of matrix has a major influence on the interlaminate shear strength which is an important design parameter for structural use under bending loads. On the other hand the in-plane shear strength is also important design factor under torsion loads. The matrix provides lateral support against the possibility of fiber bucking

under compression loading, hence influencing to some extent the compressive strength of composite material to certain extend. The interaction of fiber and matrix is also important in designing damage-tolerant structures. Finally, the process ability and defects in a composite material depend on the physical and thermal characteristics, such as viscosity, melting point, and curing temperature of matrix.

The principal factors usually need to be taken into consideration when choosing a matrix resin are:

- The mechanical strength characteristic required for composite. Such strength properties also depend upon the type of reinforcement and its arrangement within the matrix.
- The specific performance of the composite in its working environment. The matrix should be able to maintain its properties during service conditions.
- The fabrication process to be used. The resin should be easy to use in the process. The cost and shelf life of the resin are also important parameter that have to consider [11].

2.1.2 Benzoxazine Resin

Phenolic resins are widely used in various applications, from commodity and construction materials to the needs of the high technology aerospace industry. Benzoxazine resin is a novel kind of phenolic resin that can be synthesized from phenol, formaldehyde and amines [12]. Benzoxazines were first synthesized by Cope and Holy in 1940s [13].

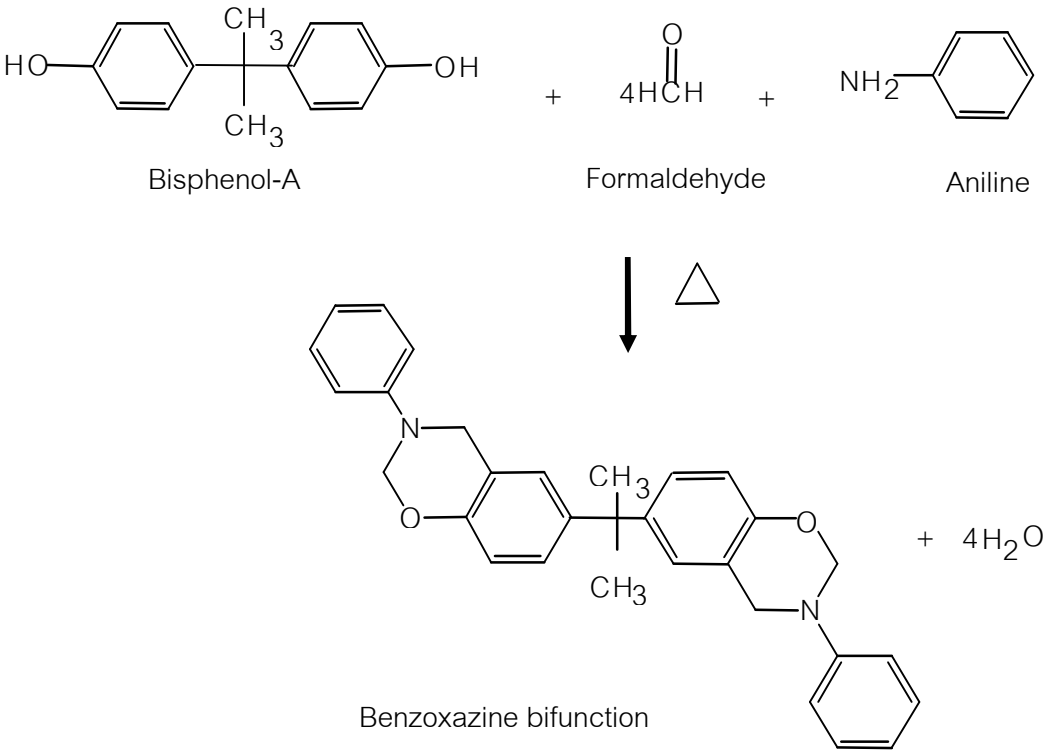

Figure 2.3 Schematic synthesis of bifunctional benzoxazine monomer.

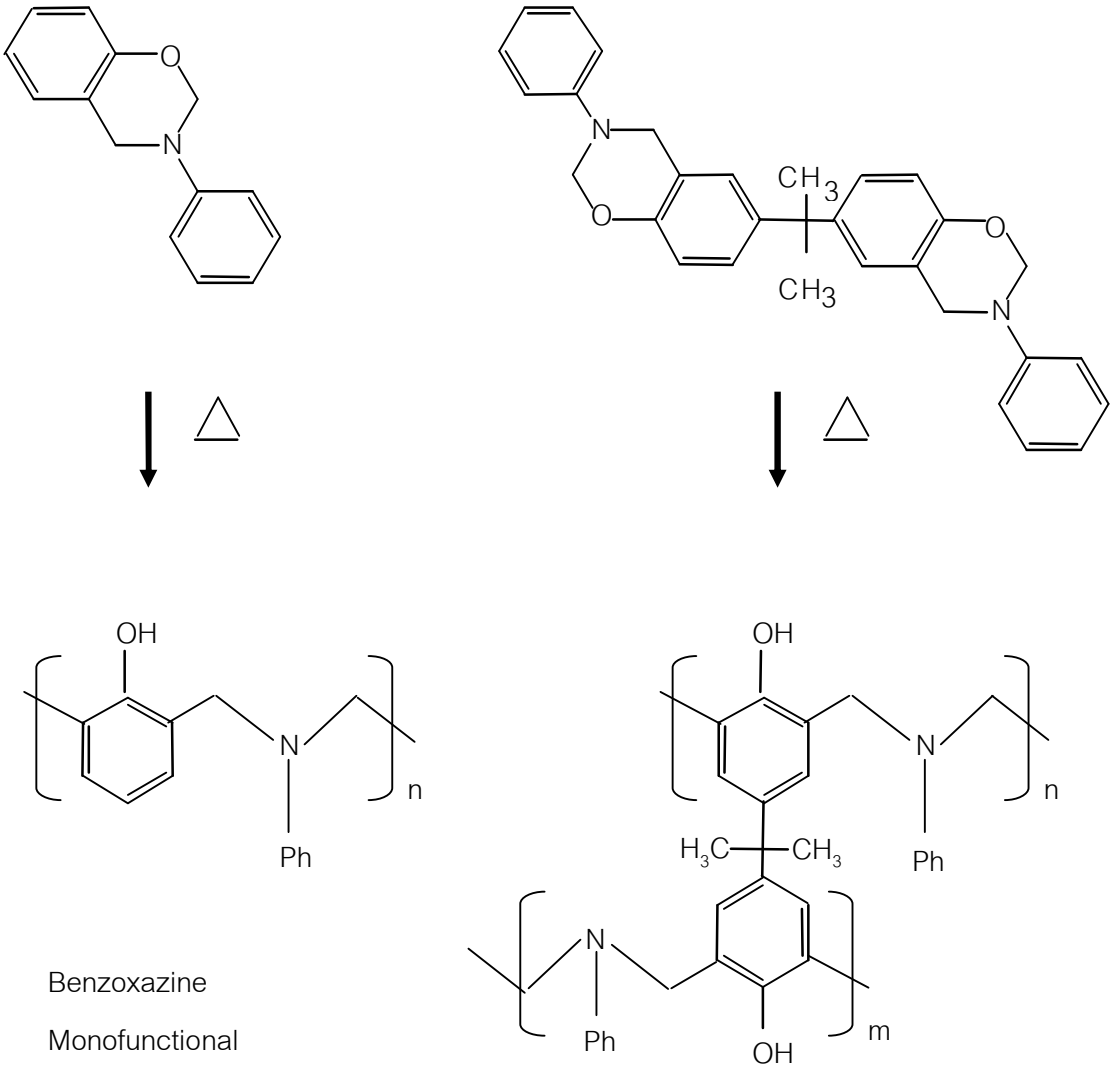

Figure 2.4 Structures of monofunctional and bifunctional.

Benzoxazine monomers are typically synthesized using phenol, formaldehyde and amine (aliphatic or aromatic) as starting materials. Different types of benzoxazine monomer can be synthesized using various phenols and amines with different substitution groups attached. These substituting groups can provide additional polymerizable sites and also affect the curing process. Therefore, benzoxazine resin can be classified into a monofunctional and a bifunctional type depending on a type of phenol i.e. benzoxazine bifunctional monomer use bi-phenol and benzoxazine monofunctional monomer use phenol to synthesize. The synthesis of benzoxazine resin

can be employed by solution or solventless methods. A novel solventless synthesis method was developed by Ishida in 1996 [14]. This method is a convenient method for preparation of benzoxazine monomer series. Stoichiometric amounts of solid bisphenol, para-formaldehyde and liquid 3-aminophenylacetylene were mixed together at 110^{o}C as illustrated in Figure 2.3. Benzoxazine resin can be polymerized by heating and do not need catalyst or curing agent as shown in Figure 2.4. The unique properties of benzoxazine resin reported in the literature include:

- Solvent-less synthesis provides almost contaminant-free monomers. Thus, we can neglect the purification process which can save a production cost and also decrease pollution from the use of solvent.
- Self-polymerized upon heating.
- No catalyst or curing agent required.
- No by-products during cure.
- Low melt viscosity.
- Near zero mold shrinkage.
- Low water absorption.
- Excellent electrical properties.
- High mechanical integrity [15-17].

The properties of polybenzoxazines compared with those of the state of art matrices were depicted in Table 2.1. Polybenzoxazines present the highest tensile properties. Their results from dynamic mechanical analysis reveal that these candidate resins for composite applications possess high moduli and glass transition temperatures, at low cross-link densities. Long-term immersion studies indicate that these materials have a low rate of water absorption and low saturation content, in addition to their satisfactory impact, tensile and flexural properties [17].

Table 2.1: Comparative properties of various high performance polymers.

Property	Epoxy	Phenolics	Toughened BMI	Bisox-phen (40:60)	Cyanate ester	P-T resin	Polybenzoxazine
Density (g/cc)	1.2-1.25	1.24-1.32	1.2-1.3	1.3	1.1-1.35	1.25	1.19
Max use temperature (°C)	180	~200	200	250	150-200	300-350	130-280
Tensile strength (MPa)	90-120	24-25	50-90	91	70-130	42	100-125
Elongation (%)	3-4.3	0.3	3	1.8	0.2-0.4	2	2.3-2.9
Dielectric constant (1MHz)	3.8-4.5	0.4-10	3.4-3.7	-	2.7-3.0	3.1	3-3.5
Cure temperature (°C)	RT-180	150-190	220-300	175-225	180-250	177-316	160-220
Cure shrinkage (%)	>3	0.002	0.007	<1	~3	~3	~0
TGA onset (°C)	260-340	300-360	360-400	370-390	400-420	410-450	380-400
Tg (°C)	150-220	170	230-380	160-295	250-270	300-400	170-340
G_{IC} (J/m^2)	54-100	-	160-250	157-223	-	-	168
K_{IC} (MPa $m^{1/2}$)	0.6	-	0.85	-	-	-	0/94

Bismaleimide (BMI), Bisoxazoline-phenolics (Bisox-phen), Phenolic-triazine resin (P-T resin), Thermogrvimetric analysis (TGA), Fracture energy (G_{IC}) and Fracture toughness plain-strain stress intensity factor (K_{IC}).

2.1.3 Urethane Elastomer

Otto Bayer et al. at I.G. Ferbenindustri, Germany in 1937 were the first to discover polyurethane (PU). The initial work was the reaction of aliphatic isocyanate with a diamine to form polyurea which was infusible and hydrophilic. Further research on this

subject demonstrated the reaction of an aliphatic isocyanate with a glycol produces new materials with excellent properties. Dupont and ICI soon recognized the desirable elastic properties of PU. Nowadays, the PU forming system has received intense attention resulting in the syntheses of various specialized forms such as plastics, rubbers, surface coatings, adhesives and fibers.

Urethane Elastomer can be regarded as a linear block copolymer shown in Figure 2.5. This segmented polymer structure can vary following properties over a wide range of strength and stiffness by modification of its three basic building block i.e. polyol, diisocyanate and chain extender.

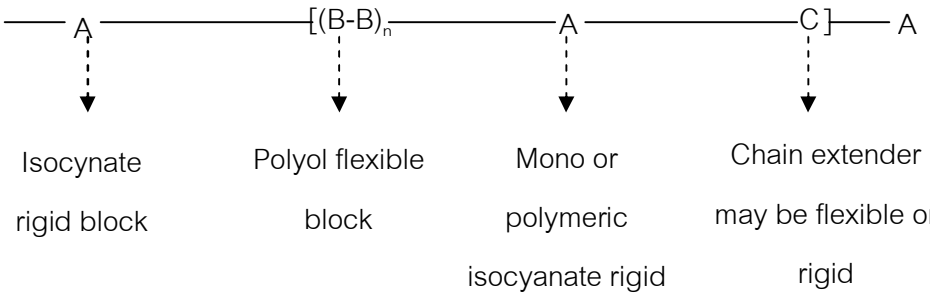

Figure 2.5: The basic unit in a urethane block polymer.

The usual route of chemical formation for all urethanes consists of polyol and diisocyanate. Initially, the diisocyanate and polyol are reacted together to form an intermediate polymer of molecular weight 15000-20000 which is called a preploymer after that it is converted into the final high molecular weight by further reaction with a diol and diamime chain extender.

The polyfunctional isocyanate used to prepare PU can be aromatic, aliphatic, cycloaliphatic or polycyclic in structure. Different diisocyanates contribute to the PU properties in different ways. For example, aromatic diisocyanates give more rigid PU than aliphatic ones, but their oxidative and ultraviolet stabilities are lower [10]. In this work, the raw materials used for the systhesis of PU prepolymer are toluene

diisocyanate (TDI) which is an aromatic diisocyanate. Most of the TDI used is a mixture of the 2,4- and 2,6-isomers. The structure formulae of toluene diisocyanate (TDI) are shown in Figure 2.6.

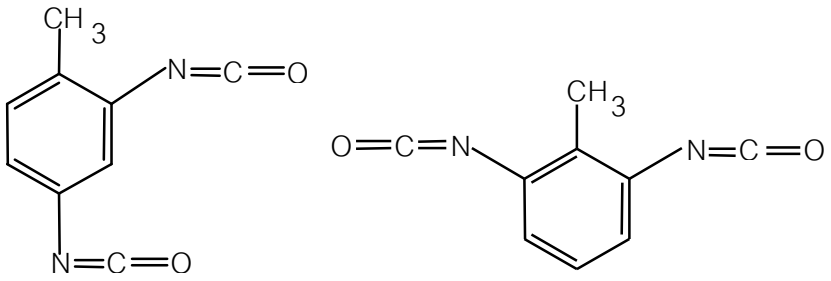

Figure 2.6 2,4 Toluene diisocyanate and 2,6 toluene diisocyanate (TDI) [18, 19].

Toluene diisocyanate is prepared by direct nitration of toluene to give a 80:20 mixture of the 2,4- and 2,6-di-nitro derivatives, followed by hydrogenation to the corresponding diaminotoluene. Though toluene diisocyanate (TDI) is stable with a relatively high-flash point, it can react with water, acid, base, organic, and inorganic compounds. The 80:20 mixture of 2,4-TDI and 2,6-TDI is, today, the most important and widely use for way application and widely used for vary application in commercial product.

The polyol component of the PU is a polyfunctional polyether (e.g., polyethylene glycol, polypropylene glycol, PTMG or polycaprolactone diol), polyester polyol (PEPO), acrylic polyol (ACPO), polycarbonate polyol, castor oil. The low molecular weight reactants result in hard and stiff polymers because of a high concentration of urethane groups. Otherwise, the use of high molecular weight polyols as the main reactants produces polymer chains with fewer urethane groups and more flexible alkyl chains. Long-chain polyols with low functionality give soft, elastomeric PU while short chain polyols of high functionality give more rigid.

In this work, polyether polyols with the fixed molecular weight of 2000 was used to synthesize our urethane prepolymer. Polyether polyols contain the repeating ether linkage –R–O–R– and have two or more hydroxyl groups as terminal functional groups.

They are manufactured commercially by the catalyzed addition of epoxies, cyclic ethers to an initiator. The most important types of the cyclic ethers are propylene oxide and ethylene oxide, with smaller quantities of butylene oxide also being consumed. These oxides react with active hydrogen-containing compounds so called initiators, such as water, glycols, polyols and amines; thus, a wide variety of compositions of varying structures, chain lengths and molecular weights is theoretically possible. By selecting the proper oxide (or oxides), initiators, and reaction conditions and catalysts, it is possible to synthesize a series of polyether polyols that range from low-molecular-weight polyglycols to high-molecular-weight resins. Most polyether polyols are produced for polyurethane applications; however, other end uses of the polyols ranging from synthetic lubricants and functional fluids to surface-active agents. In this work, the polyol used for the synthesis of our urethane prepolymer is polypropylene glycol (MW = 2000). The structure formulae of the polypropylene glycol (MW = 2000) are presented in Figure 2.7 [20].

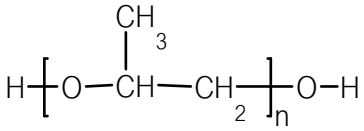

Figure 2.7 Polypropylene glycol used in this study.

Takeichi et al. studied about the synthesis and characterization of polyurethane-benzoxazine in a previous work. The polyurethane-benzoxazine films as novel polyurethane (PU)/phenolic resin alloys were prepared by blending a benzoxazine monomer (BA-a) and TDI-polyethylene adipate polyol (MW = 1000) based PU prepolymer. FT-IR spectroscopic technique was used to investigate the reaction between benzoxazine resin and urethane prepolymer. From the experiment, the mechanism of benzoxazine-urethane alloys was proposed as illustrated in Figure 2.8. The benzoxazine ring thermally opens, followed by the reaction between the OH groups and NCO groups [21].

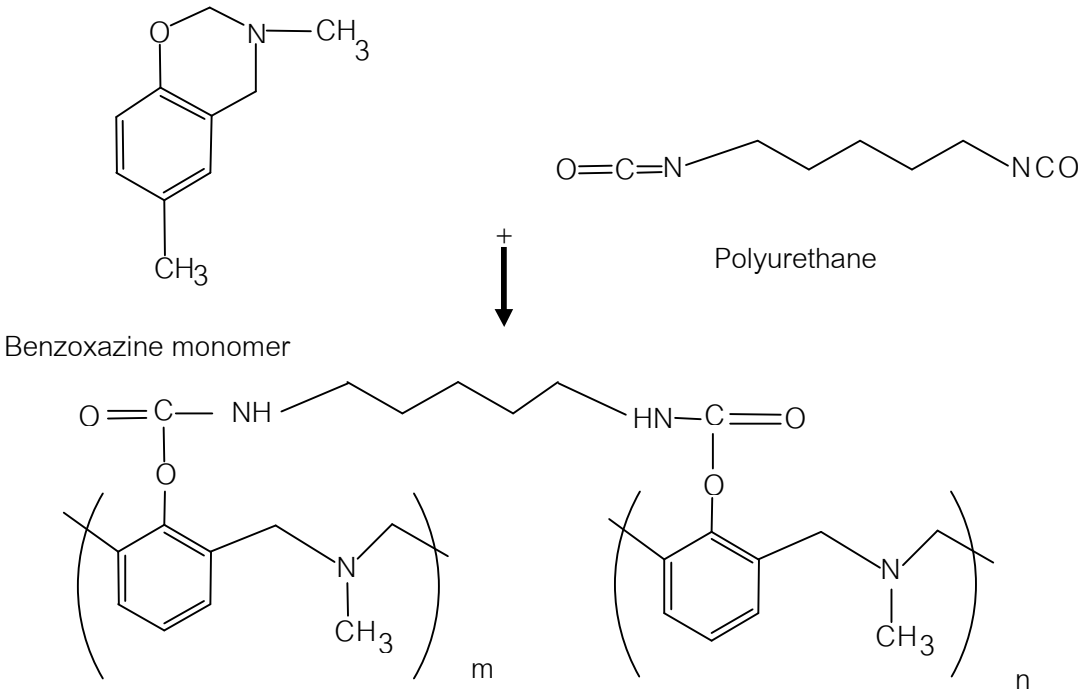

Figure 2.8 Benzoxazine-Urethane crosslinked.

2.2 Fiber-reinforced composites

Fibers are the principal constituent in a fiber-reinforced composite material. They occupy the largest volume fraction in a composite laminate and share the major portion of the load acting on a composite structure. Proper selection of the type, amount and orientation of fibers is very important; since it influences the following characteristics of a composite laminate i.e. specific gravity, tensile strength and modulus, compressive strength and modulus, fatigue strength and fatigue failure mechanisms, electrical and thermal conductivities and cost. High-performance polymeric (organic) fibers can be broadly classified into the following three main categories: (i) fibers from lyotropic liquid crystalline polymers, such as the aramid fibers (Kevlar); (ii) fibers from thermotropic liquid crystalline polymers, such as a copolymer of benzoic and naphthoic acids (Vectran); (iii) fibers from extended-chain flexible polymers, such as ultrahigh molecular weight polyethylene (Spectra, Dyneema) [11].

Fibers can be applied in a variety of frabication techniques. These include:

- Impreged mats of fibers

- Laminates of impregnated sheets of oriented fibers or woven fabrics
- Filament winding of resin-coated continous fibers around three dimension axes of rotation to form a vessle

The basic element of fabrication and design a sheet containing uniaxial oriented continous fibers. These sheets are stacked in various orientations and laminated to create a material that are controlled and tailored such that the finished product can be produced best with properties having resistance against to multiaxial static and dynamic load during their service life [22].

2.2.1 Kevlar™ Aramid Fiber

Kevlar™ aramid fiber developed in 1965 when a Du Pont research scientist synthesized a series of para-oriented symmetrical super-rigid molecular chain and fiber of ultra-high modulus [2]. Typical properties of Kevlar™ fiber are summarized in Table 2.1

In general, Kevlar™ aramid fiber has a high breaking tenacity which is several times that of metal wire, industrial nylon, and polyester yarns. It also has a much higher tensile modulus than steel wire, fiberglass, nylon, and polyester fibers. Kevlar™ has a low elongation at break, which is comparable to that of steel. It has lower density than steel and glass, which makes most Kevlar™-reinforced structures of a lighter weight for a given strength and stiffness. As an aramid, Kevlar™ fiber is inherently stable at relatively high temperatures. It has a very small shrinkage at elevated temperatures, low creep, and a rather high glass transition temperature. In addition, it is corrosion resistantance, non-conductive, and resistantance to most chemicals except strong acids and bases. These outstanding properties make Kevlar™ fiber products useful for many industrial and civilian applications.

Table 2.2: Properties of various grades of Kevlar™ fiber.

Yarn properties	Kevlar™ 29	Kevlar™ 49	Kevlar™ 68	Kevlar™ 119	Kevlar™ 129	Kevlar™ 149
Tensile strength (GPa)	2.90	2.90	2.90	3.03	3.34	2.34
Initial modulus (GPa)	71.02	119.97	99.28	55.16	96.53	144.79
Elongation (%)	3.6	2.8	3.0	4.4	3.3	1.5
Density (g/cm^3)	1.44	1.45	1.44	1.44	1.45	1.47
Moisture absorption(%)	6	4.3	4.3	-	-	1.5

Note: Yarn properties determined on 10 in twisted yarns (ASTM D-885)

2.2.2 Carbon Fiber

Carbon fiber is a generic name representing a family of fibers. Over the years, it has become one of the most important reinforcement fibers in many different types of composites, especially in polymer matrix composites [23]. Carbon and its graphite derivatives have emerged prominently in twentieth century technology. Carbon fibers are fine filament composed largely of carbon with structures and properties varying from those of amorphous carbon to those of well-developed crystalline graphite. Carbon in the graphitic form has hexagonal structure and highly anisotropic. The fibers have the largest variety of strengths and moduli. Carbon fibers are divided into high-strength and high modulus according to their mechanical properties. Possible strength of carbon fiber is estimated to be about 100 GPa. Though the theoretical tensile strength of single crystal of graphite is 150 GPa, which is the highest of all the materials known. The commercial high-strength carbon fibers have a reported maximum strength of 7 GPa [24]. The ratio of stiffness to density is very high for most carbon fiber because the

density of carbon is low. For this reason, they are the most widely used and are notably effective as reinforcing elements in advanced composite materials.

Physico-chemical properties of carbon fibers depend on the type of the precursor, manufacture conditions, the subsequent processing methods and other factors. Carbon fibers are a monocomponent system but they can be imparted with various properties often changeable in a wide range depending on the purposes and fields of application. The structure and properties of carbon fiber significantly depend on the raw material used, generally a polymer fiber. Numerous precursors have been used to produce carbon fiber. However three precursors which are being used for large-scale production of carbon fiber are PAN, rayon, and pitch. The first high-stiffness carbon fibers were produced from rayon. However, rayon-based carbon fiber did not compete with the PAN-based carbon fiber that became commercially available by the late sixties due to higher carbon yields which is 50% against 30% of rayon.

The carbon fibers produced from PAN have good-to-excellent strength up to 6895 MPa and high stiffness. Later carbon fibers were also prepared from pitch, an available by-product of the coal gasification and petrochemical industries. The properties of pitch carbon fibers are generally inferior to PAN carbon fiber. The properties of typical carbon fiber from these three precursors are shown in Table 2.3. [25].

Table 2.3: Axial tensile properties of carbon fiber.

Precursor	Tensile strength (GPa)	Tensile modulus (GPa)	Elongation at break (%)
PAN	2.5-7.0	250-400	0.6-2.5
Pitch	1.5-3.5	200-800	0.3-0.9
Rayon	~1.0	~50	~2.5

2.2.3 Glass Fiber

The basic material for making glass is sand, or silica, which has a melting point around 1750°C, too high to be extruded through a spinneret. However combining silica with other elements can reduce the melting point of glass which is produced. Fibers of glass are produced by extruding molten glass at a temperature around 1300°C, through holes in a spinneret and then drawing the filaments to produce fibers having diameters usually between 5 and 15 micron.

Several types of glass are based on silica (SiO_2) which combined with other elements to create specialty glasses. The most common types of glass fibers are following:

- A-glass is alkali or soda lime glass and is most usually used for bottles and not in fiber form.
- E-glass is the most widely used as fiber reinforced composite.
- S- and R- glasses contain a higher amount of alumina, however the higher the content of refractory solid such as alumina and silica the more difficult it is to obtain a homogenous melt and this is reflected in the cost of the final product.
- C-glass is resistant to acid environment and Z-glass also resist to alkaline environment. Type D-glass is produced to apply in a low dielectric constant [26].

Table 2.4: Properties of glass fibers.

Properties	E-glass	S-glass	C-glass
Modulus of elasticity (GPa)	7.24	8.62	-
Tensile Strength (GPa)	3.4	4.8	2.4

Table 2.5 Typical properties of glass fibers.

Property	E-glass	S-glass
Specific gravity	2.60	2.50
Young's modulus (GPa)	72	87
Tensile strength (MPa)	3450	4310
Tensile elongation, %	4.8	5.0
Coefficient of thermal expansion (μm/m/^{o}C)	5.0	5.6

2.2.4 Assembling Fiber and Yarns: Woven Fabrics

The majority of fibers used to manufacture composite armor is a high performance fiber. However fibers placed in the path of the projectile cannot hold a high speed projectile by themselves. To engage a high number of fibers, they are combined into a woven fabric, a felt material or into a non-woven cross-plied in the from of unidirectional set of fibers.

Woven fabrics are designed through interlacing yarns in two- and three-dimensional regular geometric arrangements. Two-dimensional woven fabrics are created by positioning yarns at 0^{o} and 90^{o} are the most common for armor applications. The yarns running parallel to the direction of weaving and transverse are called wrap and weft, respectively. They have three basic configurations, namely plain, twill and stain.

Plain weave is most basic of the 1 dimensional types. The wrap and weft form a simple criss-cross pattern. Each weft thread crosses the wrap threads by going over one, the under the next. Adjacent weft threads go under the wrap threads that its adjacent went over as shown in Figure (a). Twill weave is made by passing weft threads over one warp thread and then under two or more warp threads, with an offset between

rows that creates a pattern of diagonal ribs as depicted in Figure (b). Satin is more flexible type of weave, which is used to manufacture complex shapes. For example, one wrap runs over three or more weft yarn and under one weft yarn as presented in Figure (c).

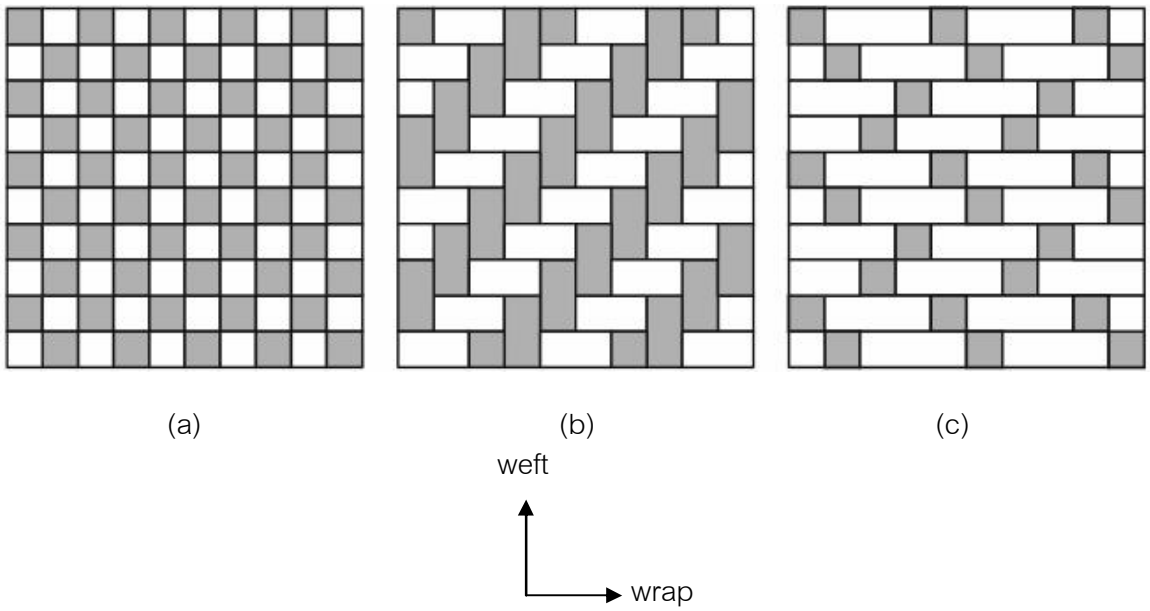

Figure 2.9 (a) Plain weave fabric, (b) 2/2 twill weave fabric and (c) 4-hardness stain weave.

Balanced weaves are fabrics in which the wrap and weft are made of threads of the same weight and number of threads per inch. The unbalanced fabric may be used to obtain different mechanical properties along the wrap and weft directions. It is well known that balanced fabrics dissipate more energy than unbalalnced ones. Nevertheless, ballistic fabrics normally have different levels of crimp in wrap and weft yarns because of the weaving process, resulting in weft yarns having lower levels of crimp than warp yarns as depicted in Figure 2.10. It is due to cause weft yarns to break preferentially to warp yarns during ballistic impacts. New generation fabrics for ballistics applications are manufactured with equal crimp in both yarns therefore they are loaded equally during ballistic impacts [27]. Furthermore, the process of weaving degrades the

mechanical properties of the yarns. Lee et al .(2002) observed that the tensile stiffness of E-glass dry yarns is reduced by 7% and the strength is reduced by 30% after processing as shown in Figure 2.11 [28].

(a) (b)

Figure 2.10 (a) Crimp in warp and (b) weft yarns from Twaron ™ CT716 fabric.

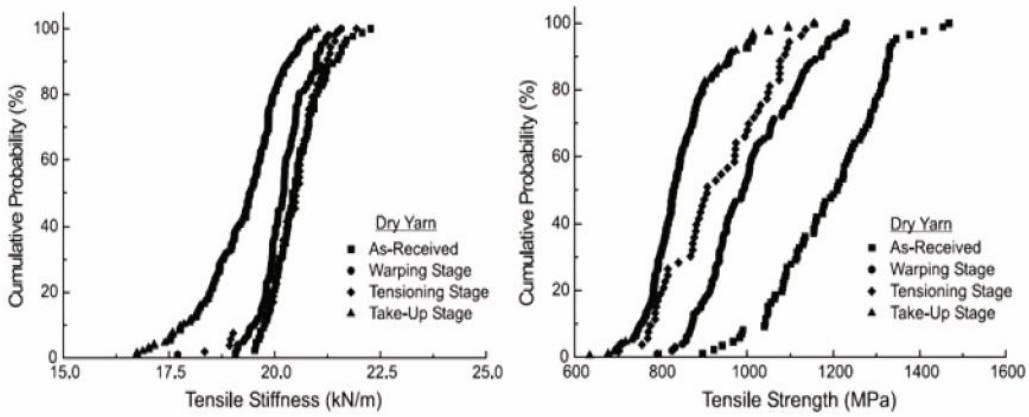

(a) (b)

Figure 2.11 Cumulative probability distribution of tensile stiffness (a) and tensile strength (b) at different weaving phases.

2.3 The Ballistic Resistance of Composite

A starting point for a description of the impact into fabric, the transverse impact into a single fiber is described first. Figure 2.12 illustrates a projectile strikes a fiber. Two types of wave propagations are generated in the fiber upon impact i.e. longitudinal and transverse. The longitudinal tensile wave travels down the fiber axis at the sound speed of the material. As the tensile wave propagates away from the impact point, the material

behind the wave front flows toward the impact point, which has deflected in the direction of motion of the impacting projectile. This transverse movement of the fiber is the transverse wave, which is propagated at a velocity lower than that of the material [4].

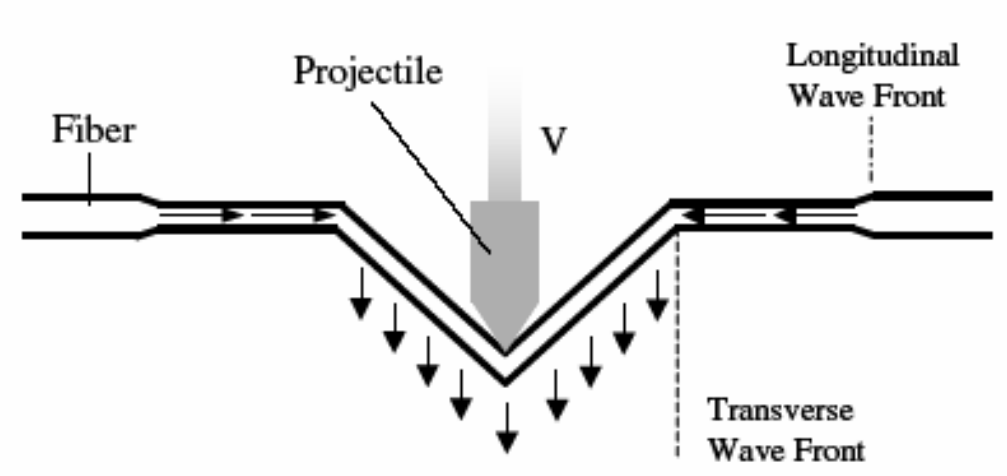

Figure 2.12 Wave propagation in a transversely impacted fiber.

Cunniff reported a projectile impacts the fabric as shown in Figure 2.12, it produces a transverse deflection in the yarns that are in direct contact with the projectile (defined as principal yarns) and generates longitudinal strain waves that propagates at the sound speed of the material down the axis of the yarns. Additionally, orthogonal yarns, defined as yarns that intersect the principal yarns, are then pulled out of the original fabric plane by the principal yarns. These orthogonal yarns undergo a deformation and develop a strain wave like those observed in the principal yarns. Analogously, these orthogonal yarns then drive yarns with which they intersect. These yarn–yarn interactions, which are a function of the friction between them, produce bowing, the misalignment of the orthogonal yarns, toward the impact point. The transverse deflection proceeds until the strain at the impact point reaches a breaking strain [29].

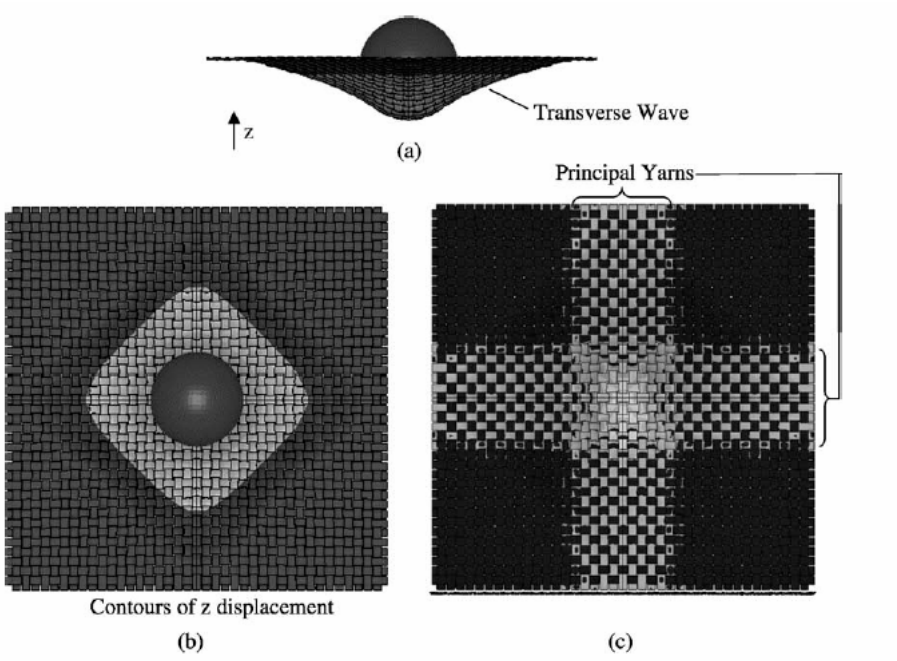

Figure 2.13 Sphere impacting single ply of fabric: (a) side view, (b) top view of z displacement contours and (c) bottom view showing principal yarns under high stress.

For residual velocity testing, by measuring the velocity of the projectile entering and exiting the specimen, the amount of energy absorbed by the composite $E_{absorption}$ is calculated as [30]:

$$E_{absorption} = 0.5\, m_{projectiles} (V_{in}^{2} - V_{out}^{2}) \quad (2.1)$$

where is the $m_{projectiles}$ mass of the projectile and V_{in} and V_{out} are the velocities entering and exiting the specimen, respectively. This type of test method is typically used for residual strength testing where penetration resistance is not required.

The term 'ballistic limit velocity, V50' is defined as the minimum velocity at which a particular projectile is expected to consistently, completely of specimen penetration. The V_{50} is the projectile velocity at which 50% of projectile will penetrate a given target, while 50% will be stopped. The military standard MIL-STD-662E was created by the army to provide a simple cost effective method for determining V_{50} the ballistic limit. It is determined by taking the average of an equal number of highest partial penetration velocities and lowest complete penetration velocities which occur within a specific

velocity range for a particular specimen configuration. The velocity range requirement is necessary since an unusually high or low data point could offset the average, causing a misrepresentation of the V_{50} ballistic limit. According to standard recommendations, five partial and five complete penetrations within a 125 ft/sec range was set as the criteria for testing.

The energy absorbed by the composite was taken as the metric for impact penetration resistance. From the V50 ballistic limit, the amount of energy E absorbed was calculated as:

$$E = 0.5 * m_p * V_{50}^{\ 2} \quad (2.2)$$

where m_p is the mass of the projectile.

2.3.1 Mechanisms for Dissipating Ballistic Impact

Upon ballistic impact, polymer composites retard the projectile by reducing its kinetic energy. Different mechanisms such as the tensile failure of fibres, the elastic deformation of the composite, interlayer delamination, back-face deformation, shear between layers in the composite, and the inertia of the composite are responsible for the absorption of energy to different extents. Among the factors which control the energy absorption are the tensile properties of the fibre, the properties of the matrix, the arrangement of the fibres in the composite and the interfacial strength., It is necessary to understand and quantify the energy absorbed by each of these mechanisms to be able to design composite materials for ballistic protection efficiently, [31].

2.3.2 Quantification of Energy Absorption by Polymer Composites upon Ballistic Impact

The mathematical model has been derived to predict the energy absorbed by the composite during ballistic impacts. It gives a value of the ballistic limit, V_0, defined as

the estimated highest velocity at which the projectile is stopped. In developing the model the following assumptions had been made:

- The projectile is rigid and remains undeformed during the impact. This was confirmed by experiments which revealed that the projectiles used in the experiment retained their shape and mass after impact.
- The energy lost in overcoming the frictional force between a projectile and a composite is negligible and the heat generated during the projectile/composite interaction is negligible.
- The mechanism of failure of the composite is uniform across its thickness. This has been confirmed subsequently by high speed photography.
- The energy absorbed in delamination is neglected.
- The kinetic energy of a projectile of mass, m, moving with a velocity, V is given by

$$\text{K.E.} = \frac{1}{2}mV^2 \tag{2.3}$$

the ballistic limit

$$E_L = \frac{1}{2}mV_0^2 \tag{2.4}$$

where V_0 is the limiting velocity.

As discussed earlier, the impact of the projectile results in the formation of a cone on a back side of the composite through the propagation of a transverse wave shown schematically in Figure 2.14.

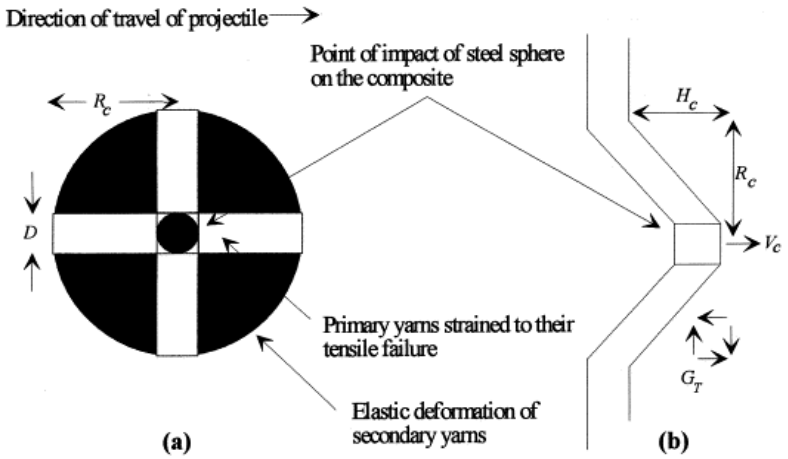

Figure 2.14 Deformation of a composite during ballistic impact by a steel sphere.

(a) plane of the back face and (b) side view.

In addition to these two major energy absorbing mechanisms, due to deformation of the primary and secondary yarns, there is a third contribution, the kinetic energy of the moving portion of the composite panel. Elements of the composite panel which are at rest before the impact are put into motion by the projectile on impact and, therefore, absorb energy through the kinetic energy of the moving cone. Thus

$$E_{Total} = E_{TF} + E_{ED} + E_{KE} \quad (2.5)$$

I. Energy absorbed in the tensile failure of primary yarns (E_{TF})

If the energy absorbed at the point of tensile failure of the composite per unit volume is E_c, then the total energy absorbed by tensile failure, $E_{TF,}$ is given by:

$$E_{TF} = E_C V \quad (2.6)$$

where D is the projectile diameter, T is the composite thickness and R_c is the radius of the cone formed on the back face of the composite.

$$E_{TF} = 4E_c R_c DT \quad (2.7)$$

II. Energy absorbed in the elastic deformation of secondary yarns (E_{ED})

The energy absorbed in elastic deformation of the composite at a strain ε can be obtained from the area under the stress/strain curve of the composite and because the stress/strain curve for the composite is linear, it is given by

$$E_{ED} = \frac{1}{2} M \varepsilon^2 \tag{2.8}$$

where M is the tensile modulus of the composite.

The yarns within the deformed zone, which are not directly impacted by the projectile, experience a different strain depending on their position. Those that are closest to the point of impact experience a strain just lower than the failure strain, while those that are farthest from the impact point do not see any strain. This imposes the following boundary conditions for the variation in strain ε, with distance from the impact point $\varepsilon=\varepsilon_0$ at r=D/2 and $\varepsilon=0$ at r=R_c, where ε_0 is the failure strain of the composite.

$$E_{ED} = \frac{\pi M \varepsilon_0^2 T}{\left(2R_C - D\right)^2}\left[\frac{R_C^4}{3} - \frac{D^2 R_C^2}{2} + \frac{D^3 R_C}{2} - \frac{D^4}{16}\right] \tag{2.9}$$

III. Kinetic energy of the cone formed on the back face of the composite upon ballistic impact (E_{KE})

The kinetic energy of the moving cone is given by

$$E_{KE} = \frac{1}{2} m_C V_C^2 \tag{2.10}$$

where m_c is the mass of the moving cone and V_c is the velocity of the moving cone.

The kinetic energy of the moving cone at the point of impact.

$$E_{KE} = \frac{1}{2}\pi R_C^2 T \rho V_C^2 \quad (2.11)$$

IV. Calculation of V_0

According to the model, the energy lost by the projectile is equal to the total energy absorbed by the composite.

$$E_L = E_{Total} \quad (2.12)$$

Using Eq.(2.4),

$$\frac{1}{2} m V_0^2 = E_{Total} \quad (2.13)$$

$$V_o = \sqrt{\frac{2}{m} E_{Total}} \quad (2.14)$$

2.3.3 Ballistic Standard of Body Armor (NIJ Standard for the Ballistic Resistance of Police Body Armor)

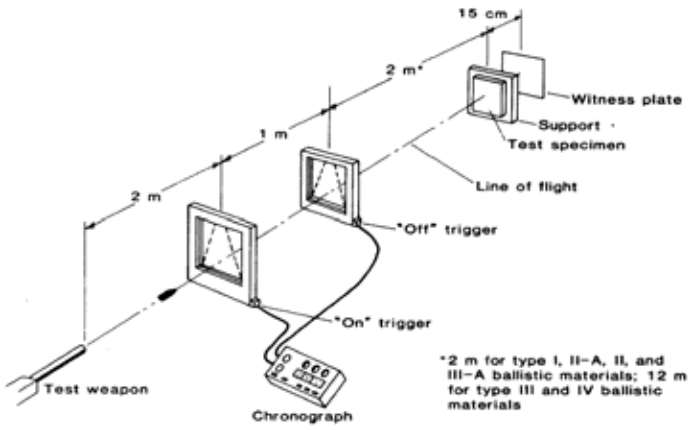

Figure 2.15 Ballistic test setup.

Police body armors covered by this standard are classified into seven types, by level of ballistic protection performance. The classification of an armor panel that provides two or more levels of ballistic protection at different locations on the ballistic panel shall be that of the minimum ballistic protection provided at any location on the panel.

Firstly, the test specimen should be conditioned at a temperature of 20 to 28°C (68 to 82°F) for at least 24 hours prior to test. Then the triggering devices are placed 2 and 3 m (6.6 and 9.8 ft.), respectively from the muzzle of the test weapon as shown in Figure 2.17, and arranged them so that they define planes perpendicular to the line of flight of the bullet. The distance between the devices should be measured with an accuracy of 1.0 mm. (0.04 in.) using the time of flight and distance measurements to calculate the velocity of each test round. After the specified test weapon has been supported, leveled, and positioned, fire one or more pretest rounds as needed through a witness plate to determine the point of impact. Place the test specimen in the support fixture and position it 5 m. (16 ft.) from the muzzle of the test weapon. Then position an imperforated witness plate 15 cm. (6 in.) beyond the test specimen. Fire a test round and record the velocity of the bullet as measured by the chronograph. Examine the witness plate to determine penetration, and examine the specimen to see if the bullet made a fair hit. If no penetration occurred, reposition the test specimen and repeat the procedure with additional test rounds until the test is completed. Space the hits as evenly as possible so that every portion of the test specimen is subject to test.

2.4 Ballistic Standard (National Institute of Justice for Body Armor Classification)

Two types of armor are classified to be soft armor and hard armor. Generally, soft armor designed to stop hand gun bullet. It is often worn in a sleeveless undergarment called a vest but is sometimes incorporated into the lining of a jacket or other outer garment. It is designed to be inconspicuous, although a person intent on detecting it might discern it under light clothing at close range in daylight. For hard armor, it is domed over soft armor. The hard armor is used for the special assignments

expecting an unusual risk of rifle fire or stabbing. The hard armors are manufactured from panels of sheet steel or titanium, perhaps coated or tiled with ceramic.

Personal body armors covered by this standard are classified into seven classes, or types, by level of ballistic performance. As of the year 2000, ballistic resistant body armor suitable for full time wear throughout an entire shift of duty is available in classification Types I, IIA, II, and IIIA, which provide increasing levels of protection from handgun threats. Type I body armor, which was first issued during the NIJ demonstration project in 1975, is the minimum level of protection that any officer should have. Officers seeking protection from lower velocity 9 mm and 40 S&W ammunition typically wear Type IIA body armor. For protection against high velocity 357 Magnum and higher velocity 9 mm ammunition, officers traditionally select Type II body armor. Type IIIA body armor provides the highest level of protection available in concealable body armor and provides protection from high velocity 9 mm and 44 Magnum ammunition.

Type IIIA armor is suitable for routine wear in many situations; however, departments located in hot, humid climates may need to carefully evaluate their use of Type IIIA body armor for their officers. Types III and IV armor, which protect against high powered rifle rounds, are clearly intended for use only in tactical situations when the threat warrants such protection.

2.4.1 Type I

This armor protects against .22 caliber Long Rifle Lead Round Nose (LR LRN) bullets, with nominal masses of 2.6 g (40 gr) impacting at a minimum velocity of 320 m/s (1050 ft/s) or less, and 380 ACP Full Metal Jacketed Round Nose (FMJ RN) bullets, with nominal masses of 6.2 g (95 gr) impacting at a minimum velocity of 312 m/s (1025 ft/s).

2.4.2 Type IIA

This armor protects against 9 mm Full Metal Jacketed Round Nose (FMJ RN) bullets, with nominal masses of 8.0 g (124 gr) impacting at a minimum velocity of 332 m/s (1090 ft/s) or less, and 40 S&W caliber Full Metal Jacketed (FMJ) bullets, with nominal masses of 11.7 g (180 gr) impacting at a minimum velocity of 312 m/s (1025 ft/s). It also provides protection against the threats mentioned in section 2.10.1.

2.4.3 Type II

This armor protects against 9 mm Full Metal Jacketed Round Nose (FMJ RN) bullets, with nominal masses of 8.0 g (124 gr) impacting at a minimum velocity of 358 m/s (1175 ft/s) or less, and 357 Magnum Jacketed Soft Point (JSP) bullets, with nominal masses of 10.2 g (158 gr) impacting at a minimum velocity of 427 m/s (1400 ft/s). It also provides protection against the threats mentioned in sections 2.10.1 and 2.10.2.

2.4.4 Type IIIA

This armor protects against 9 mm Full Metal Jacketed Round Nose (FMJ RN) bullets, with nominal masses of 8.0 g (124 gr) impacting at a minimum velocity of 427 m/s (1400 ft/s) or less, and 44 Magnum Semi Jacketed Hollow Point (SJHP) bullets, with nominal masses of 15.6 g (240 gr) impacting at a minimum velocity of 427 m/s (1400 ft/s). It also provides protection against most handgun threats, as well as the threats mentioned in sections 2.10.1, 2.10.2, and 2.10.3.

2.4.5 Type III

This armor protects against 7.62 mm Full Metal Jacketed (FMJ) bullets (U.S. Military designation M80), with nominal masses of 9.6 g (148 gr) impacting at a minimum velocity of 838 m/s (2750 ft/s). It also provides protection against the threats mentioned in sections 2.10.1, 2.10.2, 2.10.3, and 2.10.4.

2.4.6 Type IV

This armor protects against .30 caliber armor piercing (AP) bullets (U.S. Military designation M2 AP), with nominal masses of 10.8 g (166 gr) impacting at a minimum velocity of 869 m/s (2850 ft/s). It also provides at least single hit protection against the threats mentioned in sections 2.10.1, 2.10.2, 2.10.3, 2.10.4, and 2.10.5.

2.4.7 Special type

A purchaser having a special requirement for a level of protection other than one of the above standard types and threat levels should specify the exact test round(s) and minimum reference impact velocities to be used, and indicate that this standard shall govern in all other aspects.

Table 2.6: Test summary.

Bullet	Armor Type	Test Ammunition	Nominal Bullet Mass	Suggested Barrel Length	Required Bullet Velocity
	I	.22 LRHV Lead 38 Special RN Lead	2.6 g 40 gr 10.2 g 158 gr	15 to 16.5 cm 6 to 6.5 in 15 to 16.5 cm 6 to 6.5 in	320 ± 12 m/s 1050 ± 40 ft/s 259 ± 15 m/s 850 ± 50 ft/s
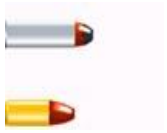	II-A	.357 Magnum JSP 9 mm FMJ	10.2 g 158 gr 8.0 g 124 gr	10 to 12 cm 4 to 4.75 in 10 to 12 cm 4 to 4.75 in	381 ± 15 m/s 1250 ± 50 ft/s 332 ± 12 m/s 1090 ± 40 ft/s
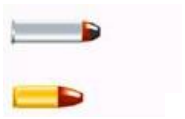	II	.357 Magnum JSP 9 mm FMJ	10.2 g 158 gr 8.0 g 124 gr	15 to 16.5 cm 6 to 6.5 in 10 to 12 cm 4 to 4.75 in	425 ± 15 m/s 1395 ± 50 ft/s 358 ± 12 m/s 1175 ± 40 ft/s
	III-A	.44 Magnum Lead SWC Gas Checked 9 mm FMJ	15.55 g 240 gr 8.0 g 124 gr	14 to 16 cm 5.5 to 6.25 in 24 to 26 cm 9.5 to 10.25 in	426 ± 15 m/s 1400 ± 50 ft/s 426 ± 15 m/s 1400 ± 50 ft/s
	III	7.62 mm 308 Winchester FMJ	9.7 g 150 gr	56 cm 22 in	838 ± 15 m/s 2750 ± 50 ft/s
	IV	30.06 AP	10.8 g 166 gr	56 cm 22 in	868 ± 15 m/s 2850 ± 50 ft/s

Abbreviations: AP - Armor Piercing, LRHV - Long Rifle High Velocity, FMJ - Full Metal Jacket, RN - Round Nose, JSP - Jacketed Soft Point, SWC - Semi-Wad cutter

CHAPTER III

LITERATURE REVIEWS

Polymer composites play an important role in ballistic protection for military and civilian personnel, because of the high strength, stiffness, and elongation provided by man-made fibers. Such composites offer many advantages over metal armor, including high durability, light weight and low maintenance costs. Various composites have been proposed in the past for use in the ballistic protection. A commonly used composite comprises a laminated structure consisting of woven or knitted fibers embedded in one or more polymer matrices [32-34].

Characteristics of matrix resin play an important role on the performance of each ballistic composite. Some important parameters for suitable matrix resins needed to be considered include its rigidity, processing ability, its viscosity, curing temperature, and shelf-life. Table 3.1 reveals some of the United States patents of polymer composite ballistic armor. The several types of fibers can be used with thermoplastics and also thermosets which have relatively broad range of properties depending on the intended applications. The matrix resins which are thermoplastic resins can be heated and softened, cooled, and hardened for limitless times without undergoing a basic alteration. On the other hand the thermosetting resins do not tolerate thermal cycling and cannot be reworked after molding. The outstanding characteristic of thermosetting resins is their inherent structural integrity, high thermal stability whereas common-typed thermoplastic polymers are more flexible and le Table 3.1: Review on United States patents of polymer composite ballistic armor [35-38].

Table 3.1: Review on United States patents of polymer composite ballistic armor.

Fiber	Matrix	Matrix Properties	Reference
1. Spectra™	Thermosetting		
	- Epoxy	- Elastomer - modulus 500,000 psi - strength 3,000 psi at high temp. below the melting point of fiber	Patent No. 4,748,064 Date: May 31, 1988 Patent No. 4,403,102 Date: Sep 6, 1983
	Matrix	**Matrix Properties**	**Reference**
	Thermoplastic elastomer		
	- thermoplastic elastomer	- areal density 4.5 oz/yd.	Patent No. 5,724,670 Date: Mar 10, 1998
	- urethanes	- Tg = -70 to 0 °C - low modulus - below the melting point of fiber	Patent No. 5,534,343 Date: Jul 9, 1996 Patent No. 4,403,102 Date: Sep 6, 1983
	- styrene-isoprene-styrene (SIS) dissolved in methylene chloride	- T_g = -55 °C - melt index = 9 g/min using - modulus 100 psi at 300% elongation	Patent No. 5,480,706 Date: Jan 2, 1996 Patent No. 5,093,158 Date: Mar 3, 1992 Patent No. 4,748,064 Date: May 31, 1988
2. Kevlar™	Thermosetting		
	- phenolic resin	- impact strength 17 J/m, 32 mm thick - T_g = 170 °C	Patent No. 5,190,802 Date: Mar 2, 1993 Patent No. 4,748,064 Date: May 31, 1988 Patent No. 4,639,387 Date: Jan 27, 1987
	- Polyester		Patent No. 4,550,044 Date: Oct 29, 1985
	- Epoxy	- elastomer - modulus 500,000 psi strength 3,000 psi at high Temp	Patent No. 5,102,723 Date: Apr 7, 1992 Patent No. 3,956,447 Date: May 11, 1976
	Thermoplastic		
	- urethanes	- Tg = -70 to 0 °C - low modulus - T_g = -55 °C	Patent No. 4,639,387 Date: Jan 27, 1987
	- styrene-isoprene-styrene (SIS)	- melt index = 9 g/min using - modulus 100 psi at 300% Elongation	Patent No. 5,480,706 Date: Jan 2, 1996

Fiber	Matrix	Matrix Properties	Reference
3. Glass Fiber	Thermosetting - phenolic - polyester	- moldable - MW. Range 800 to 5,000 or more	Patent No. 5,215,813 Date: Jan 1, 1993 Patent No. 4,639,387 Date: Jan 27, 1987 Patent No. 4,550,044 Date: Oct 29, 1985
	Thermoplastic - urethane - styrene-isoprene-styrene (SIS)	- flexibility - resistance to degradtion - T_g = -55°C - melt index = 9 g/min using - modulus 100 psi at 300% elongation	Patent No. 4,639,387 Date: Jan 27, 1987 Patent No. 4,822,439 Date: Apr 18, 1989
4. Polybenzoxazole and Polybenzothiazoe	- are not limited to thermoplastic or thermosetting		Patent No. 6,268,301 B1 Date: Jul 31, 2001
	Thermoplastics - polybenzoxazole or polybenzothiazoe	- low flammability - low smoke - high temperature stability - high chemical and solvent resistance - high strength and modulus	Patent No. 5,196,259 Date: Mar 23, 1993
5. Mixed Fibers -aramid andcarbon - aramid and glass - carbon and glass - carbon, glass and spectra	- ethylene-acrylate, methacrylate copolymer, vinyl ester phenilic polyimide, polycarbonate or the like	- high modulus - higher in impact resistance	Patent No. 4,732,803 Date: Mar 22, 1988

Some binders have been reported to be used with Kevlar™ fiber to produce ballistic composites such as 50:50 mixture of phenol formaldehyde resin and polyvinyl butyral resin. The Kevlar™ composites of this resin mixture were 27 layers of Kevlar

yielding 5.9 mm in thickness. It was capable to protect a projectile of 0.68 g steel sphere at 612 m/s strike velocity [39].

Coppage et al., 2000 patented composite fabric comprised of aramid fiber combined with PBO fiber and at least one flexible, rubbery resin (Styrene Butadiene-Styrene block copolymer) used in making ballistic armor. Its composite was able to pass the NIJ III-A (.44 magnum). The products possessed an area density of 0.75 -0.95 lb/ft^2 [37].

Phenolic resins provide a future class of preferred resins for a composite armor. Phenolic resins are inexpensive, can be handled using conventional technology, and do not bond too firmly to ballistic fiber especially Kevlar™. However, phenolics do require that moisture be driven from the resins during curing stage which is one additional step in the composite fabrication process thus the processing cost [35, 40, 41].

Polyfunctional benzoxazines were found to exhibit excellent mechanical and thermal properties with good handling capability for material processing and composite manufacturing, e.g., the glass transition temperature of 190°C, tensile modulus of 3.2 GPa, and tensile strength of 58 MPa. In addition, they offered greater flexibility than conventional phenolic resins in terms of molecular design. They do not release by-product during reactions and there are no solvent other than for the solvency which the reactants may have for each other. The other outstanding property of benzoxazine resin is its ability to undergo hybrid network formation with several other resins for tailor-made properties. This makes it possible to fine tube and enhance the properties of the ballistic armor [7, 21, 40, 41].

Recently, Rimdusit et al., 2005 improved the toughness of polybenzoxazine by alloying with isophorone diisocyanate (IPDI) based urethane prepolymers (PU) or with flexible epoxy. The toughness of alloys of rigid polybenzoxazine and the PU or epoxy systematically increases with the amount of either tougheners due to the addition of more flexible molecular segments in the polymer alloys. Interestingly glass transition

temperatures (T_g) of BA-a/PU alloys was found to be higher than those of the parent resins, i.e. 165°C for BA-a and -70°C for PU while T_g of the BA-a/PU alloys at 70/30 mass ratio determined as 220°C. However, this characteristic was not observed in case of the BA-a/flexible epoxy alloys systems. BA-a/PU alloys thus may be suitable for an application as a composite matrix to produce a ballistic armor due to the above observed thermal stability as well as the broad range of the modulus of the resulting alloys. In this study, the suitable composition ratios of the polymeric alloys between benzoxazine and urethane resins and the number of the layers of the Kevlar cloth to produce ballistic composite of level IIA [7].

Ishida and Chaisuwan (2003) reported the improvement of the mechanical properties of carbon fiber-reinforced polybenzoxazine (BA-35X) composites by amine-lerminated-butadiene-acrylonitrile (ATBN) which was used as the rubber interlayer. The thermal property of composites which was observed by dynamic mechanical analyzer, presented that the Tgs of composites remained almost constant at about 240°C until the concentration of ATBN reached 0.05%. Then, Tg started to decrease since ATBN modifier has a relatively low Tg. Moreover, this research also determined the mode II delarmination toughness (G_{IIC}) of carbon fiber-reinforced polybenzoxazine composites. The G_{IIC} increased with additional of ATBN rubber. Hence, the ATBN rubber interlayered method could be used to improve the delarmination toughness of the carbon fiber-reinforced polybenzoxazine composites due to the adhesion improvement from the rubber interlayer [42].

Lin S.P. et al (2007) investigated the polyurethane reinforced ultrahigh-molecular-weight polyethylene (UHMWPE) and aramid fiber. The standard testing using the NIJ Threat Level IIA method reveals that at a thickness of 5 mm, the UHMWPE fiber/PU composite and the aramid fiber/PU composite both exhibited bulletproof properties; in this case, the number of penetrating layers of the UHMWPE fiber/PU composite (35 layers) was greater than that of the aramid fiber/PU composite (23 layers). The standard tests using the NIJ Threat Level IIIA method at a thickness of 5 mm, the UHMWPE fiber/PU composite did not exhibit bulletproof properties, whereas the aramid

fiber/PU composite did. In contrast, standard testing using the NIJ Threat Level IIIA method at a thickness of 10 mm indicated that the UHMWPE fiber/PU composite displayed bulletproof properties similar to those of the aramid fiber/PU composite; in this case, the number of penetrating layers of the UHMWPE fiber/PU composite (67 layers) was nearly equal to that of the aramid fiber/PU composite (64 layers) [43].

Pilpel et al. (2008) investigated the ballistic panel that has a strike-face portion principally consisting of E-glass fiber and S-glass fiber. The plies weight of both glass fibers are about equal in their weight contribution to the panel. To prepare the prepreg, polypropylene and polypropylene were used as matrices. A sufficient pressure to form article in the mold is about 0.69 MPa. A molding process is about 52°C and the desired molding temperature is 171°C for polypropylene matrix and 121°C for polyethylene matrix. The first composite ply is deposed at about 90° relative to the fibers in the second composite ply. The composite laminates were observed that they passed NIJ criterion Type II, Type IIA, Type IIIA, Type III or Type IV or V_{50} [44].

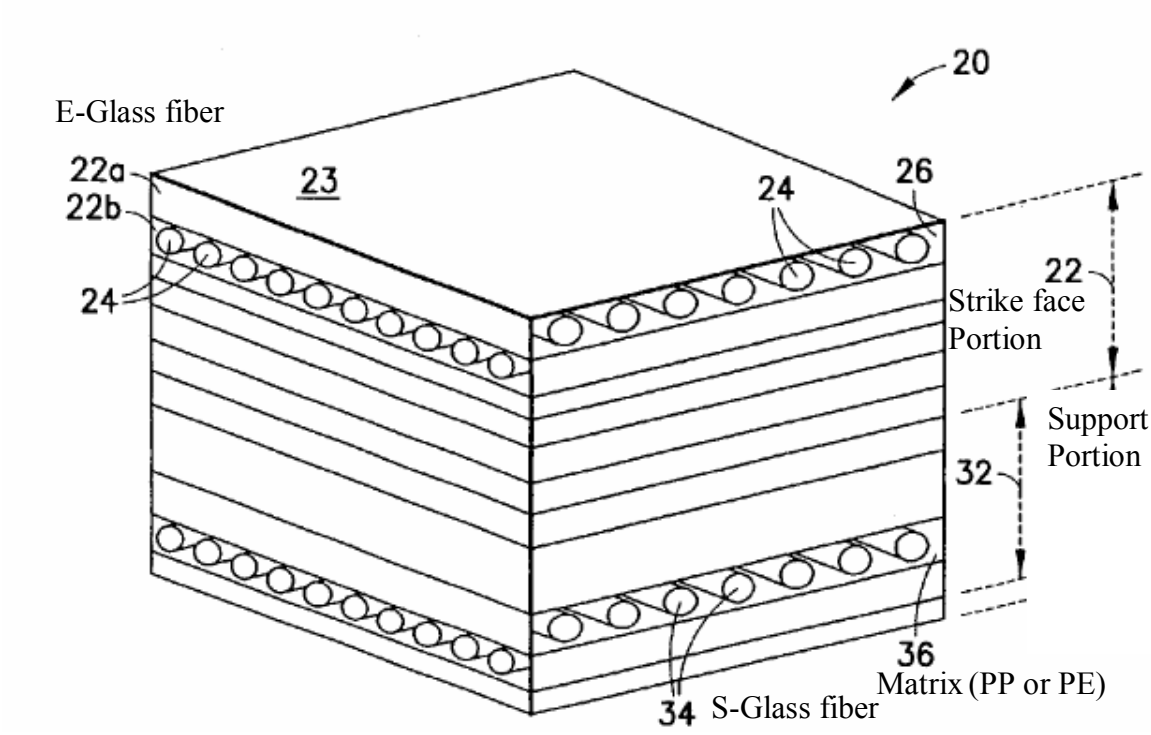

Figure 3.1 Composite ballistic panels E- and S- glass/ matrix.

Pilpel et al (2009) reported composite ballistic panels and method of use. The panels composite is shown in Figure 3.1 The composite comprise a strike face portion, which is first ply produced from E-glass and polypropylene (PP)/ or polyethylene (PE) matrix as well as support portion which is S-glass used as second ply. The fibers in one ply disposed at 90° to fibers in the other ply, are know in the art and are commercially available. The panels are tested by NIJ standard and the results are summarized in Table 3.2 [45].

Table 3.2: The results of panels tested by NIJ standard.

Material (Fiber/Matrix)	Areal Density (g/cm^2)	NIJ Standard	Velocity (m/s)
S-Glass fiber/PP	1.10-1.46	III-A	442.56-479.76
(E-Glass + S-Glass fibers at same weight)	0.98-1.708	III-A	441.96.590-543.15
S-Glass fiber/PP	4.88	III	876.01
(E-Glass + S-Glass fibers at same weight)	4.88	III	843.09
S-glass/Phenolic resin	4.88	III	889.77
S-Glass fiber/PP	1.22-2.44	IV	543.02-847.96
E-Glass + S-Glass fibers at same weight	0.83-2.44	IV	408.13-810.47

From the Table 3.2, the S-Glass fiber reinforced PP (S-Glass fiber/PP) and S-Glass and E-Glass fibers at same weight (E-Glass + S-Glass) were mentioned that they passed NIJ criterion IV. However, these results are doubtful i.e. the projectile velocities used for testing were observed to be lower than NIJ standard requirement i.e. 868±15 m/s. It is due to the weight of used bullet in the test (44 grain 30 caliber simulated shrapnel) has weight lower than the standard test of NIJ. For NIJ standard level IV (Armor-Piercing Rifle), this armor protects against 30 caliber armor piercing rounds with nominal masses of 10.8g or 166 grain.

Tanoglu et al. (2003) evaluated the effects of performing binder on mechanical properties and ballistic performance of E-glass-fiber/polyester composite. The peel strength determined by using T-peel test (ASTM D-1876-95) presented that the peel strength increased with increasing binder concentration (polyester) due to the improved adhesion between fabric and binder. The highest peel strength value was obtained from performed with about 9 wt% of binder. The composite panels were subjected to ballistic testing following NATO standard 2920 (1.1 g fragment simulating projectiles/FSPs). Figure 3.2 (a) illustrates the delamination (2.15% for front face and 8.62% back face) and intra bundle cracking type failure mode occurred within the impact damage zone of panel without binder. On the other hand, Figure 3.2 (b) shows that the panel with 3 wt% binder has a less damage and delamination (1.66% for front face and 4.74% back face). This may indicate a relatively higher energy absorbing capability of the composite with performing binder [46].

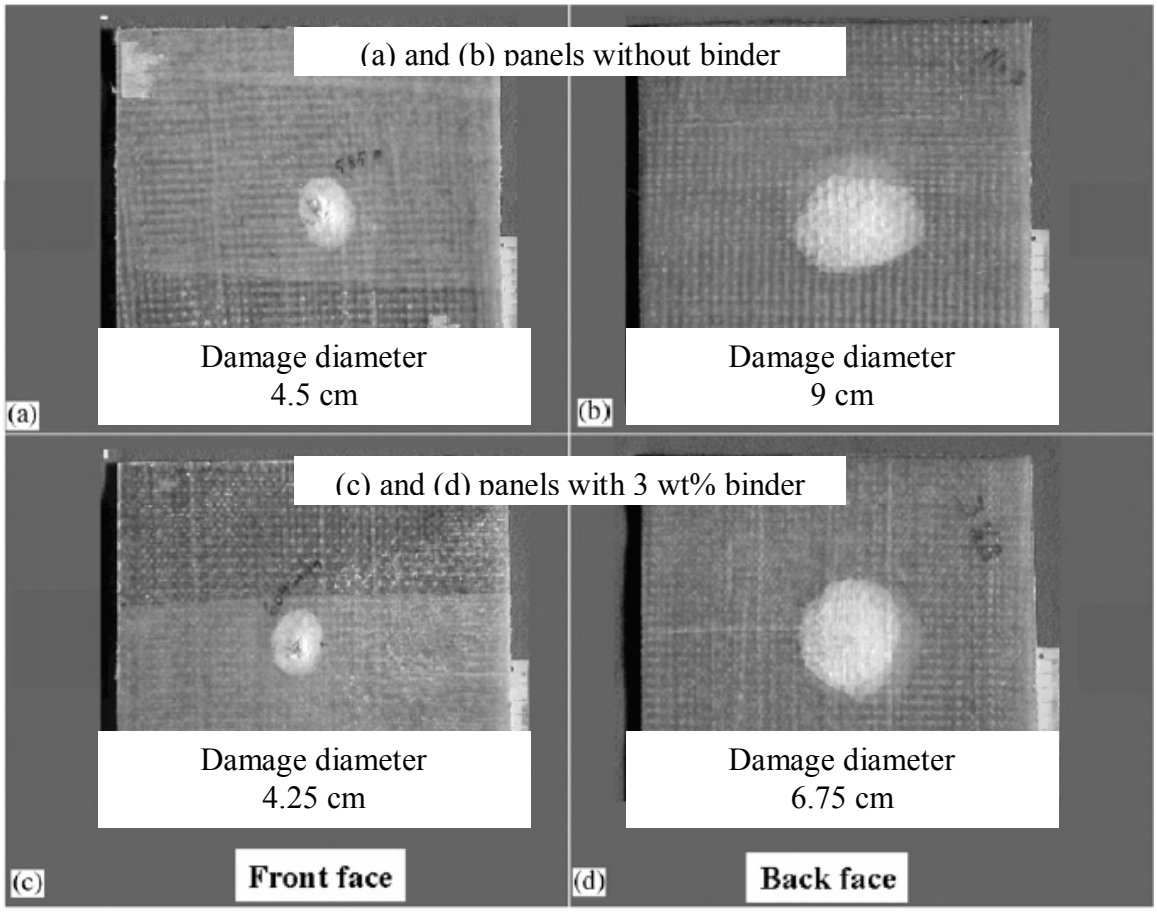

Figure 3.2 Ballistic impact damage on front and back face of composite panels.

Naik et al., (2005) investigated the energy of the projectile, which was absorbed by E-glass/epoxy composite with different energy absorption mechanisms as shown in Figure 3.3. The impact velocity of a projectile used in this study was 158 m/s. In this case, the projectile kinetic energy was 34.9 J. At the end of the ballistic impact event, cone kinetic energy, secondary yarn deformation energy, tensile failure energy, delamination energy, and matrix cracking energy were 0.56%, 87.04%, 8.16%, 3.60% and 0.64% of total impact energy respectively. As a result of this research, the major portion of projectile kinetic energy was absorbed by the deformation of the secondary yarns. In addition, the energy absorbed by the deformation of the secondary yarns has two components, i.e. elastic strain energy and plastic deformation energy. If the projectile cannot complete penetrate to the target, elastic strain energy will be transferred back to the projectile, and the projectile will be rebounded [47].

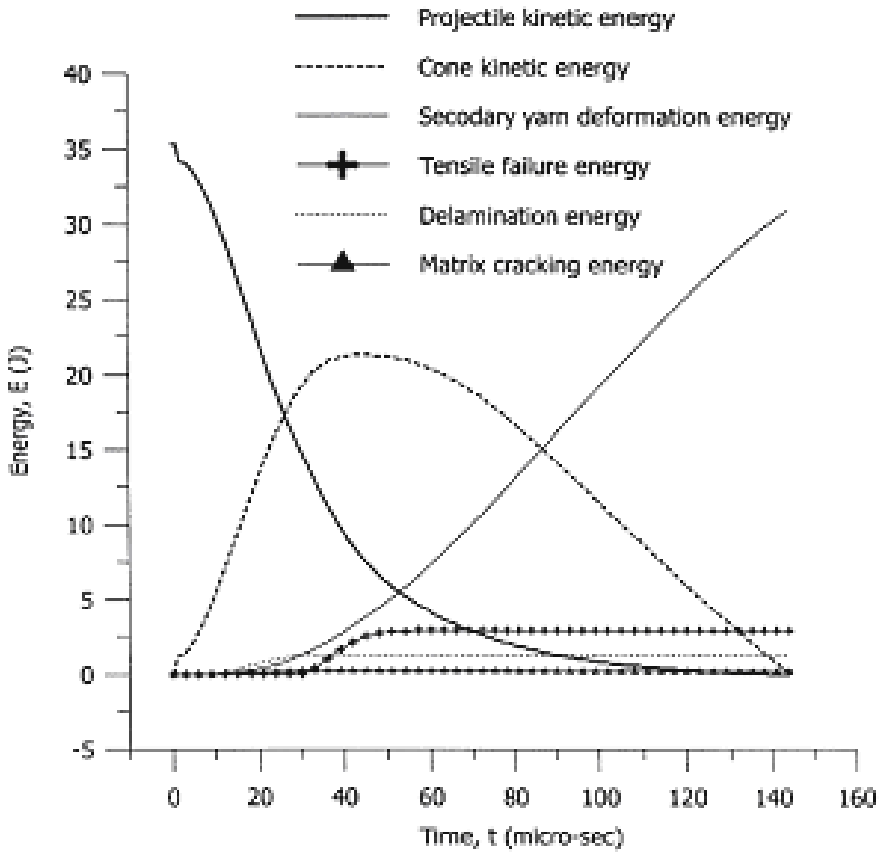

Figure 3.3 Energy absorbed by different mechanisms during ballistic impact of woven fabric E-glass/epoxy laminate.

Gellert et al., 1998 investigated the energy transfer in ballistic perforation of fiber reinforced composites. The 30 mm squares of woven fiber either impregnated with Derakane 8084 vinyl ester resin or stitched along one axis at line spacings of 30 mm. The composite panels were cured at ambient temperature in a press at a 2 MPa then post-cured for 1 h at 90°C and 2 MPa. The ballistic testing was undertaken using 5.59 mm diameter (0.22 inch Calibre). The values of ballistic limit, tensile fracture strain and apparent maximum strain in ballistic impact are exhibited in Table 3.3. Moreover, the energy data obtained from ballistic tests are illustrated in Table 3.4 [48].

Table 3.3: Properties of ballistic perforation of fiber and fiber reinforced composites.

Material	Areal Density (g/cm^2)	Ballistic limit (ms^{-1})	Tensile Fracture strain	Apparent maximum strain in ballistic impact	Tensile Strength (MPa)
E-glass composite	8.1	356±14	0.021	0.036	308
Kevlar composite	8.1	458±10	0.052	0.063	400
Spectra composite	5.5	366±14	0.074	0.045	750
Kevlar fabric	6.6	474±5	0.035	0.15 [(1)], 0.18 [(2)]	1200
Nylon fabric	5.3	422±5	0.21	0.195 [(1)], 0.16 [(2)]	365

Table 3.4: Energy data from ballistic tests.

Material	Velocity (ms^{-1})	Projectile		Penetration	Target energy term (J) Rear layer		
		Kinetic energy (J)	Kinetic Energy loss (J)		Strain	Kinetic	Dealmination
E-glass composite	370	75.3	68.2	Yes	2.5	1.2	1.5
Kevlar composite	475	124.1	115	Yes	6.3	4.0	1.3
Spectra composite	390	83.7	79	Yes	3.0	1.3	< 0.9
Kevlar fabric	466 (1)	119.4	119.2	No	74.5	0.4	-
	476 (2)	124.6	123.8	No	54.1	0.5	-
Nylon fabric	427 (1)	100.2	99	No	7	0.8	-
	441 (2)	107	78	Yes	3	1.8	-

CHAPTER IV

EXPERIMENTAL

4.1 Materials

The materials used in this research are benzoxazine resin, urethane resin, glass fiber and Kevlar™ fiber. The fiber was purchased from Thai Polyadd Limited Partnership. Benzoxazine resin is based on bisphenol, aniline and paraformaldehyde. The bisphenol A (polycarbonate grade) was supplied by Thaipolycarbonate Co., Ltd (TPCC). Paraformaldehyde and aniline were purchased from Merck Company and Panreac Quimica SA Company, respectively. Urethane prepolymer was prepared using toluene diisocyanate and polyether polyol. The toluene diisocyanate was obtained from South City Group and the poly(propylene glycol) with the molecular weights of 2000 was supported by TPI Polyol CO., LTD.

4.2 Preparation of Resins

4.2.1 Benzoxazine resin preparation

Bisphenol A, aniline, and paraformaldehyde at a 1:2:4 molar ratio were used for the synthesis of benzoxazine monomer. These three reactants were continuously mixed at about 110^{o}C for approximately 2 hours. The benzoxazine monomer was obtained as clear-yellowish solid at room temperature [14]. The product was then ground into fine powder and can be kept in a refrigerator for future-use.

4.2.2 Urethane resin preparation

The urethane prepolymer was prepared from toluene diisocyanate and poly(propylene glycol) at a stoichiometric molar ratio using various molecular weights of the poly(propylene glycol) i.e. 2000. The two reactants were directly mixed in a four-necked round bottomed flask and the mixture was continuously stirred under a nitrogen

stream at about 60°C for 2 hours to yield a light yellow prepolymer. Then, the urethane prepolymer was cooled to room temperature and was kept in a refrigerator for future-use.

4.3 Benzoxazine/Urethane Binary Mixture Preparation

The benzoxazine monomer was mixed with the urethane prepolymer to provide Ba/PU mixture at the desirable mass fraction. The mixture was heated to about 80°C in an aluminum container and was thoroughly mixed by hand for about 15-30 minutes until a homogeneous mixture was obtained. The weight ratios of the benzoxazine (BA) and urethane (PU) binary mixtures at 90/10 (BA/PU 90/10), 80/20 (BA/PU 80/20), 70/30 (BA/PU 70/30) and 60/40 (BA/PU 60/40), were evaluated as potential matrices for Kelar™-reinforced composites for a ballistic armor.

4.4 Processing of Composites

The fabrics were pre-impregnated with the binary mixture resins using the hand-lay up procedure at 80°C. The weight fraction of the fiber was kept constant at approximately 80% by weight. The molding compound was compression-molded using a compression molder. The specimens were finally kept in room temperature to cool before they were ready for characterizations.

4.5 Characterization Methods

4.5.1 Nuclear magnetic resonance spectrometer (^{1}H NMR)

^{1}H NMR spectra was used to check the chemical structure of purified benzoxazine monomer and urethane preolymer. The spractra were recorded on a Bruker DPX-300S spectrometer at the resonant frequencies at 400 MHz for ^{1}H nuclei using $CDCl_3$ as solvent and tetramethylsilane as the reference.

4.5.2 Fourier transform infrared spectroscopy (FT-IR)

FT-IR spectra were obtained with a JASCO spectrophotometer model FT-IR 4200-type A. Online FT-IR was carried out from 40 to 300 ^{o}C at heating rate 3min/ ^{o}C under nitrogen flow to investigate the curing behavior of the blend.

All of the samples used in this study were sufficiently thin to obey Beer-Lambert's law. The selected intensity data was normalized using the carbon-hydrogen symmetric deformation at 1388 cm^{-1}, which is indicated the methyl group of bisphenol-A, was chosen as internal standard to compensate for the thickness change in the samples during polymerization. The intensity peaks of reactive groups assigned by FTIR were determined conversion of curing .

$$\alpha = 1 - \frac{(A \text{ reactive band})_{T,i}}{(A \text{ reactive band})_{T,o}} \qquad (4.1)$$

where α is conversion, $A_{T,0}$ and $A_{T,i}$ are absorbance of reactive group before curing and at each temperature, respectively. To obtain more accurate quantitative results, the peak fit 4.0; a curve analysis program was used to resolve overlapped bands by using Lorentzian-Gaussian function. Calculations were continued until least squares curve-fitting converged [58].

FT-IR spectra of all samples under various curing methods were acquired by using a Spectrum GX FT-IR spectometer from Perkin Elmer. The apparatus is equipped with a KBr beam splitter and a deuterated triglycine sulfate (DTGS) detector. A small amount of a solid sample, preferably 0.5-1.0 mg, was ground and casted on a potassium bromide (KBr) disk. The sample was sufficiently thin with optical thickness of a fraction of a millimeter in compliance with the thickness specified under the Beer-Lambert's law. The sample was then mounted on a sample holder. All spectra were taken with 32 scans at a resolution of 4 cm^{-1} and a spectral range of 4000-400 cm^{-1}.

4.5.3 Differential scanning calorimeter (DSC)

The curing behavior and kinetic parameters were measured by DSC model 2910 from TA Instrument. The heating rates was 10°C/min from 30 to 300°C under nitrogen gas purging.

4.5.4 Dynamic mechanical analysis (DMA)

A dynamic mechanical analyzer (DMA) model DMA242 from NETZSCH was used to investigate specimens' dynamic mechanical properties. The dimension of each specimen was 50 mm×10 mm×2 mm. The strain was applied sinusoidally with a frequency of 1 Hz and the specimen was heated at a rate of 5°C/min from room temperature to 270°C. The storage modulus (G'), loss modulus (G''), and loss tangent (tan δ) were then obtained. The glass transition temperature was taken as the maximum point on the loss modulus curve in the temperature sweep test.

4.5.5 Flexural property measurement

A universal testing machine (model 5567) from Instron Co., Ltd. was used to determine flexural properties of composite specimens. The test method used was a three-point bending mode with a support span of 32 mm at a constant cross head speed of 0.85 mm/min. The dimension was 25 mm in width, 50 mm in length, and 2 mm in thickness. The flexural properties were determined using ASTM D 790M-93 according to the following equations:

$$E_B = \frac{L^3 m}{4bd^3} \qquad (4.2)$$

$$S = \frac{3PL}{2bd^2} \qquad (4.3)$$

where E_B = Flexural modulus (MPa)

S = Flexural strength (MPa)

P = Load at a given point on the load-deflection curve (N)

L = Support span (mm)

b = Width of beam tested (mm)

d = Depth of beam tested (mm)

m = Slope of the tangent to the initial straight-line portion of the load-deflection curve (N/mm)

4.5.6 Thermogravimetric analysis (TGA)

Thermal stability and thermal decomposition of the cured polymer alloys were studied using a Perkin Elmer's TG/DTA thermogravimetric analyzer model SII Diamond. The experiment was done using a heating rate of 20°C/min under nitrogen atmosphere. The temperature was ramped from 30°C to 900°C using a sample mass of about 15-20 mg. The degradation temperature at 5% weight loss and the char yield at 900°C were recorded for each specimen.

4.5.7 Density measurement

The density of the polymer alloys and the fiber composites were measured by water displacement method according to ASTM D792-91 (Method A). All specimens were prepared in a rectangular shape of 50 mm×25 mm×1 mm and weighted both in air and in water.

The density was calculated using the following equation:

$$\rho = \left(\frac{A}{A - B}\right) \times \rho_o \qquad (4.4)$$

where ρ = Density of the specimen (g/cm^3)

A = Weight of the specimen in air (g)

B = Weight of the specimen in liquid (g)

ρ_o = Density of the liquid at the given temperature (g/cm^3)

4.5.8 Ballistic impact test

The ballistic tests were made using 2 different classes of ammunitions. The tested composite panel was approximately 15 cm×15 cm with varied thickness depending on the number of layers of fabric cloths used. The composite panel was tested with a test weapon having an impact velocity following NIJ standard. The velocity of each shot was recorded using a triggered timer system, as shown in Figure 4.1. A test barrel was appropriately selected for the ammunition required to test the armor. The barrel test was mounted in an appropriate fixture with the barrel horizontal. Dimensions A and B shall be determined from the barrel muzzle. The backing material fixture will be rigidly held by a suitable (metal) test stand, which shall permit the entire armor and backing material assembly to be shifted vertically and horizontally such that the entire assembly can be targeted by the test barrel.

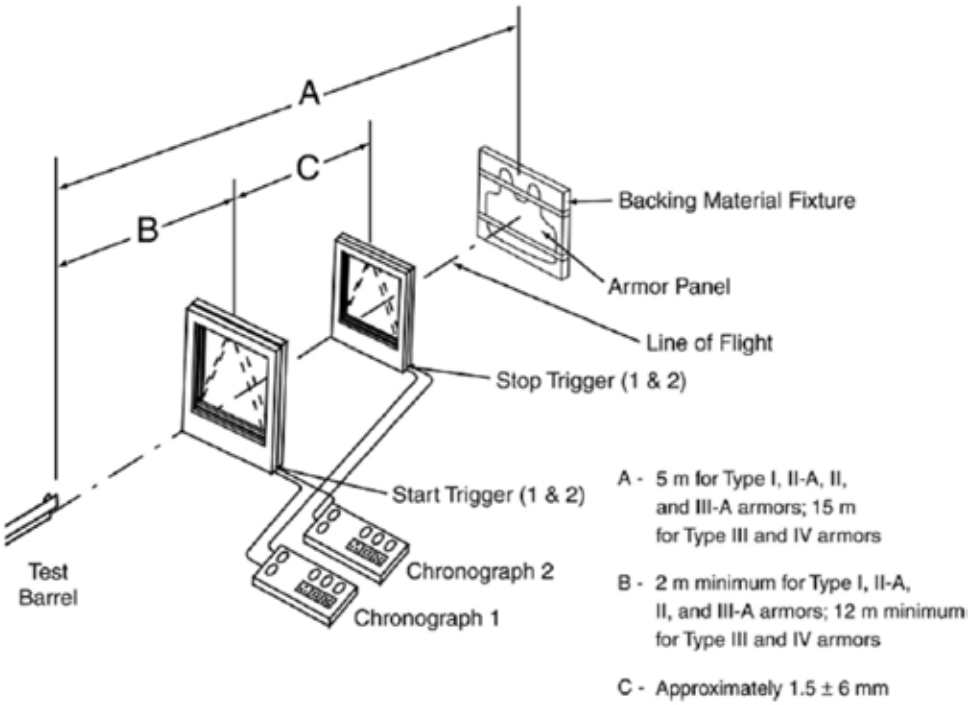

Figure 4.1 Testing scheme used for the NIJ standard ballistic test.

In this research, The ballistic impact test was preformed to evaluate the most appropriate composition of the matrix used for ballistic composite and possibility of using other reinforced-fibers such as carbon fiber and glass fiber in order to cooperate with Kevlar™ fiber i.e. the glass fiber or carbon fiber composite will be designed as strike face whereas Kevlar composite will be armor backing.

The first evaluation was performed using a test weapon having impact velocity following NIJ standard of level III-A. The dimension of the laminated specimens per one panel was 15 cm×15 cm×7mm, corresponding to 18 plies of the glass fabric and 32 plies of carbon fabric. The equipments of ballistic test are shown in Figure 4.2
The requirements and acceptance criteria for NIJ standard level III-A are following:

(a) Four complete armor samples, consisting of either a front and back set of armor panels or one full jacket; two samples per test threat.

(b) Six fair hit impacts per armor panel or jacket front and back surface, four armor panels (two front and two back) or two armor jackets for each test threat,

(c) No perforation through the panel, either by the bullet or by any fragment of the bullet or armor.

(d) No measured backface signature, (made from oil based modeling clay) depression depth greater than 44 mm (1.73 in).

The second evaluation was performed using a test weapon having impact velocity following NIJ standard of level III. The two sizes of the polymeric laminated specimens were 15 cm × 15 cm and 30 cm× 30 cm. The specimen consisted of 25 plies of each type of fiber i.e. glass fiber and Kevlar™ cloth. The fabrics were impregnated with about 20 % by weight of the BA-a resin for glass fiber and BA-a/PU (80/20) resin mixtures for Kevlar™ fiber. The equipments of ballistic test are shown in Figure 4.3. The requirements and acceptance criteria for NIJ standard level III are following:

(a) One complete armor sample, or two to six primary ballistic panels, plates or inserts, if removable from the armor sample (e.g., front panel protection only).

(b) Six fair hit impacts against each primary ballistic panel, plate(s), or insert(s).

(c) Backface signature of shot one and the highest remaining velocity shot for each armor panel, plate, or insert.

(d) No perforation by the bullet, fragment of the bullet, or fragment from the plate/insert through the armor.

(e) No measured backface signature depression depth greater than 44 mm (1.73 in).

(a.) Equipments set up following NIJ standard level III-A

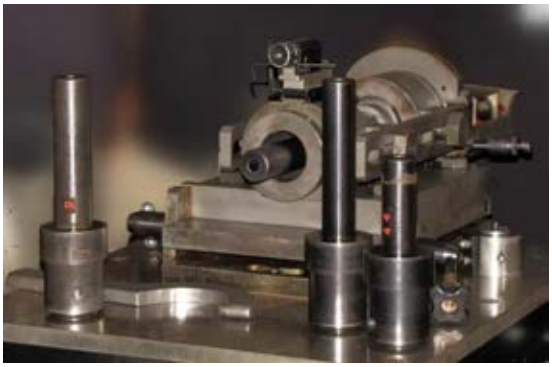

(b.) Test barrel

(c.) 44 Magnum Semi Jacketed Hollow Point

Figure 4.2 The equipments of ballistic test for NIJ standard level III-A.

(a.) Equipments set up following NIJ standard level III

(b.) Test barrel and chronographs

(c) 7.62 mm Full Metal Jacketed

Figure 4.3 The equipments of ballistic test for NIJ standard level III.

CHAPTER V

RESULTS AND DISCUSSION

5.1 Model compound from ^{1}H NMR

Urethane prepolymer was synthesized from toluene 2,4-diisocyanate and propylene gycol, with reaction between isocyanate group and hydroxyl group. Reaction of urethane prepolymer synthesis is shown in Figure 5.1. The resultant products after synthesis were characterized by ^{1}H-NMR. The ^{1}H-NMR spectrum at 1.12 ppm (a) and group of signals at 3.20-3.90 ppm (b) in Figure 5.2 (A)., are due to methyl protons and methine belonging to the internal portion of propylene glycol. Figure 5.2 (B) presents toluene 2,4-diisocyanate spectrum. Signals at 2.30 ppm (c) assigned the methyl protons belonging to aromatic proton of toluene 2,4-diisocyanate which was presented at 7.10-7.83 (d and e). Urethane prepolymer spectrum is shown in Figure 5.2 (C), signals at 1.25 ppm (f) and 4.98 ppm (g) were due to the terminal units and methine protons involved in the urethane linkages, respectively. The group of signals at 6.87-7.83 ppm (h and i) presented aromatic protons of chain end of urethane prepolymer and urethane proton formed from NCO minor reactivity in ortho position to the hydroxyl group [49].

The ^{1}H-NMR spectrum of the benzoxazine monomer was measured to confirm structure. The benzoxazine monomer structure and ^{1}H-NMR spectrum are shown in Figure 5.3 and 5.4, respectively. The methyl proton of bisphenol-A showed the signal at 1.58 ppm (a). The characteristic peaks assignable to methylene (Ar–CH_2–N) of oxazine ring and methylene (O–CH_2–N) were observed at 4.53 (b) and 5.24 ppm (c), respectively. The group of signals at 6.87-7.83 ppm (d) exhibits aromatic protron. Moreover, the disappearance of signal at 3.6 ppm indicates that the obtained monomer did not consist of methylene protron of either opening ring or dimmers [50, 51].

5.2 *In situ* Fourier Transform Infrared Spectroscopic Investigation

5.2.1 Curing Process of Benzoxazine

It is well known that benzoxazine monomer will undergo a ring-opening polymerization upon heating in the absence of initiator and catalysts. The ring-opening reaction can be monitored at the band centered near 941 and 1230 cm^{-1} assigned to trisubstituted benzene ring and C-O-C stretching mode, respectively. As the curing process proceeded, an infinite three dimensional network was formed upon benzoxazine ring opening by the breakage of C-O bond and then the benzoxazine molecule transformed from a ring structure to a network structure. During this process, the tri-substituted benzene ring, backbone of benzoxazine ring, became tetra-substituted benzene ring which led to the formation of a phenolic hydroxyl group-based polybenzoxazine (PBA-a) structure. The vibrational mode of benzoxazine polymerization is exhibited in Figure 5.5. The band centered near 1230 cm^{-1} associated with the opening of oxazine ring at C-O-C whereas the band around 941 and 1497 cm^{-1} involved with trisubstituted benzene ring. Both of these bands significantly reduced, when temperature was raised to 240°C. This phenomenon indicated a nearly complete loss of the oxazine ring. In additional, a new band at 878 cm^{-1} and 1488 cm^{-1} of the tetra-substituted aromatic ring were observed suggesting the ring opening reaction to take place *ortho* to phenolic moiety. This result was good agreement with previous work reports [52].

5.2.2 Curing Process of Benzoxazine Alloyed with Urethane Prepolymer

The reaction between benzoxazine resin (BA-a) and urethane prepolymer (PU) could also be investigated by FT-IR technique. The spectra of BA-a/PU resin mixture at a mass ratio of 60/40 during curing process at various temperatures were exhibited in Figure 5.6. The spectrum of the BA-a/PU monomer with the characteristic peaks at 1230 cm^{-1}, which was C-O-C stretching mode of the benzoxazine resin and 941 and 1497 cm^{-1} attributed to trisubstituted benzene ring. The absorption band at 1732 and 2273 cm^{-1}

were attributed to NH-C=O and N=C=O stretching of the urethane prepolymer, respectively. The absorption bands at 941, 1230 and 2273 disappeared when temperature increased from 50 to 150°C. Meanwhile, the intensity of phenolic hydroxyl group of BA-a at the wide absorption band in the range of 3100-3700 cm^{-1} also decreased. This investigation may imply that the ring-opening polymerization of BA-a took place in situ with NCO group. Our result is also in good agreement with the result previously reported by Takeichi and Guo., 2001 [53].

Recently, the urethane formation reaction was reported that it was complicated by various side reactions. Therefore, these side reactions can influence to reaction of PU prepolymer and BA-a. As depicted in Figure 5.6, the absorption band at 1689 cm^{-1} assigned to hydrogen bond of urea carbonyl which was observed at 150°C. The urea group was formed by reaction of the isocyanate containing prepolymer with amine group (which was produced from a trace amount of water and isocyanate-end group of PU), as shown in Figure 5.7. Moreover, the urethane and urea themselves can supply the labile hydrogen atoms to react with the isocyanate. This reaction forms the three-dimensional crosslink structure containing allophanate and biuret as illustrated in Figure 5.7 [54, 55]. At high temperature, both of the urethane linkage and allophante are unstable and prone to dissociation. The breakage bonds of these compounds directly generated isocyanate terminated chains. This phenomenon corresponded with the reappearance of the absorption band of NCO when temperature increased to 180°C, as shown Figure 5.6.

5.2.3 Qualitative Analysis of Ring-Opening Polymerization

Due to, the ring opening polymerization, tri-substituted benzene ring turned into tetra-substituted benzene ring and the absorption intensities associated with benzene ring changed, especially at bands and 1498 cm^{-1}. Therefore, the absorption should be a suitable index for ring-opening reaction. The conversion of ring-opening polymerization at various temperatures with the band 1498 cm^{-1} is depicted in Figure 5.8. The polymerization of BA-a monomer was observed to occur at 140°C whereas the BA-a/PU

alloys exhibited the reaction around 180°C which was higher than neat BA-a. The tri-substituted benzene ring band of neat BA-a increased to 98% at 230°C. The obtained alloys have nearly same conversion value (95%) at 260°C. These results suggested that the addition of PU tended to postpone the polymerization of benzoxazine.

5.3 Differential Scanning Calorimetry (DSC) for Curing Process Investigation

The curing reaction of the binary mixtures of BA-a and PU at various PU compositions by differential scanning calorimetry using a heating rate of 10°C/min at a temperature range of 30-300°C is depicted in Figure 5.9. From the DSC thermograms, only a single dominant exothermic peak of the curing reaction in each resin composition was observed. The exothermic peak of the neat benzoxazine resin was located at 226°C which attributed to ring-opening polymerization of ozaxine ring. The curing peak maximum was observed to shift to a higher temperature when the PU fraction in the resin mixtures increased. In Figure 5.9, the positions of the exothermic peaks of BA-a/PU resin mixtures at 90/10, 80/20, 70/30 and 60/40 mass fractions were found to be 234°C, 243°C, 245°C and 247°C, respectively.

Considering the breadth of the exotherms, the curing peaks of the binary mixtures became broader when the urethane content enhanced. Furthermore, an area under the exothermic peak was also observed to be decrease with increasing mass fraction of the PU. The heat of reaction values of the BA-a/PU resin mixtures determined from the area under the exothermic peak, were 272 J/g in BA-a/PU 100/0, 228 J/g in BA-a/PU 90/10, 205 J/g in BA-a/PU 80/20, 165 J/g in BA-a/PU 70/30 and 153 J/g in BA-a/PU 60/40. The phenomenon was possibly due to the reaction of the BA-a with the PU rendering a lower heat of reaction per mole of the specimen than the reaction of the neat BA-a. These can be attributed to the changes in the number of mole and the functional groups of each component in polymer alloys. At equal mass, the number of molecules of the PU was lower than that of benzoxazine monomers. In addition, a benzoxazine monomer is tetrafunctional while difunctional urethane prepolymer can only react with two hydroxyl groups of the polybenzoxazine. Thus, we can observe the decreasing of

the heat of reaction with decreasing benzoxazine monomers in the binary mixtures. The result is in good agreement with previous work [56].

Figures 5.10 presents glass transition temperatures (T_g) from DSC of the fully cured BA-a/PU alloys after curing at 150°C for 1 hour and 200°C for 2 hours. In this experiment, the T_g values were taken as the midpoint temperature of the change in specific heat in the transition region. From room temperature up to 300°C, there existed only single T_g in each of these BA-a/PU alloys. Additionally, the T_g's of the polymer alloys between the BA-a and the PU were found to remarkably increase with the mass fraction of the PU. The T_g of the fully cured BA-a/PU alloys were observed to be 161°C in BA-a/PU 100/0, 173°C in BA-a/PU 90/10, 182°C in BA-a/PU 80/20, 220°C in BA-a/PU 70/30 and 241°C in BA-a/PU 60/40. However, T_g of the polyurethane elastomer and the polybenzoxazine were reported to be about –70 to –20°C [53, 57] and 160 to 170°C [14], respectively. This is the unique characteristic of these polymer alloys which exhibited synergistic behaviors in their glass transition temperature making the systems highly attractive for high temperature application. Synergism in glass transition of polybenzoxazine from an addition of other resins or polymers has been observed and reported previously in various systems such as benzoxazine-epoxy [15, 41] benzoxazine-polycarprolactone [58], or benzoxazine-polydimethysiloxane [59] etc.

5.4 Investigation Types of Fiber for Strike Face Portion of Ballistic Armor

As mentioned in the objectives of this work, the other fibers such as fiber glass and carbon fiber are investigated possibility to cooperate with Kevlar™ as a strike face in order to decrease cost of Kevlar™. Both of glass and carbon fabric were impregnated with 20% by weight of BA-a resin and cured using the curing conditions as suggested in the previous section. The dimension of the laminated specimens per one panel was 15 cm×15 cm×0.7cm, corresponding to 18 plies of the glass fabric and 32 plies of carbon fabric.

Generally, the key parameter in the ballistic armor design of composite structures is the damage resistance of matrix and fiber. From previous work, Mines et al. (1999) proposed that the perforation mechanics of high velocity impact depend on factors such as fiber type, the matrix, volume fraction, the stacking sequence, the size and initial kinetic energy of the impact [60]. Furthermore, Cheng et al. (2003) observed that the penetration process can be broke down into three sequential stages i.e. (i) punching, (ii) fiber breaking and (iii) delamination [61]. Therefore, the performance of glass fabric and carbon fabric composites is performed by .44 mm Magnum Semi Jacketed Hollow Point bullets (427 ± 15m/s). The damaged areas of the composites were measured by a digital camera and ImageJ software.

Both glass fiber and carbon fiber composites can not resist the ballistic penetration. However, they can distort the bullets as clearly seen in Figure511. The damaged areas were also noticed on the back surface after impact of glass fiber and carbon fiber composites. As can observed in Figure 5.12, the back surface of one and two panels of glass fiber composite present three damaged zones i.e. first one was a central fiber breakage region, whereas the second one was a much intense delamination area surrounding the fiber breakage/perforation region. The last region was a large region with diffuse delamination. According to Caprino et al. (2007) and Will et al. (2002), the delamination area was investigated to be correlated with the maximum absorbed energy by linear relationship [62, 63]. Therefore, delamination is one parameter that indicated the ability of energy absorption. This phenomenon was not observed in one panel of carbon fiber composites as shown in Figure 5.13. Perforated hole was found in the back surface of one panel of carbon fiber composite which implied that the specimen can not dissipate the load of impact. The two panels of carbon composite were observed petaling formation at the back surface. Petaling is formed by high radial and circumferential tensile stresses after passage of the initial wave near a lip of the penetration. This deformation is the result of bending moments produced by the forward motion of the material as it is pushed ahead of the projectile [64]. As depicted in Figure 5.12 and 5.13, the fiber pull out was observed to be more in

glass fiber composite than in carbon fiber composite. The fiber pull out characteristic reveals of the energy dissipation mechanisms during ballistic impact [65].

The size of the damage and projectile velocities were measured as given in Table 5.1. The damage area at front surface where projectile entered was found to be less than the back surface. The delaminated areas of glass fiber composites on back surface were observed to be 60.21 cm^2, 31.07 cm^2 and 37.66 cm^2 for one panel, 1^{st}-two panels and 2^{nd}–two panels, respectively whereas the damaged areas of carbon composites were smaller, at 5.67 cm^2 (one panel), 10.53 cm^2 (1^{st}-two panels) and 17.86 cm^2 (2^{nd}–two panels). From previous research, Will et al. (2002) investigated that the energy dissipated by delamination is directly proportional to the delamination area [63]. Therefore, the larger delamination of glass fiber composite may imply that it has the higher energy dissipation. Due to the energy dissipation characteristic and low cost of glass fiber composite, this composite is considered as a good candidate to be used as a strike face for ballistic armor.

5.5 Thermal Degradation and Thermal Stability of BA-a/PU Reinforced with Fibers

The thermal stability of the composites was evaluated by TGA. The thermal degradation of all the samples has taken place within the programmed temperature range of 35-900^{o}C. The TGA curves of all composites and matrices are illustrated in Figure 5.14 and 5.15, respectively. Thermal decomposition in glass fiber reinforced neat benzoxazine resin found to occur in one stage attributed to decomposition of the polymer matrix at temperature between 300^{o}C and 500^{o}C. For Kevlar^{TM} reinforced benzoxazine-urethane alloys, the thermal decomposition in composites were observed in two stages. The first stage was in the same range with the decomposition of the polymer matrix in glass fiber composite. The second stage from thermogram corresponded to the decomposition temperature of Kevlar^{TM} fiber was approximately 500-600^{o}C. The degradation temperatures at 5% weight loss (T_d) of the glass fiber reinforced neat benzoxazine resin was observed to be 391^{o}C whereas Kevlar^{TM} reinforced benzoxazine alloys with the PU compositions of 0 to 40 % by weight was

ranging from 381°C to 350°C. However, both of the glass fiber reinforced neat benzoxazine resin and Kevlar™ reinforced benzoxazine alloys exhibited higher degradation temperatures than those of the polymer matrices, as illustrated in Table 5.2 It is due to the effect of high degradation temperature of the glass fiber and Kevlar™ fiber. Furthermore, the greater T_d of the composite with higher amount of the benzoxazine fraction in the matrix alloys suggested the stronger interaction between the fiber and the polybenzoxazine than between the PU portion.

Another important feature in the thermograms is the weight residue at 800°C or the char yield of the composites which is related to the flammability of materials and is essential for some ballistic armor applications. The char yield was found to be 83.35 for glass fiber composite. For the char yield of Kevlar™-reinforced benzoxazine alloys, the values systematically reduced from 36.43% to 34.61% with an incorporation of the PU from 0 to 40% by weight, as depicted in Table 5.2. In addition the values were all greater than those of the matrix alloys comparing at the same PU content.

Thermogravimetric analyzer was also used to determine the fiber content in the composites. In this research, the fibercontent in the composites was calculated using the resulting char yields from thermogravimetric analysis (TGA) following an empirical formula based on the rule of mixtures to calculate the fiber fraction.

$$X = a(W_f) + b(1 - W_f) \quad (5.1)$$

Where X is the percentage weight of TGA residue, W_f is the weight fraction of fiber, a is the percentage residual weight when 100% fiber is degraded and b is the percentage residual weight when 100% neat matrix is degraded [66].

The percent of fiber content of 79 wt% in glass fiber composite, 77 wt% in Kevlar™ fiber reinforced BA-a/PU 100/0, 83 wt% in Kevlar™ fiber reinforced BA-a/PU 90/10, 82wt% in Kevlar™ fiber reinforced BA-a/PU 80/20, 80 %wt in Kevlar™ fiber reinforced BA-a/PU 70/30 and 81wt% in Kevlar™ fiber reinforced BA-a/PU 100/0 were

obtained, as shown in Table 5.2. The calculated results confirmed that the glass fiber and Kevlar™ fiber content in each composite was about 80% by weight as prepared in the pre-impregnation stage.

5.6 Dynamics Mechanical Properties of BA-a/PU Reinforced with Fibers

The dynamic mechanical properties of the glass fiber and Kevlar composites were examined as a function of temperature. The storage modulus (E′) at temperature ranging from 30 to 300°C of glass fiber reinforced with neat benzoxazine resin and Kevlar composites reinforced with PU content in the range 0 to 40 wt% are illustrated in Figure 5.16. Generally, the storage modulus of a solid sample at room temperature provides a measure of material stiffness. The storage moduli of obtained composites were found to be 25.57 GPa for glass fiber/ neat BA-a whereas the storage moduli of Kevlar composites were systematically reduced from 16.82 GPa to 11.92 GPa with addition of the PU from 0 to 40 wt%. It is due to the incorporation of the more flexible PU molecule in the composite. This observation is in good agreement with the previous studied of benzoxazine-urethane copolymer reported by Rimdusit et al (2011) [56].

Glass transition temperature (T_g) of Kevlar fabric composites were exhibited in Figure 5.17. The T_gs of the crosslink materials were determined from the maximum of the loss modulus (E″) of the plots. From a pratical point of view, the maximum E″ is the most appropriate value to evaluate T_g. It corresponds to the initial drop from the glassy state into the rubbery state. The T_g of glass fiber reinforced neat BA-a was observed to be 182°C which was higher than neat BA-a reported at 165°C [56]. For Kevlar™ composites, they can be observed that the addition of the PU into the matrix composites was found to increase the T_g of Kevlar™ fiber composites. The T_gs of BA-a, 90/10 BA-a/PU, 80/20 BA-a/PU, 70/30 BA-a/PU and 60/40 BA-a/PU composites were determined to be 184, 187, 213, 225 and 247°C, respectively. These values were higher than those of BA-a/PU matrices which reported to be in range of 165-245°C [56]. The implication of these phenomena is probably due to the contribution of the substantial interfacial adhesion between the fibers and the polybenzoxazine alloys.

The α-relaxation peaks of the loss factor or tan δ of composites are shown in Figure 5.18. The magnitude of tanδ was observed to decrease with the increasing mass fraction of the PU resin in the alloy matrices and the peak maxima also shifted to higher temperature. The peak height of the tanδ in the vicinity of T_g was observed to be smaller with increasing PU content. Since tanδ is a ratio of a viscous to an elastic component of dynamic moduli of a specimen. Therefore, it can be implied that its decreasing height with the PU around T_g is associated with a lower segmental mobility, and thus is indicative of a higher degree of crosslinking for the urethane-rich samples as observed in our BA/PU alloy systems [58]. In other words, the polymer alloys are softer at room temperature due to the PU fraction but possess higher degree of crosslinking that can inhibit the large scale mobility at elevated temperature.

5.6.1 Effect of frequency

Frequency is found to have a direct impact on dynamic mechanical properties of materials. Figure 5.19 and 5.20 present the variation of storage modulus and tanδ of BA-a/PU 80/20 and Kevlar fiber reinforced BA-a/PU (80/20) at different frequencies i.e. 1, 5, 10, 20, 25 and 50 Hz as a function of temperature. From the plot, the tanδ values were observed to shift to higher temperature with increase of frequency. It is due to the fact that a material is subjected to a constant stress its elastic will decrease over a period of time. The material undergoes molecular rearrangement in an attempt to minimize the localized stresses. Modulus measurements at high frequency performed over short time resulted in higher values while measurements taken over long times at low frequencies resulted in low values [67]. Furthermore, the width of tanδ peak of composite was observed to be boarder than matrix. This phenomena relates to the network heterogeneity due to the interfacial bond between fiber and matrix.

5.6.2 Activation Energy for glass transition temperature

The apparent activation energy for glass transition (ΔE) can be used to characterize the relationship between the shift of glass transition temperature and

frequency. It is mentioned that T_g represents the relationship between the mobility of polymer chains and temperature whereas ΔE represents a relationship between mobility and time scale the energy barrier of transition temperature relaxation. The ΔE values for glass transition of the obtained composites can be calculated from the Arrhenius equation:

$$f = f_0 \exp(-\Delta E / RT) \quad (5.2)$$

Where *f* is the measuring frequency, f_o is the frequency when T approaches infinity and T is temperature corresponding to maximum of tanδ curve.

Figure 5.19 and 5.20 show the variation of Tg obtained from peak tanδ as a function of frequency of mechanical oscillation for neat BA-a, BA-a/PU matrices, glass fiber composite and Kevlar™ fiber composites. A good linear correlation was observed, and the activation energy was also calculated from the slope of the relationship between the frequency and glass transition temperature as depicted in Figure 5.21. The obtained activation energy values were summarized in Table 5.2. The activation energy of matrices tended to be increase with increasing amount of PU content i.e. 417 kJ/mole (BA-a), 472 kJ/mole (BA-a/PU 90/10) and 517 kJ/mole (BA-a/PU 80/20). This can be explained that in the glass transition region, the motion of molecules is governed by the crosslink density. The enhancement of crosslink density affects to the decreasing of the free volume and oscillations of molecules about mean position. As can seen in Figure 5.22, the crosslink densities of BA-a/PU alloys were calculated from Neilsen equation

$$\log\left(\frac{E'}{3}\right) = 7.0 + 293(\rho_X)$$

From Nielson's equation above, E' is a storage modulus in a rubbery plateau region, ρ_x is a crosslinked density that is the mole number of network chains per unit volume of the polymers. The obtained crosslink density increased with increasing PU fraction. Therefore increase in PU content reduces the motion of chain, which is required higher

energy to make molecule motion. For the composites, the activation energy of glass fiber reinforced BA-a and Kevlar™ reinforced BA-a/PU matrices i.e. BA-a/PU (100/0), BA-a/PU (90/10) and BA-a/PU (80/20) composite were determined to be 434, 445, 491 and 544 kJ/mole, respectively. These values were higher than those of matrices. This observation indicated the effective stress transfer between fibers and matrix, which decreased the polymer chain mobility [68].

5.7 Composites Mechanicals Properties

The flexural properties of all composites are summarized in Table 5.4. From the table, the highest flexural modulus and flexural modulus was observed in glass fiber composite which is suitable for used as hard strike face of ballistic armor. This portion is necessary to break up and distort the projectile before the composite backing spread the energy over a greater area. In case of armor backing, Kevlar™ composites were considered to be used in this portion. As illustrated in figure 5.23, the stress deflection curve of the Kevlar™ composites were 2.04 mm for BA-a, 3.37 mm for BA-a/PU (90/10), 4.27 mm for BA-a/PU (80/20), 3.37 mm for BA-a/PU (70/30) and 2.71 mm for BA-a/PU (60/40). The increased strain behavior may be caused by the addition of the more flexible PU fraction to the benzoxazine matrix. This indicates the improved flexibility of the obtained composites that can provide more deflection during ballistic impact [69]. The flexibility of Kevlar™ composites slightly decreased when PU content was greater than 30wt% which was likely from the discontinuous or imperfect network. This observation is in good agreement with our recent work. Rimdusit et al. (2009) reported the ability of network formation of BA-a/PU alloys at different composition. The presence of 30 wt% of PU in BA-a/PU alloy was observed to be the weakest network which has the highest percent of solvent extraction (20.4%) whereas 20 wt% of PU in alloy provided a zero solvent extraction value [70]. In previous work, the ballistic armor based Kevlar ™ reinforced BA-a/PU (80/20) was observed to be able resist the ballistic impact equivalent NIJ level III-A. Therefore, Kevlar™ reinforced with BA-a/PU (80/20) was suitably chosen to be used as armor backing.

5.8 Fracture Surface of Composites

The SEM studies reveal aspects of fiber bonding and adhesion between fiber and matrix. The micrographs exhibit phase information and fracture characteristics reflecting the reasons why the mechanical properties have been changed and in turn decide the mechanical properties of polymeric composites [71]. The fractured surfaces of the glass fiber and Kevlar™ composites are illustrated in Figure 5.24 a and b. The 80 wt% of glass fiber reinforced neat BA-a resin and Kevlar™ fiber reinforced BA-a/PU with presented the tight interfacial between fibers and benzoxazine matrix, which implied a good fiber interface, as illustrated in Figure 5.19 a and b. This may be explained that the glass fiber and Kevlar™ fiber can provide interaction with matrices [72, 73]. These results confirmed the observed enhancement in thermal properties of these composites.

5.9 Ballistic Impact Tests of Composite Armors

At high level ballistic impact test, NIJ level III ballistic impact, the test was performed on the composites which were assembled from glass fiber and Kevlar™ fiber composites. The dimension of the polymeric laminated specimens was 15×15 cm^2 consisted of 25 plies of each type of fiber i.e. glass fiber and Kevlar™ cloth. The fabrics were impregnated with about 20 % by weight of the BA-a resin for glass fiber and BA-a/PU (80/20) resin mixtures for Kevlar™ fiber. The glass fiber and Kevlar™ composites were assembled to form a hard armor composite i.e. the panel of glass fiber composite acted as a strike face portion and the panel of Kevlar™ composite performed as support portion. The specimen was performed by 7.62 mm AP projectile for one shot per specimen. The results of bulletproof testing of the composites were summarized in Table 5.3.

The samples consisted of glass fiber and Kevlar™ composite had two types of arrangements, i.e. 1 panel of glass fiber composite/1 panel of Kevlar™ composite as sample 3a. and 2 panels of glass fiber composite/1 panel of Kevlar™ composite as sample 3b. The total areal density of samples was 2.6 g/cm^2 for sample 3a and 4.3

g/cm^2 for sample 3b. The sample 3a can not pass this level of the NIJ standard for ballistic protection, as depicted in Figure 5.25. In case of the sample 3b, it can resist the ballistic penetration, as shown in Figure 5.26.

.As shown in Figure 5.26, the damage in glass fiber composite was more localized and circular in both front and back side whereas the damage characteristic of Kevlar^{TM} composite was observed to be a star shaped crack on front side and circular on back side. In a recent work, laminates were perforated by conical and ogival a projectile which is the characteristic of 7.62 mm AP projectile. These laminates showed localized damage but the region which was affected by the impact also increased with impact velocity. During ballistic impact of the fabric, transverse deflection was created in the principal yarns (the yarns that were in direct contact with the projectile). This, in turn interacts with orthogonal yarns (the yarns that intersect principle yarns) through the crossovers and the yarns got displaced out of the plain of the fabric. This results in deflection resembled square pyramid or star impression at the rear of the fabric or composite. The amount of energy absorbed by the composite depended upon the amount of the material that undergo deflection during impact and the velocity at which the deflection took place. The star-type crack formation in the front side of the composite laminates can be attributed to the delamination of the layers and due to back ply being pulled away from the front ply during perforation [27, 74].

In addition, the polymeric laminated specimens with approximately dimension 30 × 30 cm^2 were prepared as the sample 3c. The total weight and thickness of the hard armor composite was about 4.6 kg and 31.5 mm, respectively. In this test a 7.62 mm full metal jacket with 3 ammunitions were impacted on the same composite specimen. Figure 5.27 illustrates the ability of the hard armor composite to clearly resist the penetration of those ammunitions. From table 5.5, the delaminated area of the sample 3a, 3b and 3c had the values vary within a certain characteristic level for each panel. The observation indicates the homogeneity of the composite performance.

Generally, selection of suitable armor materials for defense application is very crucial with respect to increasing mobility of the systems as well as maintaining safety. Therefore, determining the material with the lowest possible areal density that resist the predefined threat successfully is required in armor design. Table 5.4 summarizes the ballistic armors against 7.62 mm AP projectiles were produced from various materials. From table 5.6, the areal density of the composite based glass and Kevlar™ reinforced benzoxazine alloy was significantly lower than those of reported materials e.g. aluminum alloy (10-11.5 g/cm^2) [75], multi layer metallic plates-steel/aluminum (8.1-15 g/cm^2) [76], alumina ceramic bonded steel (9.4-16.5 g/cm^2) [77], the composite based alumina ceramic/stainless/Kevalr™ reinforced benzoxazine alloy panels (7.1 g/cm^2) [78], S-glass reinforced PP (4.88 g/cm^2) and the composite panels of E-glass reinforced PP and S-glass reinforced PP (4.88 g/cm^2) [45]. Based on the outstanding characteristics of the composite based glass and Kevlar™ reinforced benzoxazine alloy make it a good candidate for light weight ballistic armor.

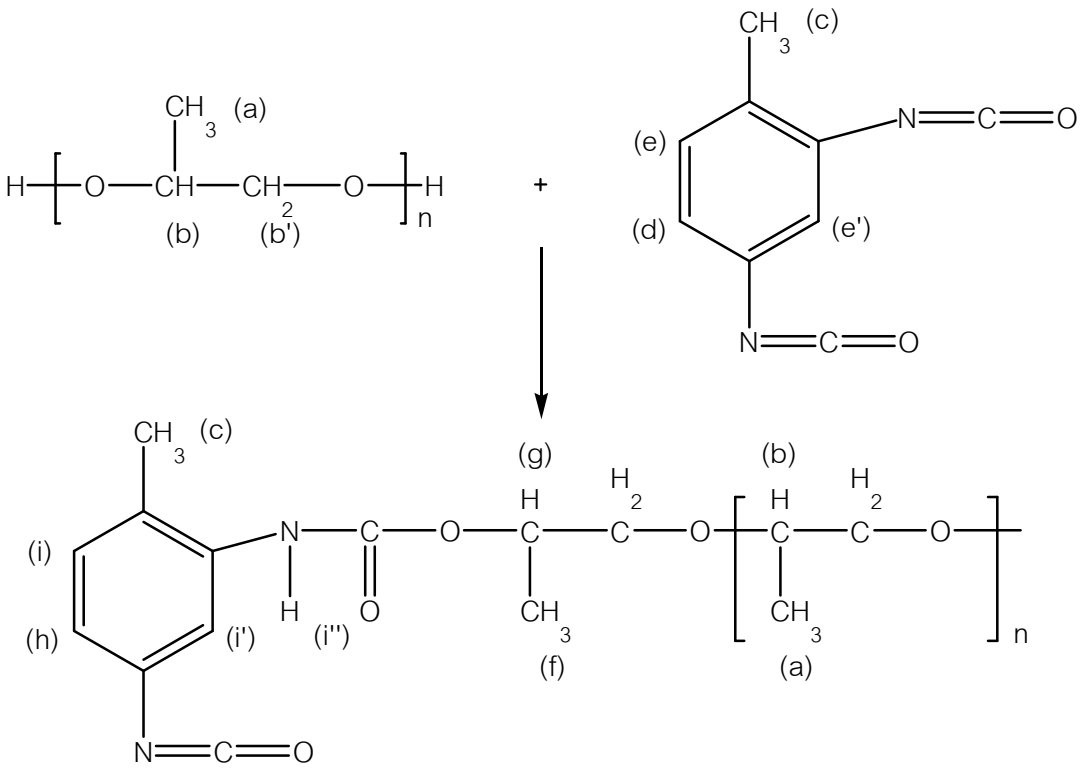

Figure 5.1 Reaction of urethane prepolymer synthesis obtained from propylene gycol and toluene 2,4-diisocyanate.

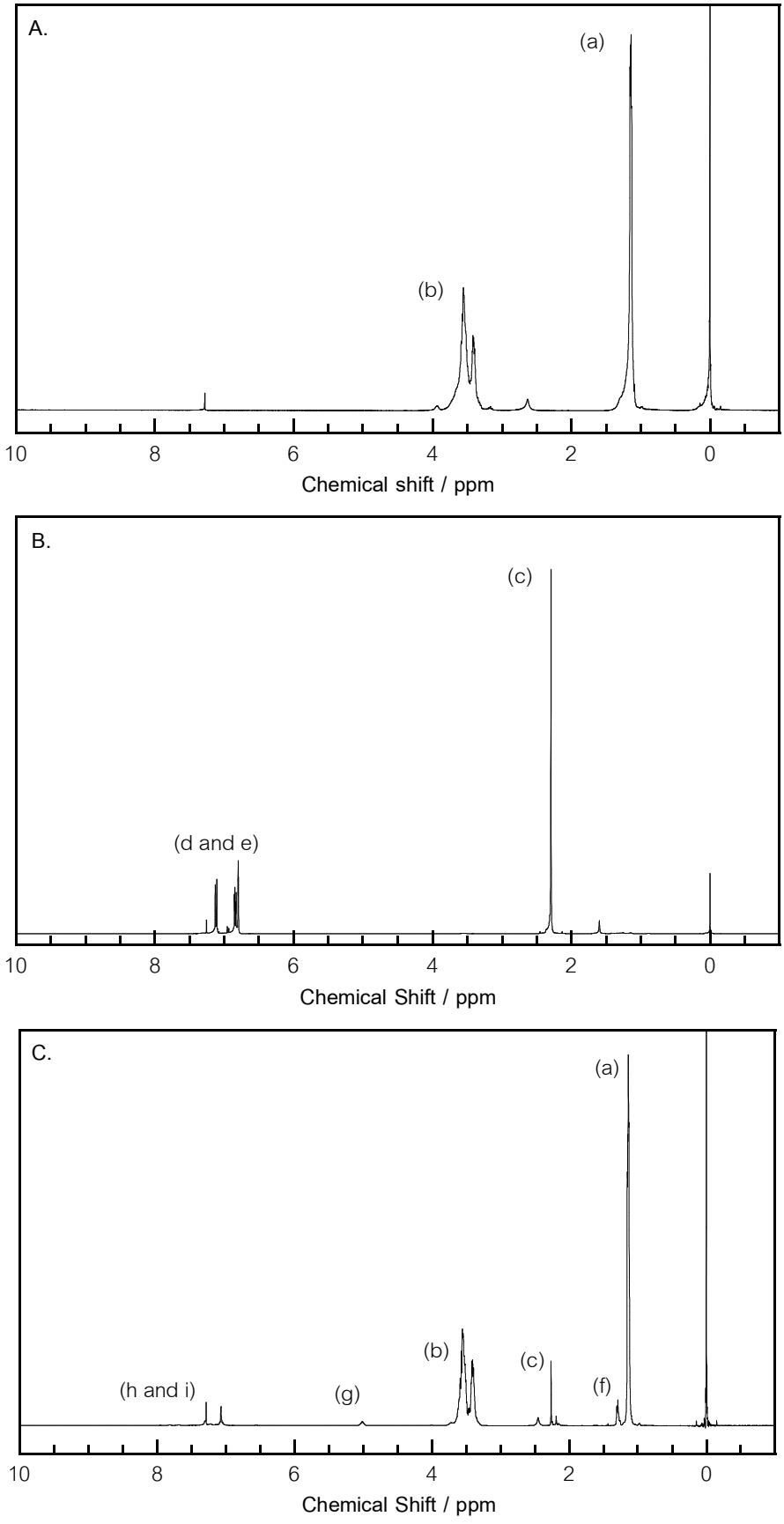

Figure 5.2 ^{1}H-NMR of (A) propylene gycol (MW 2000), (B) toluene 2,4-diisocyanate and (C) urethane prepolymer.

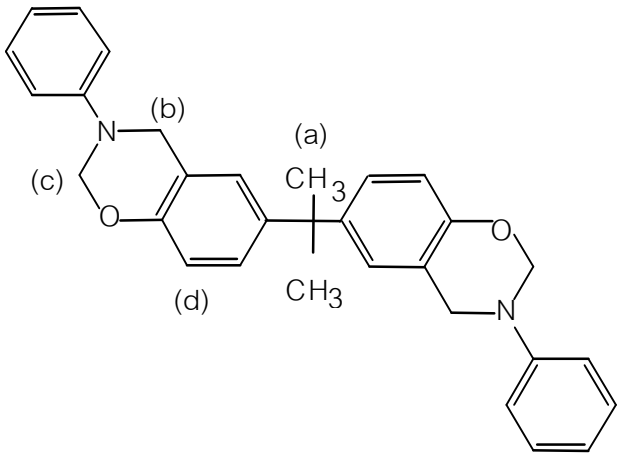

Figure 5.3 Structure of benzoxazine monomer.

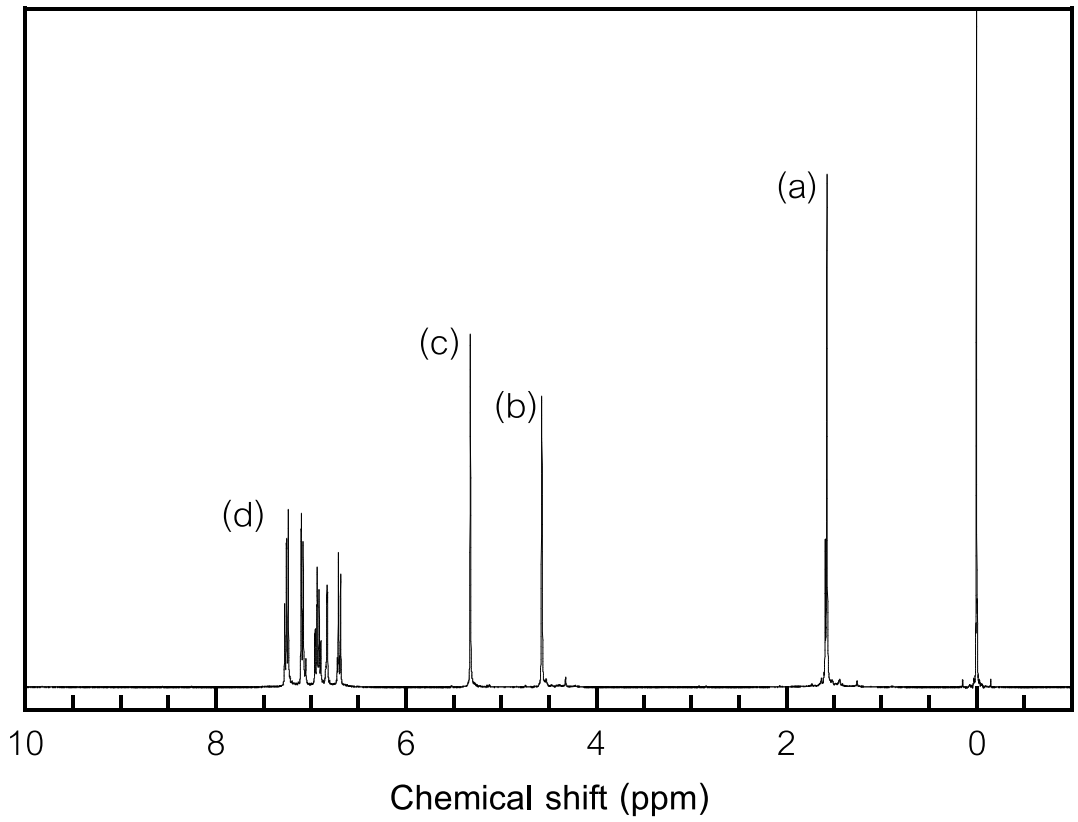

Figure 5.4 ^{1}H-NMR of the benzoxazine monomer.

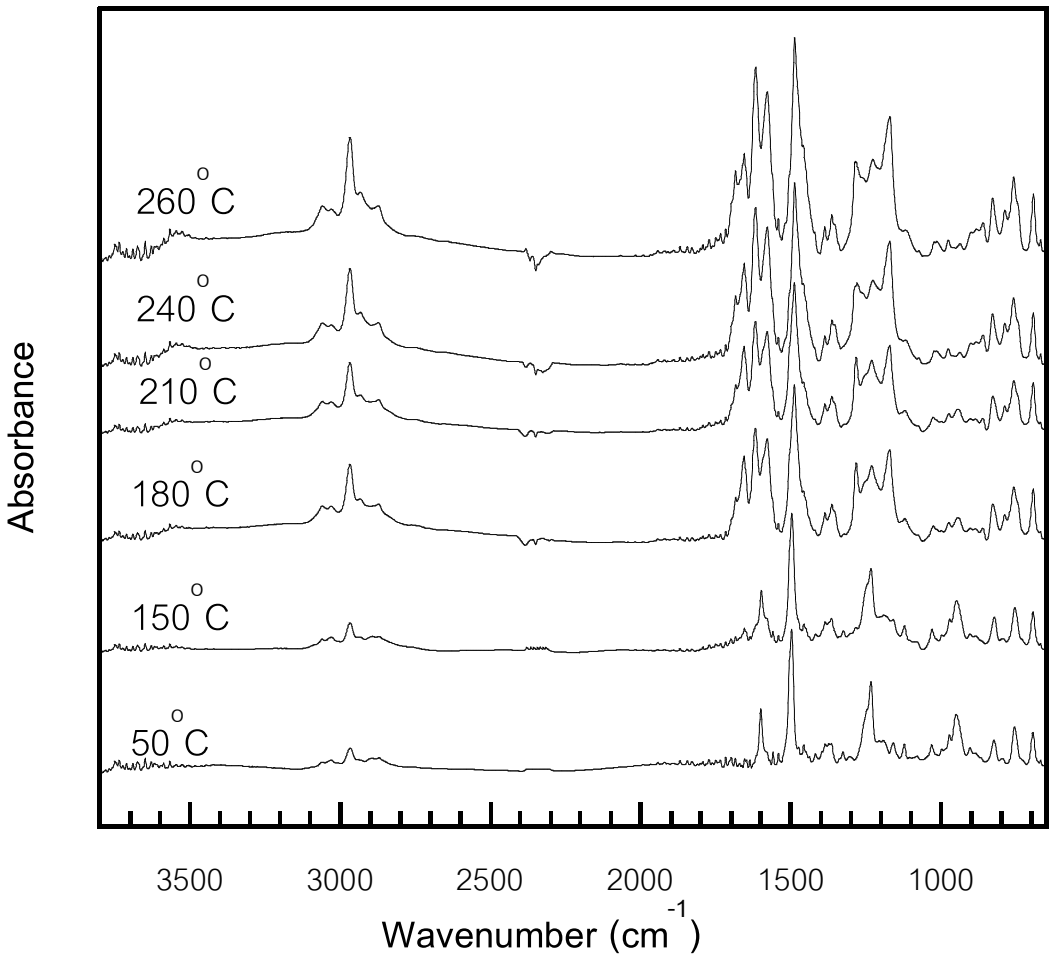

Figure 5.5 *In situ* FT-IR Spectra of benzoxazine resin during curing process.

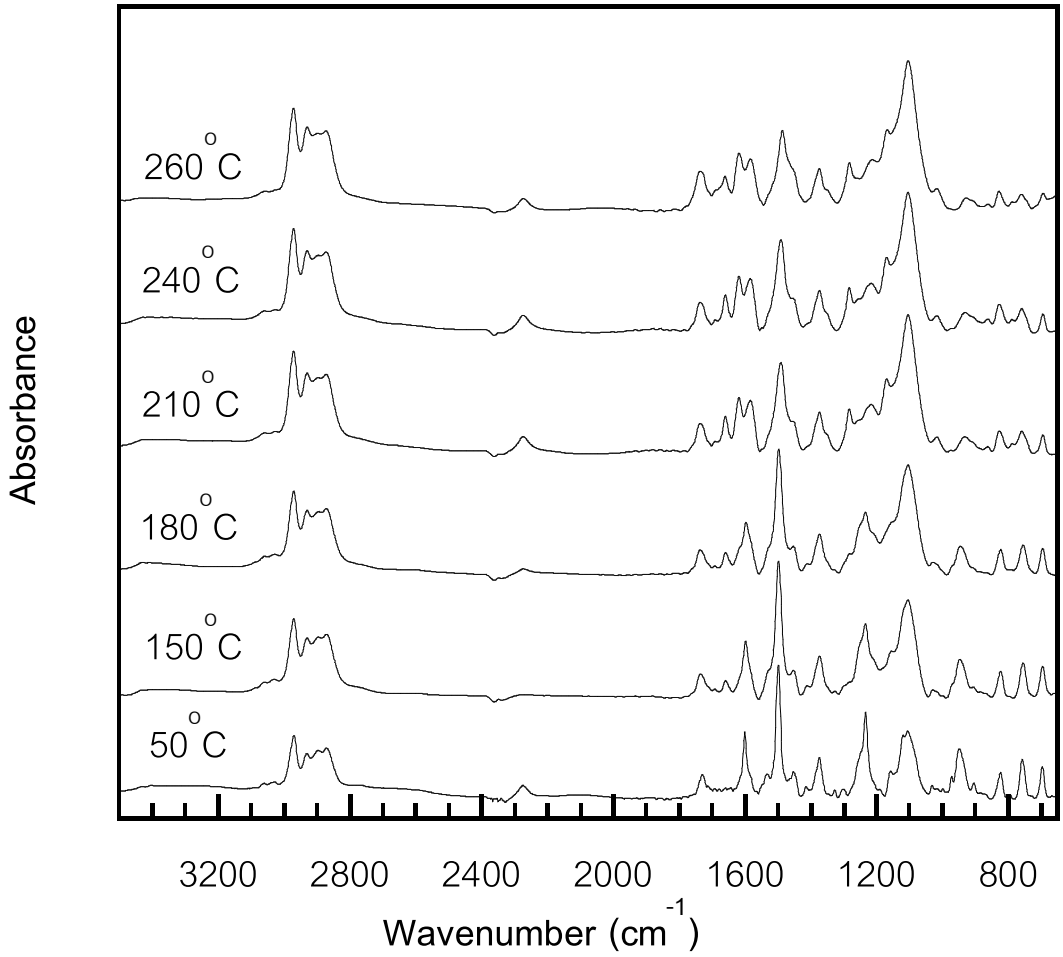

Figure 5.6 *In situ* FT-IR Spectra of BA-a/PU resin mixture at 60/40 during curing process.

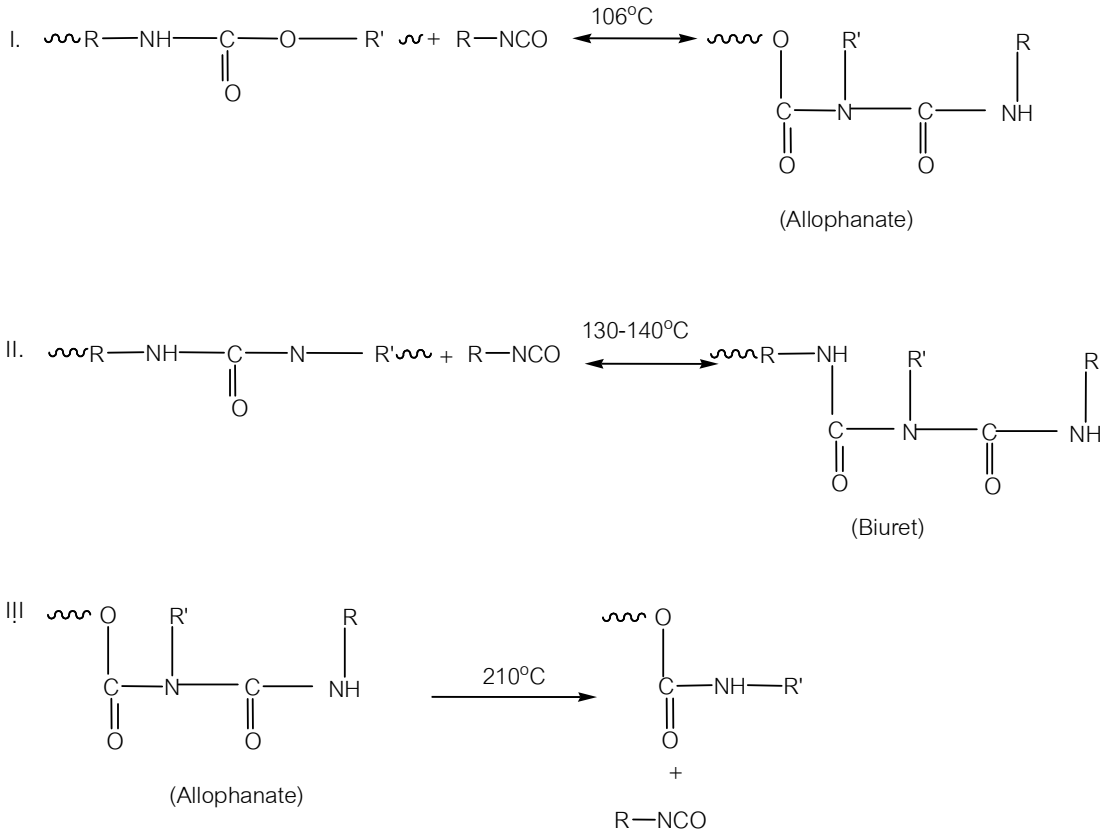

Figure 5.7 Urethane formation reactions.

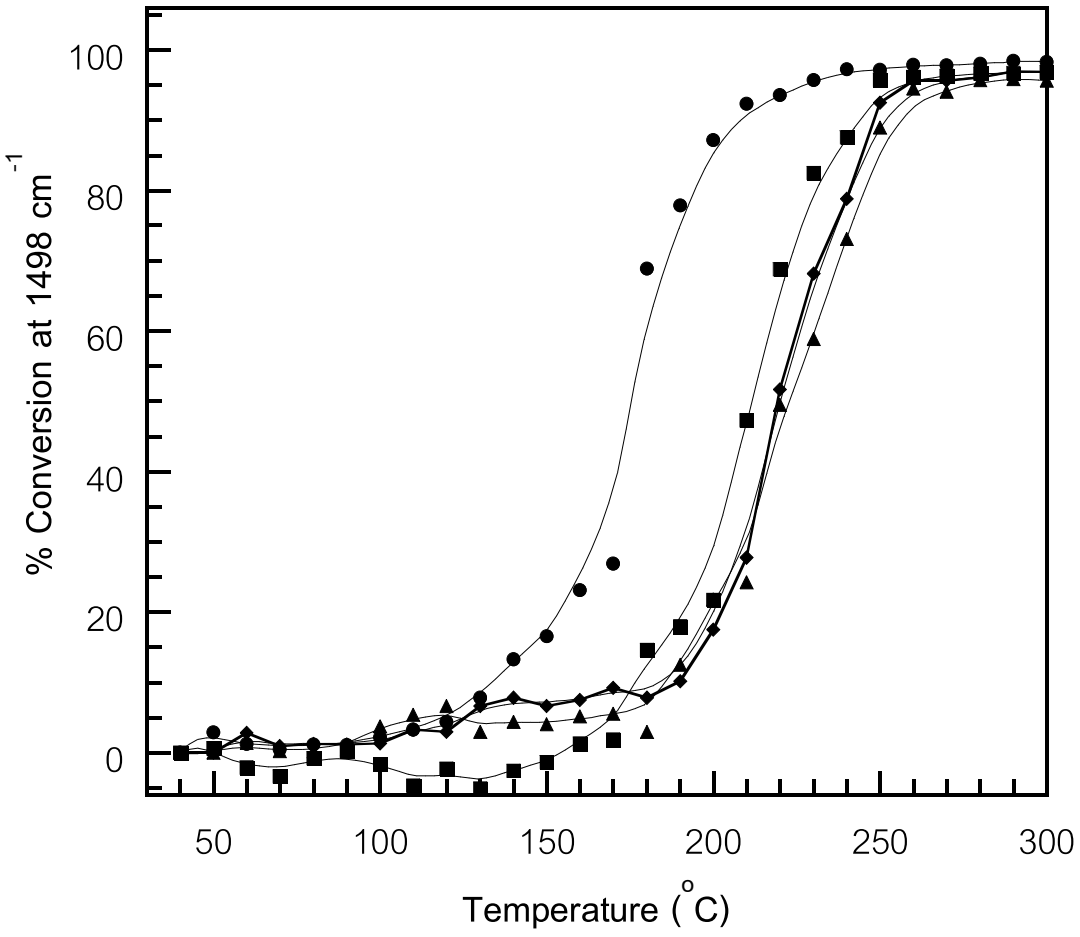

Figure 5.8 The conversion of polymerization (1497 cm^{-1}) of BA-a and BA-a/PU.

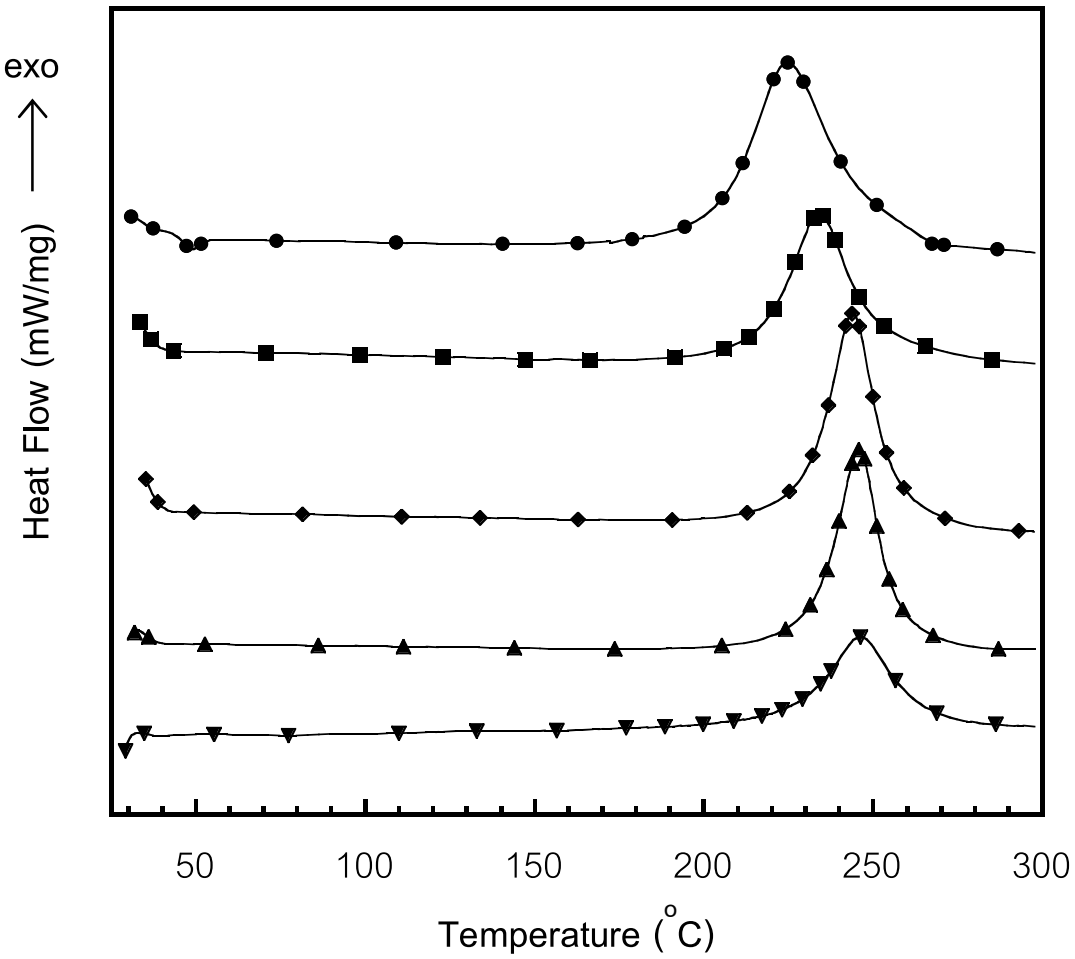

Figure 5.9 DSC thermograms of BA-a/PU resin at various compositions. (●) BA-a/PU 100/0, (■) BA-a/PU 90/10, (◆) BA-a/PU 80/20, (▲) BA-a/PU 70/30 and (▼) BA-a/PU 60/40.

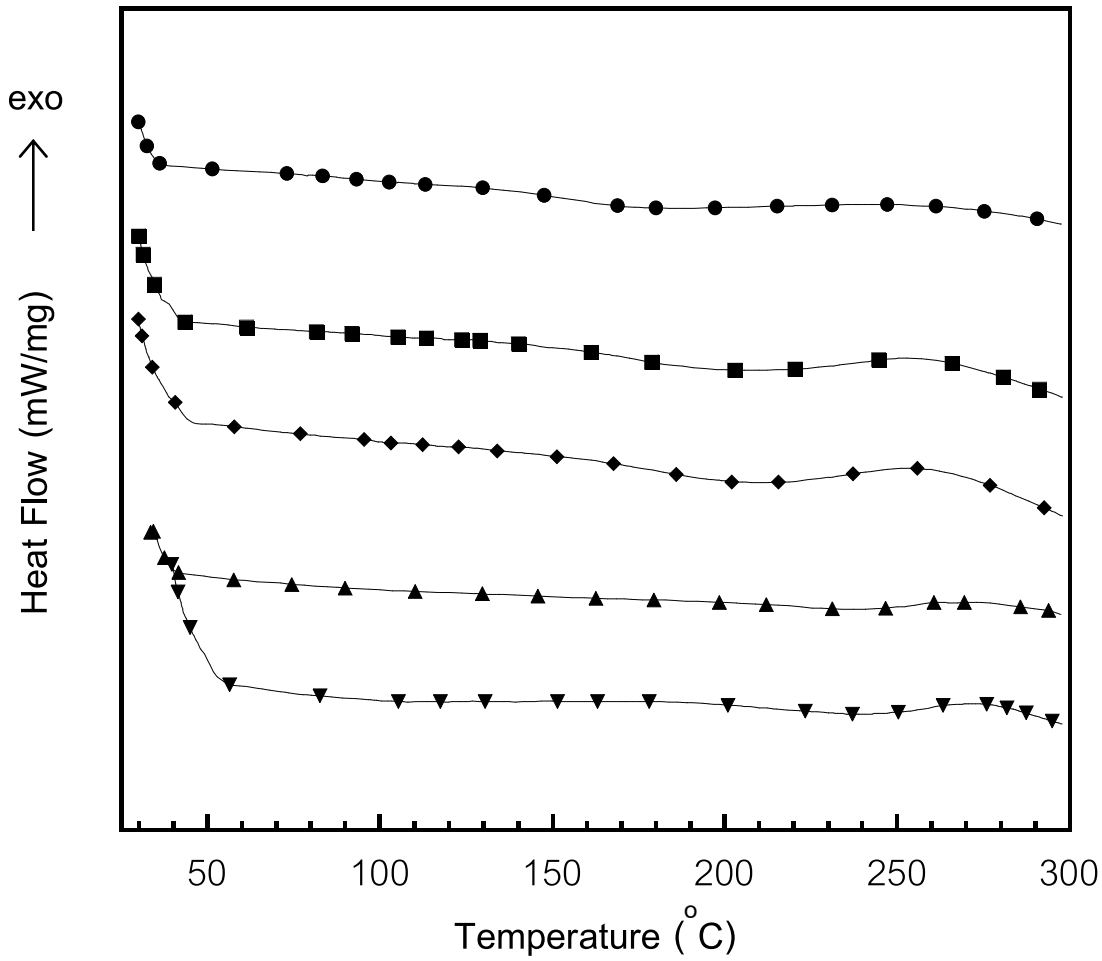

Figure 5.10 DSC thermograms showing glass-transition temperature of BA-a/PU alloys at various compositions : (●) BA-a/PU 100/0, (■) BA-a/PU 90/10, (◆) BA-a/PU 80/20, (▲) BA-a/PU 70/30 and (▼) BA-a/PU 60/40.

The deformed bullet retrieved from 1 panel of glass fiber composite

The deformed bullet retrieved from 2 panels of glass fiber composite

The deformed bullet retrieved from 1 panel of carbon fiber composite

The deformed bullet retrieved from 2 panels of carbon fiber composite

Figure 5.11 The deformed bullet after ballistic test.

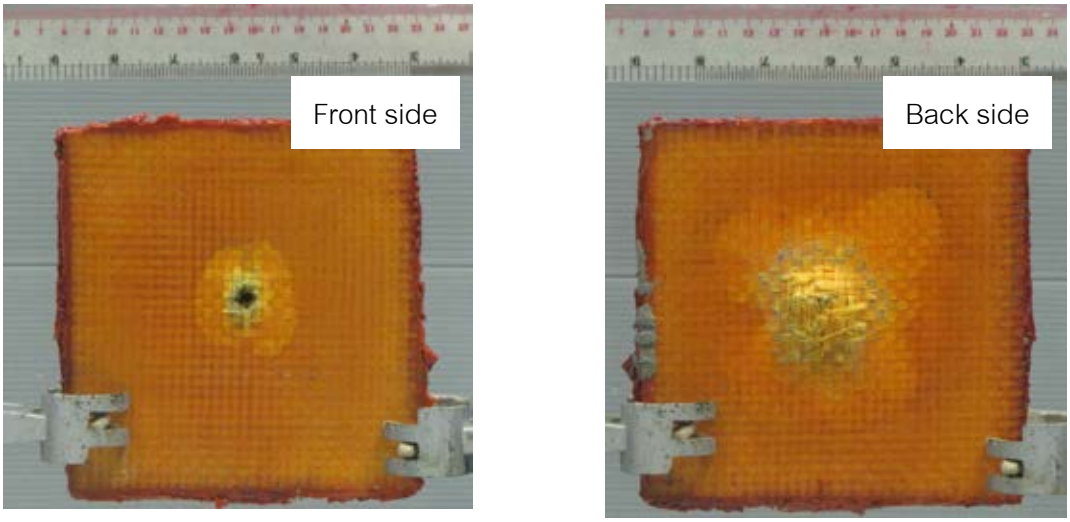

1 panel of glass fiber composite

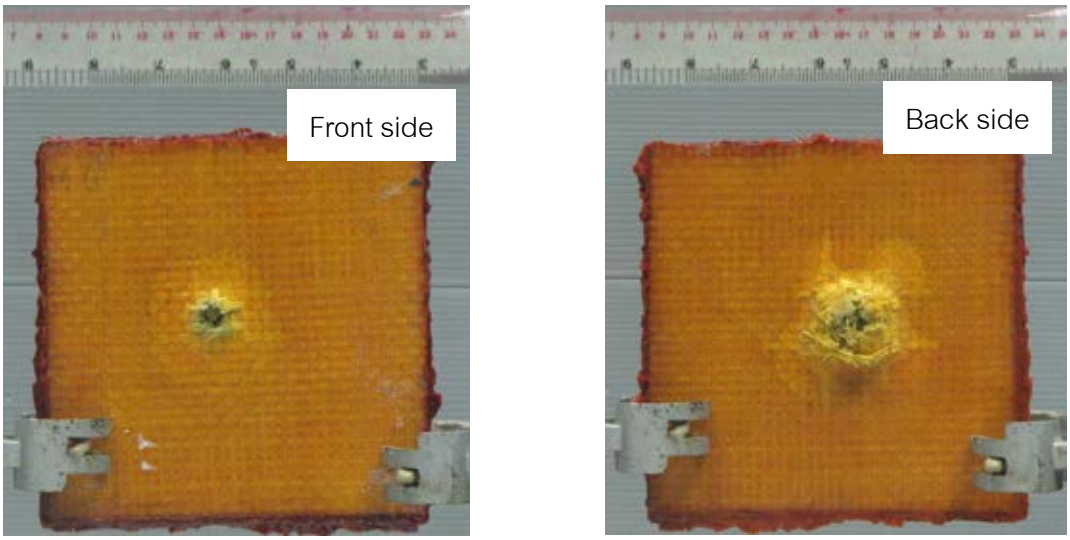

2 panels of glass fiber composite (1st panel)

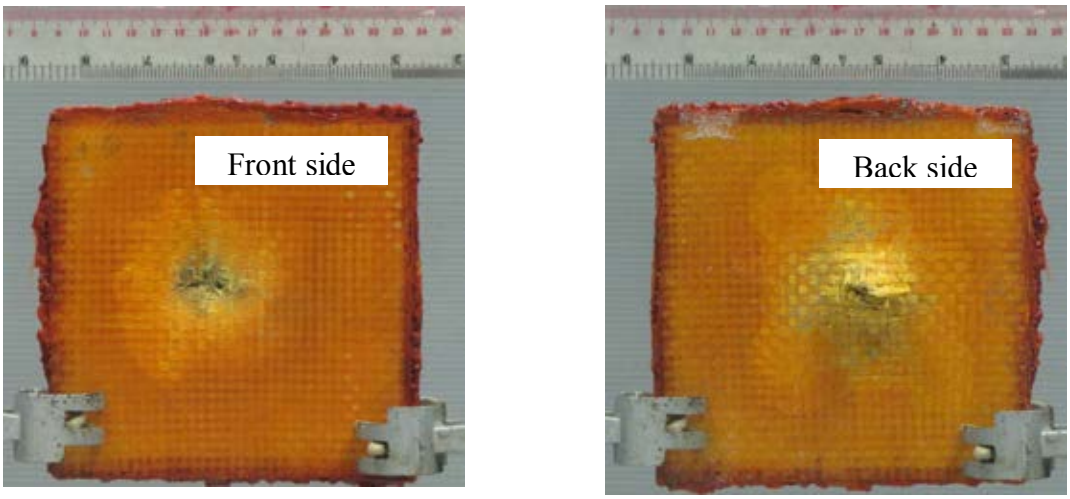

2 panels of glass fiber composite (2nd panel)

Figure 5.12 The impacted glass fiber composites.

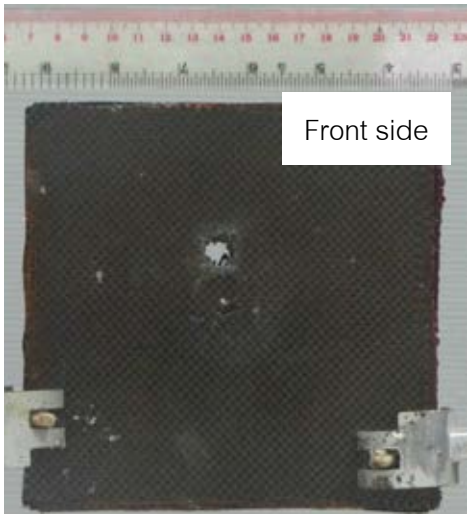

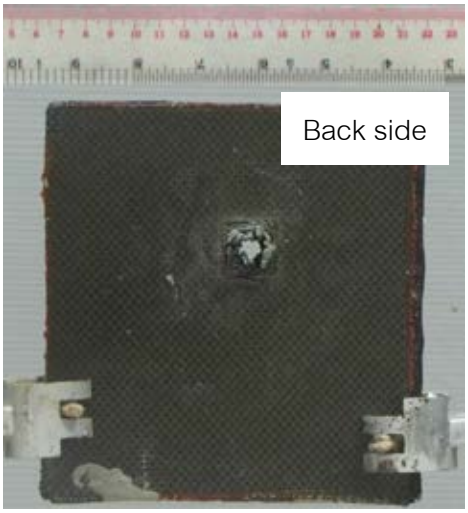

1 panel of carbon fiber composite

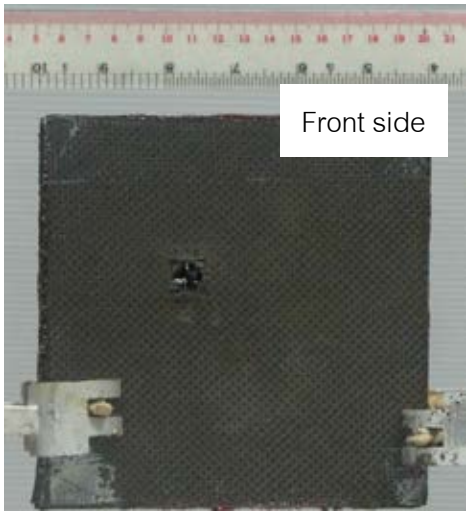

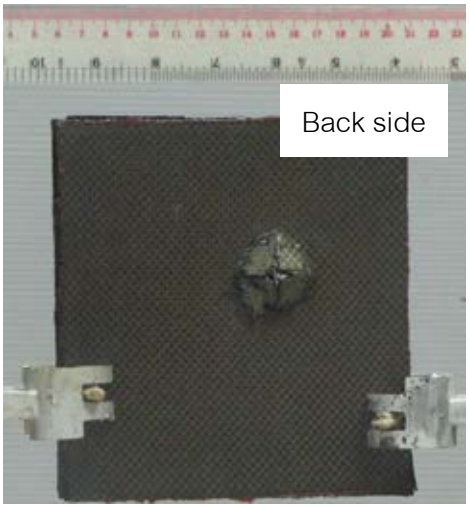

2 panels of carbon fiber composite (1st panel)

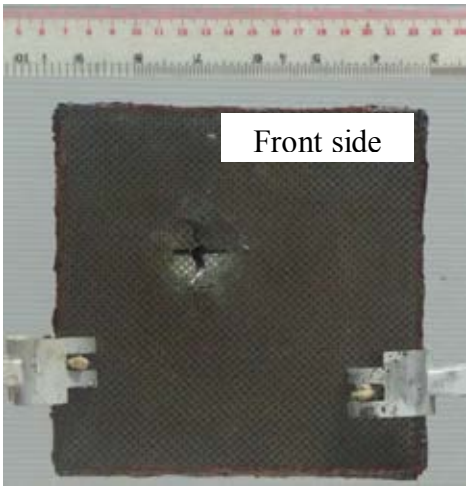

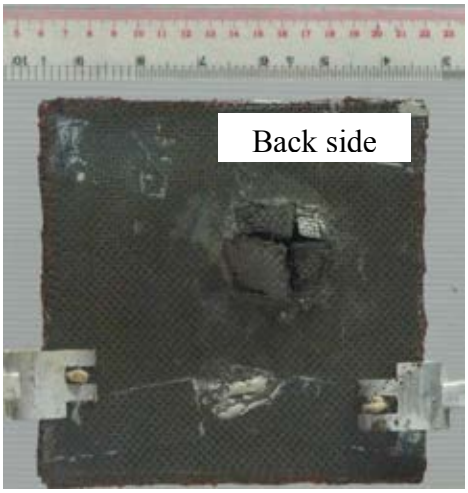

2 panels of carbon fiber composite (2nd panel)

Figure 5.13 The impacted of carbon fiber composites.

Table 5.1: The size of the damage of ballistic panel performed by .44 Magnum.

Ballistic panel	Velocity (m/s)	Perforation	Front damage area (cm^2)	Back damage area (cm^2)	Areal density (g/cm^2)
1 panel of Glass fiber composite	439.20	Yes	16.60	61.26	1.52
2 panels of Glass fiber composite (1^{st} panel)	441.65	Yes	19.21	31.07	3.53
2 panels of Glass fiber composite (2^{nd} panel)	441.65	Yes	12.04	37.66	
1 panel of Carbon fiber composite	440.61	Yes	5.09	5.67	1.04
2 panels of Carbon fiber composite (1^{st} panel)	442.0	Yes	4.95	10.53	2.07
2 panels of Carbon fiber composite (2^{nd} panel)	442.0	Yes	11.89	17.86	

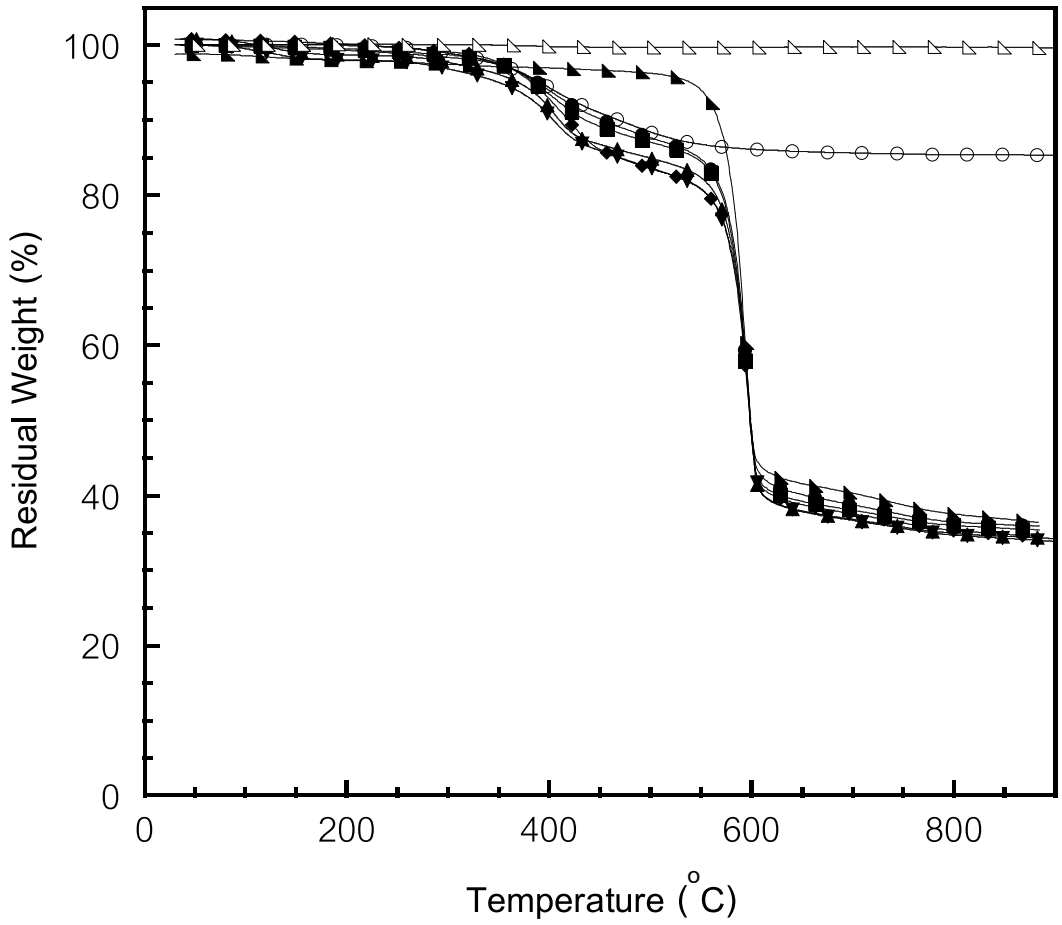

Figure 5.14 Thermal degradation of glass fiber reinforced neat BA-a (○), Kevlar™ fiber reinforced BA-a/PU alloys at various PU content: BA-a/PU 100/0 (●), BA-a/PU 90/10 (■),BA-a/PU 80/20 (◆), BA-a/PU 70/30 (▲), BA-a/PU 60/40 (▼), glass fiber and (◺) and Kevlar™ fiber (◣).

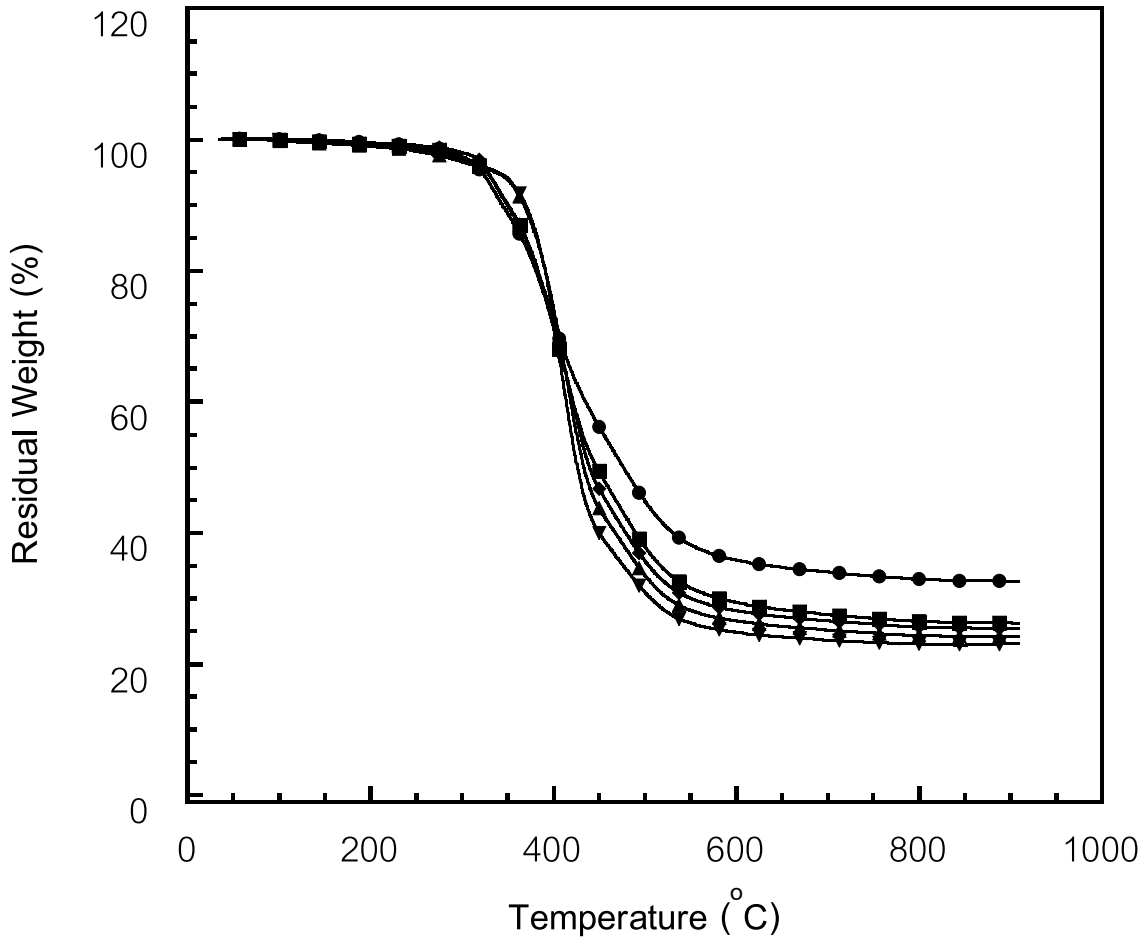

Figure 5.15 Thermal degradation of BA-a/PU alloys at various compositions : (●) BA-a/PU 100/0, (■) BA-a/PU 90/10, (◆) BA-a/PU 80/20, (▲) BA-a/PU 70/30 and (▼) BA-a/PU 60/40

Table 5.2: The thermal stability of glass fiber and Kevlar™ composites.

Samples BA-a/PU	Td at 5 wt% loss		Percent residual weight at 800°C		Percent fiber content
	Matrix	Composite	Matrix	Composite	
100/0	322	391[a]	32.88	83.35[a]	79[a]
		388[b]		36.43[b]	77[b]
90/10	327	384[b]	28.54	35.95[b]	83[b]
80/20	329	382[b]	25.60	35.29[b]	82[b]
70/30	337	370[b]	24.33	34.89[b]	80[b]
60/40	339	350[b]	22.98	34.67[b]	81[b]

a: composite based glass fiber and b: composite based Kevlar™ fiber

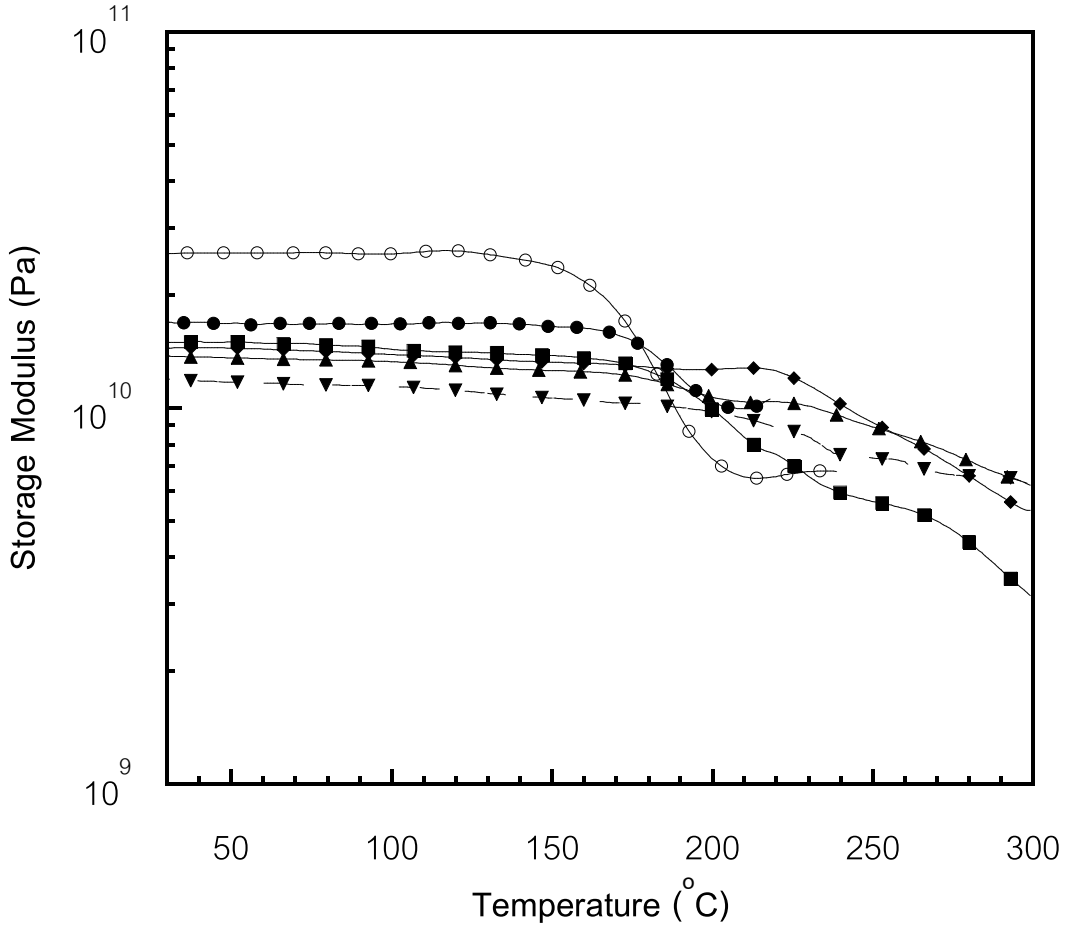

Figure 5.16 Storage modulus of glass fiber reinforced neat BA-a (○), and Kevlar™ fiber reinforced BA-a/PU alloys at various PU content: BA-a/PU 100/0 (●),BA-a/PU 90/10 (■),BA-a/PU 80/20 (◆), BA-a/PU 70/30 (▲), and BA-a/PU 60/40 (▼).

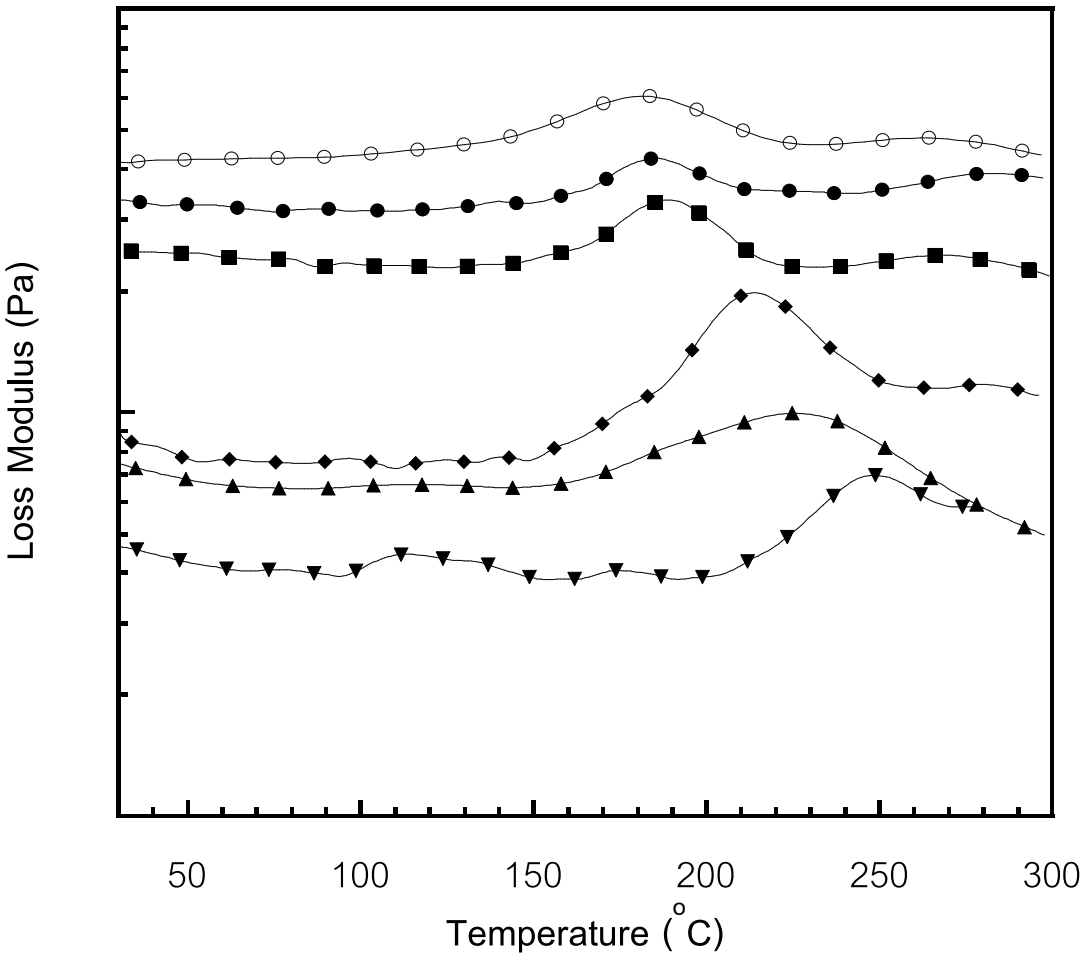

Figure 5.17 Loss modulus of glass fiber reinforced neat BA-a (○) and Kevlar™ fiber reinforced BA-a/PU alloys at various PU content: BA-a/PU 100/0 (●),BA-a/PU 90/10 (■),BA-a/PU 80/20 (◆), BA-a/PU 70/30 (▲), and BA-a/PU 60/40 (▼).

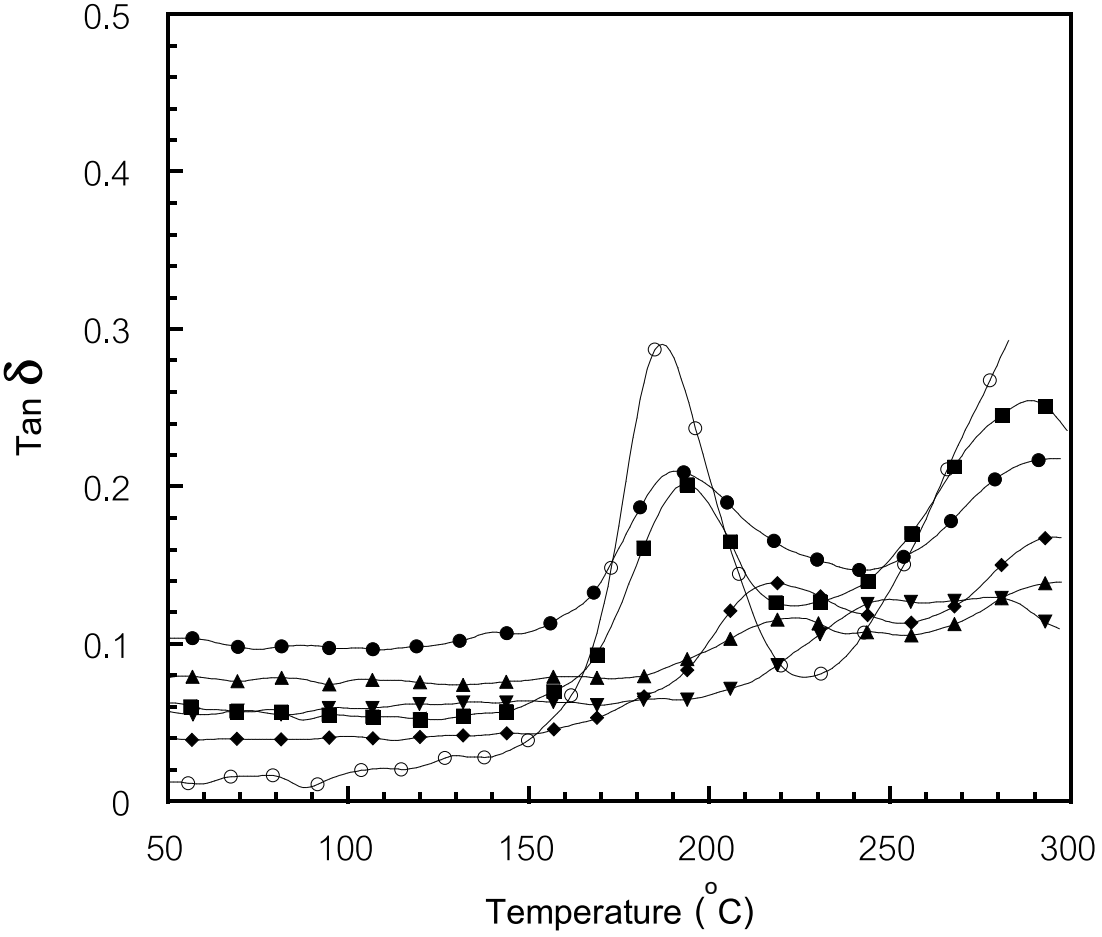

Figure 5.18 Tan δ of glass fiber reinforced neat BA-a (○) and Kevlar™ fiber reinforced BA-a/PU alloys at various PU content: BA-a/PU 100/0 (●),BA-a/PU 90/10 (■),BA-a/PU 80/20 (◆), BA-a/PU 70/30 (▲), and BA-a/PU 60/40 (▼).

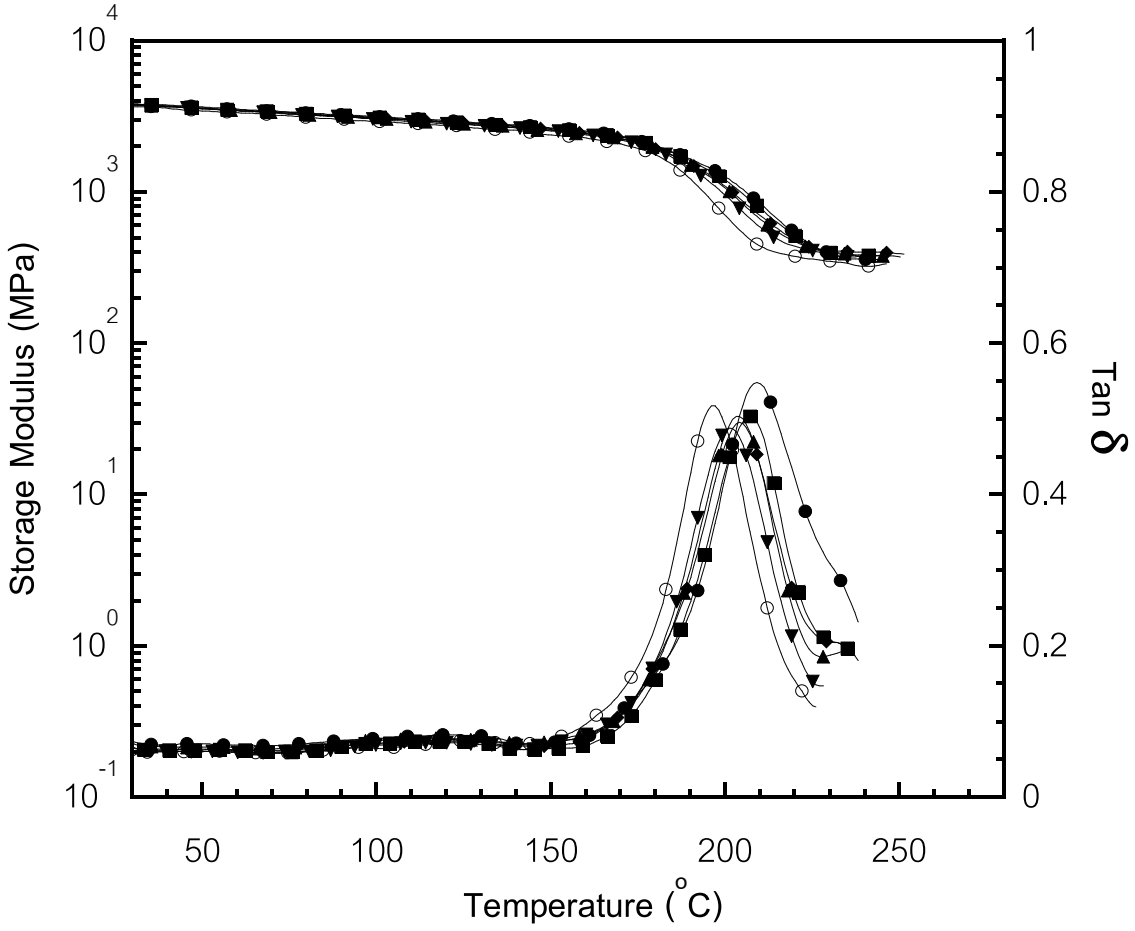

Figure 5.19 Effect of frequency on the storage modulus and Tan δ curve of BA-a/PU (80/20) at different frequencies: 1 Hz (○), 5 Hz (▼), 10 Hz (▲), 20 Hz(◆), 25 Hz s(■) and 50 Hz (●).

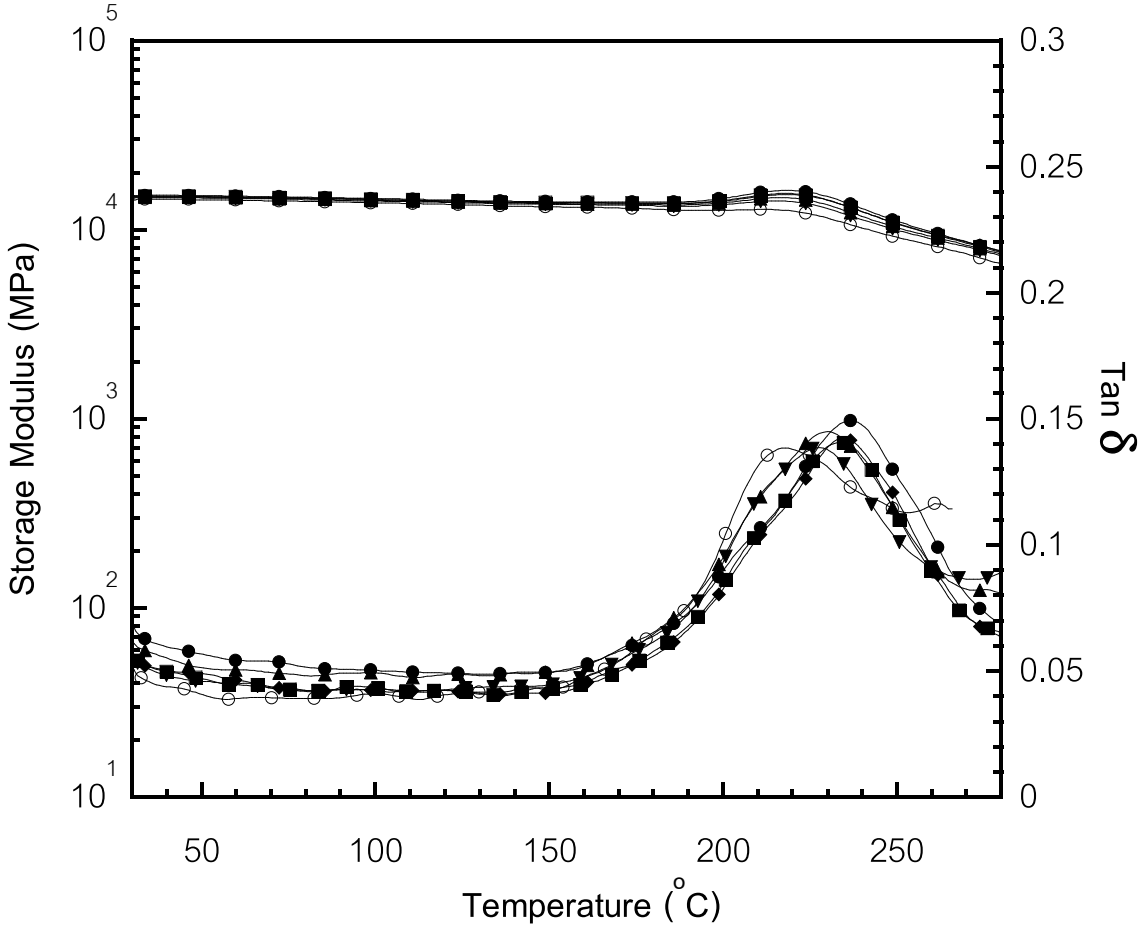

Figure 5.20 Effect of frequency on the storage modulus and Tan δ curve of Kevlar fiber reinforced BA-a/PU (80/20) at different frequencies: 1 Hz (○), 5 Hz (▼), 10 Hz (▲), 20 Hz(◆), 25 Hz (■) and 50 Hz (●).

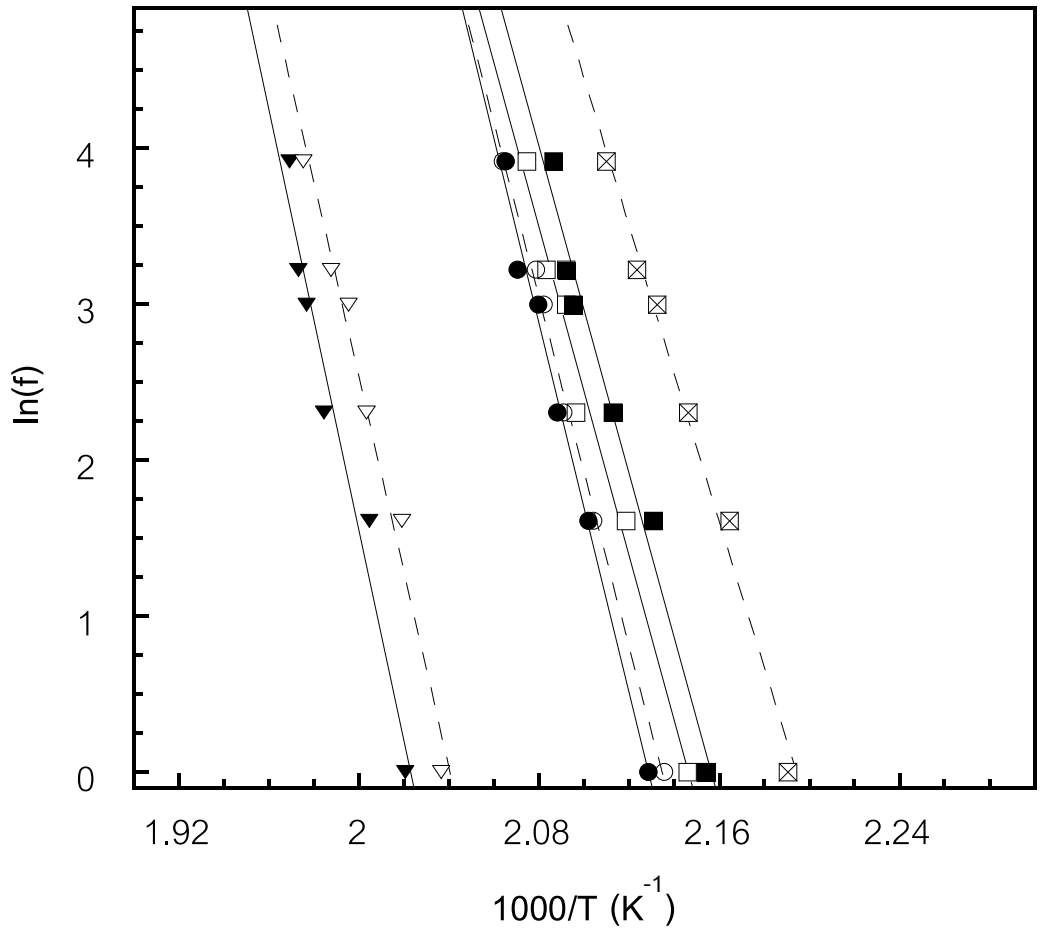

Figure 5.21 The relationship between the measurement frequency (f) and the temperature of the Tan δ peak for neat BA-a (⊠), 90/10 BA-a/PU (○), 80/20 BA-a/PU (▽), glass fiber reinforced neat BA-a (■), Kevlar™ fiber reinforced neat BA-a (□), Kevlar™ fiber reinforced neat 90/10 BA-a/PU (●) and Kevlar™ fiber reinforced neat 80/20 BA-a/PU (▼).

Table 5.3: The activation energy of matrices and composites.

Matrix BA-a/PU	Activation energy (kJ/mole)	
	Matrix	Composite
100/0	417	445[a]
		434[b]
90/10	472	491[b]
80/20	517	544[b]

a: composite based glass fiber and b: composite based Kevlar™ fiber

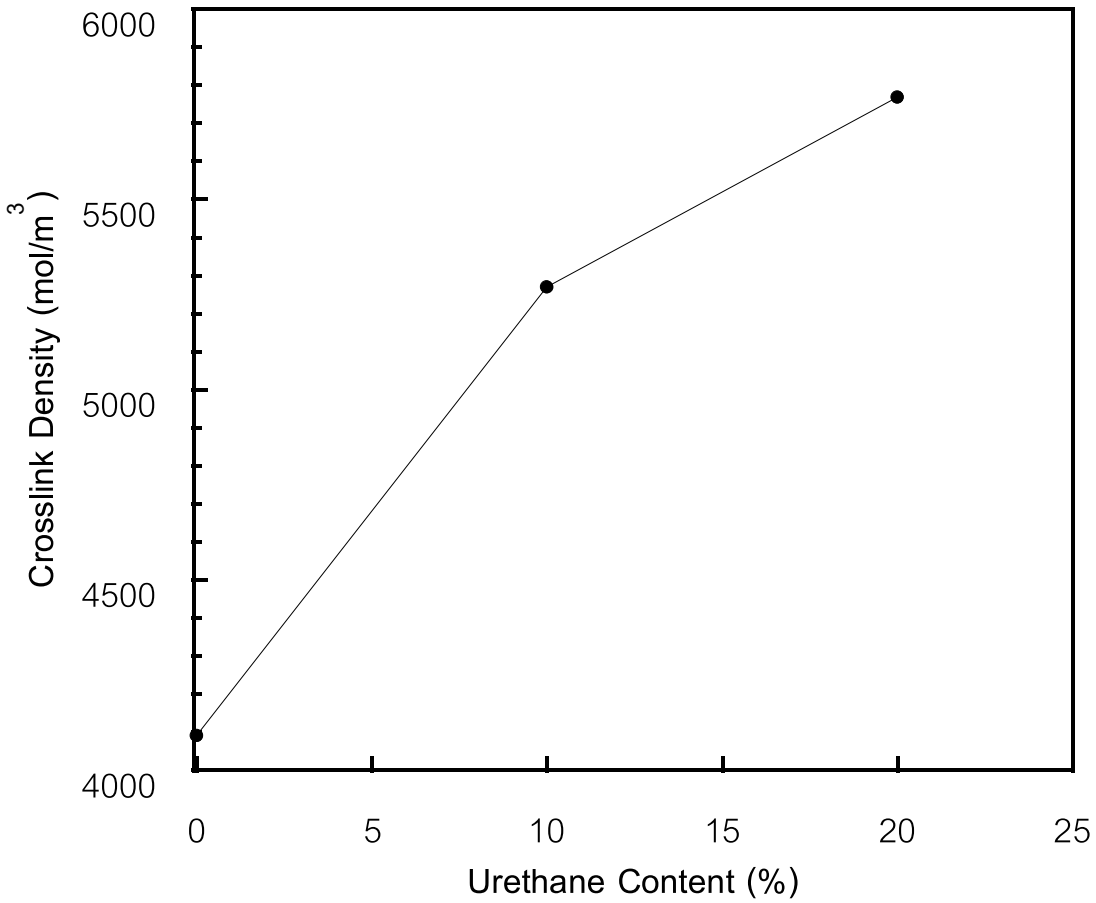

Figure 5.22 Crosslink density of BA-a/PU alloys at various PU compositions.

Table 5.4: Flexural properties of glass fiber and Kevlar™ composites.

Sample	Flexural modulus (GPa)	Flexural strength (MPa)	Flexural strain at max stress (%)
Glass fiber reinforced BA-a	506 ± 13.62	28 ± 2.04	1.19 ± 0.15
Kevlar™ fiber reinforced BA-a	153 ± 11.97	22 ± 1.27	1.26 ± 0.10
Kevlar™ fiber reinforced 90/10 BA-a/PU	127 ± 8.21	17 ± 1.19	1.27 ± 0.10
Kevlar™ fiber reinforced 80/20 BA-a/PU	104 ± 9.35	15 ± 2.25	1.35 ± 0.17
Kevlar™ fiber reinforced 70/30 BA-a/PU	95 ± 10.17	14 ± 1.29	1.19 ± 0.15
Kevlar™ fiber reinforced 60/40 BA-a/PU	74 ± 9.94	12 ± 1.51	0.87 ± 0.10

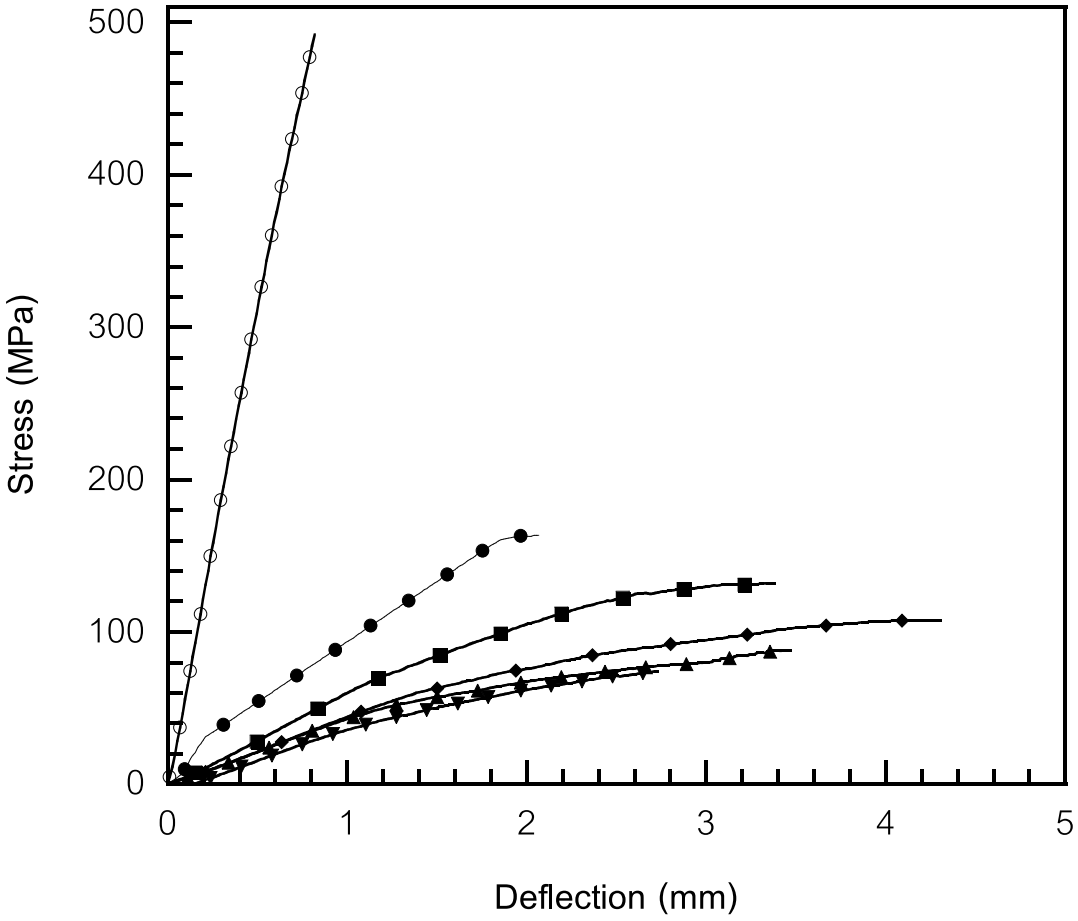

Figure 5.23 Stress-deflection curve of glass fiber reinforced neat BA-a (○) and Kevlar™ fiber reinforced BA-a/PU alloys at various PU content: BA-a/PU 100/0 (●),BA-a/PU 90/10 (■),BA-a/PU 80/20 (◆), BA-a/PU 70/30 (▲), and BA-a/PU 60/40 (▼).

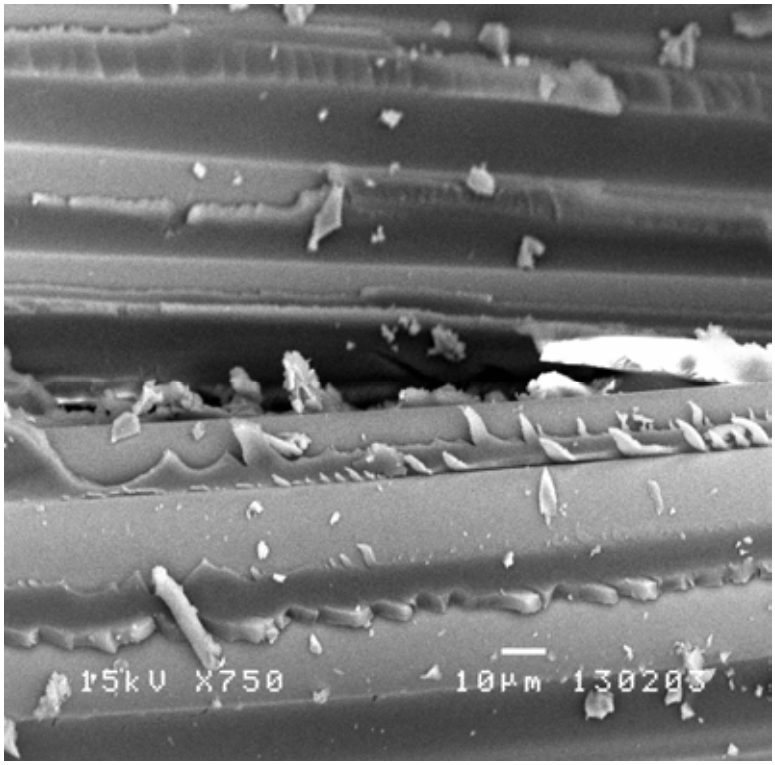

(a)

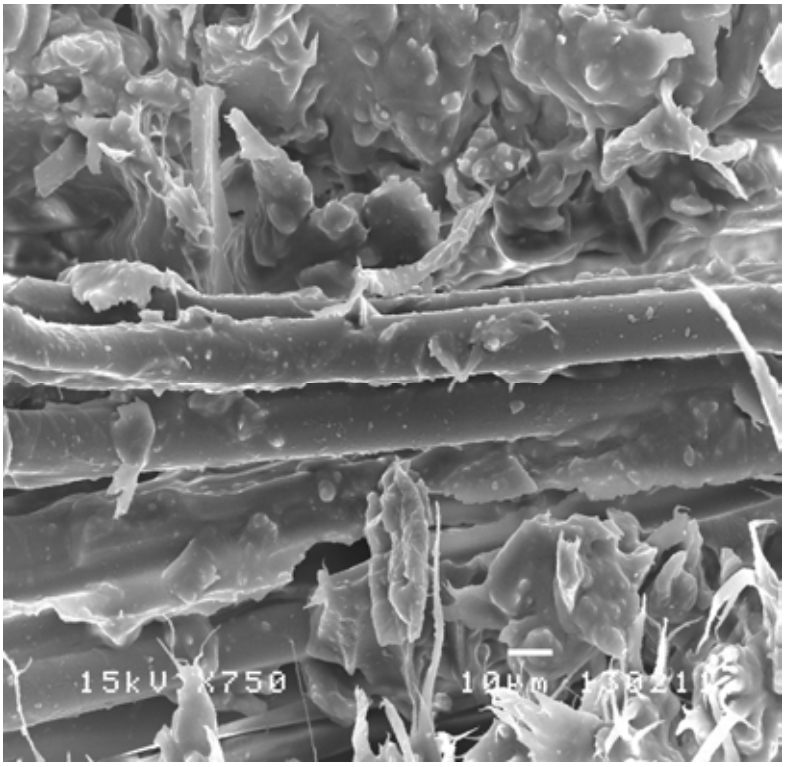

(b)

Figure 5.24 Fractured surfaces of composites: (a) glass fiber reinforced neat BA-a and (b) Kevlar™ reinforced 80/20 BA-a/PU.

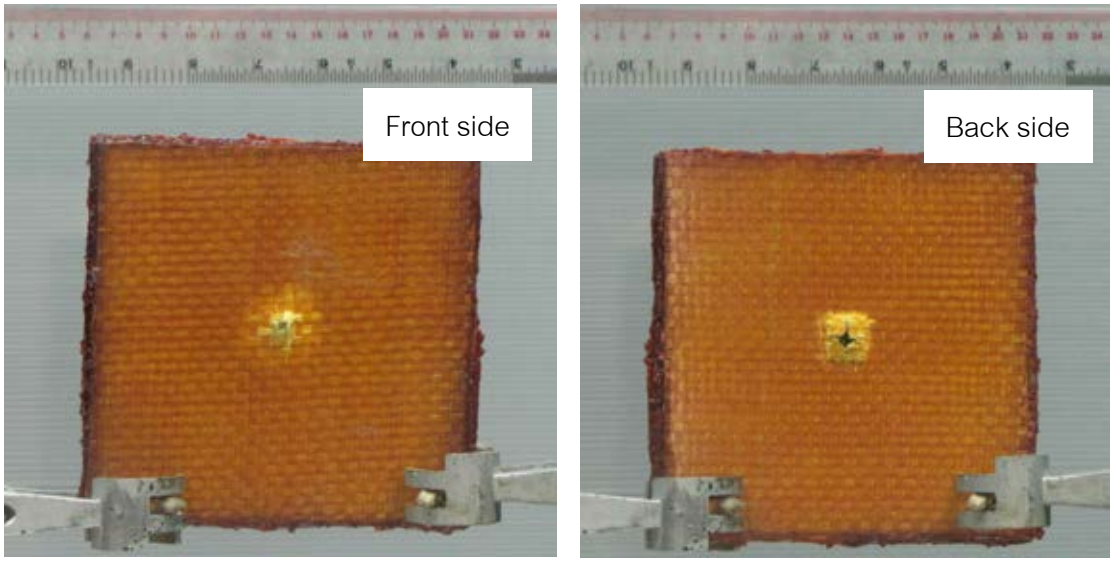

1 panel of glass fiber composite

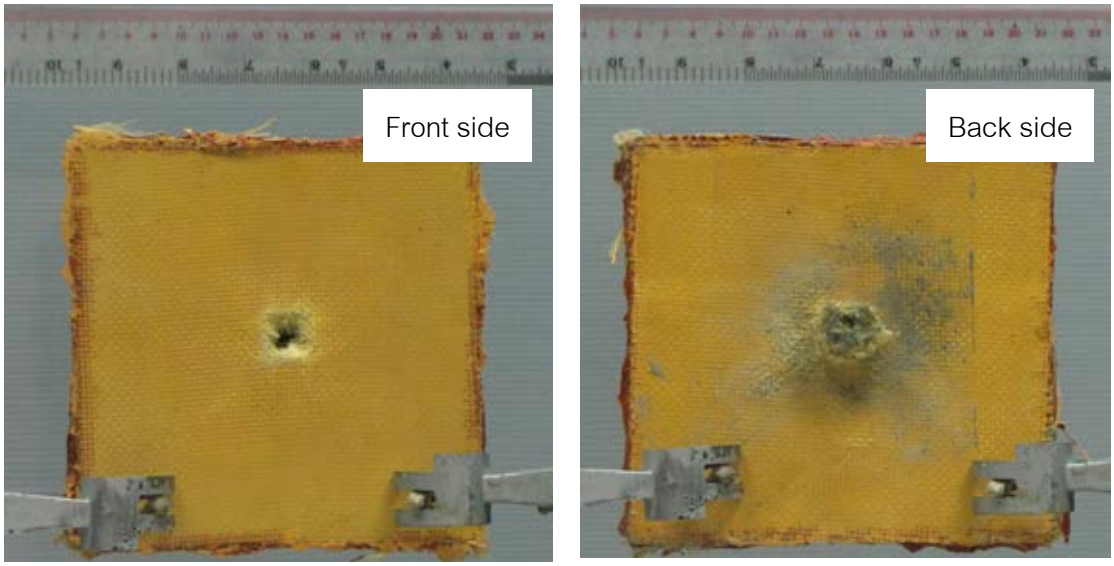

1 panel of Kevlar™ fiber composite

Figure 5.25 The hard armor consisted of 1 panel of glass fiber composite/1 panel of Kevlar™ composite.

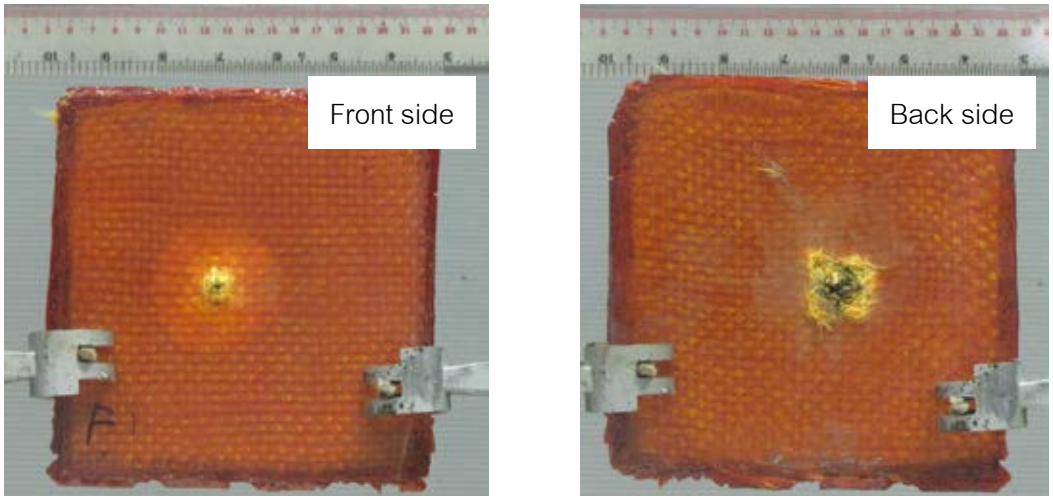

2 panels of glass fiber composite (1st panel)

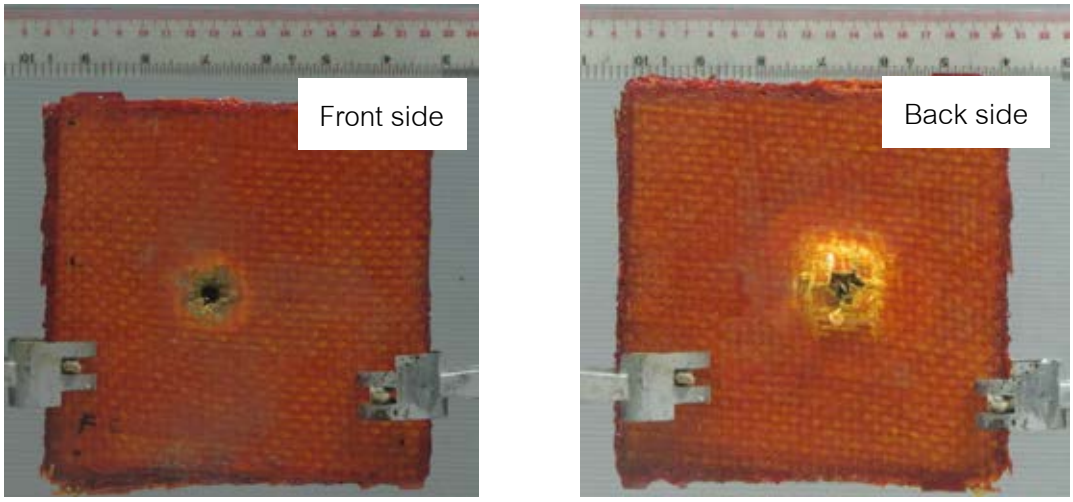

2 panels of glass fiber composite (1st panel)

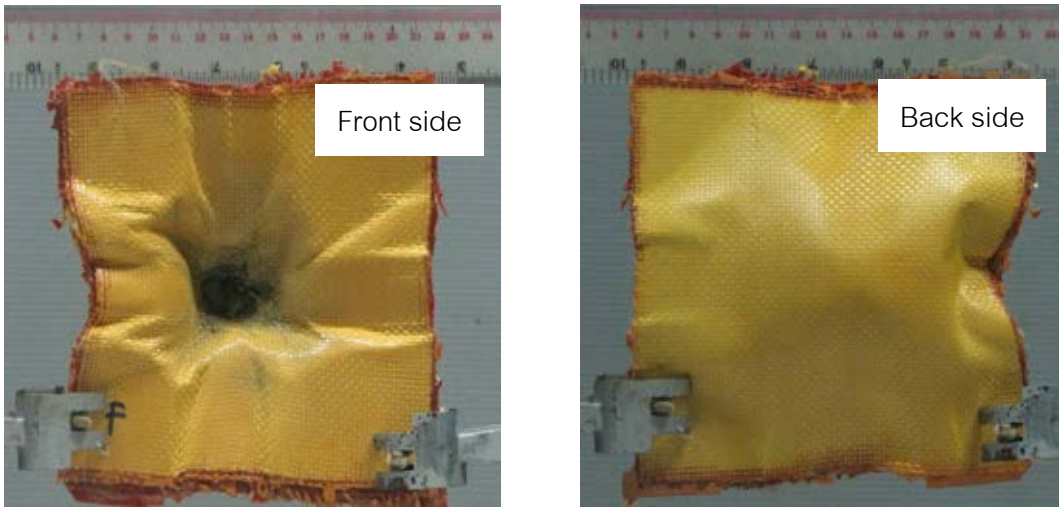

2 panels of glass fiber composite (2nd panel)

Figure 5.26 The hard armor consisted of 2 panels of glass fiber composite/1 panel of Kevlar™ composite.

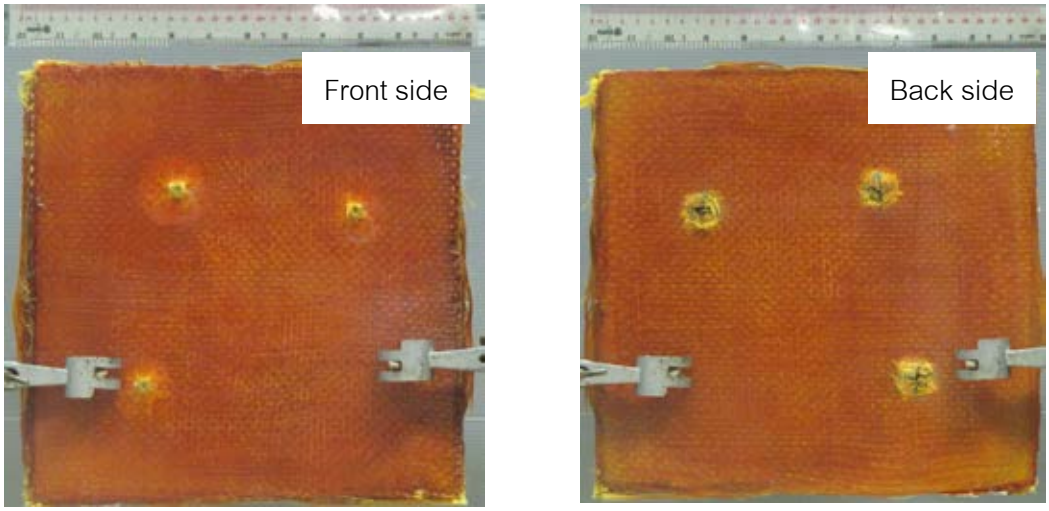

2 panels of glass fiber composite (1st panel)

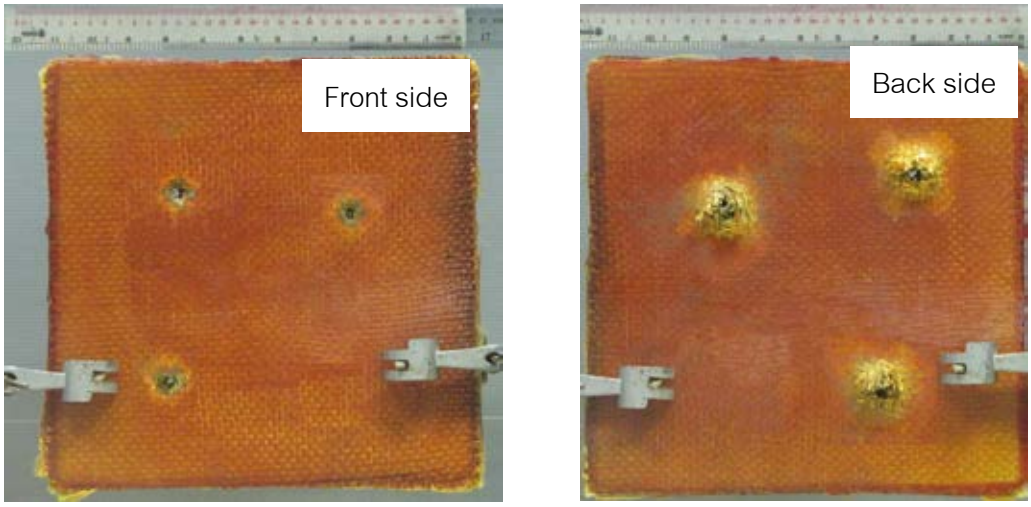

2 panels of glass fiber composite (1st panel)

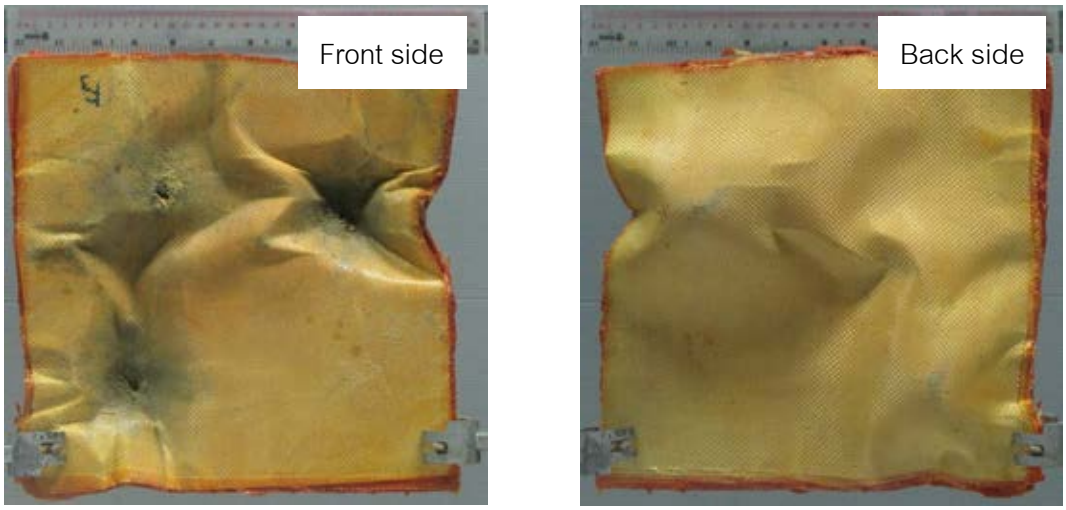

1 panel of Kevlar™ fiber composite

Figure 5.27 The hard armor consisted of 2 panels of glass fiber composite/1 panel of Kevlar™ composite (Size: 30cm × 30cm).

Table 5.5: The size of the damage and projectile velocities of 7.62 AP Winchestor.

Sample	Ballistic panel	Perforation	Front damage area (cm^2)	Back damage area (cm^2)	Areal density (g/cm^2)	Velocity (m/s)
3a	Glass fiber composite (1^{st} panel)	Yes	5.19	5.54	3.53	760.95
	Kevlar™ fiber composite (2^{nd} panel)	Yes	5.55	8.38		
3b	Glass fiber composite (1^{st} panel)	N0	6.83	9.02	4.30	832.2
	Glass fiber composite (2^{nd} panel)	No	9.68	21.80		
	Kevlar™ fiber composite (3^{rd} panel)	No	124.5	176.04		
3c	Glass fiber composite (1^{st} panel)	No	#1: 5.95 #2: 6.13 #3: 6.98	#1: 5.98 #2: 6.88 #3: 7.73	4.30	#1: 842.8 #2: 829.2 #3: 833
	Glass fiber composite (2^{nd} panel)	No	#1: 10.70 #2: 9.04 #3: 8.80	#1:33.51 #2: 28.04 #3: 24.06		
	Kevlar™ fiber composite (3^{rd} panel)	No	#1:131.18 #2: 101.65 #3: 104.25	#1:157.60 #2: 178.97 #3: 159.74		

#: The target located on composite panel

Table 5.6: The ballistic armors against 7.62 mm AP projectiles were produced from various materials.

Material	Thickness (mm)	Areal density (g/cm^2)	Velocity (m/s)
Aluminum alloy	70	10-11.5	782±5.4
Multi layer metallic plates (steel/aluminum)	12-40	8.1-15.0	775-950
Alumina ceramic bonded steel	9-12	9.4-16.5	-
Composite based alumina ceramic/stainless/Kevlar™ reinforced benzoxazine alloy	22	7.1	838
E-Glass + S-Glass fibers (at same weight)	-	4.9	843
S-glass/Phenolic resin	-	4.9	890

CHAPTER VI

CONCLUSIONS

In this research, the ballistic armor based on fiber composite was studied. The glass fiber reinforced benzoxazine resin was used as strike face whereas Kevlar™ fiber-reinforced benzoxazine alloy was armor backing plate. The suitable matrix alloy composition based on benzoxazine, and urethane resins for glass fiber and Kevlar™ fiber-reinforced composites were determined. The criteria for the evaluation of the optimal resin mixture compositions were thermal stability, mechanical properties and ballistic impact resistance of the obtained composite materials.

The structure of benzoxazine resin and urethane prepolymer were successfully synthesized as confirmed using ^{1}H NMR.

In situ FT-IR analysis confirmed the curing process of BA-a/PU matrices and evaluated the degree of curing conversion.

Processing condition of the BA-a/PU composites at 150^{o}C for 1 hour and 200^{o}C for 2 hours was achieved the fully cured stage.

Comparing two types of fibers, the glass fiber reinforced with benzoxazine resin suitable to cooperate with Kevlar™ composite.

T_g and activation energy of the composites increased with increasing PU contents, which were higher than those of BA-a/PU alloys.

The presence of glass fiber and Kevlar™ fiber in the BA-a/PU alloys enhanced both the T_d and char yield of the obtained composites.

The flexural strain behavior of Kevlar™ composites increased with addition of urethane from 0 to 20 wt%. The improved flexibility of the Kevlar™ composites can provide more deflection during ballistic impact. The highest flexural strain at break value of Kevlar™ reinforced with benzoxazine-urethane alloy (80/20 BA-a/PU) was suitably chosen to be used as armor backing plate.

SEM observation showed fractured surfaces of glass fiber reinforced benzoxazine resin and Kevlar™ fiber reinforced benzoxazine urethane alloy (80/20 BA-a/PU). From the micrograph, the tight interfacial between fibers and matrix were observed that attributed to a good fiber-matrix interface.

The hard armor composite with approximately dimension 30 × 30 cm^2 consisted of 2 panels of glass fiber reinforced benzoxazine resin and 1 panel of Kevlar™ reinforced benzoxazine urethane alloy (80/20 BA-a/PU) can resist the penetration from 7.62 mm AP projectile (838 ± 15m/s) equivalent to level III of NIJ standard. The total weight, thickness and areal density of the hard armor composite were about 4.6 kg, 31.5 mm and 4.3 g/cm^2 respectively.

REFERENCES

[1] Peter, F. M.; James, M. R.; Adam, J. B.; and Schwab, W. C. Ballistic Trauma. 2nd edition. London: Springer, 2005.

[2] Hartran, D. R.; Jutte, R. B.; and Rameg, T. W. Ballistic material, U.S. Patent 5,215,813 (1993).

[3] Grogan, J.; Tekalur, S. A.; Shukla, A.; Bogdanovich, A.; and Coffelt, R. A. Ballistic resistance of 2D and 3D woven sandwich composites. J. Sandwich Struct. Mater. 9 (2007): 283-302.

[4] Jacobs, M. J. N.; and Van Dingenen, J. L. J. Ballistic protection mechanisms in personal armour. J. Mater. Sci. 36 (2001): 3137-3142.

[5] Nunes, L. M.; Paciornik, S.; and d'Almeida, J. R. M. Evaluation of the damaged area of glass-fiber-reinforced epoxy-matrix composite materials submitted to ballistic impacts. Compos. Sci. and Technol. 64 (2004): 945-954.

[6] Larsson, F.; and Svensson, L. Carbon, polyethylene and PBO hybrid fibre composites for structural lightweight armour. Composites Part A. 33 (2002): 221-231.

[7] Rimdusit, S.; Pirstpindvong, S.; Tanthapanichakoon, W.; and Damrongsakkul, S. Toughening of polybenzoxazine by alloying with urethane prepolymer and flexible epoxy: comparative study. Polym. Eng. Sci., 45 (2005) 288-297.

[8] Liengvachiranon, C. Effect of Types of Isocyanates on Mechanical and Thermal Properties of Benzoxazine and Urethane Polymer Alloys Master's degree. Department of Chemical Engineering, Faculty of Engineering, Chulalongkorn University, 2006.

[9] Pathomsap, S. Development of Ballistic Armor from Kevlar Fiber and Polybenzoxazine Alloys Master's degree. Department of Chemical Engineering, Faculty of Engineering, Chulalongkorn University, 2005.

[10] Birley, A. W.; and Heath, R. J. Plastics Materials Properties and Applications. 2nd edition. Glasgow: Blackie, (1988).

[11] Mallick, P. K. Fiber-Reinforce Composite: Material, Manufacturing, and Design, New York: Marcel Dekker, Inc. (1993).

[12] Ghosh, N. N.; Kiskan, B.; and Yagci, Y. Polybenzoxazines-New high performance thermosetting resins: Synthesis and properties. Prog. Polym. Sci. 32 (2007): 1344-1391.

[13] Holly, F. W.; and Cope, A. C. Condensation products of aldehydes and ketones with o-aminobenzyl alcohol and o-hydroxybenzylamine. J. Am. Chem. Soc. 66 (1944): 1875-1879.

[14] Ishida, H. Process for preparation of benzoxazine compounds in solventless systems. U. S. Patent 543,516 (1996).

[15] Ishida, H.; and Allen, D. J. Mechanical characterization of copolymers based on benzoxazine and epoxy, Polymer. 37 (1996): 4487-4495.

[16] Ning, X.; and Ishida, H. Phenolic materials via ring-opening polymerization of benzoxazines: effect of molecular structure on mechanical and dynamic mechanical properties. J. Polym. Sci. Part B. 32 (1994): 921-927.

[17] Ishida, H.; and Sanders, D. P. Improved Thermal and Mechanical Properties of Polybenzoxazines Based on Alkyl-Substituted Aromatic Amines. J. Polym. Sci., Part B. Polym. Phys. 38 (2000): 3289-3301.

[18] Nair, C. P. R. Advances in addition-cure phenolic resins. Prog. Polym. Sci. 29 (2004): 401- 498.

[19] Wood, G. The ICI polyurethanes book. 2nd edition. Singapore: John Wiley&Sons, 1990.

[20] Hepburn, C. Polyurethane elastomers. 2nd edition. London: Elsevier Science Publishing, 1992.

[21] Takeichi, T.; Guo, Y.; and Agag, T. Synthesis and characterization of poly (urethane-benzoxazine) films as novel type of polyurethance/phenolic resin Composites. J. Polym. Sci. Part A. Polym Chem. 38 (2000): 4165-4176.

[22] Lawrence, E. N.; and Robert, F. L. Mechanical properties of polymers and composites. 2nd ed. New York: Marcel Dekker, Inc., 1994.

[23] Chawla, K. K. Fibrous materials, New York: Cambridge University Press, 1998.

[24] Chand, S. Review carbon fiber for composites. J. Mater. Sci. 35 (2000): 1303-1313.

[25] Smith, W. F.; and Hashemi, J. Foundations of Materials Science and Engineering, New York: The McGraw-Hill Companies Inc., 2006.

[26] Bansal, P. N. Handbook of Ceramic Composites, New York. Kluwer Academic Publishers., 2005.

[27] Tan, V. B. C.; Shim, V. P. W.; and Zeng, X. Modelling crimp in woven fabrics subjected to ballistic impact. Int. J. Impact Eng. 32 (2005): 561-574.

[28] Lee, L.; Rudov-Clark, S.; Mouritz, A. P.; Bannister, M. K.; and Herszberg, I. Effect of weaving damage on the tensile properties of three-dimensional woven composites. Compos. Struct. 57 (2002): 405-413.

[29] Cunniff, P. M. "An analysis of the system effects of woven fabrics under ballistic impact". Text Res J. 62 (1992): 495-509.

[30] Duan, Y.; Keefe, M.; and Bogetti, T. A. Cheeseman BA. Modeling the impact behavior of high-strength fabric structures. Presented at the Fiber Society Annual Technical Conference, Natick, Massachusetts. 16-18 October 2002.

[31] Morye, S. S.; Hine, P. J.; Duckett , R. A.; Carr, D. J.; and Ward, I. M. Modeling of the energy absorption by polymer composites upon ballistic impact. Compos. Sci. Technol., 60 (2000) 2631-2642.

[32] Slater., P. A. Ballistic amour composites. EROPEAN. Patent 94302402.6 (1994).

[33] Epel, J. N. Fibrous armor material. U.S. Patent 4,369,387 (1987).

[34] Park, A. D. Ballistic laminate structure in sheet form. U.S. Patent 5,395,678 (1996).

[35] Denommee, D. R. Method of making deep draw laminate articles. U.S. Patent 3,956,447 (1976).

[36] Park, A. D. Method for fabricating a ballistic laminate structure. U.S. Patent 5,547,536 (1999).

[37] Coppage, J.; Edward, A.; and Richard, W. Anti-ballistic protective composite fabric. U.S. Patent 6,127,291 (2000).

[38] Hunt, B. J.; and James, M. I. Polymer Characterization. New York, John Wiley & Sons, 1993.

[39] Yang, H. H. Kevlar Aramid Fiber. West Sussex, John Wiley&Sons, 1993.

[40] Ishida, H.; and Allen, D. J. Physical and mechanical characterization of near-zero shrinkage polybenzoxazines. J. Polym. Sci. 34 (1996): 1019-1030.

[41] Rimdusit, S.; and Ishida, H. Synergism and multiple mechanical relaxations observed in ternary systems based on benzoxazine, epoxy, and phenolic resins. J. Polym. Sci. Part B; Polym. Phys. 38 (2000): 1687-1698.

[42] Ishida, H.; and Chaisuwan, T. Mechanical property improvement of carbon fiber reinforce polybenzoxazine by rubber interlayer. Polym. Compos. 24 (2003): 597-607.

[43] Lin, S. P.; Han, J. L.; Yeh, J. T.; Chang, F. C.; and Hsieh, K. H. Composites of UHMWPE fiber reinforced PU/epoxy grafted interpenetrating polymer networks Eur Polym J. 45 (2009): 494-502.

[44] Pilpel, D. E. Composite laminate and method of manufacture. U.S. Patent 0044659 A1 (2008).

[45] Pilpel, D. E.; Richard, H.; and Johnson, R. S. S. Composite ballistic panels and method of use. U.S. Patent 7,598,185 B2 (2009).

[46] Tanoglu, M.; and Seyhan, T. A. Investigating the effect of a polyester performing binder on the mechanical and ballistic performance of E-glass fiber reinforced polyester composites. Int Adhes Adhes 23 (2003): 1-8.

[47] Naik, N. K.; Shrirao, P.; and Reddy, B. C. K. Ballistic impact behaviour of woven fabric composites: Parametric studies. Mater. Sci. Eng., A. 412 (2005): 104-116.

[48] Gellert, E. P.; and Pattie, S. D. Woodward, R. L. Energy transfer in ballistic perforation of fiber reinforce composites. J. Mater. Sci. 33 (1998): 14885-1850.

[49] Pegoraro, M.; Galbiati, A.; and Ricca, G. ^{1}H nuclear magnetic resonance study of polyurethane prepolymers from toluene diisocyanate and polypropylene glycol. J. Appl. Polym. Sci. 87 (2003): 347-357.

[50] Takeichi, T.; Kano, T.; and Agag, T. Synthesis and thermal cure of high molecular weight polybenzoxazine precursors and the properties of the thermosets. Polymer 46 (2005): 12172-12180.

[51] Ishida, H.; and Low, H. Y. Synthesis of benzoxazine functional silane and adhesion properties of glass-fiber-reinforced polybenzoxazine composites. J. Appl. Polym. Sci. 69 (1998): 2559-2567.

[52] Ishida, H.; and Sanders, D. P. Regioselectivity and network structure of difunctional alkyl-substituted aromatic amine-based polybenzoxazines. Macromolecules 33 (2000): 8149-8157.

[53] Takeichi, T.; and Guo, Y. Preparation and properties of poly(urethane-benzoxazine)s based on monofunctional benzoxazine monomer. Polym. J. 33 (2001): 437-443.

[54] Nazipov, M. M.; Tabachkov, A. A.; Elchueva, A. D.; and Liakumovich, A. G. Urethane formation in the presence of stabilizers. Russ. J. of Appl. Chem. 74 (2001): 149-153.

[55] Lapprand, A.; Boisson, F.; Delolme, F.; Mechin, F.; and Pascault, J. P. Reactivity of isocyanates with urethanes: Conditions for allophanate formation. Polym. Degrad. Stab. 90 (2005): 363-373.

[56] Rimdusit, S.; Bangsen, W.; and Kasemsiri, P. Chemorheology and Thermomechanical Characteristics of Benzoxazine-Urethane Copolymers. J. Appl. Polym. Sci. 121 (2011): 3669-3678.

[57] Takeichi, T.; Guo, Y.; and Agag, T. Synthesis and characterization of poly(urethane-benzoxazine) films as novel type of polyurethane/phenolic resin composites. J. Polym. Sci., Part A: Polym. Chem. 38 (2000): 4165-4176.

[58] Ishida, H.; and Lee, Y. H. Study of hydrogen bonding and thermal properties of polybenzoxazine and poly-(epsilon-caprolactone) blends. J. Polym. Sci. Part B: Polym. Phys. 39 (2001): 736-749.

[59] Ardhyananta, H.; Kawauchi, T.; Ismail, H.; and Takeichi, T. Effect of pendant group of polysiloxanes on the thermal and mechanical properties of polybenzoxazine hybrids. Polymer 50 (2009): 5959-5969.

[60] Mines, R. A. W.; Roach, A. M.; and Jones, N. High velocity perforation behaviour of polymer composite laminates. Int. J. Impact Eng. 22 (1999): 561-588.

[61] Cheng, W. L.; Langlie, S.; and Itoh, S. High velocity impact of thick composites. Int. J. Impact Eng. 29 (2003): 167-184.

[62] Caprino, G.; Lopresto, V.; and Santoro, D. Ballistic impact behaviour of stitched graphite/epoxy laminates. Compos. Sci. Technol. 67 (2007): 325-335.

[63] Will, M. A.; Franz, T.; and Nurick, G. N. The effect of laminate stacking sequence of CFRP filament wound tubes subjected to projectile impact. Compos. Struct. 58 (2002): 259-270.

[64] Yungwirth, C. J.; O'Connor, J.; Zakraysek, A.; Deshpande, V. S.; and Wadley, H. N. G. Explorations of Hybrid Sandwich Panel Concepts for Projectile Impact Mitigation. J. Am. Ceram. Soc. 94 (2011): S62-S75.

[65] Bazhenov, S. Dissipation of energy by bulletproof aramid fabric. J. Mater. Sci. 32 (1997): 4167-4173.

[66] Vanaja, A.; and Rao, R. Fibre fraction effects on thermal degradation behaviour of GFRP, CFRP and hybrid composites. J. Reinf. Plast. Compos. 21 (2002): 1389-1398.

[67] Joseph, P. V.; Mathew, G.; Joseph, K.; Groeninckx, G.; and Thomas, S. Dynamic mechanical properties of short sisal fibre reinforced polypropylene composites. Composites Part A. 34 (2003): 275-290.

[68] Saw, S. K.; Sarkhel, G.; and Choudhury, A. Dynamic Mechanical Analysis of Randomly Oriented Short Bagasse/Coir Hybrid Fibre-Reinforced Epoxy Novolac Composites. Fibers Polym. 12 (2011): 506-513.

[69] Nayak, N.; Sivaraman, P.; Banerjee, A.; Madhu, V.; Dutta, A.L.; and Misha, B.C. Effect of Matrix on the Ballistic Impact of Aramid Fabric Composite Laminates by Armor Piercing Projectiles. Polym. Compos. 33 (2012): 443-450.

[70] Rimdusit, S.; Mongkhonsi, T.; Kamonchaivanich, P.; Sujirote, K.; and Thiptipakorn, S. Effects of Polyol Molecular Weight on Properties of Benzoxazine-Urethane Polymer Alloys. Polym. Eng. Sci. 48 (2008): 2238-2246.

[71] Hameed, N.; Sreekumar, P. A.; Thomas, P. S.; Jyotishkumar, P.; and Thomas, S. Mechanical Properties of Poly(styrene-co-acrylonitrile)-Modified Epoxy Resin/Glass Fiber Composites. J. Appl. Polym. Sci. 110 (2008): 3431-3438.

[72] Alagar, M.; Kumar, A. A.; Mahesh, K. P. O.; and Dinakaran, K. Studies on thermal and morphological characteristics of E-glass/Kevlar 49 reinforced siliconized epoxy composites. Eur. Polym. J. 36 (2000): 2449-2454.

[73] Brown, J. R.; and Mathys, Z. Plasma surface modification of advanced organic fibres .5. Effects on the mechanical properties of aramid/phenolic composites. J. Mater. Sci. 32 (1997): 2599-2604.

[74] Tan, V. B. C.; Lim, C. T.; and Cheong, C. H. Perforation of high-strength fabric by projectiles of different geometry. Int. J. Impact Eng. 28 (2003): 207-222.

[75] Demir, T.; Ubeyli, M.; and Yildirim, R. O. Investigation on the ballistic impact behavior of various alloys against 7.62 mm armor piercing projectile. Mater. Design. 29 (2008): 2009-2016.

[76] Flores-Johnson, E. A.; Saleh, M.; and Edwards, L. Ballistic performance of multi-layered metallic plates impacted by a 7.62-mm APM2 projectile. Int. J. Impact Eng. 38 (2011): 1022-1032.

[77] Ubeyli, M.; Deniz, H.; Demir, T.; Ogel, B.; Gurel, B.; and Keles, O. Ballistic impact performance of an armor material consisting of alumina and dual phase steel layers. Mater. Design. 32(2010): 1565-1570.

[78] Kamonchaivanich, P. Effects of Diol Molecular Weight on Properties of Benzoxazine-Urethane Polymer Alloys for Ballistic Armor Applications Master's degree. Department of Chemical Engineering, Faculty of Engineering, Chulalongkorn University, 2006.

APPENDICES

APPENDIX A

Characterization of Benzoxazine/Urethane Polymer Alloys

Appendix A-1 Curing temperature of BA-a/PU alloys.

BA-a/PU systems compositions	Curing temperature (^{o}C)	Heat of reaction (J/g)
100/0 BA-a/PU	226	272
90/10 BA-a/PU	234	228
80/20 BA-a/PU	243	205
70/30 BA-a/PU	245	165
60/40 BA-a/PU	247	153

Appendix A-2 Glass transition temperature of BA-a/PU alloys.

BA-a/PU systems compositions	Glass transition temperature (^{o}C)
100/0 BA-a/PU	161
90/10 BA-a/PU	173
80/20 BA-a/PU	182
70/30 BA-a/PU	220
60/40 BA-a/PU	241

APPENDIX B

Thermal characterization of fiber-reinforced benzoxazine/urethane alloys

Appendix B-1: Density of Kevlar™ Fiber-reinforced BA-a/PU Alloys

Composition (BA-a/PU)	Density (g/cm^3)	
	Theory	Actual
100/0	2.08 (a)	2.06 (a)
	1.374 (b)	1.305 (b)
90/10	1.370 (b)	1.328 (b)
80/20	1.365 (b)	1.330 (b)
70/30	1.361 (b)	1.327 (b)
60/40	1.341 (b)	1.302 (b)

(a): Glass fiber reinforced benzoxazine resin and (b): Kevlar™ fiber reinforced benzoxazine-urethane alloys.

Appendix B-2 Dynamic mechanical properties of fibers reinforced BA-a/PU alloys

BA-a/PU system compositions	Glass transition temperature (^{o}C)	Storage modulus (GPa)
100/0 BA-a/PU	182 (a)	25.57 (a)
	184 (b)	16.82 (b)
90/10 BA-a/PU	187 (b)	14.89 (b)
80/20 BA-a/PU	213 (b)	14.39 (b)
70/30 BA-a/PU	225 (b)	13.69 (b)
60/40 BA-a/PU	247 (b)	11.89 (b)

(a): Glass fiber reinforced benzoxazine resin and (b): Kevlar^{TM} fiber reinforced benzoxazine-urethane alloys.

APPENDIX C

LIST OF PUBLICATIONS

1. P. Kasemsiri, S. Hiziroglu, and S. Rimdusit, “Characterization of Heat Treated Eastern Redcedar (*Juniperus Virginiana L.*),” *J. Mater. Proc. Tech.*, 212(6), 1324 (2012).
2. P. Kasemsiri, S. Hiziroglu, and S. Rimdusit, ‘Properties of Wood Polymer Composites from Eastern Redcedar Particles Reinforced with Benzoxazine Resin/ Cashew Nut Shell Liquid Copolymer,” *Compos. A*, 42, 1454 (2011).
3. P. Kasemsiri, S. Hiziroglu, and S. Rimdusit, “Effect of Cashew Nut Shell Liquid on Gelation, Curing Kinetics, and Thermomechanical Properties of Benzoxazine Resin,” *Thermochim Acta*, 520, 84 (2011).
4. S. Rimdusit, S. Pathomsap, P. Kasemsiri, C. Jubsilp, and S.Tiptipakorn, “KevlarTM Fiber-Reinforced Polybenzoxazine Alloys for Ballistic Impact Applications,” *Eng. J*, 15(4), 24 (2011).
5. Y. Wang, W. Su, P. Kasemsiri, S. Hiziroglu, “A comparison of the withdrawal resistance load of nails using experimental and interference approaches,” *Wood Mater Sci Eng*, 6, 213 (2011).
6. S. Rimdusit, W. Bangsen, and P. Kasemsiri, “Chemorheology and Thermomechanical Characteristics of Benzoxazine-Urethane Copolymers,” *J. Appl. Polym. Sci.*, 121, 3669 (2011).
7. P. Kasemsiri, S. Hiziroglu, and S. Rimdusit, “Development of wood Composite from Eastern Redcedar Particles Reinforced with Benzoxazine Resin/Chashew Nut Shell Liquid Copolymer,” Proceeding of 3rd International Symposium on Network Polymers, Sept. 11-14, 2011, Toyohashi, Japan, p. 60 (Oral presentation).
8. P. Kasemsiri, J. Wakita, S. Ando, and S. Rimdusit, “Thermally Reversible Light Scattering Characteristics of Benzoxazine-Urethane Alloys,” Proceeding of 1st Polymer Conference of Thailand, Oct. 7-8, 2010, Bangkok, Thailand, p. 70 (Oral presentation).
9. P. Kasemsiri, S. Hiziroglu, and S. Rimdusit, “Development of Bamboo Fiber-reinforced with Benzoxazine/Cashew Nut Shell Liquid Oil Alloys,” Proceeding of Asian Conference on Thermal Analysis and Applications (ASTA 2009) Dec. 17-18, 2009. Bangkok, Thailand, p.126 (Oral presentation).

Journal of Materials Processing Technology 212 (2012) 1324–1330

Contents lists available at SciVerse ScienceDirect

Journal of Materials Processing Technology

journal homepage: www.elsevier.com/locate/jmatprotec

Characterization of heat treated eastern redcedar (*Juniperus virginiana* L.)

Pornnapa Kasemsiri[a], Salim Hiziroglu[b], Sarawut Rimdusit[a,*]

[a] Department of Chemical Engineering, Faculty of Engineering, Chulalongkorn University, Pathumwon, Bangkok 10330, Thailand
[b] Department of Natural Resource Ecology and Management, Oklahoma State University, 303-G Agricultural Hall, Stillwater, OK 74078, USA

ARTICLE INFO

Article history:
Received 19 June 2011
Received in revised form 6 December 2011
Accepted 31 December 2011
Available online 10 January 2012

Keywords:
Heat treatment
Redcedar
Shear strength
Surface roughness

ABSTRACT

The objective of the study is to investigate the influence of heat treatment on shrinkage, density, surface roughness, water absorption, diffusion coefficient, swelling and shear strength of eastern redcedar (*Juniperus virginiana* L.) samples. The anatomical structures of samples are also observed by scanning electron microscope (SEM). Specimens are exposed to temperature levels of 120 °C, 160 °C and 190 °C for time spans of 2 and 8 h. Based on the results of this study, dimensional stability in the form of shrinkage of the samples is improved by 2.68%, 1.40% and 1.49% for tangential, longitudinal and radial grain orientations as function of heat treatment, respectively. Heat treatment also enhances surface quality of the samples based on numerical values determined from stylus type of equipment. Water absorption, swelling values and diffusion coefficient of the samples are also reduced with heat treatment. Samples exposed to heat treatment have lower shear strength values, ranging from 25.12% to 52.67%, than those of control samples. It appears that all properties evaluated in this work are affected more pronouncedly as temperature and exposure time is increased.

1. Introduction

Eastern redcedar (*Juniperus virginiana* L.) is one of the most widely distributed indigenous conifers in the eastern US. Over seven million acres of Oklahoma lands are infested with redcedar (Payne et al., 1998). Miller (2007) observed that the heartwood of redcedar is bright or dull red, and the narrow sapwood is nearly white. The wood is dimensionally stable with low shrinkage and resistant to decay with fine and uniform texture. However, eastern redcedar is underutilized as raw material for lumber manufacture due to its low value and irregular growth patterns (Bidwell et al., 2000). Currently, the wood from eastern redcedar is used for fence posts and novelty items. Eastern redcedar has encroached on 10.2 million acres in Texas and Oklahoma and there have been effort to control this species (Alemayehu et al., 1998). Eastern redcedar has serious adverse environmental impact such as degrading grasslands, increasing wildfire hazard and displacing native wildlife and plant populations reported by Hiziroglu (2007).

Properties of eastern redcedar can be improved using alternative approaches to make this species more desirable to manufacture value-added products with possible potential opportunities. Heat treatment is one of the processes which are used to enhance properties of wood. This process is also considered as eco-friendly alternative to chemically impregnated wood materials. Stamm (1956) concluded that the obtained woods properties from heat treatment process depended on several factors i.e. time, temperature, treatment atmosphere, wood species, moisture content, wood dimension and the use of a catalyst. Korkut et al. (2008) reported that the chemical modifications that occur in wood at high temperatures are accompanied by several favorable changes for its physical properties including reduced shrinkage and swelling, improved biological durability, low equilibrium moisture content, enhanced weather resistance, better thermal insulation properties and stronger decay resistance. Kocaefe et al. (2008) studied the wetting characteristics of heat treated wood by contact angle measurement. The treated wood becomes more hydrophobic which is the important factor of resistant biological attack and dimensional stability. Therefore, the heat treatment process can be used as an alternative method to make low-value wood species imitating the appearance of high-value species proposed by Gunduz et al. (2009).

Generally, the temperature and duration for heat treatment of wood varies from 180 °C to 280 °C and from 15 min to 24 h, respectively, depending on the heat treatment process, wood species, sample size, moisture content of sample, desired target mechanical properties, resistance to biological degradation and dimensional stability of the final product as observed by Kamdem et al. (2002). Temperature level has a greater influence on properties of wood than exposure time. The physical and chemical properties of wood permanently change at temperature about 150 °C and it continues with increasing temperature as reported in previous work (Mitchell, 1988).

* Corresponding author. Tel.: +662 218 6862; fax: +662 218 6877.
E-mail address: sarawut.r@chula.ac.th (S. Rimdusit).

0924-0136/$ – see front matter © 2012 Elsevier B.V. All rights reserved.
doi:10.1016/j.jmatprotec.2011.12.019

A study carried out by Korkut and Guller (2008) investigated the effects of heat treatment on physical properties and surface roughness of redbud maple. Swelling reduction in radial, tangential and longitudinal grain orientations of the treated samples at a temperature of 180 °C for 10 h was found to be 23.43%, 34.64%, and 20.04%, respectively. Such reduction rates of the samples resulting in enhanced dimensional stability are desired for better utilization of wood products. The average surface roughness (R_a) of these samples also decreased up to 15.06%. The increase in smoothness of wood is very important for some applications such as finishing and gluing in veneers. Dundar et al. (2008) concluded that veneers with rough surface of wood cause excessive resin use and may result in resin-bleed through the face veneer. In another study, the effects of thermal treatment on the mechanical and physical properties of Wild pear wood were evaluated by Gunduz et al. (2009). The thermal treatment of the samples at 160 °C for 2 h increased modulus of elasticity about 5% (from 6.27 GPa to 7.06 GPa) while their bending strength and compression strength values decreased by 7.42% and 7.55%, respectively. The swelling properties of Wild pear wood in tangential, radial and longitudinal grain orientations improved as 2.6%, 5.3%, and 8.5% swelling, respectively, as a result of heat treatment. The effect of heat treatment on mechanical properties of hazelnut wood was also studied by Korkut and Hiziroglu (2009). Maximum reduction values of 68.11%, 64.97%, and 58.75% were determined for Janka-hardness in radial, tangential grain orientations, and tension strength parallel to grain for the samples exposed to a temperature of 180 °C for 10 h, respectively. It is important that improved dimensional stability of heat-treated timber has to be balanced against the decrease in overall strength values when evaluating the effectiveness of using heat treatment for any applications. For example, the heat treatment process was applied to use with surface densification technique investigated by Gong et al. (2010) and also the interactive effect of surface densification and post heat treatment of aspen was studied. In general, the heat treatment at high temperature can assist in solving the unstable dimensional densified wood products. The densified aspen samples exposed to a temperature in ranging of 190–210 °C showed that their dimensional stability significantly improved with the observation in the reduction of radial swelling of samples from 32 to 9%.

As mentioned above various properties of heat treated different species have been reported in literature. However currently there is little information about the influence of heat treatment on some properties such as swelling, surface roughness, shear strength of eastern redcedar. Therefore the objective of this work was to evaluate various physical and shear strength properties of eastern redcedar to provide an initial data so that such treated species can be used more efficiently and effectively as value added product.

2. Materials and methods

The 70 defect free samples with dimension of 20 mm × 45 mm × 50 mm were cut from commercially produced flat sawn lumber supplied by a local sawmill. The specimens were sanded with sandpaper having 120 grits by applying 10 light strokes to each surface before they were conditioned at temperature of 20 °C with 65% relative humidity to have 12% equilibrium moisture content. Fig. 1 illustrates size and grain orientation of the samples used for the experiments. Dimension of each sample were measured and they were weighted at accuracy of 0.01 mm and 0.01 g, respectively. The density, shrinkage and roughness tests were carried out on the same samples.

Surface roughness of samples was measured by employing a fine stylus profilemeter Hommel T-500 unit equipped with a TK-300 skidless type pick-up. Five random measurements were taken

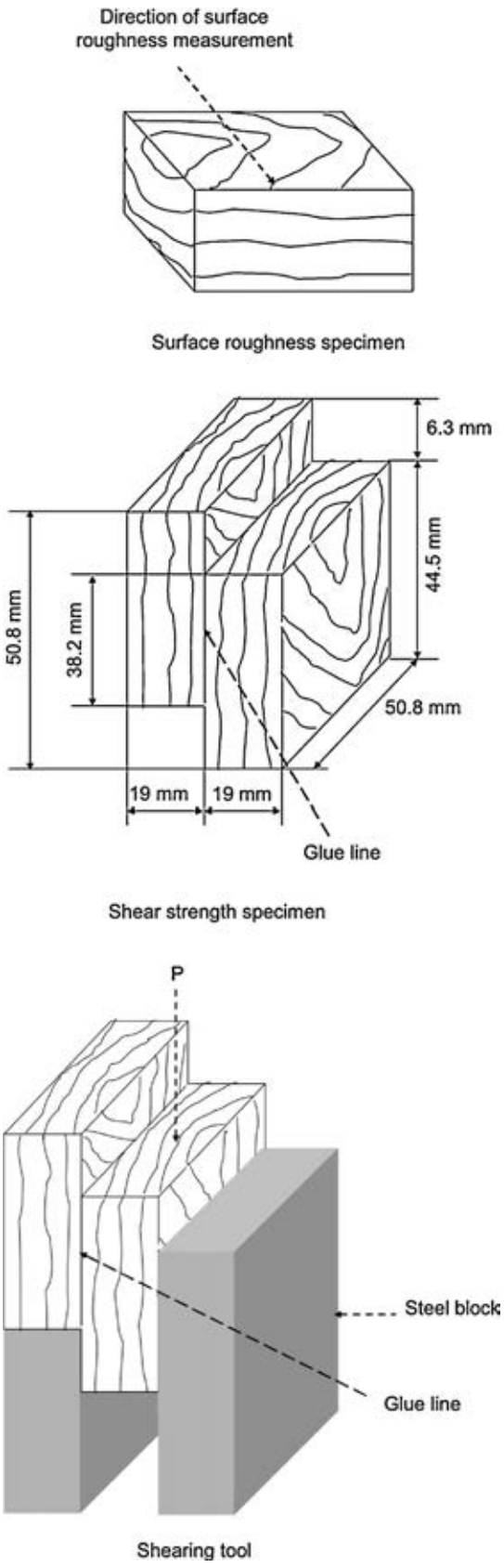

Fig. 1. Surface roughness specimens and shear strength test specimens.

from surface of sample to evaluate surface characteristics at different thermal treatment conditions. Three roughness parameters, namely average roughness (R_a), mean peak-to-valley height (R_z) and maximum roughness (R_{max}) were used to evaluate surface quality of the samples. Definitions of such roughness parameters and specifications of stylus type equipment were described by Mummery (1993). These parameters were commonly used in previous work to evaluate surface characteristic of wood products as reported by Hiziroglu (1996). Swelling measurements on the samples were conducted to 0.01 mm accuracy at three different marked positions before and after heat treatment process. Water absorption and thickness swelling characteristics of the samples were also conducted based on ASTM D 570-08. Before any testing was carried out, the thickness and weight of each sample were measured. All samples were submerged in distilled water. The samples were removed from the water tank, rinsed, wiped, weighed before they were returned to water tank at each level. The amount of water absorbed was calculated based on the mass of each sample at initial condition.

For shear strength experiment, polyvinlyacetate (PVAc) purchased from Elmer's Products, Inc. was used as adhesive applied on the both surfaces of each shear pair by brushing at a spread rate of 120 g/m^2. After adhesive application, the specimens were pressed together using a light pressure of 655 g/cm^2 for 24 h at room temperature. A total of 35 specimens were prepared for shear strength tests based on ASTM 905-03. The schematic of the test sample and shearing tool are illustrated in Fig. 1. The shear strength values of samples were determined on a Comten testing Unit equipped with a load cell having capacity of 1000 kg. The loading speed of machine during testing was adjusted to 5 mm/min.

The anatomical structures of samples were investigated by SEM. The untreated and heat treated sample (approximately 3 mm × 3 mm × 3 mm) were scraped with a blade. The sample were put under vacuum and coated with a thin film of gold using an ion sputtering device, before micrographs of the surfaces were taken.

3. Results and discussion

Table 1 displays densities and surface roughness values of all samples exposed to different heat treatments.

In general air-dry density and densities of the samples determined following each heat treatment decreased insignificantly as function of temperature and exposure time as can be seen in Table 2.

Sample exposed to a temperature of 120 °C for 2 h had the lowest density reduction as 2.10% as compared to those exposed 190 °C for 8 h having 3.25%. It seems that temperature was more prominent factor influencing reduction of density of the sample than exposure time. Similar findings were also observed in a previous work involved with heat treatment of oak samples. Korkut et al. (2010) observed that the average roughness surface of heat treated Sessile Oak had improved values up to 25.67%. This observation is in good agreement with our work. It is a well-known fact that heat treatment reduces the hydrophilic behavior of the modified wood (Homan et al., 2000) and the chemical structure of some of its elements (Raimo et al., 1996).

Table 1
Average density, surface roughness and shear strength values of the samples (values in parenthesis are standard deviation).

Heat treatment	Density	Surface roughness (μm)		
	(g/cm^3)	R_{max}	R_z	R_a
Control sample	0.49 (0.06)	46.19 (8.02)	45.88 (8.26)	5.81 (1.17)
120 °C (2 h)	0.48 (0.06)	44.71 (7.42)	33.32 (6.91)	4.43 (0.86)
120 °C (8 h)	0.46 (0.05)	40.45 (7.39)	28.96 (6.30)	4.07 (0.95)
160 °C (2 h)	0.47 (0.04)	39.33 (4.51)	30.54 (4.11)	3.86 (0.63)
160 °C (8 h)	0.45 (0.06)	37.74 (5.84)	28.77 (5.04)	3.33 (0.77)
190 °C (2 h)	0.47 (0.05)	36.45 (6.92)	27.18 (5.52)	2.25 (0.81)
190 °C (8 h)	0.44 (0.05)	31.11 (6.67)	23.67 (5.20)	1.72 (0.90)

Shrinkage reduction values of heat treated eastern redcedar specimens in three grain orientations are also summarized in Table 2. The lowest shrinkage reduction values were 2.52%, 1.09%, 1.27% for the samples exposed to a temperature of 120 °C for 2 h along tangential, longitudinal and radial grain orientations, respectively. These values were followed by the samples exposed to the same temperature for 8 h. Based on statistical analysis no significant difference was found for shrinkage values among the sample exposed temperature levels of 120 °C, 160 °C for 2 h and 8 h as well as 190 °C for 2 h at 95% confidence level. However, the sample exposed to 170 °C for 8 h resulted in significant difference in their shrinkage reduction values as compared to those of exposed 120 °C and 160 °C for both time spans. In general tangential shrinkage reduction values were determined higher than those of both radial and longitudinal values. This is an expected result since wood has the highest dimensional instability in tangential direction due to vertical orientation of microfibrils in S2 layer of the cell wall. This observation is in good agreement with previous work concluded by Barnett and Bonham (2004). The orientation of cellulose microfibrils, S2 layer made up the greatest proportion of the cell wall thickness. Therefore it was the important part which affected the physical properties such as shrinkage. Modification in chemical structure of components as mentioned above prevents the re-absorption of water molecules which have tendency attaching between and within the wood polymers, lignin, cellulose and hemicellulose. Esteves et al. (2007) reported that during heat treatment number of hydroxyl group is decreased and replaced with hydrophobic acetyl groups resulting in crosslinking between wood fibers. Such phenomenon improves dimensional stability of heat treated wood. Reduction in shrinkage values of eastern redcedar samples determined in this work resulted in lower than those observed for different species including oak in past work (Korkut et al., 2010).

Eastern redcedar has approximately 3.8% oil in its heartwood. Most of the samples used in this work had almost 95% heartwood portion of the wood with limited sapwood where there is only 1% or less oil exists. It is appears that oil should have acted some kind of barrier to heat treatment in contrast to other species

Table 2
Percent decrease in properties of treated eastern redcedar samples.

Heat treatment	Density	Shrinkage			Surface roughness		
		Tangential	Longitudinal	Radial	R_{max}	R_z	R_a
Control sample	0	0	0	0	0	0	0
120 °C (2 h)	2.10	2.52	1.09	1.27	2.41	4.66	4.52
120 °C (8 h)	2.29	2.53	1.10	1.29	2.99	5.66	5.20
160 °C (2 h)	2.47	2.56	1.27	1.39	2.76	4.80	4.78
160 °C (8 h)	2.80	2.56	1.29	1.41	4.89	7.22	5.90
190 °C (2 h)	2.63	2.57	1.38	1.45	4.29	5.57	5.90
190 °C (8 h)	3.25	2.68	1.40	1.50	8.38	9.62	10.11

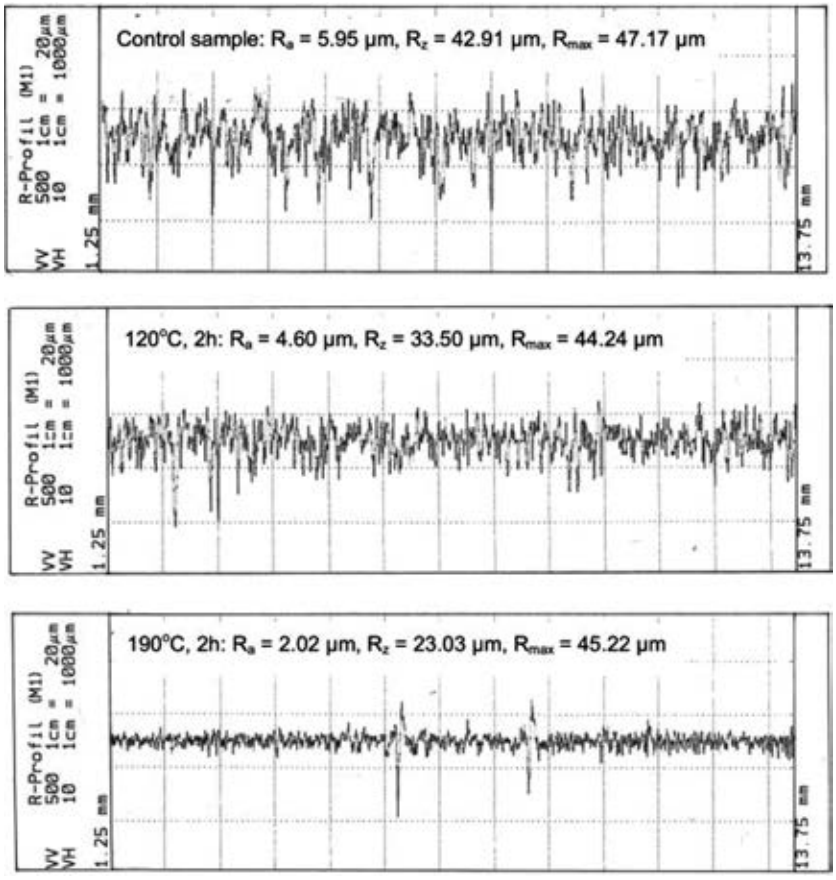

Fig. 2. Typical roughness profiles of the samples.

without having oil or other extractives in their heartwood. Therefore, reduction values in shrinkage characteristic of the samples were not more than 2.68% as in case of samples exposed to a temperature of 190 °C for 8 h. The reduction shrinkage results in the enhancement of dimensional stability which is desirable for applications such as for garden, kitchen, sauna furniture, cladding on wooden building, bathroom cabinets, floor material, musical instruments, ceilings, inner and outer bricks, doors and window joinery and a variety of other outdoor and indoor uses.

Kilic et al. (2008) observed surface roughness of samples using a fine stylus method. One of the advantages of this method is to obtain actual profile of surface and standard numerical roughness parameters, which can be calculated from the profile. Fig. 2 presents the typical profiles of treated samples at 120 °C for 2 h and 190 °C for 2 h compared with a control sample.

The surface roughness of the samples treated at three temperature levels for two the spans improved with increasing with temperature and heat exposure time, as displayed in Table 1 and Fig. 3.

While control samples had an average R_a value of 5.81 μm and 3.87 μm was determined for the specimens exposed to a temperature of 170 °C for 8 h. No significant difference was found between surface quality of the control samples and those exposed to 120 °C. However the samples exposed to 160 °C and above had substantially enhanced surface quality. For example R_a value of 3.86 μm was determined for the sample treated at temperature of 160 °C for 2 h which is 1.5 times lower than that of control sample. High temperature causes conversion of lignin into a thermoplastic condition resulting in densification and compacting of the surface roughness of the samples. Such observation was also main conclusion of past studies (Korkut et al., 2010). Rough surface of wood members can easily be eliminated by sanding however such process will not only increase overall production cost but also will cause dust problem during manufacture. Therefore, heat treatment of redcedar would be considered as alternative method to enhance its surface quality for further production steps.

Based on visual observation from photographs taken from SEM it seems that cross section of heat treated samples had rather clean

Table 3
Effect of heat treatment on water absorption, swelling and diffusion coefficients.

Heat treatment	Water absorption (%)	Swelling (%)		Diffusion coefficient ($\times 10^{-12}$ m^2/s)	
		Tangential	Radial	Tangential	Radial
Control sample	59.07	2.41	1.42	1.54	1.02
120 °C (2 h)	55.22	2.22	1.34	1.49	0.99
120 °C (8 h)	52.05	2.10	1.27	1.46	0.97
160 °C (2 h)	47.14	1.83	1.25	1.33	0.91
160 °C (8 h)	41.66	1.77	1.13	1.31	0.87
190 °C (2 h)	36.29	1.62	1.08	1.28	0.83
190 °C (8 h)	31.19	1.58	0.95	1.23	0.78

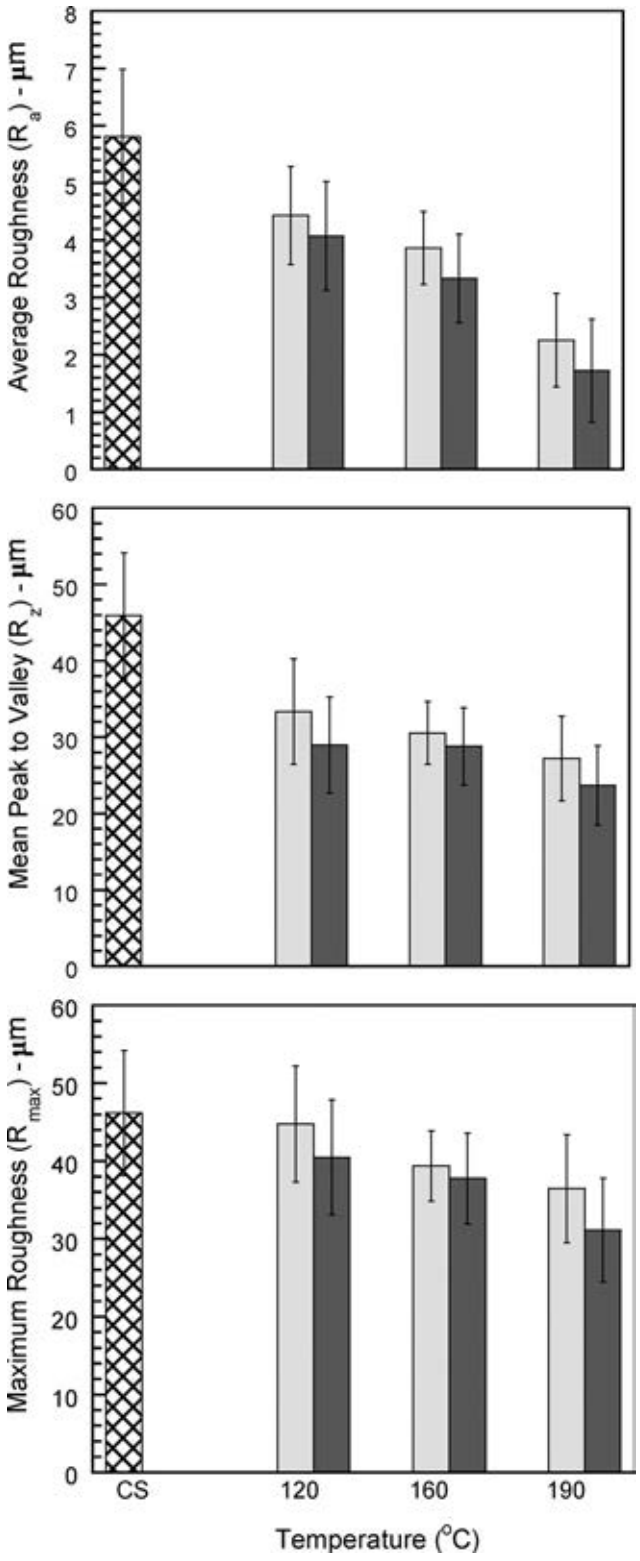

Fig. 3. Surface roughness values of the samples as function of heat treatment: (▨) control sample, (□) heat treatment at 2 h and (■) heat treatment at 8 h.

and smooth surface. Although some of the fibers are broken due to cut performed on control samples, it is still clear that heat treatment simply eliminated some of the small and broken fibers from the cell lumen as well as on the surface of the samples as can be seen from the photographs of the samples exposed to 120 and 160 °C for 2 h in Fig. 4. Surface roughness evaluation of the samples also revealed that heat treatment enhanced their smoothness.

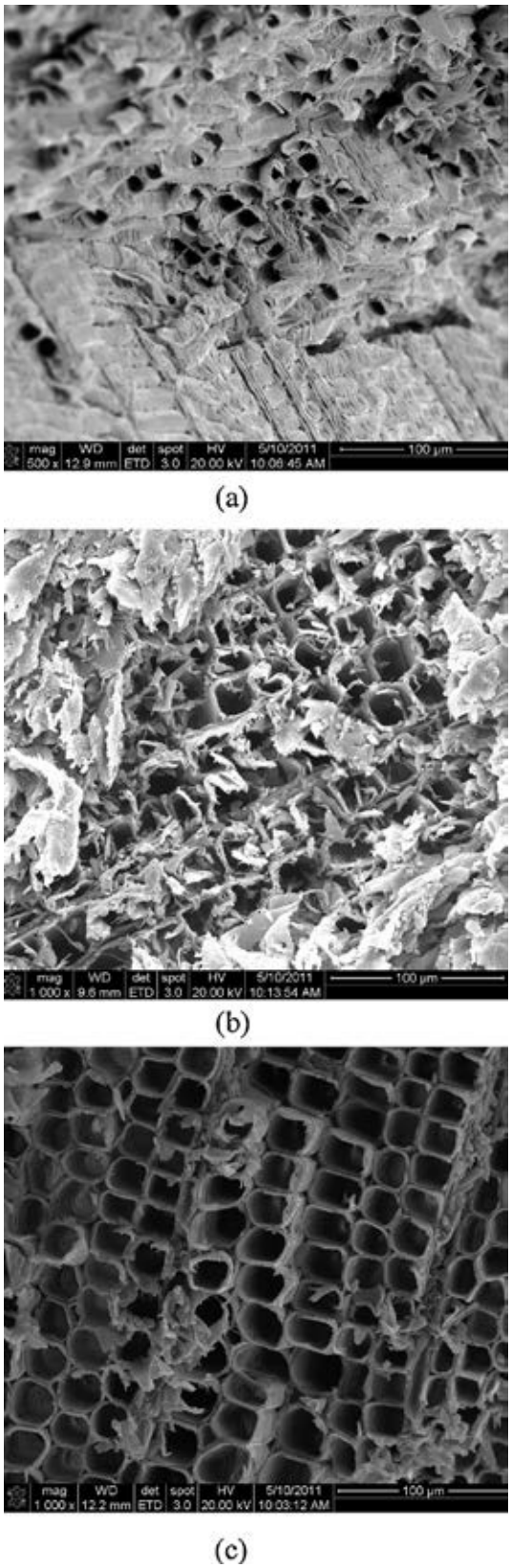

Fig. 4. Micrographs taken from cross-section of the samples by SEM: (a) control sample, (b) treated sample at 160 °C for 2 h and (c) treated sample at 190 °C for 2 h.

The values of water absorption for the heat treated redcedar are depicted in Fig. 5. The percentage of water absorbed plotted against time for all samples showed the similar behavior. The water adsorption values of the untreated and treated samples were in the

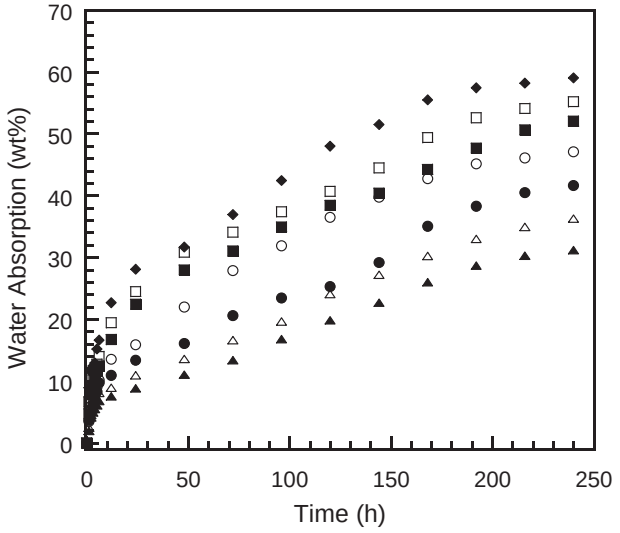

Fig. 5. Percentage water absorption of the samples at various heat treatment conditions: (♦) control sample, (□) 120 °C for 2 h, (■) 120 °C for 8 h, (○) 160 °C for 2 h, (●) 160 °C for 8 h, (△) 190 °C for 2 h and (▲) 190 °C for 8 h.

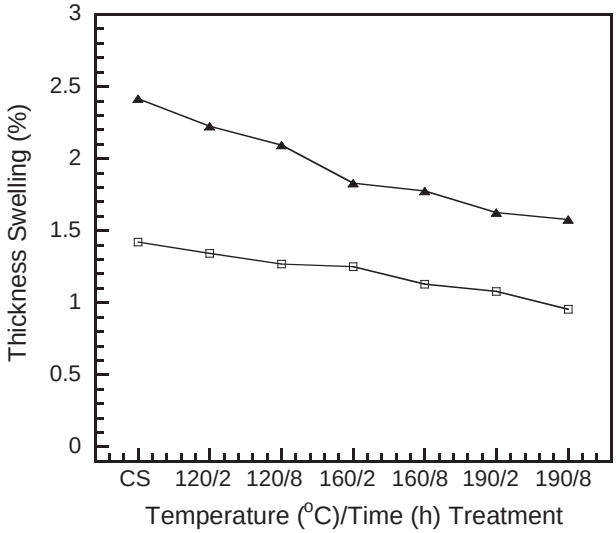

Fig. 6. Percentage thickness swelling of the samples at grain orientations: (▲) tangential grain orientation and (□) radial grain orientation.

range of 31.19–59.07% after 240 h of exposure as summarized in Table 3.

Furthermore, the water absorption of treated samples also decreased with increasing temperature and duration time of heat treatment process. This is due to the fact that heat treatment affects the wood cell polymers which consist of hemicellulose, cellulose and lignin. Among these compositions, Kocaefe et al. (2010) observed that hemicelluloses are greatly prone to thermal degradation during the treatment whereas cellulose and lignin are somewhat modified. The degradation of hemicelluloses causes of releasing of the organic acids which influences the cross-linking reduction in hydroxyl groups (OH—) and cleavage of the lignin–polysaccharide complex. The decrease in hydroxyl groups also increases the hydrophobicity of wood and results in reduction of the water absorption.

When wood is soaked in water or any liquids the liquid enters the wood up to a content which is far beyond the fiber saturation point. It is a well-known fact that all properties of wood can be influenced from water sorption. Therefore, the sorption behavior and diffusion process of solid wood are interesting for utilizations such a method by evaluating its in-service performance to help understand mold growth on wood, and for evaluating drying kinetics in wood (Neimsuwan et al., 2008). El kouali et al. (1992) investigated the diffusivity of water in wood specimens. The diffusivity can be calculated from the straight line obtained by plotting the amount of water transported through the corresponding axis as a function of the square root of time:

$$\frac{Q_t}{Q_\alpha} = \frac{4}{Th}\left(\frac{D}{\pi}\right)^{0.5} t^{0.5} \quad (1)$$

where D is diffusion coefficient, Th is the thickness of sample in tangential and radial direction, Q_t is the moisture content at time t; and Q_α the moisture content at equilibrium.

The obtained values from the fitting are shown in Table 3. The diffusion coefficient values of all samples had trend of decrease with increasing the temperature and duration time of heat treatment. This implies that the inclusion of water molecules in treated sample is less than those of control sample due to the changing structure of wood as discussed in the result of water absorption.

The percentage of swelling values in tangential and radial grain orientation of sample after immersion in water 240 h is shown in Fig. 6 and Table 3.

Both radial and tangential swelling value of treated samples significantly decreased as compared to those of untreated sample. The highest decrease of swelling value was determined for treatment condition of 190 °C for 8 h. These results also corresponded with the water absorption and diffusion coefficient of samples i.e. treated specimens had less amount of water in wood cell wall and the slow water uptake due to the decrease of the amount of wood's hydroxyl groups. As a consequence of the reduced number of hydroxyl groups the swelling of treated samples were lower as in the case of Black pine observed by Gunduz et al. (2009) (19.13% in radial and 37.61% in tangential) and Wild pear reported by Gunduz et al. (2008) (3.52% in radial and 5.29% in tangential) when the samples were compared at the same heat treatment condition. The reduction of both water absorption and swelling result in an increase in dimensional stability required for several application of wood.

The average shear strength values of the samples are presented in Fig. 7. Overall shear strength of eastern redcedar specimens decreased due to heat treatment.

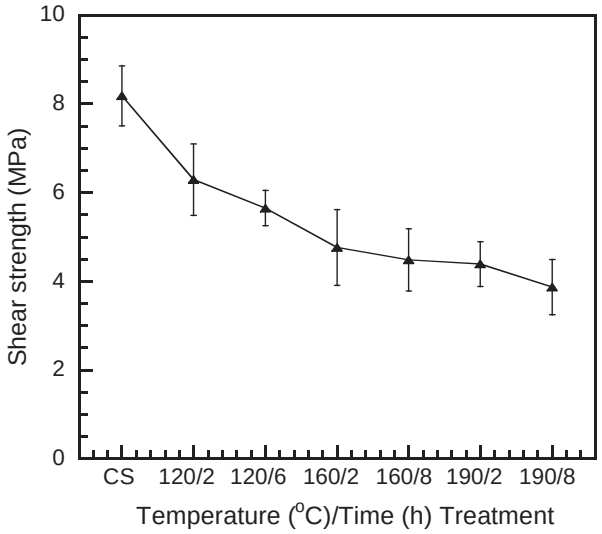

Fig. 7. Shear strength values of the samples as function of heat treatment.

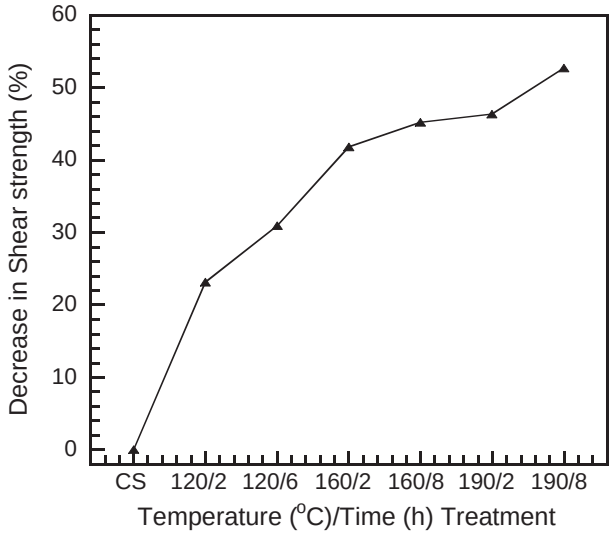

Fig. 8. Percentage decrease in shear strength values of the samples as function of heat treatment.

Such reduction was noticeable for even samples exposed to a temperature of 120 °C for 2 h having 23% reduction in the shear strength value. Maximum value was 52% for the samples exposed to 190 °C for 8 h as illustrated in Fig. 8.

There are past studies carried out to evaluate effect of heat treatment on mechanical properties of different species and they all concluded adverse influence of heat treatment on mechanical properties of the specimens such a Wild pear (Gunduz et al., 2009), Scot pine (Korkut et al., 2008), and Hazelnut wood (Korkut and Hiziroglu, 2009). Unfortunately thermal degradation and loss of chemical elements of wood is a major parameter which is responsible for negative impact of heat treatment on mechanical characteristics of the sample as reported by Yildiz et al. (2006). Kartal et al. (2008) also observed that depolymerization reactions of wood polymer including changes and loss of hemicellulose play an important role on such results of heat treated wood.

4. Conclusions

This study investigated effect of heat treatment on chemical stability, surface roughness and shear strength of eastern redcedar samples. It was observed that heat treatment has limited benefits on dimensional stability of eastern redcedar. Surface quality of the samples was enhanced noticeably as a result of heat treatment. On the other hand, shear strength of the samples tended to decrease with heat treatment. Therefore heat treatment of eastern redcedar is not recommended for applications to be used where constructional strength properties are critically desired. However, such treatment would be considered to improve surface quality of the sample for furniture and craft applications where smooth surface of the members is ideal. In further studies, it would be desirable to determine bonding and other mechanical properties such as hardness of eastern redcedar as function of temperature and exposure time to have a better understanding of heat treatment on properties of such species.

Acknowledgements

This research receives financial support from Dutsadi Phiphat Scholarship of Chulalongkorn University. Additional supports are from the Higher Education Research Promotion and National Research University Project of Thailand, Office of the Higher Education Commission (AM1076A) and 100th Anniversary of Chulalongkorn University Academic Funding. Support from Robert M. Kerr Food and Agricultural Products Center, Oklahoma State University is also acknowledged.

References

Alemayehu, D., Engle, D.M., Wittwer, R.F., Anderson, S., 1998. Pattern of growth of sapwood, heartwood, and stem volume of open-grown eastern red cedar in grasslands. South J. Appl. Forest. 22, 169–174.
American Society for Testing and Materials (ASTM D 570-08): Standard test method for water absorption of plastics. 2008, West Cohshohocken.
American Society for Testing and Materials (ASTM D 905-03): Strength Properties of adhesive bonds in shear by compression loading. 2008, West Cohshohocken.
Barnett, J.R., Bonham, V.A., 2004. Cellulose microfibril angle in the cell wall fibers. Biol. Rev. 79, 461–472.
Bidwell, T.G., Engle, D.M., Moseley, M.E., Master, R.E., 2000. Invasion of Oklahoma rangelands and forests by Eastern redcedar and Ashe juniper. Oklahoma Cooperative Extension Service Circular. E-947, Division of Agricultural Science and Natural Resources, Oklahoma State University, Stillwater, OK 74078.
Dundar, T., Akbulut, T., Korkut, S., 2008. The effects of some manufacturing factors on surface roughness of sliced Makore (*Tieghemella heckelii* Pierre Ex A. Chev.) and rotary-cut beech (*Fagus orientalis* L.) Veneers. Build. Environ. 43 (4), 469–474.
El kouali, M., Bouzon, J., Vergnaud, J.M., 1992. Process of absorption and desorption of water in a wood board with 3-dimensional transport beyond the FSP. Wood Sci. Technol. 26, 307–321.
Esteves, B., Marques, A.V., Domingos, I., Pereira, H., 2007. Influence of steam heating on the properties of pine (*Pinus pinaster*) and eucalypt (*Eucalyptus globulus*) wood. Wood Sci. Technol. 41 (3), 193–207.
Gong, M., Lamason, C., Li, L., 2010. Interactive effect of surface densification and post-heat-treatment on aspen wood. J. Mater. Process Technol. 210, 293–296.
Gunduz, G., Aydemir, D., Karakas, G., 2009. The effects of thermal treatment on the mechanical properties of wild Pear (*Pyrus elaeagnifolia* Pall.) wood and changes in physical properties. Mater. Des. 30, 4391–4395.
Gunduz, G., Korkut, S., Korkut, D.S., 2008. The effects of heat treatment on physical and technological properties and surface roughness of Camiyani Black Pine (*Pinus nigra* Arn. subsp pallasiana var. pallasiana) wood. Bioresour. Technol. 99, 2275–2280.
Hiziroglu, S., 1996. Surface roughness analysis of wood composites: a stylus method. Forest Prod. J. 46, 67–72.
Hiziroglu, S., 2007. Some of the properties of three-layer particleboard panels made from under-utilized species in Oklahoma. J. Compos. Mater. 41, 467–476.
Homan, W., Tjeerdsma, B., Beckers, E., Joressen, A., 2000. Structural and other properties of modified wood. In: World Conference on Timber Engineering, Whistler, British Columbia, Canada, pp. 1–8.
Kamdem, D.P., Pizzi, A., Jermannaud, A., 2002. Durability of heat-treated wood. Holzals Roh-und Werkstoff 60, 1–6.
Kartal, S.N., Hwang, W.J., Imamura, Y., 2008. Combined effect of boron compounds and heat treatments on wood properties: chemical and strength properties of wood. J. Mater. Process Technol. 198, 234–240.
Kilic, M., Hiziroglu, S., Gullu, C., Sezgin, Z., 2008. Influence of steaming on surface roughness of beech and sapele flooring material. J. Mater. Process Technol. 199, 448–451.
Kocaefe, D., Poncsak, S., Dore, G., Younsi, R., 2008. Effect of heat treatment on the wettability of white ash and soft maple by water. Holz. Roh. Werkst 66, 355–361.
Kocaefe, D., Poncsak, S., Tang, J.J., Bouazara, M., 2010. Effect of heat treatment on the mechanical properties of North American jack pine: thermogravimetric study. J. Mater. Sci. 45, 681–687.
Korkut, D.S., Guller, B., 2008. The effects of heat treatment on physical properties and surface roughness of red-bud maple (*Acer trautvetteri* Medw.) wood. Bioresour. Technol. 99, 2846–2851.
Korkut, S., Akgul, M., Dundar, T., 2008. The effects of heat treatment on some technological properties of Scots pine (*Pinus sylvestris* L.) wood. Bioresour. Technol. 99, 1861–1868.
Korkut, S., Hiziroglu, S., 2009. Effect of heat treatment on mechanical properties of hazelnut wood (*Corylus columa* L.). Mater. Des. 30, 1853–1858.
Korkut, S., Karayilmazlar, S., Hiziroglu, S., Sanli, T., 2010. Some of the properties of heat-treated Sessile Oak (*Quercus petraea*). Forest Prod. J. 60, 473–480.
Miller, R.B., 2007. Encyclopedia of Wood. Skyhorse, New York, pp. 1–15.
Mitchell, P.H., 1988. Irreversible property changes of small loblolly pine specimens heated in air, nitrogen, or oxygen. Wood Fiber Sci. 20 (3), 320–355.
Mummery, L., 1993. Surface texture analysis. In: The Handbook. Hommel-werke, Mulhausen, Germany, p. 106.
Neimsuwan, T., Wang, S., Taylor, A.M., Rials, T.G., 2008. Statics and kinetics of water vapor sorption of small loblolly pine samples. Wood Sci. Technol. 42, 493–506.
Payne, K.W., Wittwer, R., Anderson, S., Eisenbraun, E.J., 1998. Use of a modified Abderhalden apparatus to determine moisture and oil content of eastern redcedar. Forest Prod. J. 48, 91–93.
Raimo, A., Kuoppala, E., Oesch, P., 1996. Formation of the main degradation compounds groups from wood and its components during pyrolysis. J. Anal. Appl. Pyrol. 36, 137–148.
Stamm, A.J., 1956. Thermal degradation of wood and cellulose. Ind. Eng. Chem. 48 (3), 413–417.
Yildiz, S., Gezer, E.D., Yzldzz, U.C., 2006. Mechanical and chemical behavior of spruce wood modified by heat. Build. Environ. 41 (12), 1762–1766.

Composites: Part A 42 (2011) 1454–1462

Contents lists available at ScienceDirect

Composites: Part A

journal homepage: www.elsevier.com/locate/compositesa

Properties of wood polymer composites from eastern redcedar particles reinforced with benzoxazine resin/cashew nut shell liquid copolymer

Pornnapa Kasemsiri [a], Salim Hiziroglu [b], Sarawut Rimdusit [a,*]

[a] Department of Chemical Engineering, Faculty of Engineering, Chulalongkorn University, Pathumwon, Bangkok 10330, Thailand
[b] Department of Natural Resource Ecology and Management, Oklahoma State University, 303-G Agricultural Hall, Stillwater, OK 74078, USA

ARTICLE INFO

Article history:
Received 25 February 2011
Received in revised form 9 June 2011
Accepted 22 June 2011
Available online 29 June 2011

Keywords:
A. Wood
A. Polymer–matrix composites (PMCs)
B. Cure behavior
B. Thermal property

ABSTRACT

In this study, properties of experimentally manufactured wood polymer composites based on benzoxazine resin (BA-a) and cashew nut shell liquid (CNSL) copolymer were investigated. Specimens having as high as 75% by weight of eastern redcedar (*Juniperus virginiana L.*) particles mixed with BA-a/CNSL matrix were manufactured for property evaluation. From the experimental results, wood particles evidently lowered the curing temperature and activation energy of the BA-a/CNSL curing process. Thermal and mechanical properties of the samples were found to substantially increase with increasing amount of wood particles. Dimensional stability in a form of the thickness swelling of the specimens and overall surface quality from water immersion test were found to be comparable with those of other wood-based composite panels.

1. Introduction

Eastern redcedar (*Juniperus virginiana L.*) is one of the most widely distributed indigenous conifers in the eastern United States. Over seven million acres of Oklahoma lands are infested with redcedar [1,2]. Eastern redcedar has serious adverse environmental impact such as degrading grasslands, increasing wild fire hazards, and displacing native wildlife and plant populations. Generally, the wood from eastern redcedar is used for fence posts and novelty items. In a previous work, experimental particleboard panels were manufactured from eastern redcedar, and it was found that the basic properties of such samples were comparable with those of commercially made [3]. This process could provide a possible alternative to convert a potentially costly land management problem into a value-added product.

Adhesive cost in wood composite manufacture is the main parameter controlling overall production cost. It would be ideal to reduce adhesive percent in the composite to minimize cost of final product. However, it is well known fact that even 1% reduction in adhesive amount used in the composite would influence adversely almost all properties of the final panel product. One alternative approach to achieve reduce overall product cost would be maximizing fiber amount without changing adhesive content in the matrix. Interestingly, phenolic resins based on benzoxazine structures have a low a-stage viscosity that allows an addition of greater amount of filler [4]. Furthermore, benzoxazine resins have been reported to provide some outstanding characteristics such as having excellent thermal properties and flame retardance, molecular design flexibility, low moisture absorption, near zero shrinkage upon polymerization, low melt viscosities, and low dielectric constant [5–8]. Therefore, polybenzoxazines are widely applied in various fields including structural materials and adhesives especially when high strength properties are desired. In a recent work, it has been reported that highly filled composite panels having up to 75% wood flour can be manufactured using benzoxazine resin [9]. The high compatibility between the wood flour and the polybenzoxazine matrix was evident from the large improvement in the glass transition temperature (T_g) and char yield of the wood composites. Besides, the benzoxazine resins were also modified as ternary matrices for wood flour that consisted of benzoxazine, epoxy, and phenolic novolac resins (BEP resins). The results of these ternary system investigation suggested that an addition of epoxy resin into benzoxazine resin can reduce the liquefying temperature of wood-substituted composites from the highly filled BEP alloys at 70 wt.% of the wood flour content [10]. The relatively high flexural strength of the BEP wood composites up to 70 MPa was also achieved in the same study.

The other potential approach for reducing cost of composite material is to use inexpensive polymeric material. Consequently, to observe the easily renewable and low-cost resin is becoming a matter of necessity [11]. Recently, the development of the benzoxazine based on renewable organic material has attracted significant attention. Especially, a novel cardanol-based benzoxazine monomer having an oxazine ring in its structure can be a good candidate as binder in composite manufacture. The oxazine ring can

* Corresponding author. Tel.: +66 2 218 6862; fax: +66 2 218 6877.
E-mail address: sarawut.r@chula.ac.th (S. Rimdusit).

1359-835X/$ - see front matter © 2011 Elsevier Ltd. All rights reserved.
doi:10.1016/j.compositesa.2011.06.011

react with carbon atoms on benzene ring of cardanol, which is the main component of cashew nut shell liquid (CNSL) [12]. CNSL is a blend of naturally occurring phenol-based monomer and is traditionally obtained as by-product during the process of removing the cashew kernel from the nut. The production of CNSL is nearly 25% of the total nut weight. The main producers of cashew nut are in Asia, Africa, and South America. The major components of CNSL are anacardic acid, cardanol, and trace of cardol and 1-methylcardol. The CNSL has various applications in different industries such as friction linings, paints and varnishes, laminating resins, rubber compounding resin, urethane-based polymer, surfactant, epoxy resin, modifier agent of phenol–formaldehyde resin for plywood production, reactant of wood composite production, and intermediate compound in chemical industries [11,13–17]. Therefore, CNSL would be considered as an excellent potential material to modify the properties of benzoxazine resin possibly to reduce overall material cost in composite manufacture.

Currently, there is no information about properties of plastic-based composite using the CNSL-modified benzoxazine resin with eastern redcedar particles to produce a value-added product. Therefore, the objectives of this work are to produce composite materials from these raw materials and to evaluate the effects of eastern redcedar content in the matrix on the resulting kinetic parameters of the curing process, as well as on the physical and mechanical properties of the obtained wood-substituted composites.

2. Experimental

2.1. Materials

Benzoxazine resin (BA-a) based on bisphenol-A, aniline, and formaldehyde were used as binder to manufacture the wood composite samples. The bisphenol-A (polycarbonate grade) was supplied by Thai Polycarbonate Co., Ltd. (TPCC). Paraformaldehyde (AR grade) and aniline (AR grade) were purchased from Merck Ltd. and Rankem. The CNSL was contributed by Maboonkrong Sirichai 25 Ltd. (Thailand). Eastern redcedar (*J. virginiana L.*) chips were reduced into particles before they were separated on a shaker type screen. Particles size of the wood flour used was 400 μm.

2.2. Preparation of wood–BA-a/CSNL composites

Benzoxazine monomer was synthesized from bisphenol A, aniline, and formaldehyde at a molar ratio of 1:2:4. The monomer synthesis was based on the patented solventless synthesis technique [18]. The BA-a blended with CNSL at a fixed weight ratio of 85/15 (BA-a/CNSL) was used as a composite matrix.

Eastern redcedar particles were dried at a temperature of 100 °C for 24 h in a laboratory oven until they reached a constant weight. The ratios of wood particles to polymer matrix (%wt/wt) were prepared at 0/100, 50/50, 60/40, 75/25, and 80/20. The wood particles were compounded with the BA-a/CSNL mixture in an aluminum container at a temperature of 80 °C for at least 30 min in order to ensure complete filler wetting. The molding compound was then placed in a preheated stainless steel mold with a dimension of 60 mm × 25 mm × 3 mm and compressed in a hydraulic press using a pressure of 15 MPa at 130 °C for 0.5 h and 180 °C for 2 h. The cured specimens were cooled down at room temperature before testing.

2.3. Characterization of the composite samples

The curing behavior and kinetic parameters of the samples were evaluated by a differential scanning calorimeter (DSC) model 2910 from TA Instrument. The heating rates were 2, 3, 5, and 10 °C min^{-1} from 30 to 280 °C under nitrogen gas purging.

Densities of wood composites were determined by a water replacement method based on ASTM D 792 Method A [19]. The density of redcedar particles was determined by a pycnometer.

The dynamic mechanical analyzer (DMA) model DMA 242 from NETZSCH was employed to determine the dynamic mechanical properties and relaxation behaviors of BA-a/CNSL polymer alloy samples. The dimension of specimens was 10 mm × 50 mm × 2 mm. The test was performed in a three-point-bending mode. In a temperature sweep experiment, a frequency of 1 Hz and a strain value of 0.1% were applied. The temperature was scanned from room temperature to T_g of each specimen with a heating rate of 2 °C min^{-1} under nitrogen atmosphere. Additionally, flexural modulus and flexural strength of the wood polymer composite specimens were determined according ASTM D 790 [20] employing a Universal Testing Machine, Instron, Model 5567 equipped with a 1 kN load cell. The measurement was carried out in a three-point bending mode with a support span of 48 mm and at a crosshead speed of 1.2 mm/min. A minimum of five samples with a dimension of 25 mm × 60 mm × 3 mm were tested, and the averaged values were determined.

Water absorption and thickness swelling characteristics of the samples were conducted following ASTM D 570 [21]. Before testing, the thickness and weight of each sample were measured. All samples had been submerged in distilled water for sequential time spans of 2, 6 and 24 h up to 1 week before the samples were removed, wiped, weighed, and immediately returned to water bath at each test period. The amount of water adsorbed was calculated based on the initial conditioned mass of each sample.

Surface characteristics of samples were examined by employing a fine stylus profilemeter Hommel T-500 unit equipped with a TK-300 skidless type pick-up. Six random measurements were taken from surface of each sample to evaluate surface characteristics at dry condition and after 24 h water immersion. Three roughness parameters, namely average roughness (R_a), mean peak-to-valley height (R_z), and maximum roughness (R_{max}), were used to evaluate surface quality of the samples. Definitions of such roughness parameters and specifications of stylus type equipment were described in the literature [22].

Fracture surface of the wood composites was investigated using a scanning electron microscope (SEM) (Quanta model 600 F) at an acceleration voltage of 20 kV. Fractured samples were coated with a thin film of gold using an ion sputtering device, before micrographs of the fractured surfaces were taken.

3. Results and discussion

3.1. Curing behavior of eastern redcedar particles filled BA-a/CNSL composites

The effect of eastern redcedar particles or filler content on curing reaction of BA-a/CNSL matrix was investigated by DSC as shown in Fig. 1. The matrix showed an exothermic peak attributed to the ring-opening polymerization of oxazine ring at 214 °C. Interestingly, the exothermic peak of BA-a/CNSL system was found to be lower than that of the neat BA-a, which was reported at about 220–240 °C [23]. This result indicated that the anacardic acid in CNSL might act as a curing accelerator, which caused a shift of the exotherm of the ring-opening reaction of the benzoxazine resin to lower temperature. The thermograms at different eastern redcedar particle contents clearly revealed that the exothermic curing peak decreased with increasing eastern redcedar particle contents, i.e., 213 °C (30 wt.% filler content), 211 °C (50 wt.% filler content), and 203 °C (70 wt.% filler content). This phenomenon can be attributed to the catalytic effect of polymerization of the matrix induced by carbohydrates and lignin in wood substrates [24]. The similar

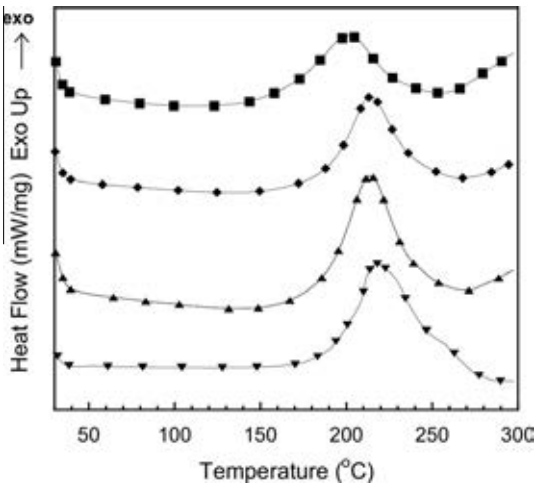

Fig. 1. DSC thermograms of samples manufactured with various filler contents: (▼) 85/15 BA-a/CNSL matrix, (▲) 30 wt.% filler content, (♦) 50 wt.% filler content, and (■) 70 wt.% filler content.

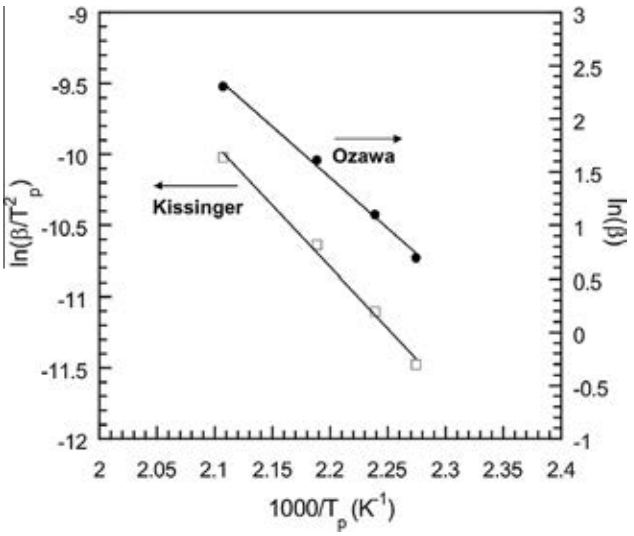

Fig. 2. (□) Krissinger method and (●) Ozawa method plots for averaged activation energy determination of 75 wt.% eastern redcedar particles filled BA-a/CNSL (85/25) resins.

conclusion was also observed in the wood composite panels manufactured using phenol formaldehyde resin [25].

A non-isothermal method in DSC experiment was used to determine the curing kinetic parameters of wood composites, which were 75 wt.% eastern redcedar particles filled the BA-a and BA-a/CNSL (85/25) resins. The activation energy of the curing process was also examined by both the Kissinger and Ozawa methods. The details of both methods were clearly described in our previous work [26].

3.1.1. Kissinger method

Kissinger method is based on a linear relationship between $(\ln \beta/T_p^2)$ against the inverse of the peak temperature of the exothermic curing reaction $(1/T_p)$. The activation energy (E_a) can be obtained as follows:

$$\ln\left(\frac{\beta}{T_p^2}\right) = \ln\left(\frac{Q_p AR}{E_a}\right) - \frac{E_a}{RT_p} \quad (1)$$

where β is a constant heating rate, $f(\alpha)$ is differential conversion function depending on reaction mechanism, and $Q_p = -[d\, f(\alpha)/d\, \alpha]$ $\alpha = \alpha_p$

3.1.2. Ozawa method

A similar method to Kissinger method is Ozawa method that relates the $\ln \beta$ and $(1/T_p)$ as follows:

$$\ln \beta = \ln\left(\frac{Q_p AR}{E_a}\right) - \ln F(\alpha) - 5.331 - 1.052\left(\frac{E_a}{RT_p}\right) \quad (2)$$

$$F(\alpha) = \int_0^{\alpha} \frac{d\alpha}{f(\alpha)}$$

where $F(\alpha)$ is a constant function

A good linear correlation was observed, and the activation energy was also calculated from the slope of the relationship between the heating rate and the reversal of the exothermic peak temperature, as illustrated in Fig. 2. Table 1 displays the average calculated activation energy values 77–81 kJ/mol and 72–76 kJ/mol for eastern redcedar particles filled BA-a and BA-a/CNSL (85/25) resins, respectively. These values are lower than around 84–87 kJ/mol the activation energy of neat benzoxazine resin previously reported [26]. This observation is good evidence that eastern redcedar particles not only decreased curing temperatures but also reduced the activation energy of the benzoxazine matrices. This would be possibly due to the catalytic effect of eastern redcedar particles as mentioned above. The decrease in curing temperature and activation energy of wood composites has a positive effect on the wood composite manufacturing, i.e., a relatively lower curing temperature or lower energy consumption can be used.

Table 1
Kinetic parameters of wood composites evaluated by Kissinger and Ozawa. methods.

Eastern redcedar/matrix (75/25 wt.%)	Methods	
	Kissinger (kJ/mol)	Ozawa (kJ/mol)
Eastern redcedar/(BA-a)	77	81
Eastern redcedar/(BA-a/CNSL)	72	76

3.2. Density measurement

One measure to evaluate the optimum packing of filler in benzoxazine matrix is density measurement [27,28]. The densities of eastern redcedar particles filled BA-a/CNSL composites as a function of the wood flour content are illustrated in Fig. 3. The theoretical densities of the composites were calculated as follows:

$$\rho_c = \frac{1}{(W_f/\rho_f) + ((1 - W_f)/\rho_m)} \quad (3)$$

where W_f is filler weight fraction, $(1 - W_f)$ is matrix weight fraction, ρ_c is composite density, ρ_f is filler density, and ρ_m is the matrix density. Based on this equation, the calculated theoretical densities value depends on weight fraction and density of the filler and the matrix based on complete wetting. The density levels of materials were 1.19 g/cm^3 for eastern redcedar particles, 1.19 g/cm^3 for polybenzoxazine, and 0.94 g/cm^3 for CNSL. The experimental results at filler contents in the range of 50–75 wt.% present a linear relationship between the density value and the filler loading.

3.3. Mechanical properties

The dynamic mechanical properties of the wood-based composites were examined as a function of temperature. The storage moduli at temperature ranging from 30 to 250 °C of BA-a/CNSL matrix and eastern redcedar particles filled with contents ranging from 50

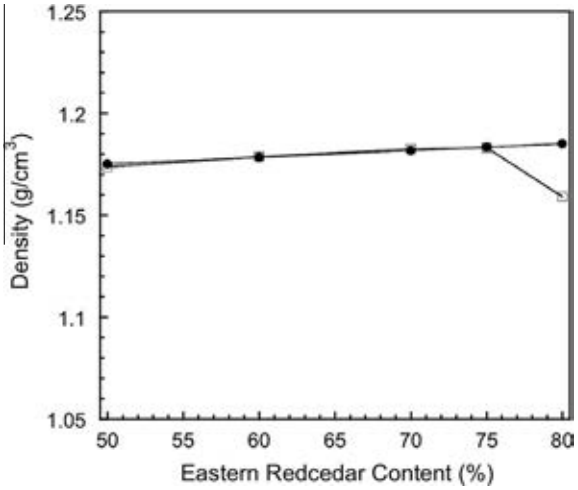

Fig. 3. Density of wood composites at various eastern redcedar contents: (□) actual density and (●) theoretical density.

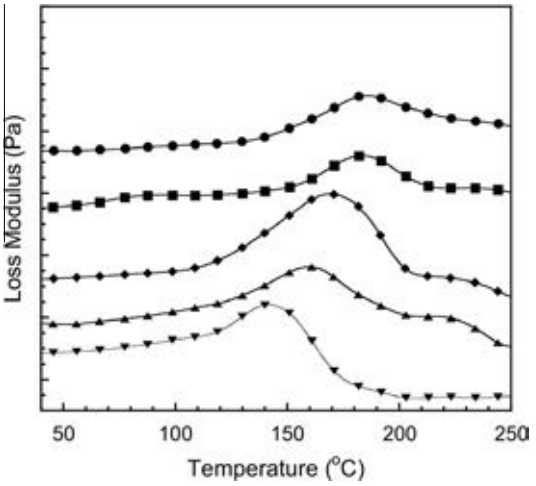

Fig. 5. Loss modulus of samples at various filler contents: (▼) 85/15 BA-a/CNSL matrix, (▲) 50 wt.% filler filled BA-a/CNSL, (♦) 60 wt.% filler filled BA-a/CNSL, (■) 70 wt.% filler filled BA-a/CNSL, and (●) 75 wt.% filler filled BA-a/CNSL.

to 75 wt.% are exhibited in Fig. 4. The room temperature moduli of the wood composites at the filler content of 75 wt.% were observed to be within the range of 4.48 GPa compared with the 3.24 GPa of BA-a/CNSL matrix. The storage modulus was maintained to be constant up to higher temperature by increasing eastern redcedar particles content. This behavior can be attributed to the effect of restriction of segmental motion of matrix possibly due to the substantial interfacial bonding between the matrix and eastern redcedar particles. Such observation is also similar to the finding of our previous studies [9,29].

Fig. 5 shows a plot of the loss modulus of the BA-a/CNSL matrix and wood composites as a function of temperature. The peak positions of the loss moduli were used to indicate the T_gs of the samples. As depicted in Fig. 5, the T_g of the BA-a/CNSL matrix was 147 °C whereas the T_gs of wood composites having eastern redcedar particles content ranging from 50 to 70 wt.% were observed to be 162 to 188 °C. This result indicated that the T_g value increased with increasing amount of the eastern redcedar particles. As explained in our previous work, the presence of the phenolic structure in lignin fraction of eastern redcedar particles and the abundance of hydroxyl moieties in the filler are believed to provide a composite system with strong interfacial bonding to the polybenzoxazine with enhanced thermal properties [9,29].

Flexural properties of the wood composites were examined, and the results are illustrated in Figs. 6 and 7. Flexural modulus values of the eastern redcedar particles filled BA-a/CNSL alloys are also depicted in Fig. 6. The average flexural modulus of wood composites ranged from 4.27 to 7.09 GPa. This values fall in the same as those of the polybenzoxazine wood composites reported in recent work [9,29]. The flexural modulus as a function of eastern redcedar particles content showed a behavior nearly identical to that of the storage modulus determined by DMA, i.e., the flexural modulus trended to increase with increasing amount of eastern redcedar particles.

Fig. 7 presents the flexural strength of wood composites. The flexural strength values trended to increase with increasing amount of eastern redcedar particles content in the samples having values ranging from 34.13 to 47.06 MPa. It should be noted that an increase in filler content enhanced the modulus and strength of samples due to reinforcing capability of the filler and matrix [29]. These flexural strengths are significantly higher than those reported wood plastic composites, e.g., 50–70 wt.% commercial wood particles reinforced HDPE (2.7–3.1 GPa) [30]. Furthermore, the

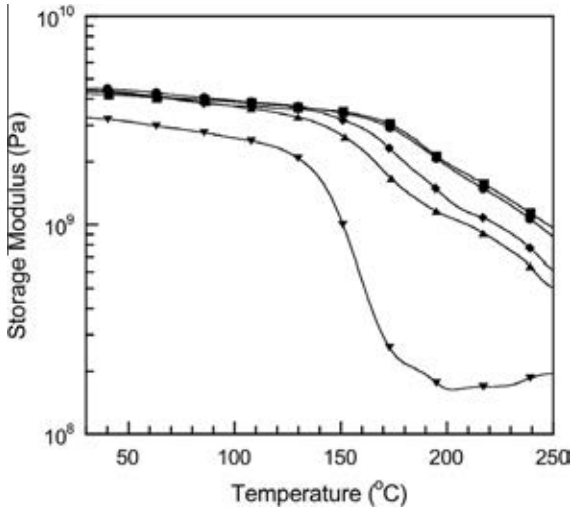

Fig. 4. Storage modulus of samples at various filler contents: (▼) 85/15 BA-a/CNSL matrix, (▲) 50 wt.% filler filled BA-a/CNSL, (♦) 60 wt.% filler filled BA-a/CNSL, (■) 70 wt.% filler filled BA-a/CNSL, and (●) 75 wt.% filler filled BA-a/CNSL.

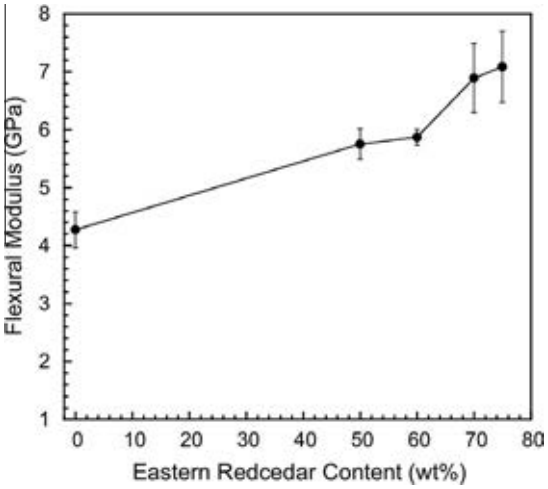

Fig. 6. Effect of wood particle content on flexural modulus of the wood composites.

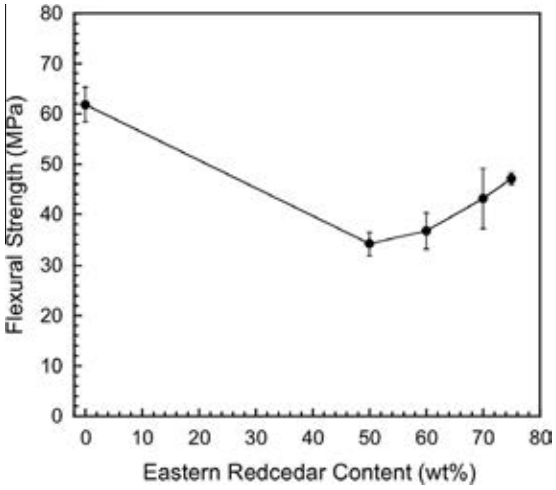

Fig. 7. Effect of wood particle contents on flexural strength of the wood composites.

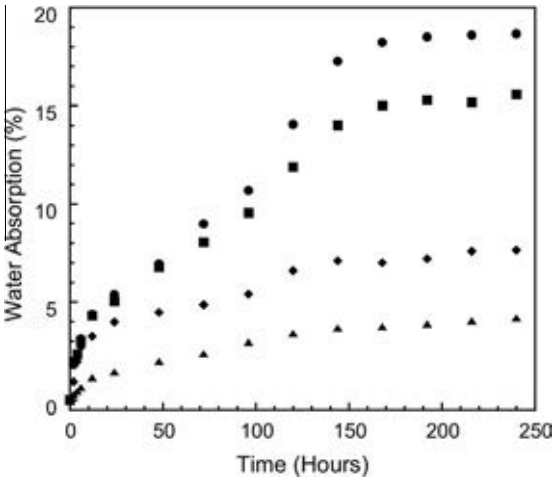

Fig. 8. Percentage water absorption of the wood composites at various filler contents: (▲) 50 wt.% filler filled BA-a/CNSL, (♦) 60 wt.% filler filled BA-a/CNSL, (■) 70 wt.% filler filled BA-a/CNSL, and (●) 75 wt.% filler filled BA-a/CNSL.

flexural modulus of wood composite in this work is higher than typical medium-density fiberboard (MDF) requirement, which requires flexural modulus to be in a range of 0.5–3 GPa. Generally, MDF is frequently used as substrate for thin overlays to manufacture furniture units [31]. These results implied that BA-a/CNSL resin strongly adhered to the eastern redcedar particles and effectively imparted good mechanical properties to the composites.

3.4. Water absorption of the wood composite samples

The values of water absorption and thickness swelling for the wood composites at varied filler loadings are shown in Fig. 8. The percentage of water absorbed plotted against time for all samples revealed a similar behavior, i.e., the samples absorbed water more rapidly during first stages (0–24 h). The water adsorption values of the samples were in range of 4.17–18.66% after 170 h of the immersion. These values were significantly lower than the water absorption values of previous works such a sisal reinforced with glyoxal–phenol–resorcinal (30%) and of bamboo/epoxy composite (40%) [32,33]. Moreover, the water absorption of all samples was also observed to increase with increasing filler content. This is likely caused by the hydrogen bonding of the water molecules to

Table 2
Diffusion case selection parameters and diffusion coefficients of the wood composites.

Eastern redcedar/matrix	n	Diffusion coefficient $\times 10^{-12}$ (m^2/sec)
50/50	0.55	1.73
60/40	0.37	1.89
70/30	0.46	2.36
75/25	0.51	3.08

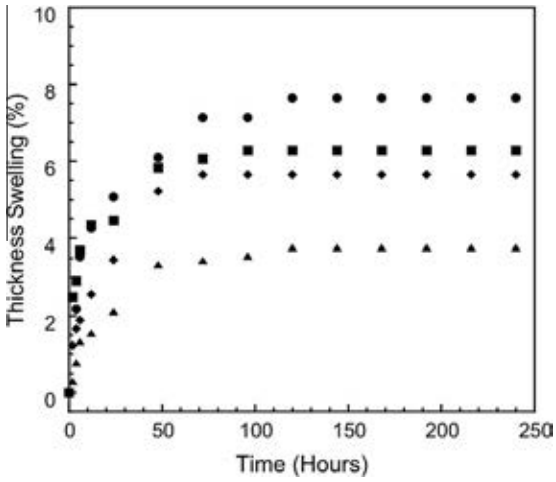

Fig. 9. Percentage thickness swelling of the wood composites at various filler contents: (▲) 50 wt.% filler filled BA-a/CNSL, (♦) 60 wt.% filler filled BA-a/CNSL, (■) 70 wt.% filler filled BA-a/CNSL, and (●) 75 wt.% filler filled BA-a/CNSL.

the free OH groups presented in the cellulosic cell wall components of the filler and by the possible diffusion of water molecules into the filler and matrix interface. Furthermore, large number of porous tubular anatomical of fiber might accelerate the penetration of water by the so-called capillary action. Therefore, with the increase in the filler content, there are more water residence sites (OH groups), which result in more absorbed water [34].

3.4.1. Kinetic of water sorption

It is necessary to study the kinetic water sorption to have better understanding of the water sorption mechanism and to minimize water uptake of materials. Generally, the analysis of the diffusion mechanism and kinetics was performed based on Fick's theory. The generalized equation can be expressed as

$$\frac{M_t}{M_\alpha} = kt^n \tag{4}$$

where M_t is the moisture content at time t, M_α is moisture content at equilibrium, and k and n are constants.

The diffusion behaviors can be classified as follows: super case II ($n > 1$), case II ($n = 1$), anomalous ($1/2 < n < 1$), classical/Fickian ($n = 1/2$), or pseudo-Fickian ($n < 1/2$). From the plots of log M_t/M_α versus log t, the obtained slope values of all samples were summarized in Table 2. The absorption of water in the eastern redcedar particles filled BA-a/CNSL approached toward the Fickian diffusion case, as the value of n were determined to be in the range of 0.36–0.54. These values were close to the value of $n = 0.5$. Generally, the water adsorption in natural fiber reinforced plastics usually follows Fickian behavior [35].

3.4.2. Transport coefficients

The diffusion coefficient (D) is the most important parameter of the Fick's model. This parameter presents the ability of solvent molecules to penetrate inside the composite structure and can be calculated using the following equation:

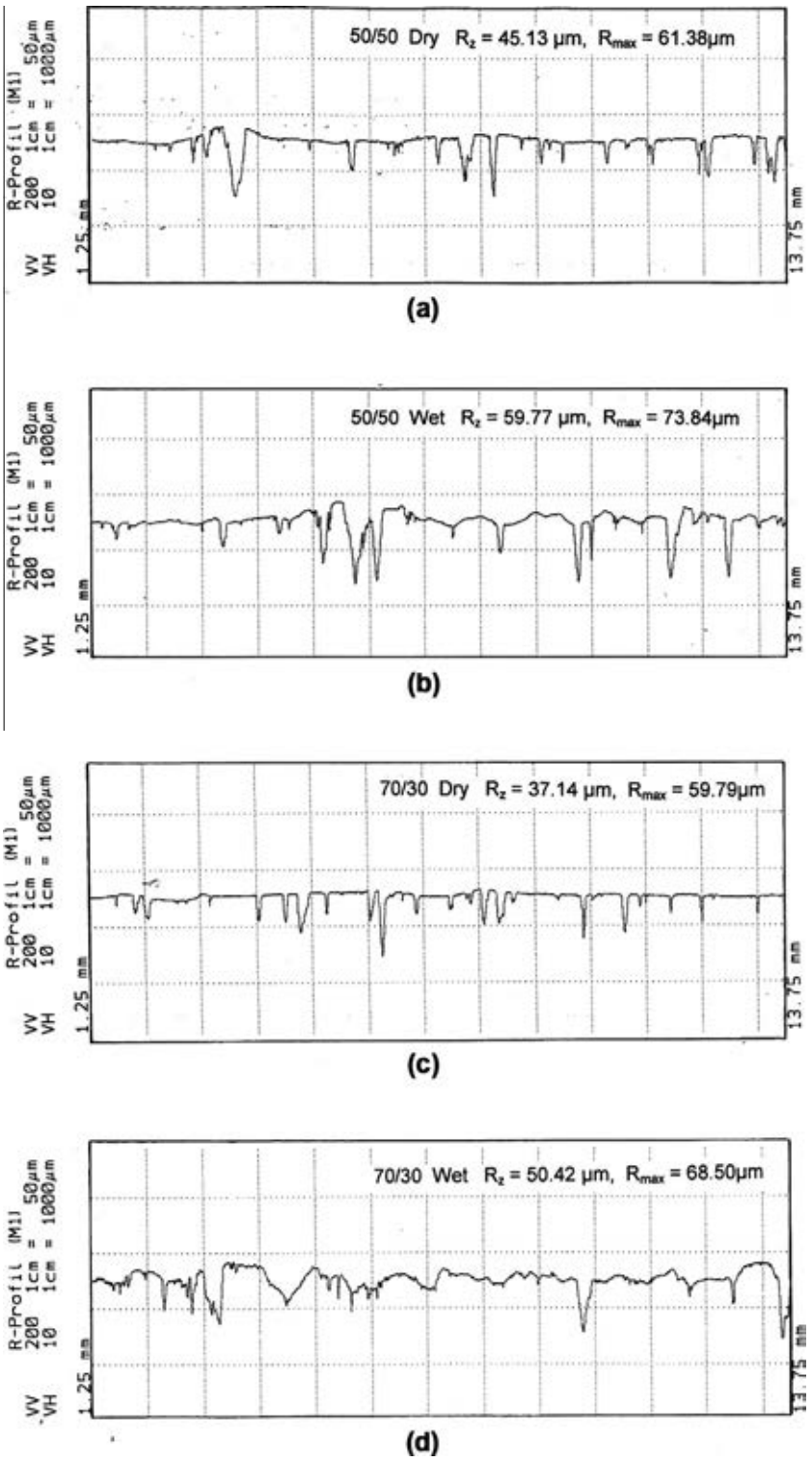

Fig. 10. Typical roughness profiles of the samples in dry and soaked condition.

$$\frac{M_t}{M_\infty} = \frac{4}{L}\left(\frac{D}{\pi}\right)^{0.5} t^{0.5} \tag{5}$$

where L is the thickness of sample.

From Eq. (5), the diffusion coefficient was obtained from the slope of the plot of M_t/M_∞ versus $(t)^{0.5}$. The obtained values from a curve fitting were shown in Table 2. The diffusion coefficient values of wood composites expectedly showed an increasing trend with increasing eastern redcedar loading. This is due to the hydrophilic characteristics of lignocellulosic fiber incorporated. Additionally, the greater natural fiber loading may increase interfacial region of the transport of the diffusant. This result is in good agreement with the results of our previous work [35].

Table 3
Surface roughness values of the wood composites.

Eastern redcedar/matrix	Surface roughness values before water immersion (μm)			Surface roughness values after water immersion (μm)			Percent increase in surface roughness values (%)		
	R_a	R_z	R_{max}	R_a	R_z	R_{max}	R_a	R_z	R_{max}
50/50	4.21	40.76	73.29	5.24	47.55	77.93	24.44	16.66	6.32
60/40	2.01	20.05	35.27	5.24	47.55	77.93	42.03	51.42	25.31
70/30	4.00	32.72	51.35	6.46	44.43	66.85	61.43	37.23	30.19
75/25	2.32	20.89	30.63	4.03	32.78	49.25	73.86	56.92	60.76

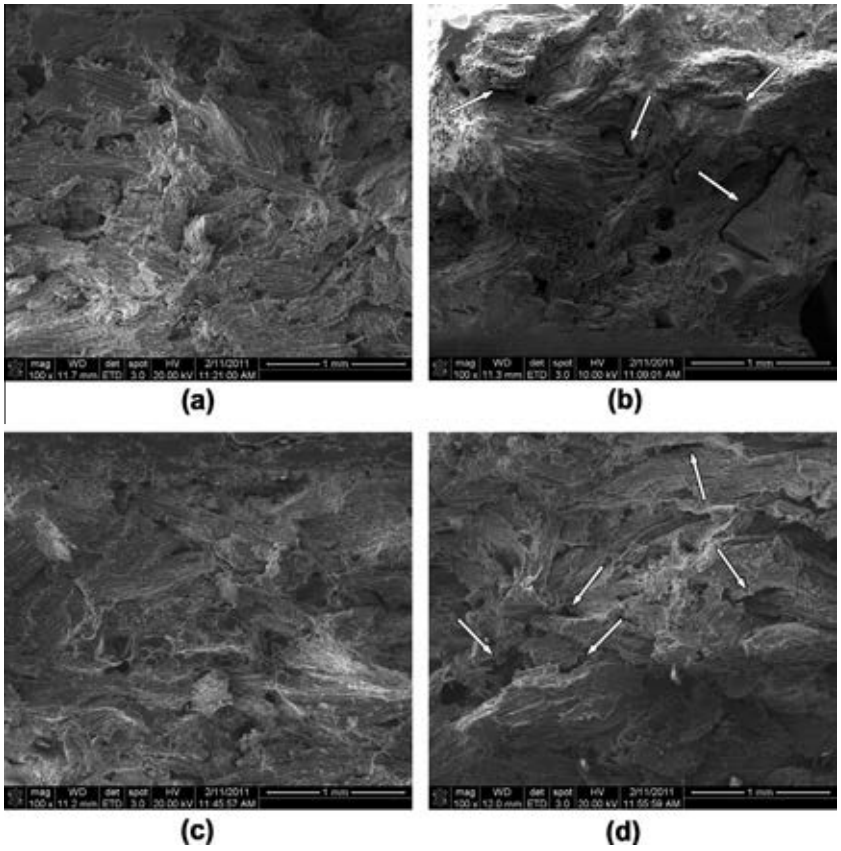

Fig. 11. Micrographs taken from cross-section of the samples by SEM (arrows show the gaps between wood and matrix due to water adsorption): (a) samples with 50% filler in dry condition, (b) samples with 50% filler in wet condition, (c) samples with 75% filler in dry condition, and (d) samples with 75% filler in wet condition.

3.5. Thickness swelling of the samples

Due to the presence of polar groups in lignocellulosic material, the polar group can attract water molecules through hydrogen bonding. This phenomenon leads to moisture build-up in fiber cell wall and in fiber matrix interface. These factors affected the swelling of fiber and the changing the dimensional behavior of the composite samples, namely thickness swelling and linear expansion [36].

The thickness swelling (TS) of the eastern redcedar filled BA/CNSL is illustrated in Fig. 9. The thickness swelling of the specimens increased with increasing eastern redcedar content in the panels similar to water absorption results. The TS value of the samples having 50–75 wt.% filler content for the 24 h water immersion varied from 2.10% to 5.06%. These values were found to be lower than those of the 55 wt.% phenolic resin reinforced with grass fiber (18.4%) [37]. Overall, TS values of the samples were within the same range of commercially produced other types of wood-based composite panels such as fiberboards having a range of 1.6–5.45 [38]. It is due to the important characteristics of BA-a/CNSL matrix and the eastern redcedar particles, i.e., the benzoxazine resin is well known as a low water adsorption material [4]. In addition, both CNSL and eastern redcedar have oil content [3]. This component in wood may act as a wax that is normally added in typical particleboard manufacturing to enhance their dimensional stability from moisture absorption. As shown in Fig. 9, the thickness swelling increased only in the initial stage and thereafter remained almost constant. After 10 days, the thickness swelling leveled off and the percentage of the TS value was observed to be within the range of 3.76–7.91%.

3.6. Surface roughness of samples

The typical roughness profiles of our wood composites are shown in Fig. 10, and the average roughness values are also summarized in Table 3. Average roughness (R_a), mean peak to valley height (R_z) and maximum roughness (R_{max}) values for the samples having 50–70 wt.% wood particles in dry condition ranged from 2.32 to 4.21 μm, from 20.05 to 40.76 μm, and from 30.63 to 73.29 μm, respectively. After 24 h water immersion, surface rough-

ness of all samples was remeasured to evaluate the change of their roughness characteristics. The percent increase in surface roughness values enhanced with increased filler content in samples, as exhibited in Table 3. This is due to water adsorption in lignocellulosic can lead to a build-up of moisture in the fiber cell wall and the interphase region between matrix and fiber. It is well known that moisture could result in swelling and dimensional instability of wood products [39]. The similar trend of the percent increase in roughness values was also observed in the panels composites exposed to 75–85% humidity [40].

3.7. Fracture surface investigation

The fractured surfaces of wood composites before and after water absorption measurement are illustrated in Fig. 11a–d, respectively. The 50 and 75 wt.% eastern redcedar filled BA-a/CNSL matrix before water immersion presented the tight interfaces between the filler and BA-a/CNSL matrix, which implied a good fiber–matrix interface. The results confirmed the observed enhancement in mechanical and thermal performance of these wood composites. After 10 days of water immersion, the fractured surfaces of samples were characterized by SEM to evaluate the existence of substantial degree of adhesion between the matrix and filler. Fig. 11c–d exhibited the voids and crack between eastern redcedar particles and BA-a/CNSL matrix attributed to the decreasing degree adhesion of filler-matrix. As mentioned above, the hydrophilic nature of the cellulosic materials caused the composite to take up a high amount of water. The water tends to be retained in the inter cell wall of the cellulosic structure of these fillers and flaws at the interface and microvoid existence in the composites [34].

4. Conclusions

Bisphenol A benzoxazine resin alloyed with cashew nut shell liquid was observed to be a good binder for natural fiber. The addition of cashew nut shell liquid and eastern redcedar particles effectively reduced the curing temperature and activation energy of benzoxazine resin. The effects of the eastern redcedar particles content on the thermal and mechanical increased with optimum amount of filler to matrix at 75/25 by weight that attributed to good compatibility between the fiber and the matrix. The wood composites at various contents of particles also showed relatively low percentages of water absorption and thickness swelling. The obtained wood composites based on eastern redcedar particles also provided an economic incentive to convert a costly land management problem into the value-added products of wood composite panels.

Acknowledgments

This research receives financial support from Dutsadi Phiphat Scholarship of Chulalongkorn University. Additional supports are from the research grant from the Thailand Research Fund (S. Rimdusit), the National Research University Project of the Ministry of Education, Thailand (AM1076A, AM006B), and 100th Anniversary of Chulalongkorn University Academic Funding. Material supplied by Thai Polycarbonate Co., Ltd. (TPCC) and Maboonkrong Sirichai 25 Ltd., are greatly appreciated. Support from Robert M. Kerr Food and Agricultural Products Center, Oklahoma State University, is also acknowledged.

References

[1] Payne KW, Wittwer R, Anderson S, Eisenbraun EJ. Use of a modified Abderhalden apparatus to determine moisture and oil content of eastern redcedar. Forest Prod J 1998;48(7–8):91–3.
[2] King SA, Lewis DK. Manufacturing solid wood products from used utility poles: an economic feasibility study. Forest Prod J 2000;50(11–12):69–78.
[3] Hiziroglu S. Some of the properties of three-layer particleboard panels made from under-utilized species in Oklahoma. J Compos Mater 2007;41(4):467–76.
[4] Rimdusit S, Ishida H. Development of new class of electronic packaging materials based on ternary systems of benzoxazine, epoxy, and phenolic resins. Polymer 2000;41(22):7941–9.
[5] Ishida H, Rodriguez Y. Catalyzing the curing reaction of a new benzoxazine-based phenolic resin. J Appl Polym Sci 1995;58(10):1751–60.
[6] Ning X, Ishida H. Phenolic materials via ring opening polymerization – synthesis and characterization of bisphenol-A based benzoxazines and their polymers. J Polym Sci Pol Chem 1994;32(6):1121–9.
[7] Ishida H, Allen DJ. Mechanical characterization of copolymers based on benzoxazine and epoxy. Polymer 1996;37(20):4487–95.
[8] Ishida H, Lee YH. Synergism observed in polybenzoxazine and poly(epsilon-caprolactone) blends by dynamic mechanical and thermogravimetric analysis. Polymer 2001;42(16):6971–9.
[9] Rimdusit S, Tanthapanichakoon W, Jubsilp C. High performance wood composites from highly filled polybenzoxazine. J Appl Polym Sci 2006; 99(3):1240–53.
[10] Jubsilp C, Takeichi T, Hiziroglu S, Rimdusit S. High performance wood composites based on benzoxazine–epoxy alloys. Bioresource Technol 2008; 99(18):8880–6.
[11] Mwaikambo LY, Ansell MP. Hemp fibre reinforced cashew nut shell liquid composites. Compos Sci Technol 2003;63(9):1297–305.
[12] Lochab B, Varma IK, Bijiwe J. Thermal behaviour of cardanol-based benzoxazines monomers and polymers. J Therm Anal Calorim 2010;102(2):769–74.
[13] Barreto ACH, Rosa DS, Fechine PBA, Mazzetto SE. Properties of sisal fibers treated by alkali solution and their application into cardanol-based biocomposites. Composites Part A 2011;42(5):492–500.
[14] Bisanda ETN, Ansell MP. Properties of sisal-CNSL composites. J Mater Sci 1992;27:1690–700.
[15] Peungjitton P, Sangvanich P, Pornpakakul S, Petsom A, Roengsumran S. Sodium cardanol sulfonate surfactant from cashew nut shell liquid. J Surfactants Deterg 2009;12(2):85–9.
[16] Papadopoulou E, Chrissafis K. Thermal study of phenol–formaldehyde resin modified with cashew nut shellliquid. Thermochim Acta 2010;512(1–2):105–9.
[17] Santos RD, Souza AA, De Paoli MA, Souza CML. Cardanol–formaldehyde thermoset composites reinforced with buriti fibers: preparation and characterization. Composites Part A 2010;41(9):1123–9.
[18] Ishida H. US Patent 5543,516; 1996.
[19] American Society for Testing and Materials (ASTM D 792). Standard test methods for density and specific gravity (relative density) of plastics by displacement. West Cohshohocken 2008; 08(01): 162–267.
[20] American Society for Testing and Materials (ASTM D 790). Standard test methods for flexural properties of unreinforced and reinforced plastics and electrical insulating materials. West Cohshohocken 2008; 08(01): 151–61.
[21] American Society for Testing and Materials (ASTM D 570). Standard test method for water absorption of plastics. West Cohshohocken 2008; 08(01): 35–38.
[22] Mummery L. Surface texture analysis. The handbook. Mulhausen, Germany: Hommel-werke; 1993. p. 106.
[23] Ishida H, Rodriguez Y. Curing kinetics of a new benzoxazine-based phenolic resin by differential scanning calorimetry. Polymer 1995;36:3151–8.
[24] Pizzi A, Mtsweni B, Parsons W. Wood-induced catalytic activation of PF adhesives autopolymerization vs. PF wood covalent. J Appl Polym Sci 1994;52:1847.
[25] Lei Y, Wu Q. Cure kinetics of aqueous phenol–formaldehyde resins used for oriented strandboard manufacturing: effect of wood flour. J Appl Polym Sci 2006;102(4):3774–81.
[26] Jubsilp C, Damrongsakkul S, Takeichi T, Rimdusit S. Curing kinetics of arylamine-based polyfunctional benzoxazine resins by dynamic differential scanning calorimetry. Thermochim Acta 2006;447(2):131–40.
[27] Ishida H, Rimdusit S. Very high thermal conductivity obtained by boron nitride-filled polybenzoxazine. Thermochim Acta 1998;320(1–2):177–86.
[28] Marcovich NE, Reboredo MM, Aranguren MI. Modified wood flour as thermoset fillers II. Thermal degradation of wood flours and composites. Thermochim Acta 2001;372(1–2):45–57.
[29] Rimdusit S, Kampangsaeree N, Tanthapanichakoon W, Takeichi T, Suppakarn N. Development of wood-substituted composites from highly filled polybenzoxazine–phenolic novolac alloys. Polym Eng Sci 2007;47(2):140–9.
[30] Balasuriya PW, Ye L, Mai YW. Mechanical properties of wood flake–polyethylene composites. Part I: Effects of processing methods and matrix melt flow behaviour. Composites Part A 2001;32:619–29.
[31] Youngquist JA. Wood handbook: wood as an engineering material. Madison, WI: US Department of Agriculture. Government Printing Office; 1987.
[32] Ramires EC, Megiatto Jr JD, Gardiat C, Gastellan A, Frollini E. Biobased composites from glyoxal–phenolic resins and sisal fibers. Bioresource Technol 2010;101(6):1998–2006.
[33] Kushwaha PK, Kumar R. Studies on the water absorption of bamboo–epoxy composites: the effect of silane treatment. Polym Plast Technol Eng 2010;49(9):867–73.
[34] Ashori A, Sheshmani S. Hybrid composites made from recycled materials: moisture absorption and thickness swelling behavior. Bioresource Technol 2010;101(12):4717–20.
[35] Espert A, Vilaplana F, Karlsson S. Comparison of water absorption in natural cellulosic fibres from wood and one-year crops in polypropylene composites

and its influence on their mechanical properties. Composites Part A 2004;35(11):1267–76.
[36] Abdul Khalil HPS, Alwani Siti M, Omar Mohd AK. Cell wall structure of various tropical plant waste fibers. Ind Crops Prod 2007;26(3):315–23.
[37] De D, Adhikari B. Grass fiber reinforced phenol formaldehyde resin composite: preparation, characterization and evaluation of properties of composite. Polym Adv Technol 2007;18(1):72–81.
[38] Roger MR. Handbook of wood chemistry and wood composites. United States of America; 2005. p. 297.
[39] Tajvidi M, Ebrahimi G. Water uptake and mechanical characteristics of natural filler–polypropylene composites. J Appl Polym Sci 2003;88(4):941–6.
[40] Ozdemir T, Hiziroglu S, Malkocoglu A. Influence of relative humidity on surface quality and adhesion strength of coated medium density fiberboard (MDF) panels. Mater Des 2009;30(7):2543–6.

Thermochimica Acta 520 (2011) 84–92

Contents lists available at ScienceDirect

Thermochimica Acta

journal homepage: www.elsevier.com/locate/tca

Effect of cashew nut shell liquid on gelation, cure kinetics, and thermomechanical properties of benzoxazine resin

Pornnapa Kasemsiri[a], Salim Hiziroglu[b], Sarawut Rimdusit[a,*]

[a] Department of Chemical Engineering, Faculty of Engineering, Chulalongkorn University, Pathumwon, Bangkok 10330, Thailand
[b] Department of Natural Resource Ecology and Management, Oklahoma State University, 303-G Agricultural Hall, Stillwater, OK 74078, USA

ARTICLE INFO

Article history:
Received 23 December 2010
Received in revised form 14 March 2011
Accepted 25 March 2011
Available online 5 April 2011

Keywords:
Cashew nut shell liquid
Benzoxazine resin
Gelation
Curing kinetics
Wood composite

ABSTRACT

Effects of cashew nut shell liquid (CNSL) on properties of a bifunctional benzoxazine resin (BA-a) have been investigated. The CNSL remarkably decreases the liquefying temperature, gel time and curing temperature of the neat benzoxazine resin. The Kissinger and Ozawa methods are used to calculate the curing kinetic parameters of BA-a/CNSL systems. The activation energy values obtained from both models show fairly consistent results i.e. the activation energy values decrease with increasing the CNSL content. It was found that optimal CNSL content from solvent extraction experiment should not exceed 20 wt% to avoid the presence of unreacted CNSL in the alloy network. Properties of bamboo fiber-reinforced BA-a/CNSL alloys are also investigated in this work. The filled BA-a/CNSL at 65 wt% of bamboo fiber shows a substantial increase in storage modulus and T_g of the composites. BA-a/CNSL alloy shows great potential as high performance lignocellulosic adhesive for wood composite applications.

1. Introduction

Benzoxazine resins are new members of phenolic based adhesives. These novel types of phenolic resins have been reported to provide some outstanding characteristics such as excellent thermal properties and flame retardance, molecular design flexibility, low moisture absorption, near zero shrinkage upon polymerization, low melt viscosities, and low dielectric constant [1–4]. Therefore, polybenzoxazines are widely applied in various fields such as structural materials and adhesives especially when high strength properties are desired.

Recently, the development of the benzoxazine-based on renewable organic material has attracted significant attention. Especially, a novel cardanol-based benzoxazine monomer contains an oxazine ring in its structure. The ring can react with carbon atoms on benzene ring of cardanol which is the main component of cashew nut shell liquid (CNSL) [5]. CNSL is a blend of naturally occurring phenol-based monomer and is traditionally obtained as by-product during the process of removing the cashew kernel from the nut. The production of CNSL is nearly 25% of the total nut weight. The main producers of cashew nut are in Asia, Africa and South America. The major components of CNSL are anacardic acid, cardanol and trace of cardol and 1-methylcardol. The CNSL has various applications in different industries such as friction linings, paints and varnishes, laminating resins, rubber compounding resin, urethane based polymer, surfactant, epoxy resin, modifier agent of phenol–formaldehyde resin for plywood production and intermediate for chemical industries. It also has potential and opportunities for development of other tailor-made polymers. This makes CNSL and their components become important for new value-added materials with possible industrial uses [6–8]. Consequently, CNSL is an excellent candidate material to modify properties of benzoxazine resin and a potential of reducing a material cost.

Currently there is no information on properties of BA-a/CNSL alloys. Therefore, effects of the benzoxazine resin modified with cashew nut shell liquid oil on the resulting processing ability and kinetic parameters of the curing process will be investigated in this research. Furthermore, the thermal properties and the adhesion performance of these alloys in wood composite will also be examined.

2. Experimental

2.1. Materials

Benzoxazine resin is based on bisphenol-A, aniline and formaldehyde. The bisphenol-A (polycarbonate grade) was supplied by Thai Polycarbonate Co., Ltd. (TPCC). Para-formaldehyde (AR grade) and aniline (AR grade) were purchased from Merck Ltd. and Panreac Quimica S.A. The CNSL was contributed by Maboonkrong Sirichai 25 Ltd. Bamboo fiber (*Dendrocalamus asper*) was supplied by Forest Products Division, Royal Forest Department, Thailand.

* Corresponding author. Tel.: +66 2 218 6862; fax: +66 2 218 6877.
E-mail address: sarawut.r@chula.ac.th (S. Rimdusit).

0040-6031/$ – see front matter © 2011 Elsevier B.V. All rights reserved.
doi:10.1016/j.tca.2011.03.020

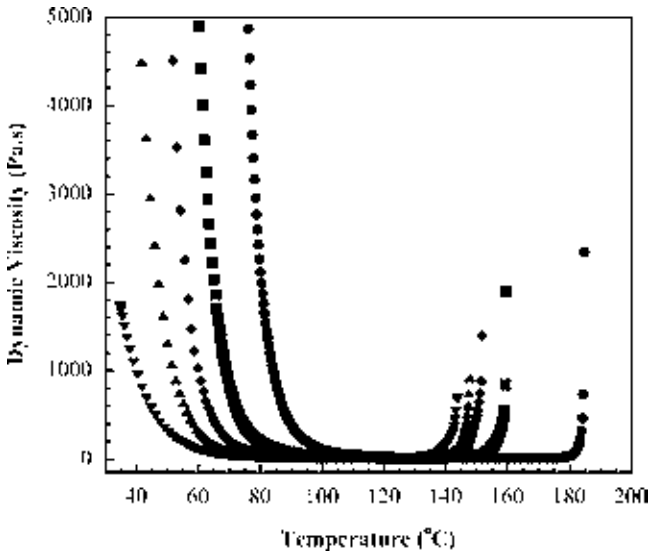

Fig. 1. Viscosity of BA-a/CNSL resin at various compositions: (●) BA-a/CNSL 100/0, (■) BA-a/CNSL 90/10, (♦) BA-a/CNSL 80/20, (▲) BA-a/CNSL 70/30 and (▼) BA-a/CNSL 60/40.

2.2. Preparation of benzoxazine–cashew nut oil matrix

Benzoxazine monomer used was synthesized from bisphenol A, aniline and formaldehyde at a molecular ratio of 1:2:4. The monomer synthesis was based on the patented solventless synthesis technique [9]. The reactants were physically mixed and heated to their melting point temperature thereafter maintained at a temperature sufficient to complete the interaction of the reactants to produce the benzoxazine monomer [10]. The BA-a blended with CNSL was used as a composite matrix and was prepared at temperature of 80 °C.

2.3. Preparation of wood-BA-a/CSNL alloy composites

Bamboo fiber was dried at temperature of 100 °C for 24 h to get a constant weight. A fixed bamboo fiber content of 65 wt% was compounded with BA-a/CSNL mixture in an aluminum container at 80 °C for at least 30 min in order to ensure fiber wet-out by the resin. Due to the relatively low viscosity of the matrix at 80 °C, the fiber can be impregnated by manual mixing following the method in Refs. [32,33]. The viscosity of all matrices was illustrated in Fig. 1. The compound was placed in a preheated 60 mm × 25 mm × 3 mm stainless steel mold and compressed in a hydraulic press using a pressure of 15 MPa and at temperature of 110 °C for 0.5 h and 170 °C for 3.5 h. The cured specimens were left to cool down at room temperature in an open mold before testing.

2.4. Evaluation of chemorheological properties

Chemorheological properties of each alloy were examined using a rheometer (Haake Rheo Stress 600, Thermo Electron Cooperation) equipped with 35 mm in diameter parallel plate geometry. The measuring gap was set at 0.5 mm. The experiment was performed under an oscillatory shear mode at 1 rad s^{-1}. The testing temperature program was ramped from room temperature at a heating rate of 2 °C min^{-1} to a temperature beyond the gel point of each resin and the dynamic viscosity was recorded.

2.5. Evaluation of curing reaction and kinetic parameters of BA-a/CSNL matrices

The curing behavior and kinetic parameters were measured by a differential scanning calorimeter (DSC) model 2910 from TA Instrument. The heating rates were 1, 3, 5 and 10 °C min^{-1} from 30 to 300 °C under nitrogen gas purging.

2.6. Evaluation of curing behavior of BA-a/CNSL blends

Fourier transform infrared spectra of all samples under various curing conditions were acquired by using a Spectrum GX FT-IR spectrometer from Perkin Elmer. All spectra were taken as a function of time with 64 scans at a resolution of 4 cm^{-1} and a spectral range of 4000–650 cm^{-1}. The powder sample was mixed with KBr powder. The mixed powder was pressed into pellet before measurement.

2.7. Mechanical properties analysis

The dynamic mechanical analyzer (DMA) model DMA 242 from NETZSCH was used to investigate the dynamic mechanical properties and relaxation behaviors of BA-a/CNSL polymer alloys. The dimension of specimens was 10 mm × 50 mm × 2 mm. The test was performed in a three-point-bending mode. In a temperature sweep experiment, a frequency of 1 Hz and a strain value of 0.1% were applied. The temperature was scanned from room temperature to T_g of each specimen with a heating rate of 2 °C min^{-1} under nitrogen atmosphere.

The flexural modulus and flexural strength of the wood composite specimens were determined according ASTM D790 employing a Universal Testing Machine, Instron, Model 5567 equipped with a 1 kN load cell. The measurement was performed in a 3-point bending mode with a support span of 48 mm and at a crosshead speed of 1.2 mm/min. A minimum of five samples with a dimension of 25 mm × 60 mm × 3 mm was tested and the averaged values were determined.

3. Results and discussion

3.1. Chemorheological properties of BA-a/CNSL resin mixtures

The complex viscosity values of the BA-a, 90/10 BA-a/CNSL, 80/20 BA-a/CNSL, 70/30 BA-a/CNSL and 60/40 BA-a/CNSL as a function of temperature are illustrated in Fig. 1. During heating, these uncured monomers became softened and viscosity rapidly decreased as temperature approached their softening points. The next stage was the lowest viscosity range of the resin mixtures as all compositions became liquid. This stage provided a processing window for the compounding process of each alloy. At the final stage, the binary mixture underwent crosslinking reactions past their gel points resulting in a sharp increase in their viscosities.

As seen from Fig. 1, the temperature of resin mixture was ramped from 40 °C up to beyond the gel point of each sample using a heating rate of 2 °C min^{-1} and a dynamic viscosity was recorded. On the left hand side of Fig. 1, the liquefying temperature of the binary mixture was indicated by the lowest temperature that the viscosity rapidly approached its minimum value. For consistency, the temperature at the viscosity value of 1000 Pa s was used to determine liquefying temperature of each resin [11]. The liquefying temperature significantly decreased with increasing amount of cashew nut shell liquid oil fraction i.e. 83 °C (BA-a), 68 °C (90/10 BA-a/CNSL), 59 °C (80/20 BA-a/CNSL), 50 °C (70/30 BA-a/CNSL) and 39 °C (60/40 BA-a/CNSL). This may be due to the fact that the CNSL is liquid while benzoxazine resin is solid at room temperature. Therefore addition of liquid (CNSL) in the solid (BA-a resin) resulted in

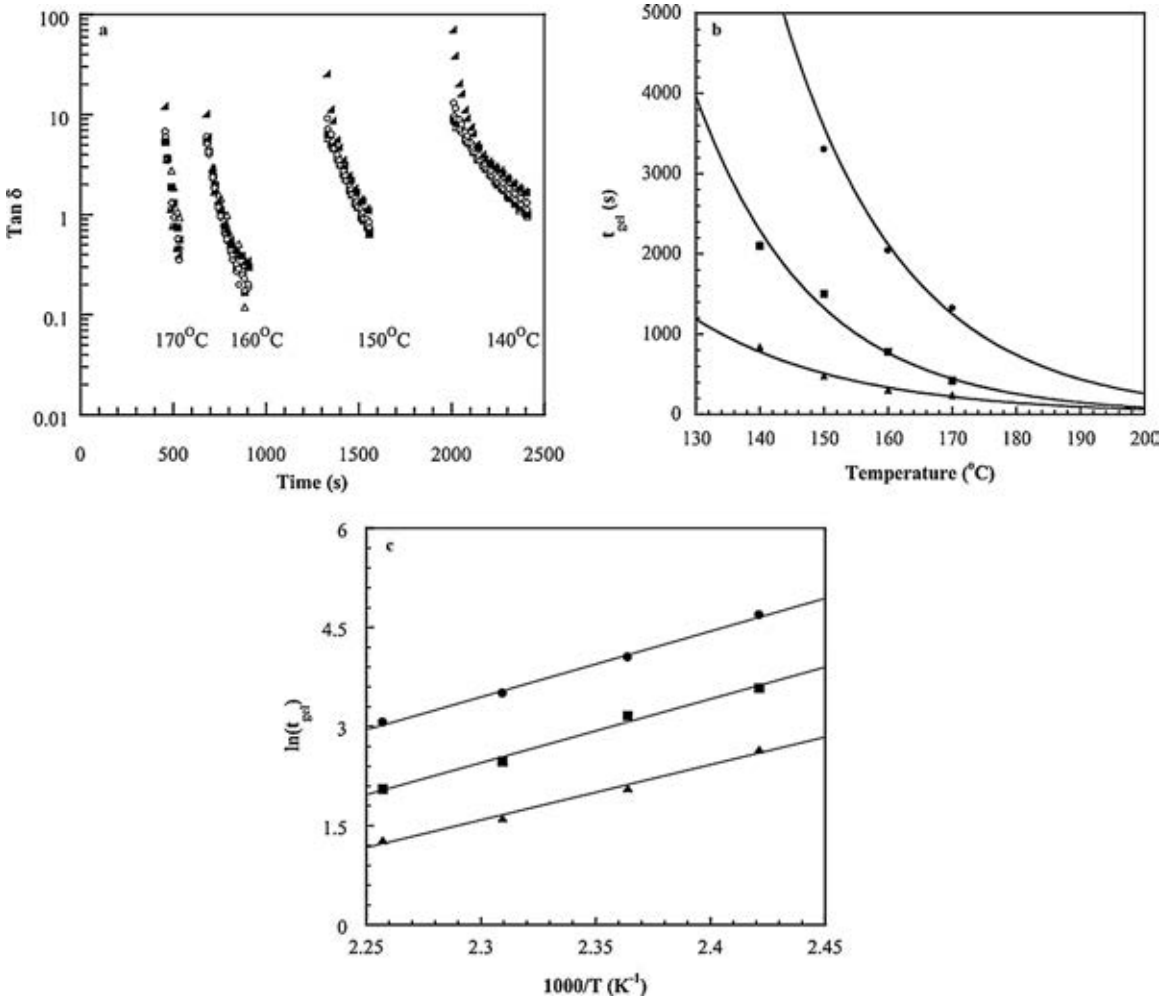

Fig. 2. (a) Effect of gel temperature on the gel time of BA-a mixed with CNSL at composition 90:10 (●) 1.6 Hz, (□) 2.8 Hz, (♦) 5.0 Hz, (△) 9.0 Hz and (▼) 15.9 Hz. (b) Gelation behavior of BA-a/CNSL revealing the gel time as a function of gel temperature at compositions: (●) BA-a/CNSL 100/0, (■) BA-a/CNSL 90/10 and (▲) BA-a/CNSL 70/30. (c) The Arrhenius plot of the gelation behavior of BA-a/CNSL at compositions: (●) BA-a/CNSL 100/0, (■) BA-a/CNSL 90/10 and (▲) BA-a/CNSL 70/30.

softer material at room temperature with lower liquefying point. The lowest viscosity at room temperature was observed in a 40 wt% CNSL system. In practice, lowering the resin liquefying temperature obviously enables the use of lower processing temperature for a compounding process, which is desirable in various applications.

On the right hand side of Fig. 1, gel temperature of each resin mixture can be evaluated. The temperature at which viscosity was rapidly raised above 1000 Pa s was used to indicate gel temperature of each resin [11]. The gel temperatures tended to decrease with increasing the CNSL content i.e. the gel temperatures of BA-a, 90/10 BA-a/CNSL, 80/20 BA-a/CNSL, 70/30 BA-a/CNSL and 60/40 BA-a/CNSL were observed to be 184, 159, 152, 147 and 143 °C, respectively. This result implied that CNSL can be not only a reactive diluent for benzoxazine resin but also a good initiator to lower the curing temperature or gel point of the benzoxazine resin.

3.2. Evaluation of activation energy of BA-a/CNSL resin mixtures

Some of the important aspects of thermosetting polymer include their gelation behavior, kinetic of gelation and the gel time. Sol–gel or gel point is one critical phenomenon that is crucial for the material processing. The gel points of samples can be accurately determined by dynamic rheological measurements which are sensitive to degree of crosslinking. In principle, elastic modulus and viscous modulus present the same power-law variation with respect to the frequency of oscillation at a gel point [12]. The corresponding expressions describing the dynamic moduli at the gel point were as follow:

$$\tan\delta = \frac{G''}{G'} = \tan\left(\frac{n\pi}{2}\right) \quad (1)$$

where G' is storage modulus, G'' is loss modulus and n is the relaxation exponent which is network specific. The above expression suggests frequency independent nature of tan δ at gel point. Experimentally, this is the point where tan δ curves of various frequencies crossover each other.

Fig. 2(a) shows the gel point of BA-a/CNSL at 90/10 mass ratio which was cured isothermally at 140, 150, 160 and 170 °C and at different frequencies i.e. 1.6, 2.8, 5, 9 and 15.6 Hz as a function of time (s). From the plot, the points that tan δ is frequency independent were at time equal 35 min (140 °C), 25 min (150 °C), 13 min (160 °C) and 7 min (170 °C) corresponding to the gel time at each temperature. The gel times of the resin mixtures expectedly decreased with increasing temperature. Gel times of other BA-a/CNSL systems at different temperatures were also obtained from the tan δ plots similar to the result in Fig. 2(a). Fig. 2(b) illustrates a relationship between gel time and temperature of BA-a/CNSL systems at varied compositions. All resin mixtures exhibited an exponential decay behavior of the gel time with increasing temperature. This could be due to the fact that raising the processing temperature increased the rate of crosslinking of BA-a/CNSL systems. As a result, the higher

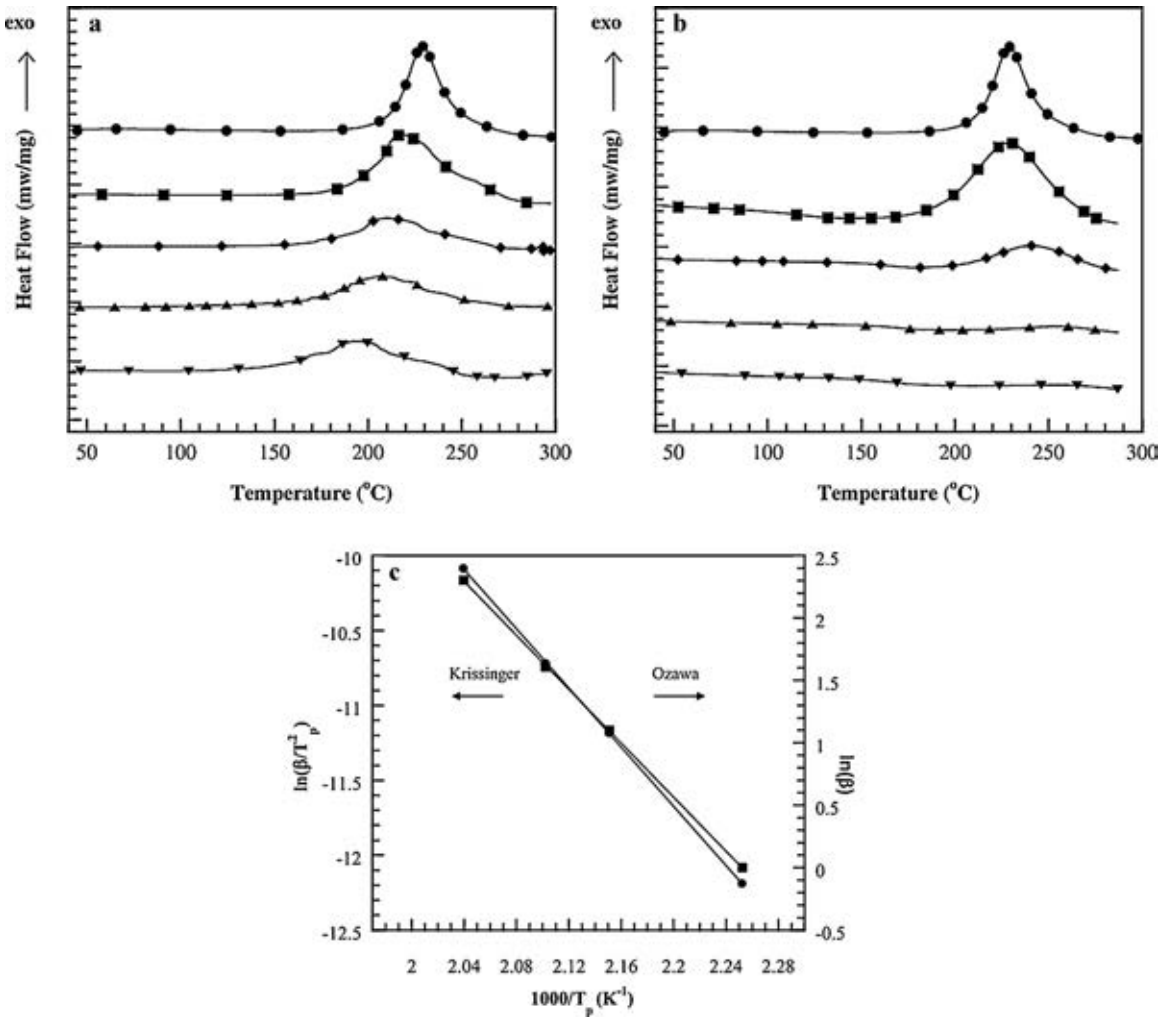

Fig. 3. (a) DSC thermograms of BA-a/CNSL resin at various compositions: (●) BA-a/CNSL 100/0, (■) BA-a/CNSL 90/10, (♦) BA-a/CNSL 80/20, (▲) BA-a/CNSL 70/30 and (▼) BA-a/CNSL 60/40. (b) DSC thermograms of BA-a at various curing conditions: (●) uncured, (■) 160 °C/1 h, (♦) 180 °C/1 h, (▲) 200 °C/1 h and (▼) 200 °C/2 h. (c) (●) Kissinger method and (■) Ozawa method plots for averaged activation energy determination of 90/10 BA-a/CNSL.

curing temperature, the faster the resin systems can reach their gel point. Additionally, from the figure, the gel time tended to decrease with increasing the CNSL content comparing at the same temperature. For instance, at 140 °C the gel time BA-a = 108 min, BA-a/CNSL 90/10 = 35 min and BA-a/CNSL 70/30 = 14 min. This result also indicated that the curing conversion of the BA-a/CNSL was raised with increasing CNSL content.

According to Winter and Chambon, $\tan\delta$ is independent of frequencies at the gel point of the polymer. The frequency independence of the loss tangent in the vicinity of the gel point has been widely used to determine the gel time (t_{gel}) in either chemical or physical gels. Additionally, activation energy of gelation process can be evaluated and calculated from the gel times at different isothermal temperatures using Arrhenius model following Eq. (2) or (3)

$$t_{gel} = A \exp\left(\frac{\Delta E}{RT}\right) \quad (2)$$

or

$$\ln(t_{gel}) = \ln A + \left(\frac{\Delta E}{RT}\right) \quad (3)$$

where t_{gel} is gel time, A is a pre-exponential factor, E is activation energy (kJ mol^{-1}) and T is temperature (K).

Fig. 2(c) displays the Arrhenius plot revealing the effect of the reactive CNSL on the gel time of BA-a resin. The activation energy calculated from the slopes of the curves was 84 kJ mol^{-1} (BA-a), 80 kJ mol^{-1} (90/10 BA-a/CNSL) and 71 kJ mol^{-1} (70/30 BA-a/CNSL). These activation energy values decreased with increasing amount of the CNSL. Moreover, the different y-intercepts at various CNSL content in Fig. 2(c) were also related to the initial temperature that material started the gelation process. The lowest y-incept value was found in 70/30 BA-a/CNSL system while the neat BA-a provided the highest value. This result implied that the presence of 30 wt% CNSL in BA-a required lower starting temperature for the gelation process than 90/10 BA-a/CNSL or neat BA-a.

3.3. Curing reaction and thermal properties of BA-a/CNSL resins

The neat benzoxazine resin (BA-a) is designed to thermally polymerize via a ring-opening addition reaction so that it does not yield any by-product. The curing reaction takes place either with or without catalyst or initiator. In general, it is a well known fact that oxazine ring opening is initiated by the presence of acidic catalysts [13]. The curing exotherms of the resin mixtures at various weight ratios of BA-a and CNSL are illustrated in Fig. 3(a). The peak exotherm and enthalpy of curing of BA-a were observed at 237 °C and 277 J g^{-1}. In the case of BA-a/CNSL mixtures, the peak exotherms and enthalpy of cure values were found to be lower than those of BA-a. When the amount of CNSL in samples increased, both peak exothermic temperature and enthalpy of cure

Table 1
Kinetic parameters evaluated from Kissinger and Ozawa methods.

BA-a/CNSL sample	Methods	
	Kissinger (kJ mol^{-1})	Ozawa (kJ mol^{-1})
100/0	84	87
90/10	82	85
70/30	74	79

values decreased i.e. 216 °C and 246 J g^{-1} (90/10 BA-a/CNSL), 207 °C and 224 J g^{-1} (80/20 BA-a/CNSL), 203 °C and 219 J g^{-1} (70/30 BA-a/CNSL) and 197 °C and 194 J g^{-1} (60/40 BA-a/CNSL). This result suggested that the anacardic acid in CNSL might act as a curing accelerator which caused a shift of the exotherm of the ring-opening reaction of the benzoxazine resin to lower temperature. The lowering of exotherms in benzoxazine systems had also been observed by the addition of other acidic protons such as poly (amide acid), clay, and titania [14–16]. In addition, the decrease of cure exotherms of BA-a/CNSL alloys may be possibly due to the presence of phenolic compounds in CNSL such as cardanol, cardol and 1-methylcardol. These phenolic compounds can act as initiator for the ring opening oligomerization of benzoxazine compounds [16]. The decrease of curing temperature of BA-a/CNSL alloys has a positive effect on the utilization of these alloys as a matrix for lignocellulosic composites i.e. a relatively lower curing temperature, or lower energy consumption, can be used. Generally, the curing or melting temperatures of wood composite molding compounds should be kept below 200 °C, except for a short period of processing time, in order to achieve samples with good mechanical integrity. A higher temperature can result in the release of volatiles, discoloration, odor, and embrittlement of the wood component [17].

The fully cured condition of BA-a and BA-a/CNSL systems was determined from the neat BA-a resin, which required the highest curing temperature among the investigated resin mixtures as depicted in Fig. 3(a). The DSC thermograms of BA-a resin after undergoing different curing conditions were shown in Fig. 3(b). The degree of conversion estimated by Eq. (4) was determined to be 20% after curing at 160 °C for 1 h, 72% after curing at 180 °C for 1 h, 96% after curing at 200 °C for 1 h and 100% after curing at 200 °C for 2 h. At the final step, the disappearance of exothermic peak of reaction indicated the fully cured of sample.

$$\%\,\text{conversion} = 1 - \left[\left(\frac{H_{rxn}}{H_o}\right) \times 100\right] \quad (4)$$

where H_{rxn} is the exothermic heat of reaction of the partially cured specimens, as determined from DSC, and H_o is the exothermic heat of reaction of the uncured resin.

3.4. Curing kinetic model of BA-a/CNSL matrix

To determine the curing kinetic parameters of BA-a/CNSL, a non-isothermal method in DSC experiment was used. The methods are widely used to study dynamic kinetics of thermosetting polymers as proposed by Kissinger and Ozawa. The detail of each method was described in the literatures [18,19].

From the non-isothermal DSC result of 90/10 (BA-a/CNSL) by using this multi heating rate data according to the Kissinger and Ozawa method, a good linear relationship between the heating rate and the reversal of the exothermic peak temperature can be obtained as shown in Fig. 3(c). The activation energy can also be calculated from the slope of the plot. The average activation energy values of BA-a and BA-a/CNSL are summarized in Table 1. The average activation energy of BA-a resin was calculated to be 84-87 kJ mol^{-1}. This values fall in the same range as those in our previous report [19]. The average activation energy of BA-a/CNSL system trended to decrease with increasing amount of CNSL content in the resin mixture i.e. 82–85 kJ mol^{-1} for 90/10 (BA-a/CNSL) and 74–79 kJ mol^{-1} for 70/30 (BA-a/CNSL). The decreasing activation energy of BA-a with increasing content of acid media was also observed in polybenzoxazine-clay hybrid nanocomposite [20]. Furthermore, a decrease of activation energy upon increasing CNSL content also had similar trend as that obtained from Arrhenius model in the gelation process.

3.5. Curing behaviors of BA-a blended with CNSL

The curing behavior of BA-a blend with CNSL was monitored by FT-IR spectroscopy. Fig. 4 shows example of FT-IR spectra in case of BA-a/CNSL at a fixed mass ratio of 80/20. In Fig. 4(a), the characteristic infrared adsorption bands of CNSL were observed at 990 and 912 cm^{-1} which correspond to phenol containing the pendent chain at meta position. The bands at 1264 and 1156 cm^{-1} were assigned to the symmetric and asymmetric stretching of the bounding C=C, respectively and the peak at 1588 cm^{-1} also related to the stretching of carbon double (C=C). The characteristic bands at 1650 cm^{-1} was assigned to (C=O) of anacardic. The peaks at 2852 and 2922 cm^{-1} corresponded to asymmetric and symmetric stretching of CH_3 and the peak around 3320 cm^{-1} was characteristic of the stretching of OH [21–23]. For BA-a/CNSL, as shown in Fig. 4(b) the characteristic adsorption peak of BA-a were 940 and 1232 cm^{-1}, which were assigned to the benzoxazine mode of the benzene ring that is adjacent to oxazine ring and trisubstituted benzene of the oxazine ring, respectively. According to the polymerization mechanism reported by Dunkers and Ishida [24], the oxazine ring is opened by the breakage of a C–O bond in it. Thereby the benzoxazine molecule was transformed from a ring structure to a network structure. During this process, the tri-substituted benzene ring, the backbone of the benzoxazine ring, became tetra-substituted. The indication of the ring-opening polymerization of BA-a was observed from the decrease of the absorption at 940 and 1232 cm^{-1} and the appearance of new adsorption band at 1487 cm^{-1} which is tetra tetra-substituted as shown in Fig. 4(c). Furthermore, the other adsorption bands of carbonyl group appeared in the region of 1750–1550 cm^{-1} which is assigned to the strong interaction between BA-a polymer and carboxylic acid. Especially, the appearance of the band at 1285 cm^{-1}

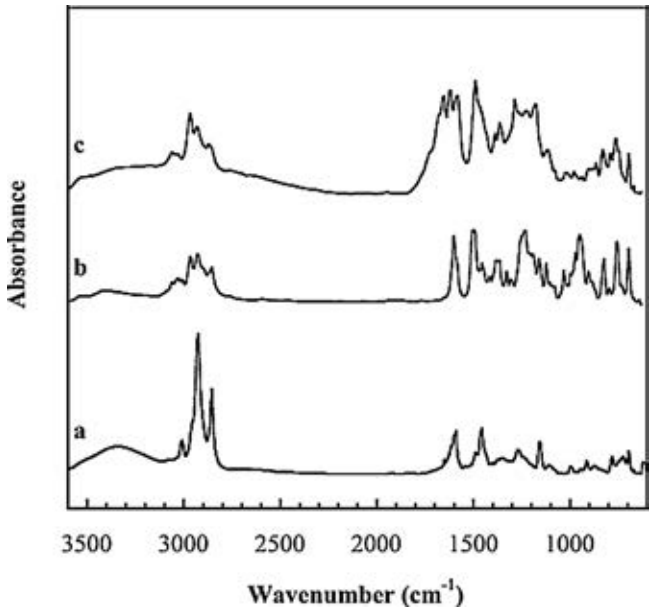

Fig. 4. IR spectra of (a) uncured CNSL, (b) uncured BA-a/CNSL 80/20 and (c) cured BA-a/CNSL 80/20 at 200 °C/2 h.

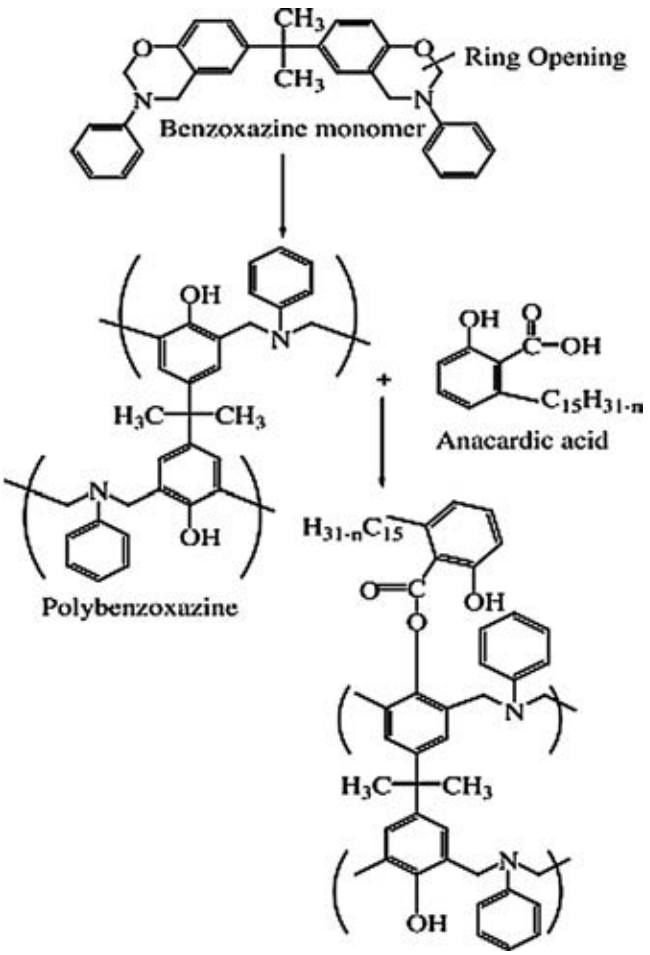

Scheme 1. A possible reaction between BA-a and CNSL.

could be assigned to the aromatic ester (Ar–COOR) that might from during curing reaction of BA-a/CNSL. This result may implied that the reaction between the phenolic (OH) of polybenzoxazine and carboxylic acid of CNSL component could occur as shown in Scheme 1. The similar reaction was also observed in the system of benzoxazine alloyed with poly (amide acid) [16].

3.6. Dynamic mechanical properties of BA-a/CNSL polymer matrix

Dynamic mechanical properties of the BA-a/CNSL alloys as a function of temperature are displayed in Fig. 5(a). The storage modulus (E') of a solid sample at room temperature provides a measure of material stiffness. The storage moduli of fully cured alloys were found to be 5.6 GPa for BA-a, 4.8 GPa for 90/10 (BA-a/CNSL), 4.7 GPa for 80/20 (BA-a/CNSL), 4.0 GPa for 70/30 (BA-a/CNSL) and 3.9 GPa for 60/40 (BA-a/CNSL). The storage moduli at room temperature of BA-a/CNSL polymers systematically decreased with increasing amount of CNSL. The decrease of storage moduli in alloys can be explained by the plasticizing effect of the CNSL on the polybenzoxazine. Though, the presence of CNSL in BA-a resulted in a more ductile polymer hybrids, the storage moduli values of BA-a/CNSL matrix were still higher than those of major unfilled thermosets used as wood composite matrices including phenolic resin (1 GPa) [25], and unsaturated polyester (8.8×10^{-3} GPa) [26].

Furthermore, the rubbery plateau modulus value in Fig. 5(a) can be used to determine crosslink density of the alloy network. In the past, some researchers have attempted to apply theory of rubber elasticity to quantify crosslink density and molecular weight between crosslinks/entanglements of network forming polymer. However, this theory is strictly applicable to lightly crosslinked materials. For highly crosslinked polymer network, the Gaussian distribution of the chain between crosslink is no longer applied and its crosslink density is more precisely estimated by the Nielson equation,

$$\log\left(\frac{E'}{3}\right) = 7.0 + 293\left(\frac{\rho}{M_c}\right) \quad (5)$$

where E' (dynes cm^{-2}) is the storage modulus in a rubbery plateau region, ρ (g cm^{-3}) is the density of the material at room temperature and M_c (g mol^{-1}) is the molecular weight between crosslink points [4,27,28]. From the results, addition of CNSL content from 0 to 30 wt% provided a maximum in the crosslink density of BA-a/CNSL alloys i.e. 3383 mol m^{-3} (BA-a), 4517 mol m^{-3} (BA-a/CNSL 90/10), 4357 mol m^{-3} (BA-a/CNSL 80/20), and 3471 mol m^{-3} (BA-a/CNSL 70/30). This behavior also implied that only a certain content of CNSL i.e. ~10–20 wt%, yielded highly crosslinked net-

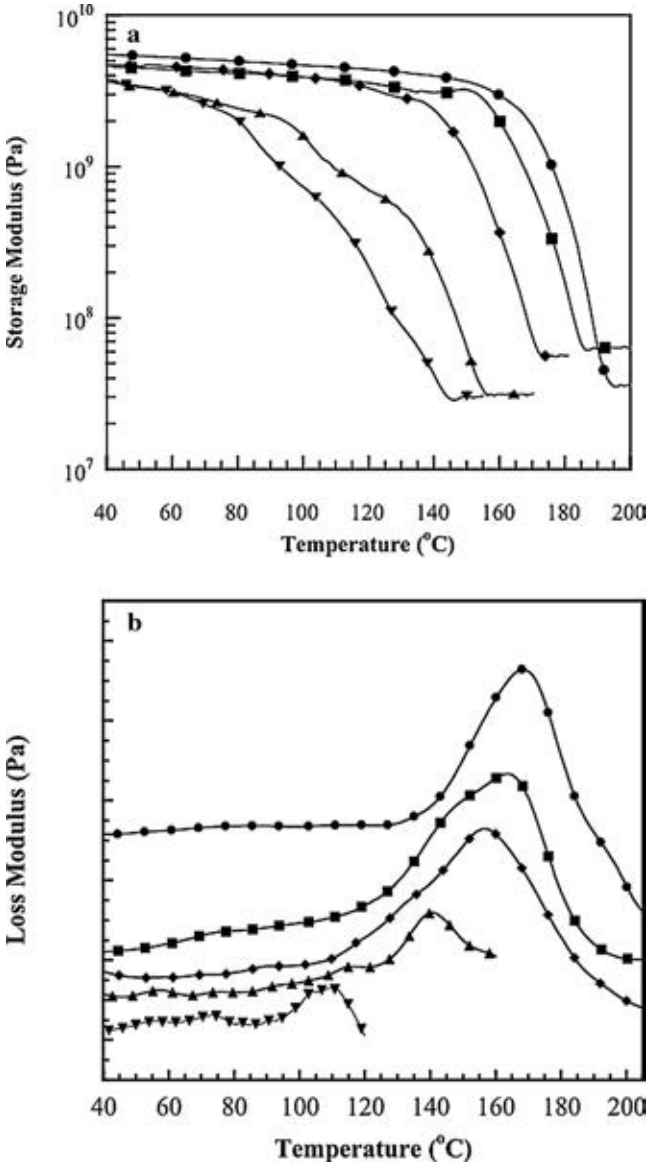

Fig. 5. (a) Storage modulus of BA-a/CNSL alloys obtained from fully cured condition at various CNSL compositions: (●) BA-a/CNSL 100/0, (■) BA-a/CNSL 90/10, (♦) BA-a/CNSL 80/20, (▲) BA-a/CNSL 70/30 and (▼) BA-a/CNSL 60/40. (b) Loss modulus of BA-a/CNSL alloys obtained from fully cured condition at various CNSL compositions: (●) BA-a/CNSL 100/0, (■) BA-a/CNSL 90/10, (♦) BA-a/CNSL 80/20, (▲) BA-a/CNSL 70/30 and (▼) BA-a/CNSL 60/40.

Table 2
Swelling and solvent extraction properties of BA-a/CNSL alloys.

Composition (BA-a/CNSL)	% Swelling	% Solvent extraction
100/0	1.78	0.95
90/10	0.96	0.10
80/20	2.87	0.30
70/30	6.63	1.01
60/40	15.4	10.6

work structure due to the possibly network formation between benzoxazine resin and anacardic acid in CNSL. This optimal content is similar to the optimal amount of phenolic novolac resin in the same type of polybenzoxazine [31] or the optimal content of epoxy resin in the polybenzoxazine [3].

Glass transition temperatures (T_g) of fully cured BA-a/CNSL polymer alloys were obtained from Fig. 5(b). The T_gs of the crosslink materials were determined from the maximum of the loss modulus (E'') of the figure. From a practical point of view, the maximum E'' is the most appropriate value. It corresponds to the initial drop from the glassy state into the rubbery state. The T_g of BA-a and BA-a/CNSL alloys was found to decrease when the CNSL content increased with the values ranging from 168 °C in BA-a to 110 °C in 60/40 BA-a/CNSL. This is probably due to the fact that the T_g of typical cashew nut shell liquid oil cured with cobalt naphthenate is reported to be about 60 °C [29] whereas the neat polybenzoxazine possesses a higher T_g of 165 °C. Consequently, the T_gs of the alloy systems became lower as the CNSL content increased. Moreover, the decreasing T_gs of BA-a/CNSL alloys may be due to the aliphatic nature of CNSL thus it can act as a plasticizer especially when the excess amount of CNSL presents in the polybenzoxazine. The decrease in the T_g of polybenzoxazine was also observed when benzoxazine resin was alloyed with phenolic novolac and novel glycidyl phosphine oxide [29,30].

3.7. Investigation of network formation ability of BA-a/CNSL alloys

The network formation ability of the BA-a/CNSL matrices at different composition of CNSL was assessed by solvent extraction method. In the test, the alloy specimens were immersed in chloroform for 15 days. After the immersion, it was observed that BA-a, 70/30 BA-a/CNSL and 60/40 BA-a/CNSL showed a deep color change of solvent due to a release of significant amount of extractives from each specimen. In addition, when the amount of CNSL in the polymer alloys was 30 wt% or greater, specimen disintegration from the solvent extraction test was observed. Beyond 30 wt% of CNSL, it was expected that excessive amount of CNSL might cause the formation of discontinuous network or network clusters. On the other hand, 80/20 BA-a/CNSL specimen exhibited slight color change and 90/10 BA-a/CNSL specimen showed almost no color change of the solvent. The percentages of swelling and solvent extraction are summarized in Table 2. It is clear that the optimum of CNSL i.e. 10 wt%, provided a near-zero solvent extraction value with the lowest degree of swelling. These results also suggested that the optimal content of CNSL of 10 wt% can contribute to a more perfect network formation of BA-a polymer. The solvent extraction results were also consistent with the crosslink density results of these alloys.

3.8. Characterization of BA-a/CNSL composites reinforced with bamboo fiber

The storage moduli as a function of temperature of the 65 wt% of bamboo fiber filled BA-a/CNSL alloys are plotted in Fig. 6(a). From the plot, the storage moduli at room temperature of the composites were observed to be in a range 3.7–6.3 GPa. It is clearly seen that all of the BA-a/CNSL alloys reinforced with 65 wt% bamboo fiber had significantly higher storage modulus values than those of unfilled BA-a/CNSL alloys. This is due to the reinforcing effect of bamboo fiber on the BA-a/CNSL matrices implying the substantial interfacial bonding between the alloy matrix and the bamboo fiber. From our previous reports, the presence of the phenolic structure in lignin fraction of woodflour and the abundance of hydroxyl moieties in the filler is believed to provide a composite system with strong interfacial bonding to the polybenzoxazine [32,33].

Fig. 6(b) exhibits a plot of the loss modulus of BA-a/CNSL filled with 65 wt% of bamboo fiber. As previously mentioned, the peak position of the loss modulus was used to determine T_g of each sample. It was evident that the T_g of the wood composites increased with an increase in polybenzoxazine fraction in the BA-a/CNSL alloys similar to the unfilled systems. The T_gs of BA-a, 90/10 BA-a/CNSL, 80/20 BA-a/CNSL, 70/30 BA-a/CNSL and 60/40 BA-a/CNSL composites were determined to be 181, 178, 168, 133 and 113 °C, respectively. The values were also higher than those of the unfilled

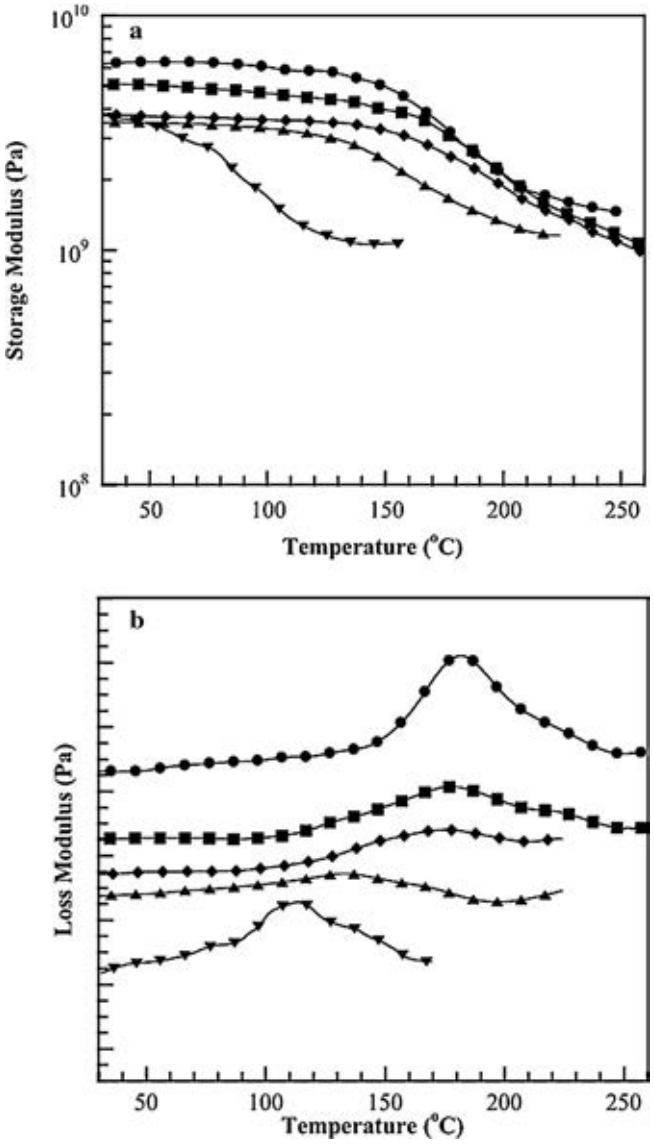

Fig. 6. (a) Storage modulus of BA-a/CNSL reinforced with bamboo at various CNSL compositions: (●) BA-a/CNSL 100/0, (■) BA-a/CNSL 90/10, (♦) BA-a/CNSL 80/20, (▲) BA-a/CNSL 70/30 and (▼) BA-a/CNSL 60/40. (b) Loss modulus of BA-a/CNSL reinforced with bamboo at various CNSL compositions: (●) BA-a/CNSL 100/0, (■) BA-a/CNSL 90/10, (♦) BA-a/CNSL 80/20, (▲) BA-a/CNSL 70/30 and (▼) BA-a/CNSL 60/40.

matrices suggesting significant interfacial bonding between the bamboo fiber and the polymer alloys.

3.9. Flexural properties of bamboo fiber composites based on BA-a/CNSL matrices

Flexural properties of bamboo fiber filled BA-a/CNSL alloys are depicted in Fig. 7(a). The average flexural modulus of our bamboo fiber composites was ranging from 3.9 to 6 GPa. The flexural modulus as a function of CNSL content showed a behavior nearly identical to that of the storage modulus determined by DMA i.e. the flexural modulus trended to decrease when the amount of CNSL increased. From Table 3, the flexural modulus of the bamboo-filled BA-a/CNSL alloys was significantly higher than those of reported wood plastic composites e.g. 50–70 wt% commercial wood particles reinforced HDPE (2.7–3.1 GPa) [34], 40 wt% bamboo fiber reinforced HDPE (3.1 GPa) [35] and 39 wt% bamboo fiber reinforced unsaturated polyester (3.6 GPa) [36]. Fig. 7(a) also exhibits flexural strength of the bamboo composites to be ranging from 54 to 66 MPa. The flexural strength of the composites was found to slightly decrease when the amount of CNSL increased. However, the bamboo filled BA-a/CNSL showed flexural strength higher than those major wood

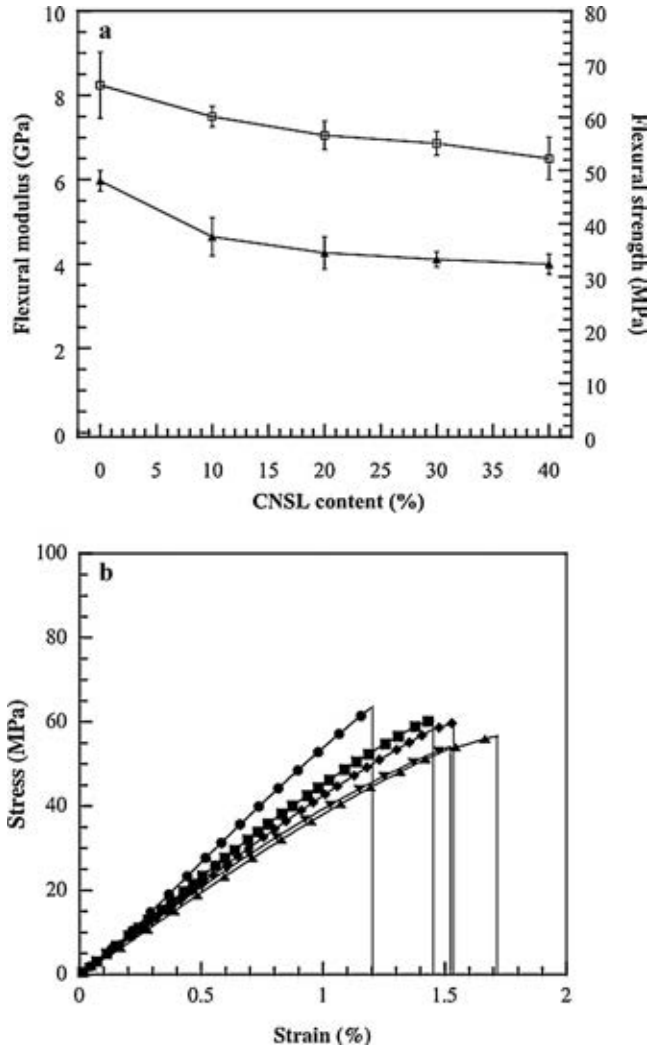

Fig. 7. (a) Effect of CNSL content on mechanical properties of bamboo composite: flexural modulus (▲) and flexural strength (□). (b) Flexural stress and strain relationship of bamboo-reinforced BA-a/CNSL reinforced with bamboo fiber at various CNSL compositions: (●) BA-a/CNSL 100/0, (■) BA-a/CNSL 90/10, (♦) BA-a/CNSL 80/20, (▲) BA-a/CNSL 70/30 and (▼) BA-a/CNSL 60/40.

Table 3
Flexural modulus and flexural strength of various natural fiber-reinforced composites.

Composite type	Mass fraction of fiber (wt%)	Flexural modulus (GPa)	Flexural strength (MPa)
Commercial wood flake reinforced HDPE	50–70	2.7–3.1	18–31
Bamboo fiber reinforced HDPE	40	3.1	21
Bamboo fiber reinforced unsaturated polyester	39	3.6	–

plastic composite products listed in Table 3.

Fig. 7(b) illustrates flexural stress and strain curves of bamboo reinforced BA-a/CNSL matrices. From the figure, flexural strains at break of the composites were 1.20% BA-a, 1.45% BA-a/CNSL (90/10), 1.55% BA-a/CNSL (80/20), 1.71% BA-a/CNSL (70/30) and 1.52% BA-a/CNSL (60/40). The improved strain behavior may be caused by the addition of the more flexible CNSL fraction to the polybenzoxazine matrix. Additionally, the area under the flexural stress–strain curve refers to the energy absorption capability of the alloy materials which indicated the toughness of materials. The area under the curve tended to increase slightly with the amount of CNSL in the alloys i.e. 37 MPa at BA-a/CNSL (100/0), 40 MPa BA-a/CNSL (90/10), 42 MPa BA-a/CNSL (80/20), 43 MPa BA-a/CNSL (70/30), and 38 MPa BA-a/CNSL (60/40). The slight decrease of the toughness when CNSL content was greater than 30 wt% was likely from the discontinuous or imperfect network formed from the presence of excess amount of CNSL in the polybenzoxazine as discussed in the solvent extraction experiment.

4. Conclusions

An addition of cashew nut shell liquid oil in benzoxazine resin can substantially reduce the liquefying temperature, gel time, curing temperature and activation energy of the benzoxazine resin. A benzoxazine resin alloyed with cashew nut shell liquid oil was developed as highly processable matrices for wood composite products. The bamboo fiber content as high as 65% by weight was able to be incorporated into the obtained matrices due to the relatively low melt viscosity of the BA-a/CNSL mixtures. The obtained bamboo fiber-reinforced composites exhibited good compatibility between the fiber and the matrices thus attributed to enhancement on glass transition temperature and mechanical integrity of the samples.

Acknowledgements

This research receives financial support from Dutsadi Phiphat Scholarship of Chulalongkorn University. Additional supports are from the Thailand Research Fund (S. Rimdusit), the National Research University Project of the Ministry of Education, Thailand (AM1076A and AM006B), and 100th Anniversary of Chulalongkorn University Academic Funding. Material supplied by Thai Polycarbonate Co., Ltd. (TPCC), Forest Products Division, Royal Forest Department, Thailand and Maboonkrong Sirichai 25 Ltd., are greatly appreciated.

References

[1] H. Ishida, Y. Rodriguez, J. Appl. Polym. Sci. 58 (1995) 1751–1760.
[2] X. Ning, H. Ishida, J. Polym. Sci. A: Polym. Chem. 32 (1996) 1121–1129.
[3] H. Ishida, D.J. Allen, Polymer 37 (1996) 4487–4495.
[4] H. Ishida, Y.H. Lee, Polymer 42 (2001) 6971–6979.
[5] B. Lochab, I.K. Verma, J. Bijwe, J. Therm, Anal. Calorim 102 (2010) 769–774.
[6] E.T.N. Bisanda, M.P. Ansell, J. Mater. Sci. 27 (1992) 1690–1700.
[7] P. Peungjitton, P. Sangvanich, S. Pornpakakul, A. Petsom, S. Roengsumran, J. Surfact. Det. 12 (2009) 85–89.

[8] E. Papadopoulou, K. Chrissafis, Thermochim. Acta 512 (2011) 105–109.
[9] H. Ishida, US Patent 5,543,516, 1996.
[10] N.N. Ghosh, B. Kiskan, Y. Yagci, Prog. Polym. Sci. 32 (2007) 1344–1391.
[11] C. Jubsilp, T. Takeichi, S. Rimdusit, J. Appl. Polym. Sci. 104 (2007) 2928–2938.
[12] H.H. Winter, F. Chanbon, J. Rheol. 30 (1986) 367–382.
[13] H. Ishida, D.J. Allen, J. Appl. Polym. Sci. 79 (2001) 406–417.
[14] T. Agag, H. Tsuchiya, T. Takeichi, Polymer 45 (2004) 7903–7910.
[15] T. Takeichi, R. Zeidam, T. Agag, Polymer 43 (2002) 45–53.
[16] T. Takeichi, Y. Guo, S. Rimdusit, Polymer 46 (2005) 4909–4916.
[17] J.A. Youngquist, Wood-based Composites and Panel Products, Wood Hand Book, U.S. Department of Agriculture Government Printing Office, Madison, WI, 1999.
[18] M.V. Alonso, M. Oliet, J.M. Perez, F. Rodriguez, J. Echeverria, Thermochim. Acta 419 (2004) 161–167.
[19] C. Jubsilp, S. Damrongsakkul, T. Takeichi, S. Rimdusit, Thermochim. Acta 447 (2006) 131–140.
[20] D.R. Yei, H.K. Fu, W.Y. Chen, F.C. Chang, J. Polym. Sci. B: Polym. Phys. 44 (2006) 347–358.
[21] F.G. Souza, J.C. Pinto, G.E. de Oliveira, B.G. Soares, Polym. Test. 26 (2007) 720–728.
[22] L.Y. Mwaikambo, M.P. Ansell, J. Mater. Sci. 36 (2001) 3693–3698.
[23] R. Chelikani, Y.H. Kim, D.Y. Yoon, D.S. Kim, Appl. Biochem. Biotechnol. 157 (2009) 263–277.
[24] J. Dunkers, H. Ishida, J. Polym. Sci. A: Polym. Chem. 37 (1999) 1913–1921.
[25] M. Das, D. Chakraborty, J. Reinf. Plast. Compos. 28 (2009) 1339–1348.
[26] A.L. Pothan, Z. Oomen, S. Thomas, Compos. Sci. Technol. 63 (2003) 283–293.
[27] H. Ishida, D.P. Sanders, J. Polym. Sci. B: Polym. Phys. 38 (2000) 3289–3301.
[28] D.C.C. Lam, A.C.M. Chong, Mater. Sci. Eng. A 281 (2000) 156–161.
[29] R. Ikeda, H. Tanka, H. Uyama, S. Kobayashi, Polymer 43 (2002) 3475–3481.
[30] M.A. Espinosa, M. Galia, V. Cadiz, Polymer 45 (2004) 6103–6109.
[31] S. Rimdusit, N. Kampangsaeree, W. Tanthapanichakoon, T. Takeichi, N. Suppakarn, Polym. Eng. Sci. 45 (2007) 140–149.
[32] S. Rimdusit, W. Tanthapanichakoon, C. Jubsilp, J. Appl. Polym. Sci. 99 (2006) 1240–1253.
[33] C. Jubsilp, T. Takeichi, S. Hiziroglu, S. Rimdusit, Bioresour. Technol. 99 (2008) 8880–8886.
[34] P.W. Balasuriya, L. Ye, Y.W. Mai, Compos. Part A 32 (2001) 619–629.
[35] H. Liu, Q. Wu, G. Han, F. Yao, Y. Kojima, S. Suzuki, Compos. Part A 39 (2008) 1891–1900.
[36] K.M.M. Rao, K.M. Rao, A.V.R. Prasad, Mater. Des. 31 (2010) 508–513.

ENGINEERING JOURNAL

Kevlar™ Fiber-Reinforced Polybenzoxazine Alloys for Ballistic Impact Applications

Sarawut Rimdusit [1,*], Somsiri Pathomsap[1], Pornnapa Kasemsiri[1], Chanchira Jubsilp[2], and Sunan Tiptipakorn[3]

1Polymer Engineering Laboratory, Department of Chemical Engineering, Faculty of Engineering, Chulalongkorn University, Bangkok 10330, Thailand
2Department of Chemical Engineering, Faculty of Engineering, Srinakharinwirot University, Khong 16, Ongkharak, Nakhonnayok 26120, Thailand
3Department of Chemistry, Faculty of Liberal Arts and Science, Kasetsart University, Kamphaeng Saen, Nakhon Pathom 73140, Thailand
E-mail: sarawut.r@chula.ac.th*

Abstract. A light weight ballistic composites from Kevlar™-reinforcing fiber having polybenzoxazine (BA)/urethane prepolymer (PU) alloys as a matrix were investigated in this work. The effect of alloy compositions on the ballistic composite properties was determined. The increase of the elastomeric PU content in the BA/PU alloy resulted in samples with tougher characteristics; the storage modulus of the Kevlar™-reinforced BA/PU composites increased with increasing the mass fraction of polybenzoxazine. A ballistic impact test was also performed on the Kevlar™-reinforced BA/PU composites using a 9 mm handgun and it was found that the optimal composition of BA/PU alloys should be approximately 20wt% of PU. The extent of the delaminated area and interfacial fracture were observed to change with the varied compositions of the matrix alloys. The appropriate thickness of Kevlar™-reinforced 80/20 BA/PU composite panel was 30 plies and 50 plies to resist the penetration from the ballistic impact equivalent to levels II-A and III-A of NIJ standard. The arrangement of composite panels with the higher stiffness panel at the front side also showed the best efficiency ballistic penetration resistance.

Keywords: Polymer alloys, Kevlar™ fiber, ballistic composite, polybenzoxazine, urethane prepolymer.

ENGINEERING JOURNAL Volume 15 Issue 4
Received 23 June 2011
Accepted 3 September 2011
Published 1 October 2011
Online at http://www.ej.eng.chula.ac.th/eng/
DOI:10.4186/ej.2011.15.4.23

DOI:10.4186/ej.2011.15.4.23

1. Introduction

In the past, protective armors were traditionally made of metals. With the development of the thermoplastic polymers and synthetic fibers in recent years, hard armor systems with lighter weight have been produced, which combine the use of metals, and/or ceramics with polymeric fabrics as well as fiber-reinforced polymer composites. The development of armor materials has been focused on reducing the weight of the existing armor materials because the reduction of weight could helps in saving energy as well as increasing mobility [1, 2]. During the Vietnam War, it was reported that soft armors prepared from fabrics of fiber glass and nylon were used for ballistic protection [3]. Some of the commercial fibers used to manufacture armors include aramids (Kevlar^{TM} or Twaron^{TM}) [4], nylon fiber [5], polyethylene fiber (Spectra^{TM} or Dyneema^{TM}) [6, 7], and carbon fiber [8, 9]. The fibers should provide excellent impact resistance required for ballistic armors, and have high sonic velocity and high specific energy absorption as well as the capability to distribute kinetic energy upon ballistic impact [5]. Typical polymeric materials used in ballistic applications are ultra high molecular weight polyethylene (i.e. Dyneema^{TM}) and para-aramid fibers (i.e. Kevlar and Twaron). In general, Kevlar has been introduced as ideal type of base material for ballistic protection due to its outstanding thermal properties and high tensile properties. Its highly crystalline and highly oriented fine structure result in high modulus required for enhanced sonic velocity [3, 6, 10]. Consequently, the fiber is considered as a major reinforcing constituent for ballistic composites in this work. In composite material, even though each parent material (i.e. the fiber and the matrix) cannot provide ballistic resistant properties by itself; the combination of the two components had been found to exhibit an enhanced level of ballistic protection.

In general, an enhanced ballistic performance of light-weight armor requires its ability to deform and/or break-up the projectiles into small fragment and prevent the penetration of the projectile by absorbing projectile's kinetic energy. Absorption of kinetic energy of the composite composes of several mechanisms, including tensile failure of fibers, elastic deformation of composite, interlayer delamination, shear between layers in the composite, and inertia effect. Kinetic energy is absorbed and attributed according to key factors such as fiber mechanical properties, direction of fiber arrangement, matrix properties and interfacial strength [11-15].

Recently, the types of matrix binders for ballistic composites are such as thermoplastic resins [16, 17], thermosetting resin [12, 18, 19], and the alloys between thermoplastics and thermosets [14]. Other binders for Kevlar^{TM}-reinforced composites consisted of urethanes [15], epoxy resin [20, 21], polyester [22] styrene-isoprene-styrene [23]. In general, the function of the matrix resin is to hold the fibers firmly together in a three-dimensional array of crossing layers. The selection of a resin for the ballistic composite depends on its required characteristics such as rigidity, environmental resistance to thermal, wear, combustibility, process ability, and shelf-life. The amount of resin necessary to consolidate the fibers has been reported to be approximately 75-80 wt% [24, 25]. If the amount of resin used is substantially increased above the desired amount the matrix, it results in a major part of the armor volume weakening the materials. However, if the resin is less than that required to wet all fibers, this causes the fibers in the composite have not enough properties to consolidate and held in the proper position upon impact; then, the fiber tends to separate relatively easily allowing the projectile to pass through before the fiber absorb force [26]. In general, the resins used as a binder in ballistic armor have an adhesive characteristic with respect to the fiber, while the tensile strength of the resin should be lower than that of the fiber. That is, upon impact, the fiber will function predominantly to transmit impact force along its longitudinal axis. In principle, it is required that the resin should not hold the fiber too rigidly along the surface but allow some small amount of movement of the fiber surface longitudinally within the resin. Obviously, the composite structure resists and provides a limited fiber spreading transversely to the fiber axis upon projectile impact. In some previous works [19, 26], phenolic resins provide a future class of preferred resins for a composite armor. Phenolic resins are inexpensive and easy to handle employing conventional technology. However, they do not bond too firmly to ballistic fiber (especially Kevlar fiber); the moisture is driven from the resins during a curing stage (one additional step in the composite manufacturing process). Polybenzoxazine, a novel class of phenolic resins, has a wide range of mechanical and physical properties that can be tailored to various needs. The polymer can be synthesized by ring-opening polymerization of the aromatic oxazines with no by-products released upon curing, [27]. The property balance of the material renders the polymer

with very low A-stage viscosity, near-zero shrinkage, low water absorption, and fast development of mechanical properties as a function of curing conversion [28-30].

In this study, polybenzoxazine alloying with urethane elastomer used as matrix for ballistic armor composites were evaluated due to one major outstanding property of benzoxazine resin related to an ability to form hybrid network with several other resins for tailor-made behaviors [31-34]. Urethane elastomer was also used to alloy with benzoxazine resin to improve thermal stability and mechanical properties of the resulting polymer hybrids [34]. In this work, the word "alloy" was used in stead of "blend" because there has been evident from some previous works [35-37] that the chemical bonding were generated between polybenzoxazine and urethane elastomer. This makes it possible to fine tune and enhance the properties of the ballistic armor composites.

2. Experimental

2.1. Raw Materials

The materials are benzoxazine resin, urethane prepolymer and Kevlar™ from DuPont. Benzoxazine resin based on bisphenol-A, paraformaldehyde and aniline was synthesized by patented solventless method [27]. The bisphenol-A was supplied by Thai Polycarbonate Co., Ltd (TPCC). Paraformaldehyde and aniline were purchased from Merck Company, and Panreac Quimica SA Company, respectively. The obtained benzoxazine resin is clear-yellowish solid at room temperature. Urethane prepolymer was prepared from isophorone diisocyanate and polyether polyol (diol, MW=2000) using dibutyltin dilaurate as a catalyst. The isophorone diisocyanate was supplied by Degussa-Huls AG and the polyether polyol was available from TPI Polyol Co., Ltd. The urethane prepolymer is clearly viscous liquid at room temperature and it was kept in a refrigerator.

2.2. Composite Processing

The benzoxazine resin was mixed with the urethane prepolymer to provide BA/PU mixtures at the desirable mass fraction. The mixture was heated to about 80^{o}C in an aluminum pan and was thoroughly mixed manually for about 15-30 minutes until it was homogeneous. The weight ratios of binary mixtures at 90/10, 80/20, 70/30, and 60/40 BA/PU resins were evaluated as potentially matrices for Kelar^{TM}-reinforced composites.

The Kevlar^{TM} fabrics were compounded with binary mixture resins using the hand-lay up procedure at 80^{o}C. The weight fraction of fibers was kept constant at 70-80%. The molding compound was compression-molded using a compression molder at 160^{o}C for 2 hours. The samples were then post-cured in an oven at 170^{o}C, 180^{o}C, and 200^{o}C, each step for 2 hours. The fully cured specimens were left at room temperature and used for further characterization.

2.3. Sample Characterization

Dynamic mechanical analyzer (DMA) model DMA242 from NETZSCH was used to investigate the viscoelastic properties of the specimens. The strain at amplitude of 30 μm was applied sinusoidal with a frequency of 1 Hz. The specimen was heated at the rate of 5^{o}C/min from room temperature to 270^{o}C and the specimen dimension was 50mm×10mm×2 mm.

Thermal decomposition characteristic of the cured polymer alloys and the composites were studied using a thermogravimetric analyzer from Perkin Elmer (Diamond TG/DTA). The experiment was measured using a heating rate of 20^{o}C/min under nitrogen atmosphere. The temperature was ramped from 30^{o}C to 880^{o}C using the sample mass of about 15-20 mg.

Instron Universal testing machine, Model-5567 was used to determine flexural properties of composite specimens. The test method used was a three-point bending mode according to ASTM D790-00 (Method I) with a support span of 32 mm with a constant cross head speed of 0.85 mm/min. The specimen dimension was 50mm×25mm×2mm.

The ballistic tests were made using three different ammunitions. The tested composite plate with a dimension of 12.7cm×12.7cm was prepared; each plate was impacted with one projectile. The Kevlar^{TM}–reinforced polybenzoxazine alloy plates were 3.2 mm in thickness corresponding to two 10-

DOI:10.4186/ej.2011.15.4.23

ply laminates. The laminates with 20 plies were tested using a 9mm handgun with a standards grains round lead projectiles having a lead outer coating. The first experimental locations chosen for projectile impact were selected so as to evaluate the most suitable composition of the matrix alloys. In addition, the laminates with 20 and 30 plies were tested with standard 124 grains round lead projectile with a copper outer coating (Full Metal Jacket) typically used in the 9mm handgun. The impact velocity used was recommended by the NIJ standard for level II-A protection. The laminates with 40, 50 and 60 plies were tested with a test weapon, meeting the impact velocity according to standard for level III-A. Measured average velocity was determined as 426 m/s for the tests. The velocity of each shot was measured using a triggered timer. The damaged areas on each sample were evaluated.

Interfacial bonding of the composites after they were impacted was evaluated using a scanning electron microscope (JEOL, model JSM-5800LV) at an acceleration voltage of 15 kV. All specimens were coated with thin film of gold using an ion sputtering device (Balzers, model SCD040) for 4 minutes to have a thickness of approximately 30nm. The obtained micrographs were used to evaluate qualitatively the interfacial interaction between the matrix resin and the fiber and to study the mechanisms of ballistic energy absorption.

3. Results and Discussion

3.1. Properties of Cured BA/PU Alloys

The dynamic mechanical properties of the BA/PU polymer alloys are shown in Fig. 1. All specimens, i.e., 100/0 BA/PU, 80/20 BA/PU, 70/30 BA/PU, and 60/40 BA/PU were fully cured to yield highly cross-linked structure. As seen in Fig. 1, the storage moduli (E′) in the glassy state of the BA/PU polymer alloys expectedly decreased with increasing the PU fraction due to the incorporation of the more flexible structure of PU in the alloys as already described by Rimdusit et al. [35]. The urethane prepolymer molecule contains a large number of ether linkages in which the internal movement of the molecules is very active compared with the rigid phenolic structure of the polybenzoxazine resulting in the lowering of the stiffness of the alloys. From Fig. 1, the storage moduli at room temperature of the BA/PU polymer alloys were systematically reduced from 5.7 GPa to 1.4 GPa with the addition of the PU from 0 to 40 wt%. On the other hand, the modulus in the rubbery plateau moduli tended to increase with the mass fraction of the PU. This could be implied that the crosslink density of the fully cured specimens increased with increasing the PU content. Theoretically, the relationship between the crosslink density and the rubbery plateau modulus could be exhibited as presented in Eq. (1) [36, 37].

$$E' = 3\upsilon_e RT \tag{1}$$

where E' is the rubbery plateau modulus at T_g+50°C in MPa, (υ_e) is crosslink density in mol/m^3, R is gas constant and T is absolute temperature at T_g+50°C. The calculated values of crosslink density crosslink density are shown in Table 1.

Table 1. Calculated values of crosslink density of the BA/PU Alloys.

BA/PU alloys	Tg (°C)	Rubbery plateau modulus at T_g+50°C (MPa)	Calculated Crosslink density (mol/m^3)
100/0	165	92.8	22.4
80/20	175	168.8	39.1
60/40	220	365.2	69.6

When the crosslink density increases with PU content as shown in Table 1, the mobility of the molecular chain in the alloy decreases. This could relate to the glass transition temperature of the alloys. Glass transition temperatures (T_gs) of the BA/PU polymer alloys were also detected in the dynamic mechanical thermograms based on the maxima of their loss moduli (E″) as also shown in Fig. 1. The T_g values of the BA/PU polymer alloys showed a synergistic behaviors as T_gs were observed to increase to

the values greater than that of both parent polymers with increasing the amount of the PU fraction. The T_gs of the PU and the polybenzoxazine were reported to be about -70°C and 165°C, respectively [35]. However, the T_gs of the fully cured BA/PU polymer alloys were observed to be 165°C in 90/10 BA/PU, 175°C in 80/20 BA/PU, 217°C in 70/30 BA/PU, and 220°C in 60/40 BA/PU. From Fig. 1, the increase of PU content resulted in the increase in the crosslink density of the polymer alloy. This could be observed from the increase of the storage modulus in the rubbery plateau region and the T_gs as previously reported [35]. The phenomenon was attributed to the additional crosslinking caused by the reaction between an isocyanate group of urethane resin and a hydroxyl group of polybenzoxazine after the phenolic hydroxyl group from the ring opening of benzoxazine resin was produced [38-39].

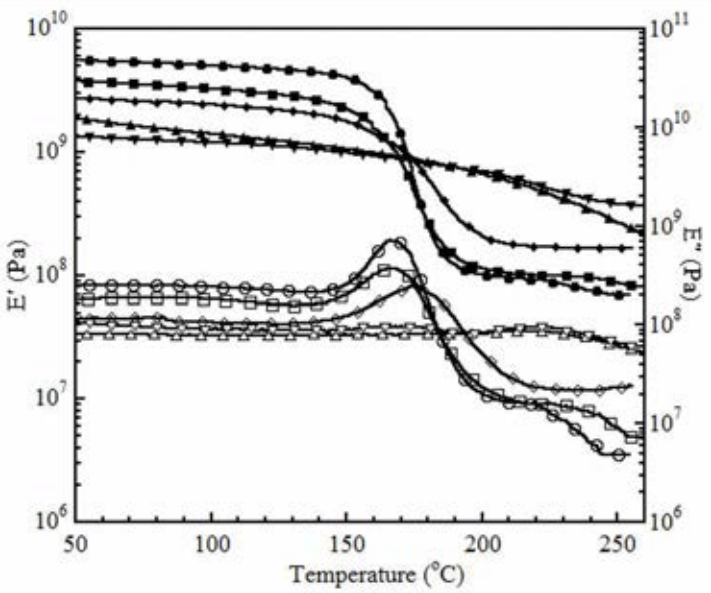

Fig. 1. Viscoelastic properties of the BA/PU alloys at various mass compositions:
E′ (●) 100/0, (■) 90/10, (♦) 80/20, (▲) 70/30, (▼) 60/40;
E″ (○) 100/0, (□) 90/10, (◊) 80/20, (Δ) 70/30, (▽) 60/40.

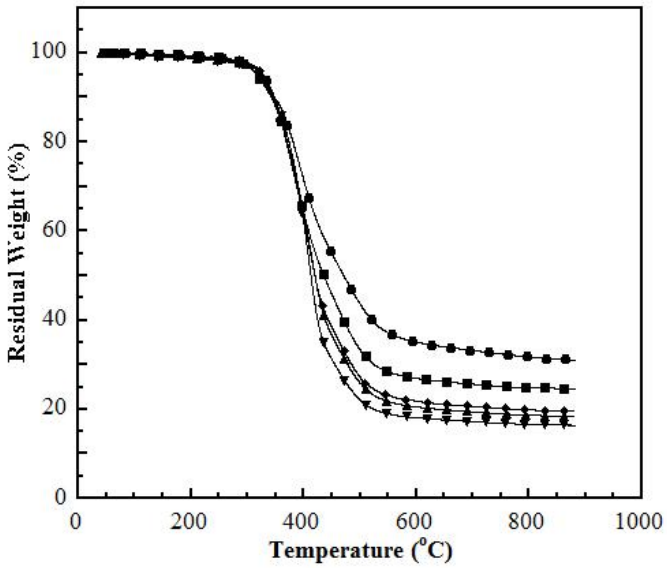

Fig. 2. TGA thermograms of the BA/PU polymer alloys at various compositions:
(●) 100/0, (■) 90/10, (♦) 80/20, (▲) 70/30, (▼) 60/40.

Figure 2 shows a TGA profile of the polybenzoxazine and BA/PU polymer alloys at investigated compositions. Generally, degradation temperature (T_d) is one of the key parameters needed to be considered for high temperature applications. The results of this study revealed that the T_d of the polymer alloys were significantly higher than that of the polybenzoxazine. The T_d of the

DOI:10.4186/ej.2011.15.4.23

polybenzoxazine at 5% weight loss was determined to be 315°C whereas the T_d values of the BA/PU polymer alloys were approximately 326°C. These results could be due to the reaction of the isocyanate of the PU and the hydroxyl group of the polybenzoxazine helped increase a crosslink density of the polymer alloys as explained earlier. Therefore, one benefit of incorporating the PU into the polybenzoxazine network was to improve the thermal stability of the polybenzoxazine as a result of crosslinking density enhancement. In addition, the residual weight at 800°C of the BA/PU polymer alloys was found to decrease with increasing the PU fraction in the polymer alloys which was consistent with the value previously reported [35]. This can be explained as the structure of the polybenzoxazine contained a more thermally stable benzene rings compared to the mostly aliphatic structure of the diol in the urethane. Consequently, the addition of the PU resulted in the lowering of the char yield in the polymer alloys.

3.2. Properties of Kevlar™-reinforced BA/PU Alloys

3.2.1. Dynamic Mechanical and Mechanical Properties

The dynamic mechanical analysis of the Kevlar™-reinforced alloys is shown in Fig. 3. In the figure, the storage moduli of Kevlar™-reinforced BA/PU alloys at 0- 40 wt% of PU with the fibers kept at 80 wt% were presented. It could be noticed that the storage moduli of the composites systematically decreases with increasing the PU fraction in the polymer alloys as a matrix of the composites, i.e., 16.4 GPa for Kevlar™-reinforced 100/0 BA/PU alloys to 2.8 GPa for Kevlar™-reinforced 60/40 BA/PU alloys. Moreover, the T_gs obtained from the maxima of the loss moduli curve of the Kevlar™-reinforced BA/PU alloys were found to increase with increasing the amount of the PU fraction, i.e., 180°C in 90/10 BA/PU, 195°C in 80/20 BA/PU, 218°C in 70/30 BA/PU, and 235°C in 60/40 BA/PU as also shown in Fig. 3. In addition, T_gs of Kevlar-reinforced composites were significantly higher than those of the neat BA/PU alloys comparing at the same mass fraction of the PU in the alloys. In general, the T_gs of urethane elastomer and polybenzoxazine were reported to be about 70°C and 165°C, respectively [36]. In our study, T_gs of the copolymers were also found to increase with the mass fraction of urethane. This enhancement in the T_g could be attributed to the increase in the crosslink density of the binary systems as previously observed in the DMA investigation of the resulting copolymers [36]. Furthermore, this phenomenon could be due to the substantial interfacial adhesion between the fiber and the matrix [40] .

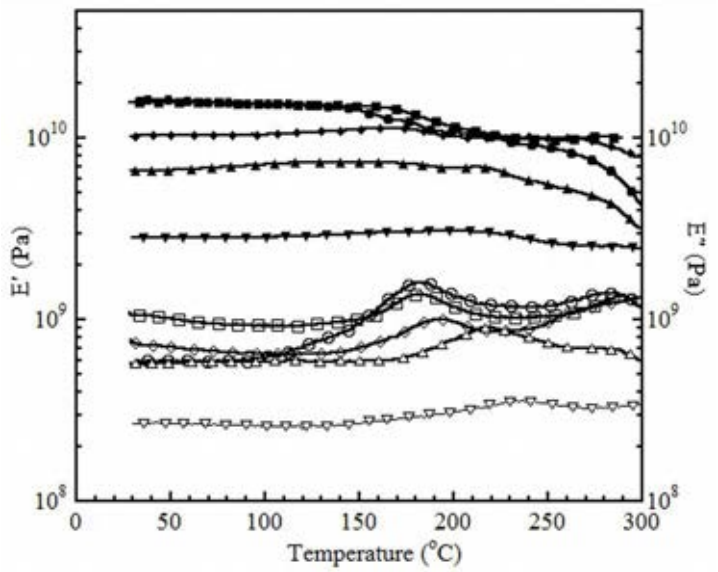

Fig. 3. Viscoelastic properties of Kevlar™-reinforced BA/PU alloys at various mass compositions:
E′ (●) 100/0, (■) 90/10, (♦) 80/20, (▲) 70/30, (▼) 60/40;
E″ (○) 100/0, (□) 90/10, (◊) 80/20, (Δ) 70/30, (▽) 60/40.

Flexural properties of the Kevlar™-reinforced polybenzoxazine alloys were depicted in Fig. 4. It could be observed that the flexural strength of the alloys was decreased with the PU content from 163 MPa (of pure polybenzoxazine) to 52 MPa (at 40wt% of PU). We also observed the strengths of the

composites decrease in a linear manner with the increase of the PU in the matrix alloys. In addition, flexural moduli of the composites were found to significantly decrease with increasing the amount of the PU in the alloys from 18.3 GPa at 0 wt% of PU to about 7.5 GPa at 40 wt% of PU as illustrated in Fig. 4. The phenomenon was due to the fact that the addition of the rubbery urethane polymer into the rigid polybenzoxazine was able to lower either the strength or the stiffness of the resulting polybenzoxazine alloys.

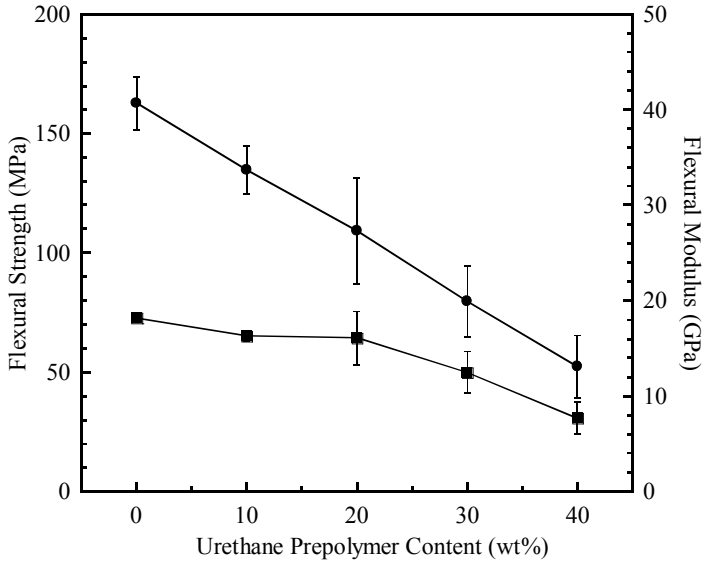

Fig. 4. Flexural properties of the Kevlar^{TM}- reinforced BA/PU alloys at various PU contents: (●) Flexural strength; (■) Flexural modulus.

3.2.2. Thermal Stability of the Composites

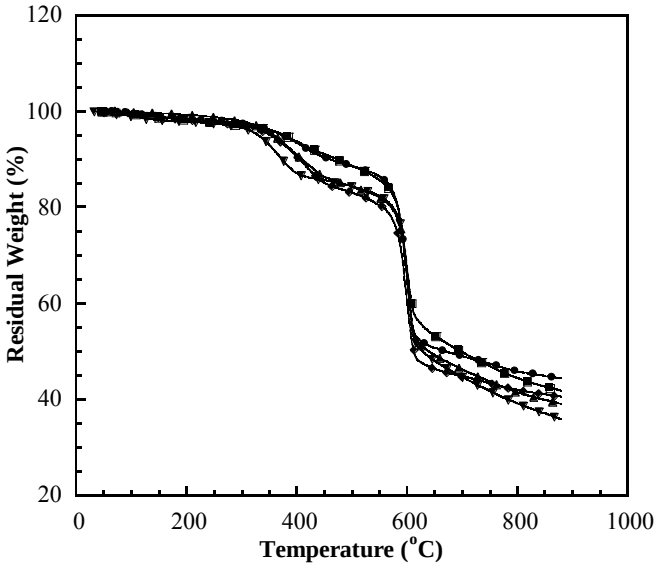

Fig. 5. Thermal degradation behaviors of the Kevlar^{TM}-reinforced BA/PU alloys at various mass ratios of BA/PU: (●) 100/0, (■) 90/10, (♦) 80/20, (▲) 70/30, (▼) 60/40.

From Fig. 5, the degradation temperatures (T_ds) at 5% weight loss of Kevlar^{TM}-reinforced polybenzoxazine alloys were found to increase systematically with increasing the mass fraction of the polybenzoxazine in the alloys. The T_d at 5% weight loss of the Kevlar^{TM}-reinforced polybenzoxazine alloys with the PU compositions of 0 to 40% by weight was ranging from 374°C to 329°C. Another

important feature in the thermograms is the weight residue at 800°C or the char yield of the composites which is related to the flammability of materials and is essential for some ballistic armor applications.

When the armor is penetrated, the heat is generated. The material could first decompose by thermally initiated mechanisms or thermo-oxidative decomposition. It has been reported that char could decrease the diffusion rate of decomposed, flammable gases toward the flame front and decrease the burning of the material [41]. The char yield was found to systematically reduce from 45.8 % to 39.1% with an incorporation of the PU from 0 to 40% by weight. This could be attributed to the fact that urethane contained aliphatic structure, while polybenzoxazine contained benzene rings [42]. Therefore, the increase in urethane content leads to the increase in aliphatic structure having less thermal stability and less char yield [38-39]. However, these values were all greater than those of the matrix alloys comparing at the same PU fraction. This is due to the fact that the char yields of the composites also included the additional residue of the Kevlar™ fiber which possessed a char yield of 44% at 600°C [3].

3.2.3. Firing Tests of the BA/PU Composite Armors

A series of ballistic tests were performed on the composite laminates which were made of Kevlar™ fabric impregnated with BA/PU mixtures and cured using the curing condition as suggested in the experimental section. The Kevlar™ fabric used has the areal density of about 0.016 g/cm^2. The dimension of the laminated specimens was 25.4mm×25.4mm×1.8mm, corresponding to 10 plies of the Kevlar™ cloth impregnated with about 20% by weight of the BA/PU mixtures. The densities of the composites were determined to be 1.26 g/cm^{3}at 60/40 BA/PU, 1.28 g/cm^{3}at 70/30 BA/PU, 1.29 g/cm^3 at 80/20 BA/PU, 1.30 g/cm^3 at 90/10 BA/PU and 1.31 g/cm^3 at 100/0 BA/PU.

3.2.3.1. Low Level Ballistic Impact Test

The composite laminates fabricated with a thickness of 10 plies of the Kevlar™ at various the BA/PU alloy compositions mentioned above were tested using a 9mm handgun with standard lead projectiles having lead outer-coating. From the test results, the composite consisted of only 10 piles of Kevlar™ could not protect ballistic impact from the standard lead projectiles. Therefore the 20 piles of Kevlar™ panels i.e. 10/10 panel arrangement, at all BA/PU alloy compositions were selected for the following tests. Moreover, the bisphenol A-based epoxy-Kelar™ composites (cured by amine hardener) at the same fiber content were also used to compare its ballistic impact performance with our BA/PU matrix alloys. From the fire test, although both composites with the 10/10 configuration of the composite panels could not resist the projectiles, the polybenzoxazine alloy composite panel exhibited obviously higher energy absorption than the epoxy composites. This could be noticed from the greater delaminated area of the polybenzoxazine composites in Figs. 6(a)-6(d). From Table 2, Figs. 6(c) and 6(d), the firing results also indicated that the 90/10 and the 80/20 mass ratios of the BA/PU matrix alloys exhibited ballistic penetration resistance in comparison with the other compositions of 100/0 BA/PU matrix as well as the epoxy matrix. However, only the composite from the 80/20 BA/PU matrix alloy exhibited 100% ballistic penetration resistance. In Fig. 6(d), the ballistic impact performance of the Kevlar™-reinforced 80/20 BA/PU alloys revealed relatively larger delaminated area than those of the epoxy matrix (Fig. 6(a)) and the polybenzoxazine matrix (Fig. 6(b)). The delaminated area has been known to be one major component of the energy absorption mechanisms in ballistic impact. Further increase the PU mass fractions to 30 wt% and 40 wt% in the composite matrices resulted in a poor ballistic impact resistance. This phenomenon confirms the necessity of identifying optimal fiber-matrix interactions in order to yield a composite system with outstanding ballistic performance. The variation in the BA/PU alloy compositions could allow an optimal interaction between the alloy matrix and its reinforcing fiber, which leads to obtaining the outstanding ballistic performance.

As previously mentioned and reported in the literature [14], the kinetic energy absorption of composite material composes several mechanisms, including tensile failure of fibers, elastic deformation of composites, interlayer delamination, shear between layers in the composite, and inertia effect. Kinetic energy absorption may be attributed to basic factors such as mechanical properties of the composite's constituent direction of fiber arrangement, as well as interfacial strength. Fracture morphology of the composite specimen is sometimes used to qualitatively evaluate the possible kinetic

energy absorption of the material. The fracture surfaces of Kevlar^{TM}-reinforced BA/PU alloys at various compositions of PU are depicted in Figs. 7(a)-7(d). The results reveals that the fracture surfaces near the center of ballistic impact of the Kevlar^{TM}- reinforced 80/20 BA/PU alloy (Fig. 7(b)) exhibited substantial level of adhesive failure in which the fibers were largely stripped off the matrix materials with only small fragments of the matrix remained adhere to the fibers. This fracture phenomenon could be clearly distinguished from that of the 60/40 BA/PU composites (Fig. 7(d)), which showed much lower degree of interfacial failure. The weaker mechanical properties due to the excessive presence of the soft PU component might be one reason of the observed predominantly cohesive failure in this composite. In other case, too strong adhesion between the Kevlar^{TM} fibers and the BA/PU matrix alloy might be attributed to the poor ballistic performance of the matrix resulting in the low degree of composite delamination mechanism. These results also confirmed the effect of the BA/PU alloy compositions on the interaction between the Kevlar^{TM} fibers and the alloy matrices and thus the ballistic performance of obtained polymer composites.

Consequently, the selection of a suitable matrix resin that renders the most energy absorption characteristics with particular reinforcing fiber used is crucial to the successful ballistic performance of the composite armor. It could be noted that the BA/PU alloy seemed to render a synergistic behavior in ballistic performance at the composition of 80/20 BA/PU with the most outstanding ballistic performance. Therefore, The 80/20 BA/PU alloy was further used to fabricate the composite armors for higher protection level evaluation.

Table 2. Comparison of resistance to penetration of low level ballistic impact test for different types of matrix with 10 piles/panel and 10/10 arrangement.

Type of Matrix	**Resistance to Penetration**		**Remark**
	First panel	**Second panel**	
Epoxy	No	No	-
Polybenzoxazine	No	No	-
90/10 BA/PU	Yes	Yes	-
80/20 BA/PU	Yes	Yes	100% ballistic penetration resistance

DOI:10.4186/ej.2011.15.4.23

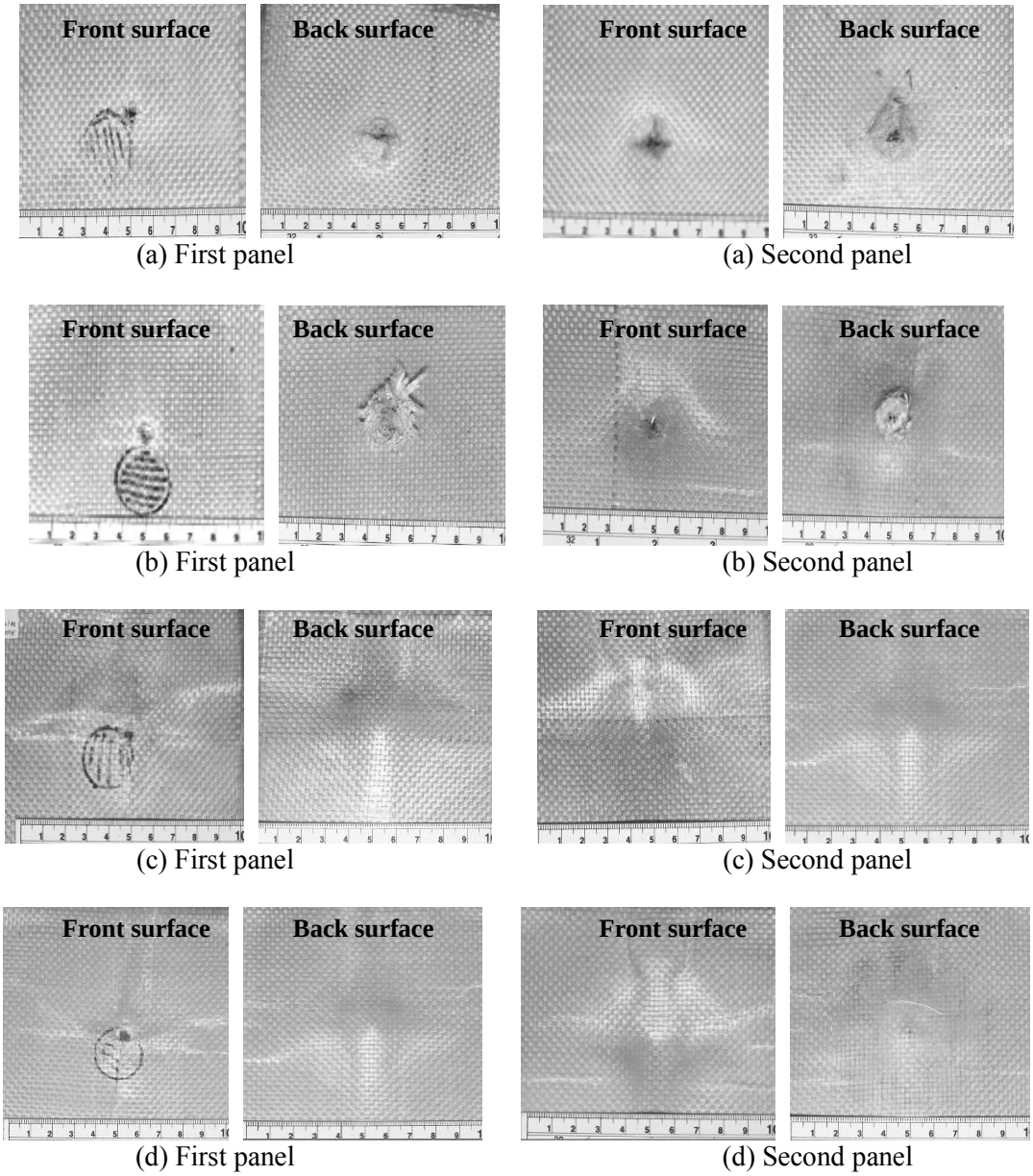

Fig. 6. Damaged and delaminated area of 10 piles/panel with the samples arrangement of 10/10 after impact with standard lead projectiles with lead outer-coating typically used in 9 mm: (a) Kevlar^{TM}-reinforced epoxy; (b) Kevlar^{TM}-reinforced polybenzoxazine; (c) Kevlar^{TM}-reinforced 90/10 BA/PU; (d) Kevlar^{TM}-reinforced 80/20 BA/PU.

DOI:10.4186/ej.2011.15.4.23

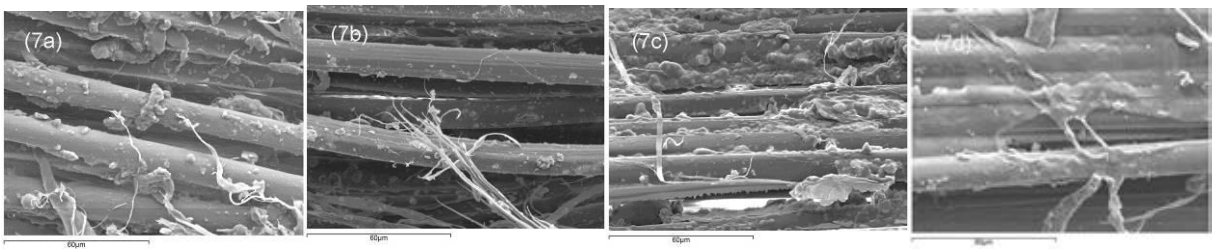

(a) (b) (c) (d)

Fig. 7. SEM images of the fracture surface of the composites after impacted with standard lead projectiles (x 1000 magnification): (a) Kevlar^{TM}-reinforced polybenzoxazine; (b) Kevlar^{TM}-reinforced 80/20 BA/PU; (c) Kevlar^{TM}-reinforced 70/30 BA/PU; (d) Kevlar^{TM}-reinforced 60/40 BA/PU.

3.2.3.2. Ballistic Impact Test of NIJ Level II-A

The ballistic impact velocities required by NIJ standard for level II-A was used to study the effect of the composite panel thickness and arrangement based on the Kevlar^{TM}-reinforced 80/20 BA/PU alloys. The samples were prepared approximate thicknesses of 1.8mm, 3.5mm, and 5.0mm for panel manufactured 10, 20, and 30 pile composites, respectively. The areal densities were 0.48 g/cm^2 for the 10 piles, 0.48 g/cm^2 for the 20 piles, and 0.70 g/cm^2 for the 30 piles panel composites. The Kevlar^{TM}-reinforced 80/20 BA/PU composite samples with 20 piles, and 30 piles were tested in the NIJ standard. The 20-ply composites were arranged in 2 patterns, i.e., 10/10 and 20/0 configurations. In case of the 30-ply composites, they were arranged in 3 patterns, i.e., 10/10/10, 20/10/0, and 30/0/0 configurations.

The penetration resistance results of the composite after impact with projectile velocities for the NIJ level II-A ballistic test are shown in Table 3. All samples were fired with a 9 mm handgun, which is known to have a greater impact velocity than that required by the NIJ standard of level II-A. The individual value for the deformed depth as well as the averaged diameter of the damaged area of the BA/PU composites after impacted with the projectiles was reported. From the table, all composite laminates assembled to have a combined thickness of 20 plies of the Kevlar^{TM} did not pass this level of the NIJ standard for ballistic protection. Eventually in the 30-ply composite arrangements, none of these samples was perforated by the level II-A projectiles as seen in Table 3 and Fig. 8. From the delaminated area measurement, it is apparent that a sample with an arrangement of the 20-ply panel in front of the 10-ply panel (20/10 configuration) (Fig. 8(b)) exhibited the best ballistic performance. The damaged area of this sample arrangement was significantly smaller than those of the other two arrangements, i.e., the 10/10/10 (Fig. 8(a)) and 30/0/0 (Fig. 8(c)) configurations. Therefore, the arrangement of composite panel in the firing test was found to be one important factor on the ballistic performance of the composites. The front panel with at least 20 plies of Kevlar^{TM} cloth was thus necessary for the level II-A resistance of perforation and was supposed to possess sufficient properties to destroy or deform this type of projectile. As a result, the kinetic energy was substantially reduced before piecing through the rear plate of 10 piles thickness. Moreover, the energy might also be dissipated via the inertia effect when the projectile passed through the gap between the two plates. However, the front plate of the 10/10/10 (Fig. 8(a)) configuration composite was found to possess insufficient mechanical integrity to destroy the projectiles. Consequently, a relatively large portion of the impact energy could still be transferred to the adjacent plate and caused relatively large damaged area to the rear plate. In the other hand, although, the 30/0/0 (Fig. 8(c)) configuration composite possessed relatively high stiffness enough to substantially deform the projectile, this sample lacked the energy dissipation by an inertia effect as likely to occur in the 20/10 (Fig. 8(b)) configuration. As a result, a larger damaged area comparing with the 20/10/0 configuration composite was observed. The cross-sections of the front plate of the tested composites with 20/10/0 and 30/0/0 arrangements are also illustrated in Fig. 9(a) and Fig. 9(b), respectively, revealing the macroscopic delamination of the Kevlar^{TM}'s cloth in the 20 plies and 30 plies thick composites.

DOI:10.4186/ej.2011.15.4.23

Table 3. Effect of number of piles and panel arrangement of Kevlar^{TM}-reinforced 80/20 BA/PU composites after ballistic impact at projectiles velocities required by NIJ standard level II-A.

Configuration	Penetration resistance	Damage dimension of the rear plate	
		Depth (mm)	Diameter (mm)
10/10	No	-	-
20/0	No	-	-
10/10/10	Yes	10.8	69.5
20/10/0	Yes	7.8	44.5
30/0/0	Yes	8.7	66.6

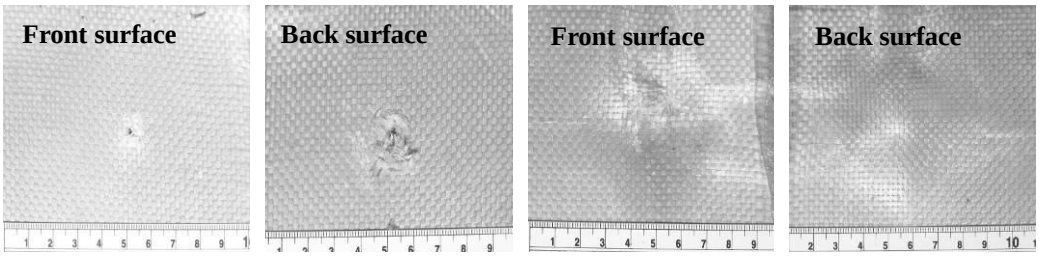

(a) First panel (10 piles/panel) (a) Second panel (10 piles/panel)

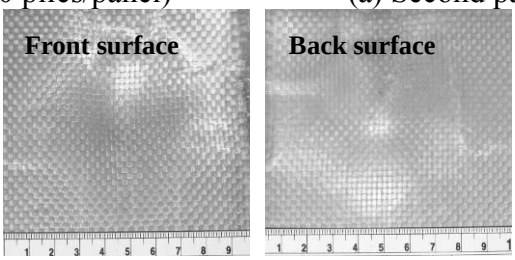

(a) Third panel (10 piles/panel)

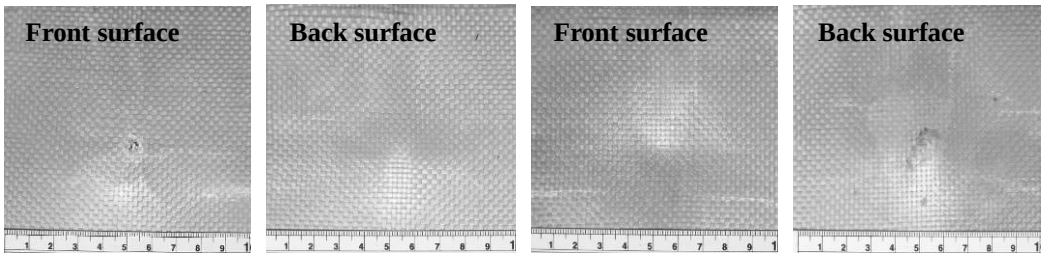

(b) First panel (20 piles/panel) (b) Second panel (10 piles/panel)

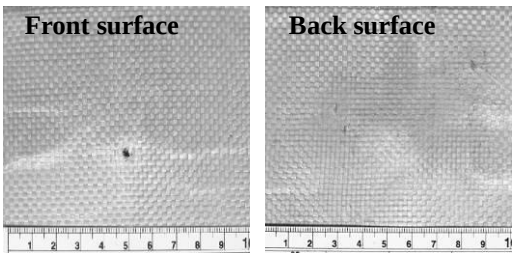

(c) First panel (30 piles/panel)

Fig. 8. Damaged and delaminated area of sample after impact with projectiles velocities required by NIJ standard for level II-A with the sample arrangement of: (a) 10/10/10, (b) 20/10/0, and (c) 30/0/0.

DOI:10.4186/ej.2011.15.4.23

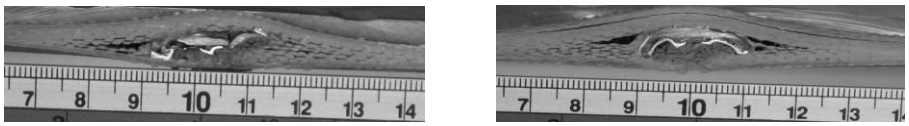

(a) (b)

Fig. 9. Damaged panel cross-sections of specimen that could stop projectiles at velocities required by NIJ standard for level II-A: (a) first panel of sample having arrangement of 20/10/0; **(**b**)** first panel of sample having arrangement of 30/0/0.

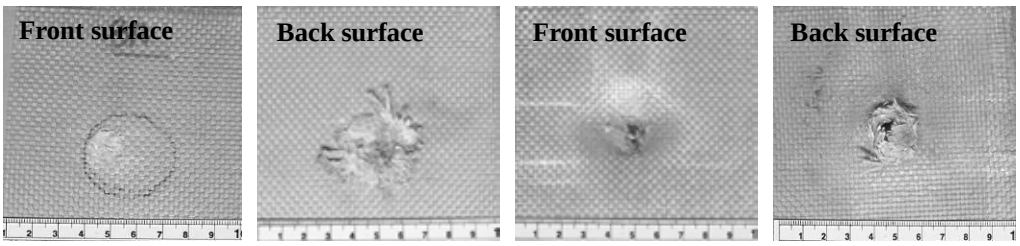

(a) First panel (20 piles/panel) (a) Second panel (10 piles/panel)

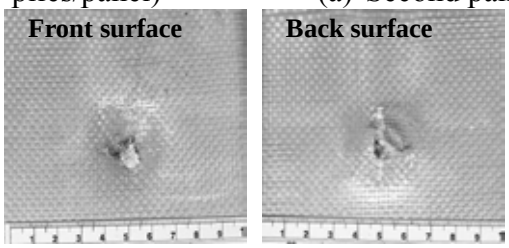

(a) Third panel (10 piles/panel)

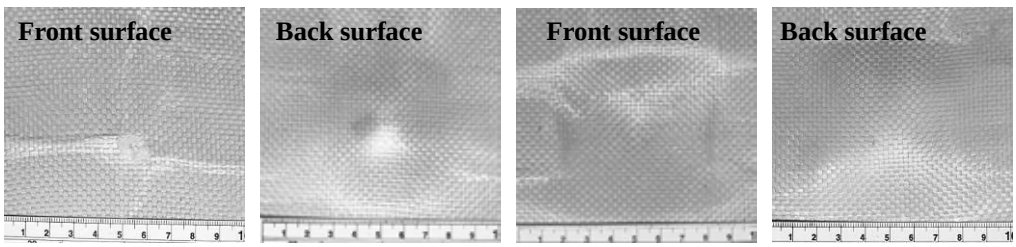

(b) First panel (30 piles/panel) (b) Second panel (20 piles/panel)

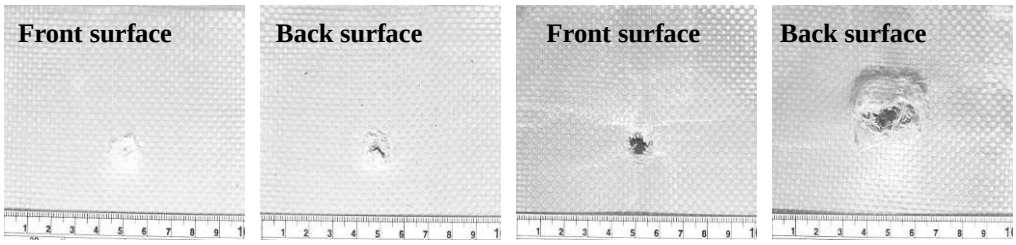

(c) First panel (10 piles/panel) (c) Second panel (10 piles/panel)

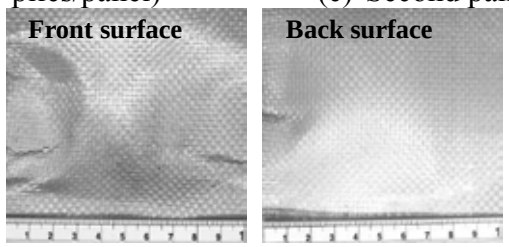

(c) Third panel (30 piles/panel)

Fig. 10. Damaged and delaminated area of sample after impact with projectiles velocities required by NIJ standard for level III-A with the sample arrangement of: (a) 20/10/10, (b) 30/20/0, and (c) 10/10/30.

DOI:10.4186/ej.2011.15.4.23

Table 4. Effect of number of piles and panel arrangement of Kevlar^{TM} reinforced 80/20 BA/PU composites after ballistic impact at projectiles velocities required by NIJ standard level III-A.

Configuration	Impact velocity (m/s)	Penetration resistance	Damage dimension of the rear plate	
			Depth (mm)	Diameter (mm)
10/10	426	No	-	-
20/0	430	Yes	13.6	93.3
10/10/10	429	Yes	19.5	119.1
20/10/0	429	Yes	11.0	90.3
30/0/0	431	Yes	10.1	66.1

3.2.3.3. Ballistic Impact Test of NIJ Level III-A

In this investigation, the Kevlar^{TM}-reinforced 80/20 BA/PU composite with the combined thickness of 40, 50, and 60 piles were subjected to a ballistic impact evaluation at a projectile velocity required by NIJ standard for level III-A. This III-A level test is currently the reported maximum level of protection based on polymer composites. The composites with the combined thickness of 40 plies had one type of arrangement, i.e. 20/10/10 configuration whereas that of 50 plies had two types of arrangements, i.e. 30/20/0, and 10/10/30 configurations. In the case of the samples of 60 plies, the arrangements were set to be 30/20/10/0, and 30/10/10/10 configurations. The test outcomes are listed in Table 4. In addition, Fig. 10 also shows of the photographs of some composites tested in this protection level revealing damaged or delaminated areas of the composites.

From Table 4, it is apparent that the test weapon with standard 124 grains round lead projectile with a copper outer coating (Full Metal Jacket) typically used in the 9mm handgun having a speed required by level III-A could be stopped with at least 50 plies of the composites. The damage area evaluation confirmed that the arrangement of composite panels had an important effect on their ballistic protection. It can be seen that the composite with 30/20/0 arrangement rendered the damaged depths and diameters smaller than those of the composite with the 10/10/30 arrangement. This result implied that the composite arrangement for level III-A protection needed at least 30-ply composite panel as a front plate in the impact direction. The sufficiently stiff panel seemed to play a crucial role as to deform the shape of the projectile as discussed previously.

In the combined 60-ply thick composite panels, the arrangement was set to be 30/20/10, and 30/10/10/10 configurations. These two types of arrangements were again found to lead to different damaged areas and deformed depths. The composite with 30/10/10/10 configuration rendered less damaged area than that of composite with 30/20/10 configuration. Since the number of the Kevlar^{TM} plies combined was the same in each tested sample, the sample arrangement with the thicker panel of 30 piles for level III-A to be on the front and was found to be essential in the successful ballistic impact resistance of the composites with lower degree of sample deformations.

4. Conclusions

In this study, the suitable matrix alloy based on benzoxazine, and urethane resins for Kevlar^{TM} fiber-reinforced composite armor was determined. The synergism in the T_g can be observed in Kevlar^{TM}-reinforced BA/PU alloys. This phenomenon was due to the addition of urethane prepolymer is attributed to improve crosslinked density of the matrix alloys. However, the increase of the PU fraction significantly lowered the stiffness and degradation behavior of the composites. The results of low level ballistic impact test of the 20-ply Kevlar^{TM}-reinforced composites revealed that only the composite from the 80/20 BA/PU matrix alloy exhibited 100% ballistic penetration resistance. The studies of specimen's thickness and the arrangement of the composite panels indicated that the suitable thickness having 30 piles of the Kevlar^{TM} cloth can protect the ballistic impact at level II-A, whereas the 50 ply-thick composite was able to protect the ballistic impact of NIJ level III-A. Furthermore, the arrangement of composite panels was also found to significantly affect the ballistic performance of our composites with the thicker and stiffer panel should be placed in the front face of the composite panel assembly to yield best ballistic resistance.

Acknowledgments

This research receives financial supports from the National Metal and Materials Technology Center (Thailand), the Research Grant for Research Scholar of the Thailand Research Fund, and from the National Research University Project (AM1076A) of the Ministry of Education, Thailand. Bisphenol-A, isophorone diisocyanate, and diols were kindly provided by Thai Polycarbonate Co. Ltd. (Thailand), Degussa- Huls AG (Thailand), and TPI Polyol Co., Ltd. (Thailand), respectively.

References

[1] A. R. Sabet, M. H. Beheshty, and H. Rahimi, "High velocity impact behavior of GRP panels containing coarse-sized sand filler," *Polym. Compos.*, vol. 29, no. 8, pp. 932-938, 2008.

[2] W. J. Cantwell and J. Morton, "The impact resistance of composite materials - a review," *Composites*, vol. 22, no. 5, pp. 347-362, 1991.

[3] H. H. Yang, *Kevlar Aramid Fiber*, Chichester, England: John Wiley&Sons, 1993.

[4] R. H. Zee and C. Y. Hsieh, "Energy loss partitioning during ballistic impact of polymer composites," *Polym. Compos.*, vol. 14, no. 3, pp. 265-271, Jun, 1993.

[5] B. Z. Jang, L. C. Chen, L. R. Hwang, J. E. Hawkes, and R. H. Zee, "The response of fibrous composites to impact loading," *Polym. Compos.,* vol.11, no. 3, pp. 144-157, Jun, 1990.

[6] M. J. N. Jacobs and J. L. J. Van Dingenen, "Ballistic Protection Mechanisms in Personal Armour," *J Mater Sci*, vol. 36, no. 13, pp. 3137-3142, Jul, 2001.

[7] R. H. Zee, C. J. Wang, A. Mount, B. Z. Jang, and C. Y. Hsieh, "Ballistic response of polymer composites," *Polym. Compos.,* vol. 12, no. 3, pp.196-202, Aug, 2004.

[8] H. Ishida and T. Chaisuwan, "Mechanical property improvement of carbon fiber reinforced polybenzoxazine by rubber interlayer," *Polym. Compos.,* vol. 24, no. 5, pp.597-607, Oct, 2003.

[9] S. B. Shen and H. Ishida, "Development and characterization of high-performance polybenzoxazine composites," *Polym. Compos.,* vol. 17, no. 5, pp.710-719, Oct, 1996.

[10] S. Chabba, M. van Es, E. J. van Klinken, M. J. Jongedijk, D. Vanek, P. Gijsman, and A. C. L. M. van der Waals, "Accelerated aging study of ultra high molecular weight polyethylene yarn and unidirectional composites for ballistic applications," *J. Mater. Sci.,* vol. 42, no. 8**,** pp. 2891-2893, Apr, 2007.

[11] N. K. Naik, P. Shrirao, and B. C. K. Reddy, "Ballistic impact behaviour of woven fabric composites: Parametric studies," *Mater. Sci. Eng.,* vol. A412, pp.104-116, Dec, 2005.

[12] C. Ulven, U. K. Vaidya, and M. V. Hosur, "Effect of projectile shape during ballistic perforation of VARTM carbon/epoxy composite panels," *Compos. Struct.,* vol. 61, no. 1-2, pp. 143-150, Jul, 2003.

DOI:10.4186/ej.2011.15.4.23

[13] M. V. Hosur, S. M. W. Islam, U. K. Vaidya, A. Kumar, P. K. Dutta, and S. Jeelani, "Dynamic punch shear characterization of plain weave graphite/epoxy composites at room and elevated temperatures" *Compos. Struct.,* vol. 70, no. 3, pp. 295-307, Sep, 2005.
[14] S. S. Morye, P. J. Hine, R. A. Duckett, D. J. Carr, and I. M. Ward, "Modelling of the energy absorption by polymer composites upon ballistic impact," *Compos. Sci. Technol.,* vol. 60, no. 14, pp. 2631-2642, Nov, 2000.
[15] M. Grujicic, B. Pandurangan, K. L. Koudela, and B. A. Cheeseman, "A computational analysis of the ballistic performance of light-weight hybrid composite armors," *Appl. Surf. Sci.*, vol. 253, no. 2, pp.730-745, Nov, 2006.
[16] J. N. Epel, "Fibrous armor material," U.S. Patent, 4,639,387 (1987).
[17] W. N. Smith, Jr., "Light weight armor," U.S. Patent, 4,732,803 (1988).
[18] X. F. Wu, G. Ghoshal, M. Kartashov, Z. Aslan, J. A. Turner, and Y. A. Dzenis, "Experimental characterization of the impact-damage tolerance of a cross-ply graphite-fiber/epoxy laminate," *Polym. Compos.,* vol. 29, no. 5, pp. 534-543, May, 2008.
[19] L. A. Pilato, "Ballistic resistant laminate," U.S. Patent, 5,190,802 (1993).
[20] D. R. Denommee, "Method of making deep drawn, laminated articles," U.S. Patent, 3,956,447 (1976).
[21] N. John, "Structural sandwich panel with energy-absorbing material pierced by rigid rods," U.S. Patent, 5,102,723 (1992).
[22] I. Rosenberg and W. K. Ansite, "Ballistic resistant armor panel and method of constructing the same," U.S. Patent, 4,550,044 (1985).
[23] L. H. Li, Y. D. Kwon, and D. C. Prevorsek, "Sulfamoyl hydrogen bond donating groups on thermal solvents for image separation systems," U.S. Patent, 5,480,760 (1996).
[24] A. D. Park, "Thin film color filter for liquid crystal display," U.S. Patent, 5,395,678 (1996).
[25] A. D. Park, "Method for fabricating a ballistic laminate structure," U.S. Patent, 5,547,536 (1999).
[26] G. A. Harpell, I. Palley, S. Kavesh, and D. C. Prevorsek, "Ballistic-resistant composite article," U.S. Patent, 4,748,064 (1988).
[27] H. Ishida, "Process for preparation of benzoxazine compounds in solventless systems," U.S. Patent, 5,543,516 (1996).
[28] H. Ishida and D. J. Allen, "Physical and mechanical characterization of near-zero shrinkage polybenzoxazines," *J. Polym. Sci. Pol. Phys.*, vol. 34, no. 6, pp. 1019-1030, Apr, 1996.
[29] N. N. Ghosh, B. Kiskan, and Y. Yagci, "Polybenzoxazines—New high performance thermosetting resins: Synthesis and properties," *Prog. Polym. Sci.,* vol. 32, no. 11, pp. 1344-1391, Nov, 2007.
[30] C. P. R. Nair, "Advances in addition-cure phenolic resins," *Prog. Polym. Sci.,* vol. 29, no. 5, pp. 401-498, May, 2004.
[31] H. Ishida and D. J. Allen, "Mechanical characterization of copolymers based on benzoxazine and epoxy," *Polymer,* vol. 37, no. 10, pp.4487-4495, Sep, 1996.
[32] S. Rimdusit and H. Ishida, "Synergism and multiple mechanical relaxations observed in ternary systems based on benzoxazine, epoxy, and phenolic resins," *J. Polym. Sci. Polym. Phys.,* vol. 38, no. 13, pp.1687-1698, Jul, 2000.
[33] C. Jubsilp, T. Takeichi, and S. Rimdusit, "Effect of novel benzoxazine reactive diluent on processability and thermomechanical characteristics of Bi-functional polybenzoxazine," *J. Appl. Polym. Sci.,* vol. 104, no. 5, pp. 2928-2938, Jun, 2007.
[34] T. Takeichi, Y. Guo, and S. Rimdusit, "Performance improvement of polybenzoxazine by alloying with polyimide: effect of preparation method on the properties," *Polymer,* vol. 46, no. 13, 4909-4916, Jun, 2005.
[35] S. Rimdusit, C. Liengvachiranon, S. Tiptipakorn, and C. Jubsilp, "Thermomechanical characteristics of benzoxazine-urethane copolymers and their carbon fiber-reinforced composites," *J. Appl. Polym. Sci.,* vol. 113, pp. 3823-3830, Feb, 2009.
[36] P. J. Flory, *Principles of Polymer Chemistry*, Ithaca: Cornell University Press, 1953.
[37] I. M. Ward, *Mechanical Properties of Solid Polymers*, New York: Wiley Interscience, 1971.

[38] T. Takeichi, Y. Guo, and T. Agag, "Synthesis and characterization of poly(urethane-benzoxazine) films as novel type of polyurethane/phenolic resin composites", *J. Polym. Sci.: Part A: Polym. Chem.*, vol. 38**,** no. 22, pp. 4165-4176, 2000.

[39] T. Takeichi and Y. Guo, "Preparation and Properties of Poly(urethane-benzoxazine)s Based on Monofunctional Benzoxazine Monomer", *Polymer J.*, vol. 33, no**.** 5, pp. 437-443, 2001.

[40] X-L. Xie, C. Y. Tang, X. P. Zhou, R. K. Y. Li, Z. Z. Yu, Q. X. Zhang, and Y. W. Mai. "Enhanced Interfacial Adhesion between PPO and Glass Beads in Composites by Surface Modification of Glass Beads via In Situ Polymerization and Copolymerization", *Chem. Mater.,* vol. 16*,* pp. 133-138, 2004.

[41] H. Ishida and T. Agag, *Handbook of Benzoxazine Resins*, 2011, pp. 12.

[42] S. Tiptipakorn, S. Damrongsakkul, S. Ando, K. Hemvichian, and S. Rimdusit, "Thermal degradation behaviors of polybenzoxazine and silicon-containing polyimide blends", *Polym. Degrad. Stabil*., vol. 92, no. 7, pp. 1265-1278, 2007.

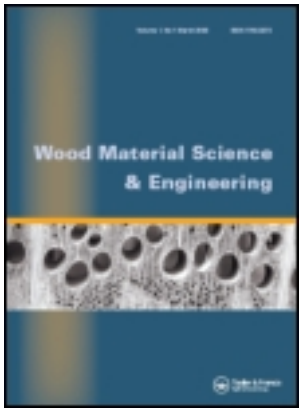

Wood Material Science & Engineering
Publication details, including instructions for authors and subscription information:
http://www.tandfonline.com/loi/swoo20

A comparison of the withdrawal resistance load of nails using experimental and interference approaches

Yiren Wang [a], Wen-ching Su [a], Pornnapa Kasemsiri [b] & Salim Hiziroglu [c]

[a] Department of Forest Products and Furniture Engineering, National Chaiyi University, Chaiyi City, Taiwan

[b] Department of Chemical Engineering, Faculty of Engineering, Chulalongkorn University, Bangkok, Thailand

[c] Department of Natural Resource Ecology & Management, Oklahoma State University, Stillwater, Oklahoma, USA

Available online: 02 Nov 2011

To cite this article: Yiren Wang, Wen-ching Su, Pornnapa Kasemsiri & Salim Hiziroglu (2011): A comparison of the withdrawal resistance load of nails using experimental and interference approaches, Wood Material Science & Engineering, 6:4, 213-218

To link to this article: http://dx.doi.org/10.1080/17480272.2011.619279

Wood Material Science and Engineering, 2011; 6: 213–218

ORIGINAL ARTICLE

A comparison of the withdrawal resistance load of nails using experimental and interference approaches

YIREN WANG[1], WEN-CHING SU[1], PORNNAPA KASEMSIRI[2] & SALIM HIZIROGLU[3]

[1]*Department of Forest Products and Furniture Engineering, National Chaiyi University, Chaiyi City, Taiwan,* [2]*Department of Chemical Engineering, Faculty of Engineering, Chulalongkorn University, Bangkok, Thailand, and* [3]*Department of Natural Resource Ecology & Management, Oklahoma State University, Stillwater, Oklahoma, USA*

Abstract

The objective of this study was to determine and predict the withdrawal resistance or pull-out load of common wire nails embedded in radial, tangential and cross-sectional grain orientation of Douglas fir (*Presudotsuga menziesii*) and sugar maple (*Acer sacharum*) samples. Four lead-hole diameters of 1.5, 2.0, 2.5 and 3.0 mm were used to create various interference fits. Nails with a diameter of 3.38 mm were driven into the samples to a depth of 10 mm for the experiments. The overall withdrawal resistance of Douglas fir samples was found to be lower than that of maple samples. Strength values of each sample increased with decreasing lead-hole diameters. No significant difference was found between withdrawal resistance values from radial and tangential sections in either species. However, significantly lower values were obtained for the cross-sections of the samples than for the two other sections. Ratios between predicted pull-out load values of the nails from both species based on the finite element numerical interference approach were very close to experimental measurements, with ratios ranging from 0.93 to 1.09. The results provide better understanding of the behaviour and performance of pull-out resistance for building systems.

Keywords: *Common wire nails, Douglas fir, maple, withdrawal strength.*

Introduction

In general, the stability of any building system consisting of interconnected components is directly related to the performance of the fastening elements. Common wire nails are widely used for different applications of wood constructions because of their good performance and low cost. Therefore, knowledge of the withdrawal strength of nails for wooden elements will provide useful information about the stability and durability of the materials in the building system. Various research projects have been carried out to evaluate the withdrawal strength characteristics of different types of nails, including annularly threaded, helically threaded, cement-coated and galvanized nails, but little testing has been done on common wire nails with different lead-hole diameters (Feldborg & Johansen, 1972; Ehlbeck, 1976; McLain, 1997; Rammer & Zelinka, 2004; Celebi & Kilic, 2007). In one of these studies it was concluded that design withdrawal values for bright nails were underestimated by 40–60% (Skulteti *et al.*, 1997). In general, the density of wood and the nail diameter were the main parameters influencing the withdrawal strength properties of the nails (Stern, 1976). The withdrawal resistance of threaded nails embedded in various species has also been studied (Stern, 1976; Wills *et al.*, 1996).

Withdrawal strength is a function of moisture content, nail penetration depth, diameter of the nails, and density and grain orientation of the wood. The grain orientation of the samples significantly influences the overall strength properties as well as the fastening characteristics of wood. If the nail is driven to parallel to the wood fibre along the longitudinal direction, withdrawal resistance is reduced to 50–75% compared with that of a nail driven across the grain orientation in either radial or tangential section (Forest Products Society, 1999). The withdrawal strength of annularly threaded nails embedded in

Correspondence: S. Hiziroglu, Department of Natural Resource Ecology & Management, Oklahoma State University, Stillwater, OK 74078-6013. E-mail: salim.hiziroglu@okstate.edu

(Received 23 April 2011; accepted 27 August 2011)

ISSN 1748-0272 print/ISSN 1748-0280 online
http://dx.doi.org/10.1080/17480272.2011.619279

southern pine lumber was investigated to determine the effect of nail diameter and galvanization on withdrawal resistance (Rammer & Mendez, 2008). When the findings from this study were compared with results using common nails, it was concluded that common wire nails had lower values than those of galvanized nails.

Although numerous studies have been carried out to evaluate the withdrawal strength of different types of nail embedded in pine and other softwood species, little information has been documented on the withdrawal strength of common wire nails in Douglas fir and maple. Therefore, the objective of this study was to determine experimentally the withdrawal resistance of common wire nails with four lead-hole diameters, which would create different interference fits, driven into three sections of Douglas fir and maple samples, and to compare these test values to calculated values using the finite element interference approach.

Materials and methods

Defect-free Douglas fir (*Presudotsuga menziesii*) and sugar maple (*Acer sacharum*) samples were conditioned in a climate chamber with a temperature of 20°C and a relative humidity of 65% until they reached an equilibrium moisture content of 12%. Flat-sawn specimens for tangential section and quarter-sawn specimens for radial section nail withdrawal strength had dimensions of 170 × 50 × 35 mm, while cross-section samples had dimensions of 50 × 50 × 35 mm. Figure 1 illustrates the sample size and grain orientation of each type of sample. Table I shows the number of samples and their specifications. Nails with a diameter of 3.38 mm were driven into radial and tangential surfaces of Douglas fir and maple with four randomly arranged lead-hole diameters, 1.5, 2.0, 2.5 and 3.0 mm, using an MTS testing system at a cross-head speed of 30 mm min^{-1}. The smaller cross-section specimen carried only one nail at a time for different lead-hole diameters. After nails were driven into the sample, they were kept in a climate-controlled room for a week before the pull-out test. The MTS unit was also used for a pull-out test at a cross-head speed of 2 mm min^{-1}.

Theoretical approach

When a nail is driven into wood, the pressure between the nail and the wood contact surface is produced by interference fits. The driving behaviour of a nail into wood with a lead hole is very similar to the axial pressing of a shaft into a hub with interference fit.

For a typical cylindrical surface assembled by interference fitting one or two isotropic materials with each other, contact pressure can be calculated analytically by Lame's equation (Timonshenko, 1941; Collins, 2003):

$$p = \frac{\Delta}{2\left[\frac{a}{E_h}\left(\frac{b^2+a^2}{b^2-a^2}+\nu_h\right)+\frac{d}{E_s}\left(\frac{d^2+c^2}{d^2-c^2}-\nu_s\right)\right]} \quad (1)$$

where p = contact pressure, Δ = diametrical interference, E = Young's modulus, v = Poisson ratio, h = hub (outer cylinder), s = shaft (inner cylinder), a = hub inner radius before assembly, b = hub outer radius before assembly, c = shaft inner radius before assembly, and d = shaft outer radius before assembly.

Once the contact pressure has been determined, the load used to pull the shaft apart from the hub can be calculated by the following friction model:

$$F = \mu \times p \times A \quad (2)$$

where F = withdrawal load, μ = coefficient of friction, p = contact pressure, and A = contact area.

After the hub and shaft have been constructed, the hollow diameter of the hub increases and the outer diameter of the shaft decreases. The difference in the diametrical deformation between the hub and shaft is the diametrical interference (Δ). However, owing to the large difference in the moduli of elasticity between the nail and the wood, all deformation is contributed by the wood rather than by the steel nail. The diametrical interference is equal to the diametrical difference between the nail and lead-hole diameters. The orthotropic characteristics of wood, with three moduli of elasticity, three shear moduli and three Poisson ratios with respect to the longitudinal, tangential and radial directions, are too complex to apply Lame's equation to the wood–nail joint. For instance, the assumption of axial symmetrical deformation in the cylindrical hub and shaft is no longer true owing to the orthotropic characteristics of wood and the shape of the wood into which the nail is driven. Lame's equation is also restricted to two-dimensional stress analysis and the case of two cylinders with the same axial length. The finite element approach is a powerful tool in such situations, having the advantage of being applicable to any arbitrary shape comprising any materials or combinations of different materials. Prasad *et al.* (1994) analysed the stress in a hollow shaft using the finite element method for a hub–shaft system and achieved good agreement with the results from Lame's equation. Zhang *et al.* (2000) applied Lame's equations and three-dimensional finite element stress analysis to interference fits in a ring gear–wheel connection. They found that three-dimensional finite element

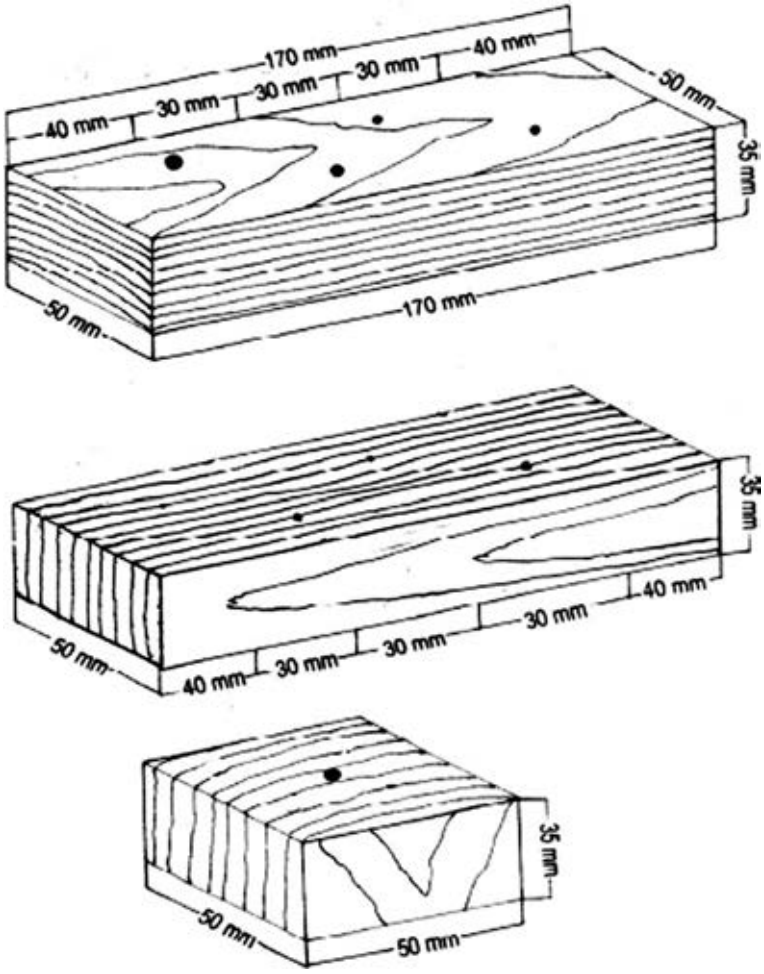

Figure 1. Schematics of the samples with three grain orientations used for the experiment.

analysis gave more complete and accurate results. Because of the high value of modulus of elasticity of a steel nail, the nail could be treated as a rigid body. The diametrical displacement is thus contributed only by the wood. The displacement vector $\{u_h\}$ of the lead hole in wood and the nodal forces $\{P\}$ acting along the contact plane by virtue of the interference could be formulated by [K] $\{u_h\} = \{P\}$, where [K] is the stiffness matrix of the wood.

The contact pressures and withdrawal loads (pull-out loads) of nails with different lead-hole diameters were approximated using numerical analysis software, ANSYS, within the scope of finite element analysis (Kohnke, 1996). To take advantage of the geometric symmetry of the problem, a three-dimensional axisymmetric model was analysed. Since the stresses at the interface between the nail and wood were the main concern, a finer mesh was used in this region, as illustrated in the quarter meshed model wood–nail joint in Figure 2. The wood and nail were modelled using SOLID186 elements. The contact surfaces were modelled using CONTA174 and TARGE170 elements on the wood and nail surfaces, respectively. The

Table I. Experimental design.

	Maple		Douglas fir	
Section	No. of nails	No. of samples (dimensions, mm)	No. of nails	No. of samples (dimensions, mm)
Tangential	4	10 (170 × 50 × 35)	4	10 (170 × 50 × 35)
Radial	4	10 (170 × 50 × 35)	4	10 (170 × 50 × 35)
Cross-section	1	40 (50 × 50 × 35)	1	40 (50 × 50 × 35)
Average moisture content (%)	–	12.0	–	11.8
Average density ($g\,cm^{-3}$)	–	0.56	–	0.45

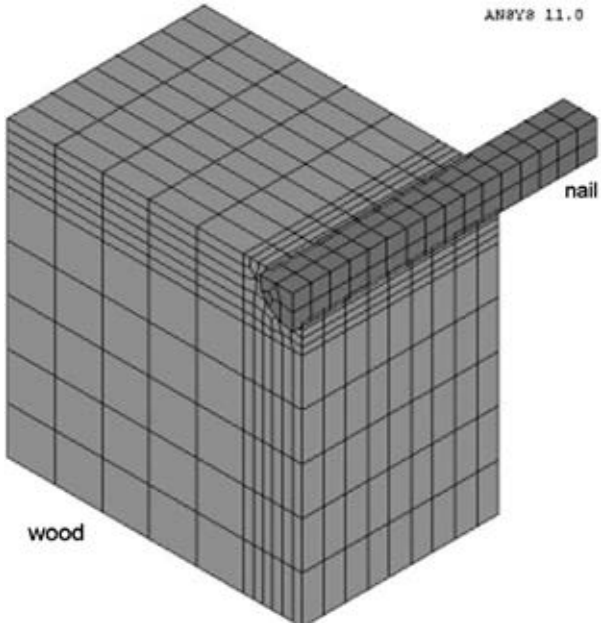

Figure 2. Illustration of meshed sample used for theoretical calculations.

Young's moduli and shear moduli of sugar maple and Douglas fir used in the simulation and shown in Table II are from Bodig and Jayne (1982). The Poisson ratios of both wood species are those given in the *Wood handbook* (Forest Products Society, 1999). The nail is isotropic, with a measured modulus of elasticity of 170,356 MPa and an assumed Poisson ratio of 0.3 for isotropic material.

Results and discussion

Table III displays average experimentally and theoretically calculated pull-out load values and maximum contact pressure for radial, tangential and cross-sections of the samples from both species. In general, maple samples gave higher pull-out values than Douglas fir samples. The average pull-out value of the nails with four different lead-hole diameters in radial sections of maple was 1001.5 N, while the corresponding value for Douglas fir was 287.5 N, which is 2.48 times lower. The high density of maple would be a major reason for this finding. The values for the other two sections of both species showed a similar trend. It appears that pull-out values increased with decreasing lead-hole diameter in all sections of samples of both species. A smaller lead-hole diameter with a fixed nail diameter would cause a larger interference fit. Consequently, a smaller lead-hole diameter would have a higher pull-out load. Both species showed the lowest pull-out load values in cross-sections, followed by tangential and radial sections. Low pull-out values in the cross-section can be related to the limited resistance of the tubular structure of wood against the driving the force of the nails. In a previous study, the withdrawal resistance of nails embedded in cross-sections of the samples was 50–75% lower than that of both radial and tangential sections (Forest Products Society, 1999). Statistical analysis showed significant differences between pull-out test values from the two species at the 95% confidence level, but regarding the grain orientation of the samples, no statistical difference was found between radial and tangential sections. However, values determined on cross-sections of the samples were significantly different from those of the other two sections, at the 95% confidence level.

Table II. Moduli and Poisson ratios of wood.

	Modulus[a] (MPa)					Poisson ratio[b]			
Species	E_L	E_R	E_T	G_{LR}	G_{LT}	G_{RT}	μ_{LR}	μ_{LT}	μ_{RT}
Maple	13,810	1,310.69	677.8	1,012.84	752.9	254.6	0.424	0.476	0.349
Douglas fir	11,259	939.07	588.81	771.52	720.50	79.43	0.292	0.449	0.390

Note: [a]Bodig and Jayne (1982) Appendix I; [b]Wood Handbook (1999).

Table III. Experimental and theoretical pull out resistance values of the samples.

Section	Lead-hole diameter (mm)	Maple				Douglas fir			
		Pred. (*n*)	Meas. (*n*)	Ratio (Pred./ Meas.)	Max. contact pressure (MPa)	Pred. (*n*)	Meas. (*n*)	Ratio (Pred./ Meas.)	Max. contact pressure (MPa)
R	1.5	1157	1150	1.00	104.4	275	291	0.94	51.4
	2.0	1034	1015	1.02	93.7	295	294	1.00	46.8
	2.5	1060	1009	1.05	84.2	305	290	1.05	42.1
	3.0	875	830	1.05	66.5	276	274	1.00	36.8
T	1.5	1045	1044	1.00	103.4	234	253	0.92	50.7
	2.0	808	781	1.03	93.7	257	253	1.01	46.8
	2.5	894	857	1.04	81.9	257	241	1.06	41.8
	3.0	742	726	1.02	65.1	233	222	1.05	36.0
X	1.5	955	956	0.99	47.5	206	221	0.93	28.1
	2.0	815	797	1.02	42.1	232	219	1.05	23.6
	2.5	621	608	1.02	35.5	222	212	1.04	17.8
	3.0	585	581	1.00	24.6	217	199	1.09	11.2

Note: Pred. = predicted; Meas. = measured.

Contact pressure values exhibited a similar trend. They increased with decreasing lead-hole diameter for samples from both species. Nails driven into the cross-section resulted in significantly lower contact pressure values than those of both tangential and radial sections of the samples. It appears that the low density and the anatomical structure of Douglass fir are key parameters, resulting in lower contact pressure values than those of maple, similarly to the pull-out test findings.

A computer program was used to predict the pull-out values of the samples for four lead-hole diameters in three sections. As can be seen from Table II, the experimental and predicted pull-out values were similar to each other, with ratios ranging from 0.93 to 1.09, suggesting that such an approach could be used to predict accurately the pull-out characteristics when common wire nails are driven into the samples.

Conclusions

Common wire nails embedded in Douglas fir and maple were tested to determine their pull-out resistance. Additional parameters considered were the grain orientation of the samples and the lead-hole diameter, which influenced the overall resistance values. Maple samples had the highest pull-out strength value of 1005.5 N in radial grain orientation. Results from experimental tests and theoretical calculations were comparable to each other, having ratios close to 1.0. In further studies, the pull-out resistance of similar types of nails embedded in wood samples with various penetration depths could be determined to obtain more comprehensive information on their characteristics.

Acknowledgements

Support by National Chaiyi University, Chaiyi, Taiwan for Dr Yiren Wang's one-year sabbatical leave in the Department of Natural Resource Ecology & Management, Oklahoma State University, is greatly appreciated.

References

Bodig, J. & Jayne, B. A. (1982). *Mechanics of wood and wood composites* (pp. 384–38). New York: Van Nostrand Reinhold.

Celebi, G. & Kilic, M. (2007). Nail and screw withdrawal strength of laminated veneer lumber made up hardwood and softwood layers. *Construction and Building Materials*, *21*, 894–900.

Collins, J. (2003). *Mechanical design of machine elements and machines* (p. 372). New York: John Wiley & Sons.

Ehlbeck, J. (1976). Withdrawal resistance of threaded nails in wood used for building construction in Germany. *Proceedings of the 30th Annual Forest Products Research Society Meeting*. Madison, WI: Forest Products Society.

Feldborg, T. & Johansen, M.(1972). *Withdrawal resistance of nails* (SBI Rep. No. 74). Copenhagen: Statens Byggeforskning Institut. (In Danish.)

Forest Products Society (1999). *Wood handbook—Wood as an engineering material* (Gen. Tech. Rep. FPL-GTR-113). Madison, WI: USDA, Forest Service, Forest Products Laboratory.

Kohnke, A. P. (1996). *ANSYS Theory reference*. SAS IP.

McLain, T. (1997). Design axial withdrawal strength from wood. II. Plain-shank common wire nails. *Forest Products Journal*, *47*(6), 103–109.

Prasad, N. S., Sashikanth, P. & Ramamutri, V. (1994). Stress distribution in interference joints. *Computers and Structures*, *51*, 535–540.

Rammer, D. & Mendez, A. M. (2008). Withdrawal strength of bright and galvanized annularly threaded nails. *Frame Building News*, April, 59–67.

Rammer, D. & Zelinka, S. L. (2004). Review of end grain nail withdrawal research (Gen. Tech. Rep. FPL-GTR-151).

Madison, WI: USDA, Forest Service, Forest Products Laboratory.

Skulteti, M., Bender, D. A., Winistorfer, S. G. & Pollock, D. G. (1997). Withdrawal strength of ring shank nails embedded in southern pine lumber. *Transactions of the ASAE*, *40*, 451–456.

Stern, E. (1976). *Performance of pallet nails and staples in 22 southern hardwoods* (Bull. 145). Blacksburg, VA: Wood Research and Wood Construction Laboratory, Virginia Polytechnic Institute and State University.

Timonshenko, S. (1941). *Strength of material. Part II. Advanced theory and problems*. New York: D. Van Nostrand.

Wills, B. L., Winistorfer, S. G., Bender, D. A. & Pollock, D. G. (1996). Threaded nail fastener—Research and standardization needs. *Transactions of the ASAE*, *39*, 661–668.

Zhang, Y., McClain, B. & Fang, X. D. (2000). Design of interference fits via finite element method. *Journal of Mechanical Science*, *42*, 1835–1850.

Chemorheology and Thermomechanical Characteristics of Benzoxazine-Urethane Copolymers

Sarawut Rimdusit, Wanchat Bangsen, Pornnapa Kasemsiri

Polymer Engineering Laboratory, Department of Chemical Engineering, Faculty of Engineering, Chulalongkorn University, Pathumwan, Bangkok 10330, Thailand

Received 18 June 2010; accepted 16 January 2011
DOI 10.1002/app.34170
Published online 12 April 2011 in Wiley Online Library (wileyonlinelibrary.com).

ABSTRACT: In this research, processability and some important thermomechanical properties of polybenzoxazine (BA-a) modified with a highly flexible urethane elastomer (PU) are discussed. This copolymer has been reported to show synergy in its glass transition temperature and some mechanical properties thus provides a fascinating group of high temperature polymers with enhanced flexibility. The results reveal that a processing window of the BA-a/PU mixtures is widened with the increasing urethane prepolymer fraction, that is, the liquefying temperature is lowered and the gel point shifted to higher temperature with the amount of the PU. Synergism in glass transition temperature (T_g) of this copolymer was clearly confirmed, i.e., T_g's of the BA-a/PU alloys were significantly greater than those of the parent resins, i.e., BA-a ($T_g = 166°C$) and PU ($T_g = -70°C$). In addition, flexural modulus was found to systemically decrease from 5.4 GPa of the neat polybenzoxazine to 2.1 GPa at 40% by weight of the PU. Flexural strength of the alloys also shows a synergistic behavior at the BA-a/PU ratio of 90/10. Coefficient of thermal expansion of the polymer alloys were also found to show a minimum value at BA-a/PU = 90/10. © 2011 Wiley Periodicals, Inc. J Appl Polym Sci 121: 3669–3678, 2011

Key words: copolymers; crosslinking; gelation; thermosets

INTRODUCTION

Polybenzoxazine, a novel kind of phenolic resin, is one of new thermosetting plastics. The curing of this resin involves ring-opening polymerization without a catalyst or a curing agent and does not produce any by-products during cure which might cause void in the products. Polybenzoxazine possesses various useful properties such as high ability to synthesize from inexpensive raw materials, low melt viscosity before cure resulting in its high processability, no by-product during cure, near zero volumetric shrinkage after processing, low water absorption, high thermal stability, and excellent mechanical properties.[1–3] However, the application of this polymer is limited to certain areas due to its rather high rigidity. In principle, toughness of polybenzoxazine can be enhanced by two major strategies. The first strategy is by utilizing a novel molecular design of benzoxazine resins such as a synthesis of linear aliphatic diamine-based benzoxazine and a utilization of high molecular weight benzoxazine precursors.[4] Second method is by alloy formation or copolymerization with flexible resins or polymers such as urethane elastomer,[5–7] flexible epoxy,[6,8] poly (ε-caprolactone),[9] poly(imide-siloxane),[10] and polydimethylsiloxane.[11] The latter strategy is a relatively versatile and simple method to improve mechanical property or thermal stability of polybenzoxazine.

Recently, benzoxazine resin (BA-a) alloyed with urethane prepolymer (PU) had been developed by Takeichi et al. The resulting hybrid films were prepared by blending BA-a monomer and PU which was synthesized from 2,4-toluene diisocyanate and adipate polyol (Mw 1000). The obtained films showed a single glass transition temperature suggesting no phase separation in the resulting alloys. The properties of the films ranged from elastomers to plastics depending on the amount of benzoxazine fraction in the alloys.[4] Other BA-a/PU alloy systems were investigated by Yeganeh group. The PU structure used in this system had glycidol as a blocking agent of urethane prepolymers. The T_g of this system was found to increase with increasing BA-a content.[12] Furthermore, a series of phenol end-functionalized urethane prepolymers was prepared by Yeganeh et al. These telechelic oligomers were used as a

Correspondence to: S. Rimdusit (sarawut.r@chula.ac.th).
Contract grant sponsor: National Research University Project of the Ministry of Education, Thailand; contract grant number: AM006B and AM1076A.
Contract grant sponsor: Thailand Research Fund, 100th Anniversary of Chulalongkorn University Academic Funding.
Contract grant sponsor: Dutsadi Phiphat Scholarship of Chulalongkorn University.
Contract grant sponsor: TRF-MAG Scholarship.

macro initiator for ring opening polymerization of benzoxazine monomers. Thermal stability of the resulting networks was improved by increasing PU molecular weight as well as BA-a content.[13] Interesting characteristics of some, benzoxazine-urethane alloy systems were also observed by Rimdusit et al. According to this report, benzoxazine resin (BA-a) was alloyed with isophorone diisocyanate/polyether polyol (Mw 2000) based PU. The obtained alloys not only provided expected enhancement on their flexibility but also exhibited synergism in glass transition temperature (T_g). The T_g value as high as 220°C of this alloy system was observed when 30 wt % of PU was added.[6,7] Synergism in glass transition of polybenzoxazine from an addition of other resins or polymers has been observed and reported previously in various systems such as benzoxazine-epoxy,[8,14] benzoxazine-urethane,[6,7] benzoxazine-polycarprolactone,[9] or benzoxazine-polydimethysiloxane[11] etc.

From the substantial enhancement on flexibility and the observed synergistic behaviors in T_g of benzoxazine-urethane alloys discussed above, other essential properties of the alloys including their processability or chemorheological characteristics and some thermomechanical properties as a function of alloy compositions will be examined in this work. The chemorheological characteristic is one of the crucial phenomena for material processibility. The sol-gel transition and time for gelation obtained from rheological property measurement are important factors to control desirable products with appropriate processing conditions and methods.

EXPERIMENTAL

Materials

Materials used in this research are benzoxazine resin and urethane prepolymer. Benzoxazine resin is based on bisphenol-A, aniline, and formaldehyde. The bisphenol-A (polycarbonate grade) was supported by Thai Polycarbonate Co., Ltd. (TPCC). Para-formaldehyde (AR grade) was purchased from Merck Company and aniline (AR grade) was contributed by Panreac Quimica S.A. Company. Urethane prepolymer was prepared using polypropylene glycol polyol at a molecular weight of 2000 with toluene diisocyanate (TDI). The toluene diisocyanate was obtained from the South City Group whereas the polypropylene glycol polyol at a molecular weight of 2000 was kindly supplied by TPI Polyol Co., Ltd.

Matrix resin preparation

Benzoxazine monomer (BA-a) was synthesized from bisphenol A, aniline, and paraformaldehyde at a 1 : 2 : 4 molar ratio. This resin was prepared based on a patented solventless method.[11] The resulting benzoxazine monomer is solid at room temperature with transparent yellow color. The as-synthesized monomer was ground into fine powder and was taken for material characterization.

The urethane prepolymer was prepared by using propylene glycol at a molecular weight of 2000 with 2,4-tolulene diisocyanate (TDI) at a 1 : 2 molar ratio. Small amount of dibutyltin dilaurate (DBDT) was used as a catalyst for the synthesis. The two reactants for urethane resin preparation were stirred under a nitrogen stream at 70°C for 2 h. 0.075% by weight of dibutyltin dilaurate was used as a catalyst. After the completion of the reaction, the obtained clear and viscous urethane prepolymers were cooled to room temperature and kept in a nitrogen-purged, closed container.

Benzoxazine/urethane polymer alloys preparation

The benzoxazine monomer (BA-a) was blended with the urethane prepolymers (PU) to provide BA-a/PU mixtures. Each resin was measured at the desirable mass fraction. The mixture was then heated to about 100°C in aluminum pan and mixed until a homogeneous mixture was obtained. The molten resin mixture was poured into an aluminum mold and step-cured in an air-circulated oven at 150, 170, 180, 190°C for 1 h each and 200°C for 2 h. Part of the mixture was taken for differential scanning analysis. The specimen was finally left to cool down to room temperature and was then ready for material characterizations.

Characterization methods

Chemorheological properties measurement

Chemorheological properties of each alloy were examined using a Rheometer (Haake Rheo Stress 600, Thermo Electron Cooperation) equipped with 20 mm in diameter parallel plate geometry. The measuring gap was set at 0.5 mm. The experiment was performed under an oscillatory shear mode at 1 rad/s. The testing temperature program was ramped from room temperature at a heating rate of 2°C/min to a temperature beyond the gel point of each resin and the dynamic viscosity was recorded.

Differential scanning calorimetry

The curing behavior and glass transition temperature of benzoxazine resins alloyed with urethane elastomer were examined using a differential scanning calorimeter (DSC) model 2910 from TA Instruments. The thermogram was obtained using a heating rate of 10°C/min from room temperature to

300°C under nitrogen atmosphere maintained to be constant at 50 mL/min. The sample with a mass in a range of 3–5 mg was sealed in an aluminum pan with lid.

Density measurement

The densities of benzoxazine resins alloyed with urethane prepolymer were determined by water displacement method according to the ASTM D 792-91 (Method A). The dimension of specimens was in rectangular shape 25 mm × 50 mm × 2 mm.

Dynamic mechanical analysis

The dynamic mechanical analyzer (DMA) model DMA242 from NETZSCH was used to investigate the dynamic mechanical properties and relaxation behaviors of BA-a/PU polymer alloys. The dimension of specimens was 10 mm × 50 mm × 2 mm. The test was performed in a three-point bending mode. In a temperature sweep experiment, a frequency of 1 Hz and a strain value of 0.1% were applied. The temperature was scanned from −150°C to the temperature beyond the glass transition temperatures (T_g) of each specimen with a heating rate of 2°C/min under nitrogen atmosphere. The storage modulus at glassy state was correlated to molecular rigidity of the polymer network whereas the storage modulus at rubbery plateau was dependent on crosslink density of the network.

Thermogravimetric analysis

The degradation temperature (Td) and char yield of the BA-a/PU polymer alloys were studied using a DSC-TGA Q600 SDT from TA Instruments. The testing temperature program was ramped at a heating rate of 20°C/min from room temperature to 900°C under nitrogen atmosphere. The purge nitrogen gas flow rate was maintained to be constant at 100 mL/min. The sample mass used was measured to be ~ 10–20 mg. Degradation temperature of each specimen was determined from the temperature at 5% weight loss whereas char yield was obtained the weight residue at 800°C.

Thermomechanical analysis

The coefficient of thermal expansion (CTE) was measured with a Perkin–Elmer Instrument Technology SII Diamond thermal mechanical analyzer (TMA). The dimension of specimens was 2 mm × 2 mm × 2 mm and had flat surfaces. The specimen was heated from room temperature to the temperature beyond the glass transition temperature at a heating rate of 10°C/min.

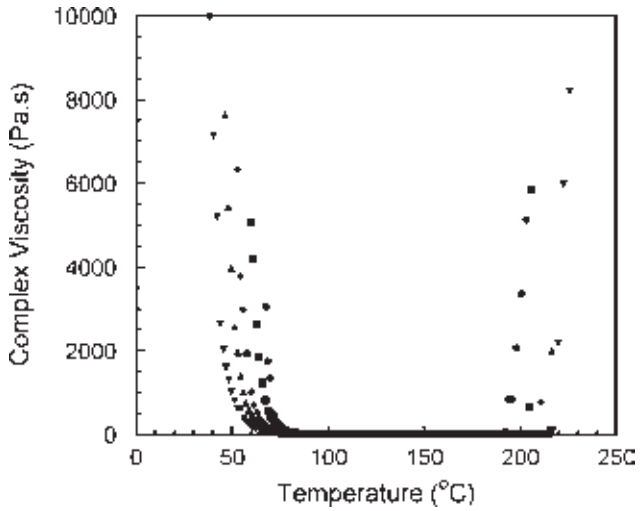

Figure 1 Viscosity of BA-a/PU resin at various compositions: (●) 100/0, (■) 90/10, (◆)80/20, (▲)70/30, and (▼)60/40.

Universal testing machine (Flexural Mode)

The flexural properties of the BA-a/PU polymer alloys were determined using a universal testing machine (model 5567) from Instron Co., Ltd. The test method was a three-point bending mode with a supporting span of 32 mm and tested at a crosshead speed of 0.85 mm/min. The dimension of the specimens is 25 mm × 50 mm × 2 mm according to ASTM D790M-93. The measured properties are averaged from eight specimens.

Hardness measurement (Shore D)

The hardness of polymer alloys samples was also measured using a shore D hardness tester (model ES-720G) from Micro Photonics. The specimens were 25 mm × 50 mm × 2 mm, and had flat surfaces following ASTM D2240.

Water absorption measurement

Water absorption measurement was conducted in accordance with ASTM D570 using a specimen dimension of 25 mm × 50 mm × 2 mm. Three samples of each composition were submerged in deionized water. The specimens were periodically removed and dried by wiping for weight measurements after which they were immediately returned to the water bath.

RESULTS AND DISCUSSION

Chemorheological behaviors

The effect of BA-a/PU resin mass ratios on chemorheology of the resin mixtures, which are miscible giving homogenous and transparent liquid, is shown in Figure 1. In the rheograms, all resin mixtures

showed a relatively high viscosity at room temperatures due to the solid state nature of these resin mixtures. They were transformed into liquid when the temperature was raised to their liquefying point (i.e., left side of the rheograms). At this point, the complex viscosity of all resin mixtures rapidly decreased. For consistency, the temperature at the viscosity value of 1000 Pa.s was investigated as a liquefying temperature of each resin.[15,16] From the figure, it can be seen that the increasing urethane polymer fraction in the resin mixtures led to the lowering of their liquefying temperatures. This is due to the fact that the urethane prepolymer used is liquid while the BA-a resin is solid at room temperature. Therefore, the addition of the liquid urethane prepolymer in the solid BA-a resin caused the shifting of the transition from solid state to liquid state to lower temperature. From the above convention, the liquefying temperature of BA-a/PU resins 100/0, 90/10, 80/20, 70/30, and 60/40 were determined to be 71°C, 67°C, 60°C, 57°C, and 51°C, respectively. All resin mixtures became liquid after liquefying point that was the lowest viscosity of each resin system and is normally termed the A-stage viscosity. Lowering the resin liquefying temperature obviously enables the use of lower processing temperature of a compounding process, which is desirable in various composite applications.

Furthermore, at the end of the A-stage viscosity or at higher temperature, the resin mixtures underwent crosslinking reactions past their gel points, which was defined as a transition of liquid (sol) to solid (gel), (i.e., the right side of the rheograms), resulting in a sharp increase in their viscosities. In this case, the maximum temperature at which the viscosity was rapidly raised above 1000 Pa.s was used as gel temperature of each resin.[15,16] From the figure, the gel point of the BA-a/PU resin mixture increased with increasing mass fraction of the urethane prepolymer. The gel temperature of BA-a/PU resins 100/0, 90/10, 80/20, 70/30, and 60/40 were determined to be 196, 205, 210, 216, and 219°C, respectively. These results suggested that the urethane prepolymer had effect on the curing reaction of the benzoxazine monomer. In other words, the processing window of the BA-a/PU resin mixtures was widened with an addition of the urethane prepolymer. Therefore, one advantage of adding urethane into BA-a/PU resin mixtures was to modify chemorheological behaviors of the benzoxazine resin. The widest processing window was $\sim$ 70 to 215°C for BA-a/PU of 60/40 compared with the range of 90 to 195°C of the neat BA-a. This behavior provides BA-a/PU resins with sufficiently broad processing window for a typical compounding process in a composite manufacturing.

Figure 2 exhibits the effect of urethane prepolymer content on complex viscosity of BA-a/PU resin mixtures determined at 120°C. From the experiment, the complex viscosity of the benzoxazine-urethane resin mixtures significantly increased with increasing the amount of the urethane prepolymer as the urethane resin had much higher melt viscosity than that of the neat benzoxazine resin. This might be due to the higher molecular weight of the urethane prepolymer compared with that of the benzoxazine resin. The complex viscosity of BA-a/PU resin mixture at 0, 10, 20, 30, and 40% mass fractions of the PU were determined to be 0.11, 0.21, 0.44, 0.78, and 1.01 Pa.s, respectively. In practice, the lower viscosity of the resin can enhance the ability of the resin to accommodate greater amount of filler and increase filler wettability of the resin during the compounding process in a composite material preparation.[15,16]

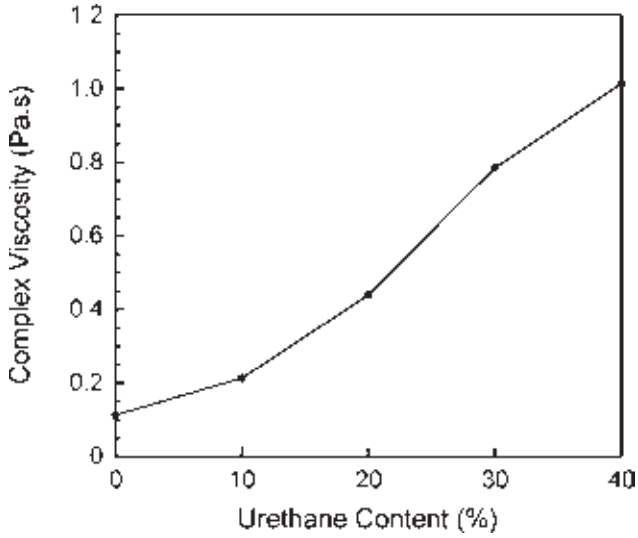

Figure 2 Effect of urethane content on viscosity of BA-a/PU resins determined at 120°C.

Density measurement of BA-a/PU polymer alloys

In this work, density measurement of all fully cured BA-a/PU specimens was performed to investigate the presence of void in the specimens. Figure 3 shows the density of specimens with various urethane contents comparing with their theoretical density. The calculated one was based on the basis that the densities of the polybenzoxazine and urethane prepolymer were 1.19 g/cm^3 and 1.06 g/cm^3.[17,18] Furthermore, the theoretical densities of the BA-a/PU polymer alloys were determined to be 1.190, 1.177, 1.164, 1.151, and 1.138 g/cm^3 in BA-a/PU 100/0, 90/10, 80/20, 70/30, and 60/40, respectively. Whereas the measured densities at 100/0, 90/10, 80/20, 70/30, and 60/40 mass ratios of the BA-a/PU alloys were found to be 1.188, 1.177, 1.160, 1.148, and 1.133 g/cm^3, respectively. In the result, the densities of the polymer alloys were observed to

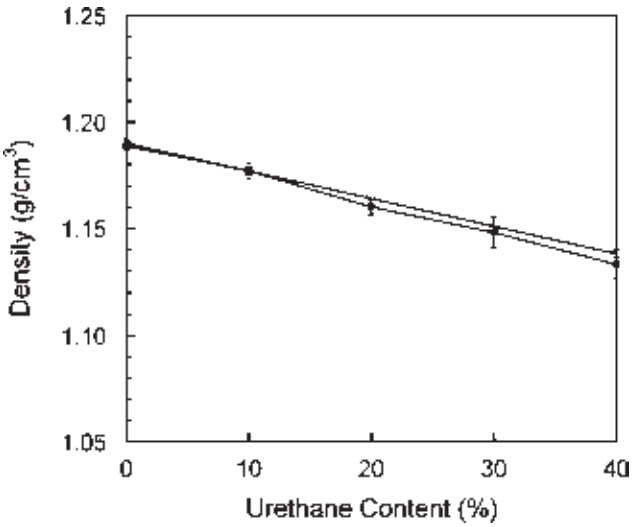

Figure 3 Density of BA-a/PU alloys at various compositions: (□) Theory density and (●) Actual density.

systematically decrease with increasing PU fraction suggesting that the theoretical and actual density of the BA-a/PU alloys followed the rule of mixture. Moreover, it can be observed that the actual densities were about the same with the values slightly lower than those of the theoretical densities. Because of the rather high melt viscosity of the urethane prepolymer, adding more urethane prepolymer directly affected on the mixing behavior and the obtained densities were normally slightly lower than the theoretical values. The phenomenon is likely to be caused by the presence of voids in the specimens as a result of mixing difficulty from an addition of the more viscous PU fraction into the benzoxazine resin.

DMA of the BA-a/PU polymer alloys

Transition temperatures of all BA-a/PU polymer alloys were also determined using DMA since the technique is highly sensitive to even minor transitions or relaxations. DMA senses any change in molecular mobility in the sample when temperature is raised or lowered. The dynamic modulus is one of the most important properties of materials for structural applications. Typically, mechanical damping is often the most sensitive indicator in determining all kinds of molecular motions, which are taking place in polymeric materials particularly in solid state. Figure 4 plots the loss modulus (E'') curves of the benzoxazine-urethane alloys at various compositions which had been fully cured to yield the crosslink structures of the infinite network as a function of temperature. The T_g of the alloys can be roughly estimated from the maximum peak temperature in the loss modulus curve of each specimen. From the figure, we can see that the T_g of the neat polybenzoxazine was determined to be 165°C whereas those of the polymer alloys were about 177, 192, 220, and 245°C in BA-a/PU 90/10, 80/20, 70/30, and 60/40. Therefore, adding PU into the polybenzoxazine can substantially increase the T_g of the polymer alloys. Synergistic behavior of the T_g of the alloys was evidently observed, i.e., T_g's of all alloys were greater than those of the BA-a and the PU, i.e., 165°C[15,16] and −70°C,[5,19] respectively. This is the unique characteristic of these polymer alloys as it exhibited synergistic behaviors in their glass transition which makes the systems highly attractive for high temperature application. The synergistic behavior of these polymer alloys has been discussed more elaborately in our previous work[6,7] as to be due to the substantial enhancement in crosslink density of the alloys by the presence of urethane portion in the network. Both the rigidity of the polybenzoxazine and the enhancement on crosslink density from the urethane provided the synergism in glass transition temperature of the resulting polymer alloys. The possible network formation scheme or illustration between the ring-opening reaction of benzoxazine resin and urethane resin has been suggested in the work by Takeichi et al.[5]

Figure 5 shows the storage modulus (E') of BA-a/PU alloys at various compositions. From the figure, three areas including the glassy state, the transition region, and the rubbery plateau were obtained for each sample. Ordinarily, the storage modulus of the materials decreased with increasing temperature. At room temperature, the storage modulus in a glassy state of the BA-a/PU binary systems was expectedly found to systematically decrease with increasing PU mass fraction. We can see that the storage moduli of the BA-a/PU alloys were reduced from 5.2 GPa to 1.8 GPa with the addition of the PU from 0 to 40% by weight. As a consequence, the presence of the

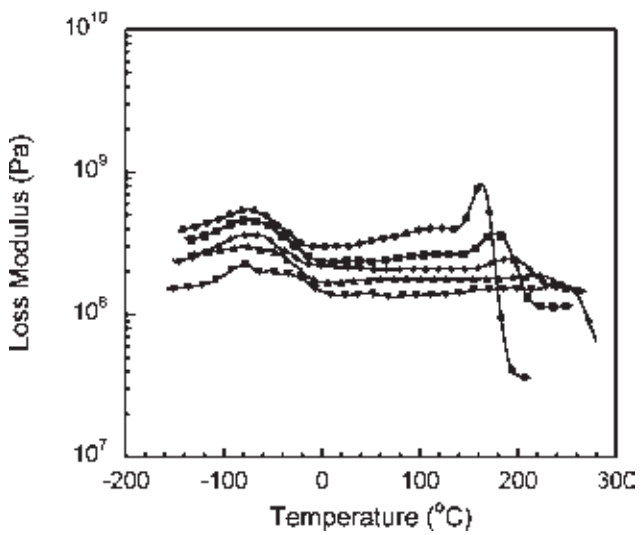

Figure 4 Loss modulus of BA-a/PU alloys at various compositions: (●) 100/0, (■) 90/10, (◆) 80/20, (▲) 70/30, and (▼) 60/40.

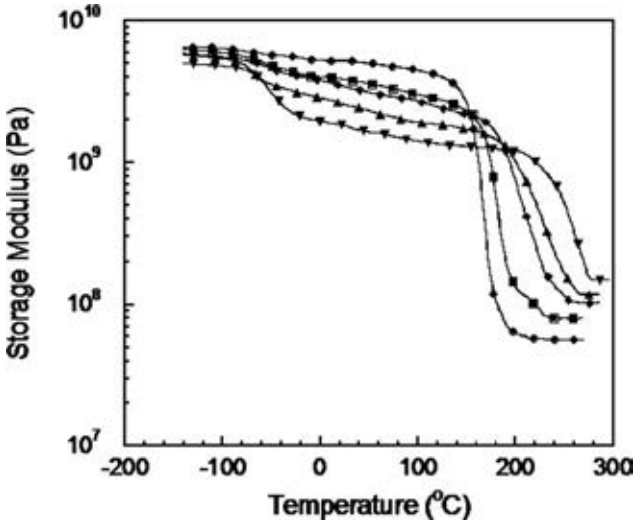

Figure 5 Storage modulus of BA-a/PU alloys at various compositions: (●) 100/0, (■) 90/10, (◆) 80/20, (▲) 70/30, and (▼) 60/40.

more flexible PU in the copolymers resulted in the more flexible polymer hybrids as seen from the lower room temperature modulus.

Effects of urethane prepolymer on the storage modulus in the rubbery plateau region of their polymer alloys are illustrated in Figure 6. From the figure, the storage modulus in the rubbery plateau region tended to increase with the mass fraction of the PU which was an opposite trend to the storage modulus in the glassy state. The storage moduli in the rubbery plateau region were systematically increased from 56 MPa to 148 MPa with an addition of the PU fraction from 0 to 40% by weight. This suggested that the increase in the PU content in the polymer alloys possibly resulted in an enhancement of the crosslink density of the fully cured specimens which was closely related to the rubber plateau modulus. For a tight network structure, i.e., rubbery plateau modulus is greater than 10^7 Pa such as in our case, the non-Gaussian character of the polymer network becomes more and more pronounced and the equation from theory of rubbery elasticity no longer holds. The approximate relation expressed in eq. (1) below proposed by Neilsen[20,21] is thus preferred and is reported to better describe the elastic properties of dense network, e.g., in epoxy systems.[3,22,23]

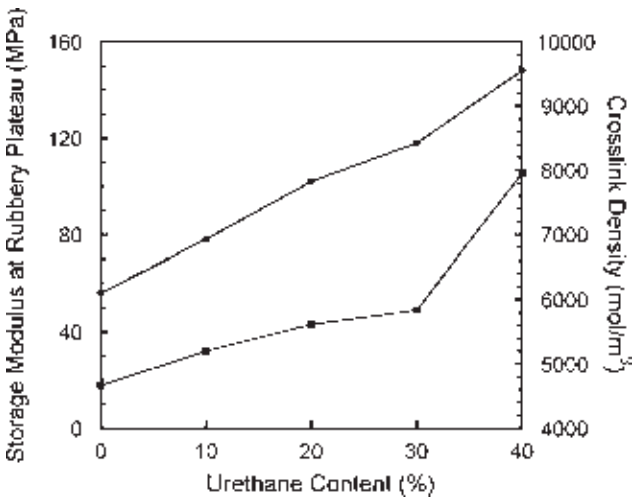

Figure 6 Storage modulus at rubbery plateau and crosslink density of BA-a/PU alloys at various compositions: (●) Storage modulus at rubbery plateau and (■) Crosslink density.

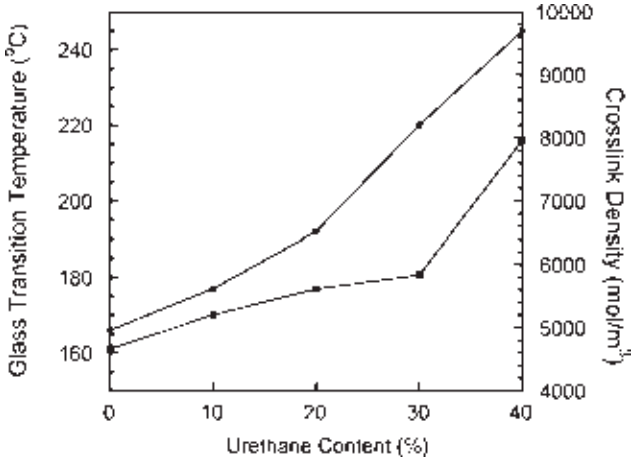

Figure 7 Glass transition temperature and the crosslink density of BA-a/PU alloys at various compositions: (●) Glass transition temperature and (■) Crosslink density.

$$\log\left(\frac{E'}{3}\right) = 6.0 + 293(\rho/M_c) \quad (1)$$

where E' (Pa) is the storage modulus in a rubbery plateau region, ρ (g/cm^3) is the density of the material at room temperature, and M_c (g/mol) is the molecular weight between crosslink points. The crosslink density of our polymer alloys was found to increase with the mass fraction of the urethane prepolymer. The crosslink density of the BA-a/PU polymer alloys was estimated to be 4338 mol/m^3 in BA-a/PU 100/0, 4829 mol/m^3 in BA-a/PU 90/10, 5227 mol/m^3 in BA-a/PU 80/20, 5443 mol/m^3 in BA-a/PU 70/30, and 5779 mol/m^3 in BA-a/PU 60/40.

In addition, the effect of molecular weight between crosslinks (i.e., inversely proportional to its crosslink density) on a T_g of a copolymer or a nonuniform polymer network can be accounted for using the equation also proposed by Neilsen.[21,24]

$$T_g - T_{g(0)} = \frac{k}{M_c} \quad (2)$$

The number average molecular weight between crosslinks is M_c. $T_{g(0)}$ is the glass transition temperature of the uncrosslink polymer. Figure 7 illustrates

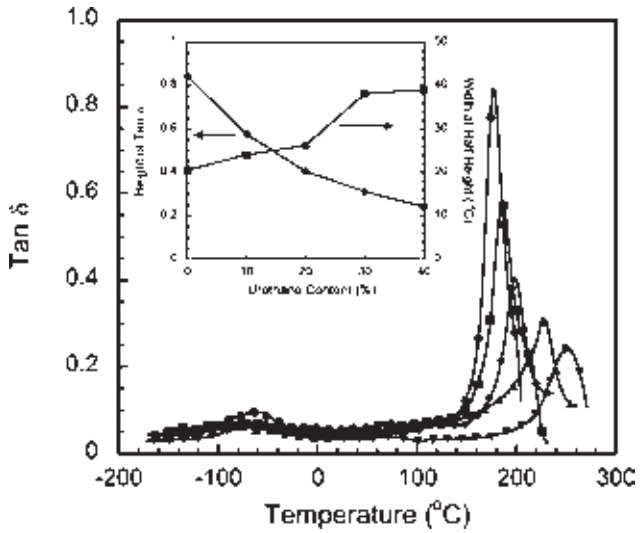

Figure 8 Tan δ of BA-a/PU alloys at various compositions: (●) 100/0, (■) 90/10, (◆) 80/20, (▲) 70/30, and (▼) 60/40.

the T_g from loss modulus and crosslink density of BA-a/PU alloys at various compositions. As seen from this figure, the T_g of the polymer network increased when its crosslink density in the alloys increased, which is in good agreement with our DMA results.

Tan δ or loss tangent curves, obtained from the ratio of energy loss or viscous part (E'') to storage energy or elastic part (E′) of dynamic modulus of material, are shown in Figure 8. The T_g of the polymer alloys can also be determined from the maximum peak temperature on the tan δ curve of each sample. As shown in the figure, T_g's of the alloys were observed to shift to higher temperature when the urethane prepolymer content in the alloys increased. Furthermore, an inset of Figure 8 illustrates the magnitude of the tan δ peak maximum reflecting the large scale mobility associated with α relaxation. The peak height of the tan δ was found to decrease with increasing the mass fraction of the PU. This confirmed the reduction in segmental mobility of polymer chains with increasing crosslink density as PU fraction in the alloy increased. The width at half height of the tan δ relates to the network homogeneity. The width at half height of the tan δ curves of our BA-a/PU polymer alloys were broader in the PU rich systems implying network heterogeneity to be more pronounced with an increasing amount of the PU.[8]

Thermal degradation of BA-a/PU polymer alloys (TGA)

Thermal degradation of BA-a/PU polymers was investigated by thermogravimetric analysis (TGA). Figure 9 shows the degradation temperature and char yield at various urethane contents under nitrogen atmosphere. The T_d's of the neat polybenzoxazine and the polyurethane were determined to be 325°C and 305°C whereas their alloys showed the T_d values of 326, 327, 334, and 336°C in BA-a/PU 90/10, 80/20, 70/30, and 60/40. As evidently seen in the figure, the T_d's of the polymer alloys were found to be slightly higher than that of the neat polybenzoxazine. Consequently, synergistic behavior of T_d of these alloys were also observed, i.e., the T_d's of all alloys were greater than that of the neat BA-a (325°C) and the neat PU (305°C). Therefore, an incorporation of the PU into the polybenzoxazine was found to enhance thermal stability of the polybenzoxazine. These results might be due to the reaction of the isocyanate in urethane prepolymer and the hydroxyl of the polybenzoxazine to increase a crosslink density of the polymer alloys as aforementioned.

Another interesting feature in the TGA thermograms is the percent residual weight of our polybenzoxazine alloys which reported at 800°C under N_2 atmosphere. It can be seen that the residual weight of the BA-a/PU alloys were found to systematically decrease with increasing PU fraction. This is due to the fact that polybenzoxazine possessed higher char yield value of about 29% while no char residue was found for the polyurethane used. The chemical structure of the polyurethane composed of a less thermally stable aliphatic structure of the polypropylene glycol polyol compared with the prevalent benzene rings in the molecular structure of the polybenzoxazine. The char yields of BA-a/PU alloys at 10, 20, 30, and 40% mass fractions of the PU were determined to be 24.1 wt %, 23.4 wt %, 20.7 wt %, and 18.7 wt %, respectively. This result is also

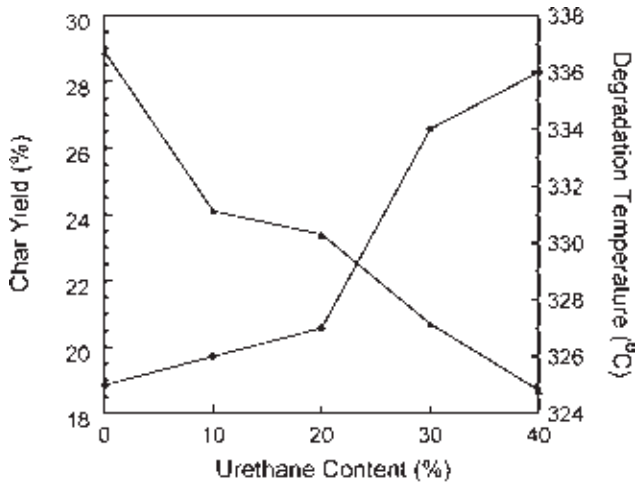

Figure 9 Thermal degradation of BA-a/PU alloys at various compositions: (▲) Char yield and (●) Degradation temperature.

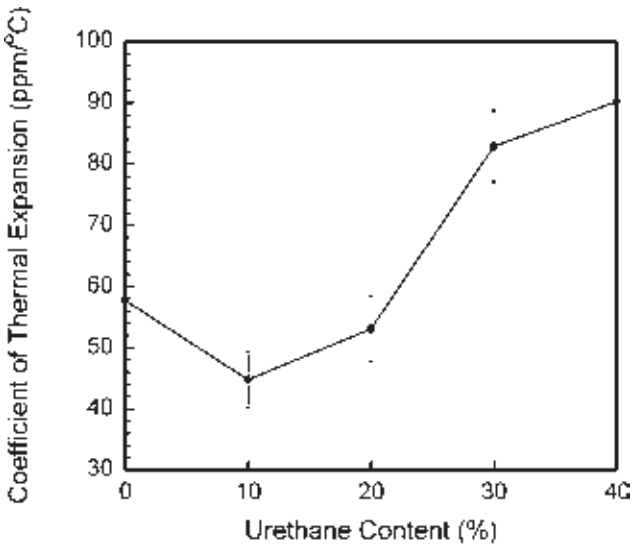

Figure 10 Effect of urethane content on coefficient of thermal expansion of BA-a/PU alloys at various compositions.

consistent with those reported by Takeichi et al. and Takeichi.[5,19]

Coefficient of thermal expansion of BA-a/PU polymer alloys

During heat transfer, the energy that is stored in the intermolecular bonds between atoms changes. When the stored energy increases, so does the length of the molecular bonds. As a result, solids typically expand in response to heating and contract on cooling. This dimensional response to temperature change is expressed by its CTE. Figure 10 exhibits the CTE characteristics of BA-a/PU alloy specimens at various urethane mass fractions. The CTE values of BA-a/PU 100/0, BA-a/PU 90/10, BA-a/PU 80/20, BA-a/PU 70/30, and BA-a/PU 60/40 were determined to be 57.7, 44.7, 53.0, 82.8, and 90.2 ppm/°C, respectively. It was clearly observed the CTE of our alloys did not show a linear relationship with the composition of the alloys but also exhibited a synergistic behavior with the minimum CTE value at BA-a/PU 90/10 mass fraction. The CTE of BA-a/PU at 90/10 and 80/20 weight ratios were found to be lower than that of the neat polybenzoxazine and increased to higher values when the amount of PU fraction was greater than 20 wt %. In principle, the addition of the PU which is more expansible than BA-a due to its elastomeric nature, the resulting BA-a/PU alloys should result in an increase in their CTE values as observed in the PU content of greater than 20% by weight region. The observed synergistic behavior in CTE of these polymer alloys in the vicinity of 10–20% by weight of implied that the effect of crosslink density enhancement in the alloy's CTE dominated the effect of the higher expansion of the PU provided that the PU mass fraction was maintained below 20% by weight.

Flexural properties of BA-a/PU polymer alloys

In this investigation, the specimens for flexural analysis were loaded until failure and the stress–strain curves were obtained for each sample. The flexural strength of a thermosetting resin is influenced by a number of interrelated system parameters including T_g, molecular weight between crosslinks, crosslink density, free volume, chemical structure, network irregularity and perfection, and many other contributing factors.[25] Flexural properties (flexural strength, flexural modulus, and elongation at break) of BA-a/PU polymer alloys were shown in Table I. The flexural strength of the neat polybenzoxazine was determined to be 130 MPa. Interestingly, the strength values of the BA-a/PU alloys were observed to exhibit also a synergistic behavior with the maximum flexural strength value of 142 MPa observed at the BA-a/PU mass ratio of 90/10. In addition, with an increase of the PU fraction (i.e., 20 wt %, 30 wt %, and 40 wt %), the flexural strength values were found to decrease systematically. Those flexural strengths of the BA-a/PU alloys were determined to be 120, 89, and 60 MPa in BA-a/PU 80/20, 70/30, and 60/40. This finding coincides with the phenomenon found in CTE and T_g as discussed earlier. Our result is also in good agreement with the result previously reported by Rimdusit et al.[6]

The maximum flexural modulus value of 5.5 GPa belonged to neat polybenzoxazine. The flexural modulus was also found to linearly decrease with increasing amount of PU for all BA-a/PU alloy systems. The flexural modulus values of BA-a/PU alloys were 4.1 GPa, 3.4 GPa, 2.5 GPa, and 2.1 GPa for BA-aPU of 90/10, 80/20, 70/30, and 60/40 mass ratios, respectively. The flexural modulus shows a behavior nearly identical to that of the storage modulus at room temperature determined by DMA. This phenomenon was due to the fact that the addition of the softer urethane resin into the benzoxazine resin was expected to lower the stiffness of the

TABLE I
Flexural Properties of BA-a/PU Copolymers at Various Compositions

PU content (%)	Flexural strength (MPa)	Flexural modulus (GPa)	Flexural strain at break (%)
0	130	5.5	2.5
10	142	4.1	3.5
20	120	3.4	3.8
30	89	2.5	4.1
40	60	2.1	5.1

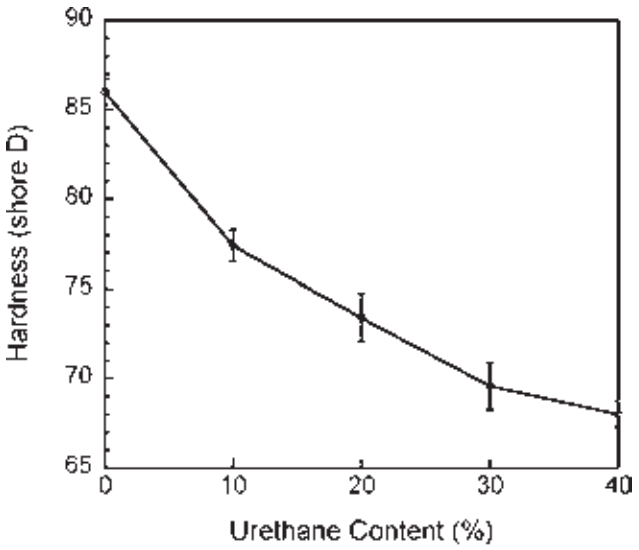

Figure 11 Effect of urethane content on surface hardness of BA-a/PU alloys at various compositions.

polybenzoxazine alloys as a result of an elastomeric nature of the PU used.[5,19]

The effect of urethane prepolymer on the flexural strain at break of polybenzoxazine as can be seen in Table I. The flexural strain at break of polybenzoxazines alloyed with urethane prepolymer at 0, 10, 20, 30, and 40% were determined to be 2.5, 3.5, 3.8, 4.1, and 5.1, respectively. Normally, the addition of the more flexible urethane prepolymer to the rigid polybenzoxazine matrix should also contribute to the increased strain at breakage for the alloys.[5,19]

Surface hardness of BA-a/PU polymer alloys

Hardness is defined as the resistance offered by a specimen to the penetration of a hardened steel truncated cone (Shore-A), pointed cone (Shore-D), or a spherical or flat indenter (foam hardness). In this study, Shore-D hardness was measured on a scale that was graduated from 0 to 100 divisions; 0 denoting the lowest and 100 the highest degree of hardness. In Figure 11, the surface hardness (Shore D) values of the BA-a/PU polymer alloys at different PU content were presented. As expected, the surface hardness of the polymer alloys was found to systematically decrease with increasing PU fraction. An addition of PU to BA-a was found to diminish the resistance of the BA-a deformation. The surface hardness values of the fully cured BA-a/PU alloys were observed to be 86, 77, 73, 69, and 68 shore D in BA-a/PU 100/0, 90/10, 80/20, 70/30, and 60/40. The surface hardness of the urethane was reported to be $\sim$ 40 shore D.[26] As a consequence, the hardness of the BA-a/PU alloys tended to follow a simple rule of mixture. This phenomenon was similar to hardness values of polyurethane reinforced with aluminum oxide (Al_2O_3) particles reported by Zhou et al.[27]

Water absorption of BA-a/PU polymer alloys

Figure 12 shows percent water absorption of BA-a/PU alloys versus time. It can be seen in this figure that the percent water absorption value of BA-a alloyed with the PU tended to increase with an addition of the PU. Moreover, the percent water absorption was observed to increase sharply in the first 24 h of the test, and reach a plateau value of 1.3% in BA-a/PU 100/0, 2.0% in BA-a/PU 90/10, 2.8% in BA-a/PU 80/20, and 4.3% in BA-a/PU 70/30, and 4.7% in BA-a/PU 60/40. To explain the diffusion in the material, the generalized equation can be expressed as

$$\frac{M_t}{M_\alpha} = k_n t_n \tag{3}$$

where M_t is the mass of sample at time t and M_α the mass of sample at saturation or infinite time.

The diffusion behaviors can be classified as: super case II ($n > 1$), case II ($n = 1$), anomalous ($1/2 < n < 1$), classical/Fickian ($n = 1/2$), or pseudo-Fickian ($n < 1/2$).[28] From the plots of log M_t/M versus log t, the obtained slope of the neat polybenzoxazine was about 0.71 implied that its diffusion behavior was an anomalous type. The slopes of the BA-a/PU polymer alloys were determined to be in a range of 0.23–0.32 suggesting Fickian type diffusion behavior.

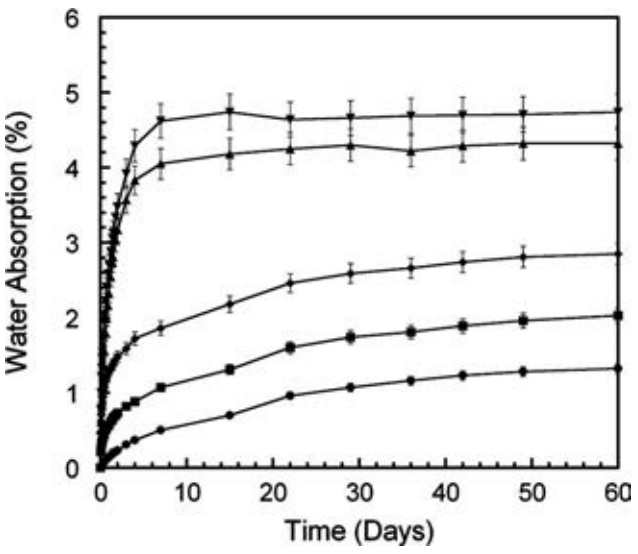

Figure 12 Percentage water absorption of BA-a/PU alloys at various compositions: (●) 100/0, (■) 90/10, (◆) 80/20, (▲) 70/30, and (▼) 60/40.

CONCLUSIONS

An addition of urethane resin in BA-a/PU resin mixtures was found to substantially widen their processing window. Density of the alloys decreased with the urethane contents. Synergism in thermal stability was clearly observed in these polymers. The phenomenon was explained by an ability of the PU fraction to substantially enhanced crosslink density of the resulting polymer alloys. Furthermore, the char yield of the BA-a/PU alloys was found to systematically increase with the increasing amount of the BA-a fraction. Whereas the CTE of the alloys was observed to show a minimum at the BA-a/PU = 90/10 mass ratio. The flexural strength of the BA-a/PU alloys exhibited the ultimate value at BA-a/PU = 90/10 mass ratio whereas the flexural modulus, flexural strain at break and surface hardness showed behaviors following a rule of mixing. Last but not least, BA-a fraction in the alloy was used to effectively lower the water absorption of the resulting polymer.

Thai Polycarbonate Co., Ltd. for bisphenol-A supply is gratefully acknowledged. In addition, the authors thank Centre of Research and Technology Development, Mektec Manufacturing Corp. (Thailand), Chulalongkorn University, for the kind support on the use of Thermal Gravimetric Analyzer (TGA) and Thermal Mechanical Analyzer (TMA).

References

1. Ishida, H.; Rodriguez, Y. Polymer 1995, 36, 3151.
2. Ning, X.; Ishida, H. J Polym Sci Part A: Polym Chem 1994, 32, 1121.
3. Ishida, H.; Lee, Y. H. Polymer 2001, 42, 6971.
4. Takeichi, T.; Kano, T.; Agag, T. Polymer 2005, 46, 12172.
5. Takeichi, T.; Guo, Y.; Agag, T. J Polym Sci Part A: Polym Chem 2000, 38, 4165.
6. Rimdusit, S.; Pirstpindvong, S.; Tanthapanichakoon, W.; Damrongsakkul, S. Polym Eng Sci 2005, 45, 288.
7. Rimdusit, S.; Mongkhonsi, T.; Kamonchaivanich, P.; Sujirote, K.; Thiptipakorn, S. Polym Eng Sci 2008, 48, 2238.
8. Ishida, H.; Allen, D. J Polymer 1996, 37, 4487.
9. Ishida, H.; Lee, Y. H. J Polym Sci Part B: Polym Phys 2001, 39, 736.
10. Takeichi, T.; Agag, T.; Zeidam, R. J Polym Sci Part A: Polym Chem 2001, 39, 2633.
11. Ardhyananta, H.; Kawauchi, T.; Ismail, H.; Takeichi, T. Polymer 2009, 50, 5959.
12. Yeganeh, H.; Razavi-Nouri, M.; Ghaffari, M. Polym Eng Sci 2008, 48, 1329.
13. Jamshidi, S.; Yeganeh, H.; Mehdipour-Ataei, S. Polym Adv Technol 2010, 1634.
14. Rimdusit, S.; Ishida, H. J Polym Sci Part B: Polym Phys 2000, 38, 1687.
15. Ishida, H. U. S. Pat. 5,543,516 (1996).
16. Rimdusit, S.; Kampangsaeree, N.; Tanthapanichakoon, W.; Takeichi, T.; Suppakarn, N. Polym Eng Sci 2007, 45, 140.
17. Jubsilp, C.; Takeichi, T.; Rimdusit, S. J Appl Polym Sci 2007, 104, 2928.
18. Ishida, H.; Allen, D. J. J Appl Polym Sci 1996, 34, 1019.
19. Takeichi, T.; Guo, Y. Polym J 2001, 33, 437.
20. Neilsen, L. E. J Macromol Sci Rev Macromol Chem 1969, 3, 69.
21. Neilsen, L. E.; Landel, R. F. Mechanical Properties of Polymers and Composites; Marcel Dekker: New York, 1994.
22. Levita, G.; De Petris, S.; Marchetti, A.; Lazzeri, A. J Mater Sci 1991, 26, 2348.
23. Lam, D. C. C.; Chong, A. C. M. Mater Sci Eng A 2000, 281, 156.
24. Rodriguez, E.; Larranaga, M.; Mondragon, I.; Vazquez, A. J App Polym Sci 2006, 100, 3895.
25. Morgan, R.; Kong, F. M.; Walkup, C. M. Polymer 1984, 25, 375.
26. Xiao, H. X.; Frisch, K. C. Advances in Urethane Ionomer; Technomic Publishing: Lancaster, 1995.
27. Zhou, R.; Lu, D. H.; Jiang, Y. H.; Li, Q. N. Wear 2005, 259, 676.
28. Neogi, P., Ed. Diffusion in Polymers; Marcel Dekker: New York, 1996.

Symposium

BAEKELAND 2011

3rd International Symposium on Network Polymers

Program and Abstracts

September 11-14, 2011

Hotel Nikko Toyohashi

Toyohashi, Japan

14:30	L26	Characterization of Polybenzoxazine Modified with Dianhydrides S. Rimdusit, C. Jubsilp, B. Ramsiri, T. Takeichi (Chulalongkorn University, Thailand)
14:45	L27	Degradation kinetic of polybenzoxazine modified with aromatic tetracarboxylic dianhydride C. Jubsilp, T. Takeichi, S. Rimdusit (Srinakharinwirot University, Thailand)
15:00	L28	Novel class of phenolic resin of hybrid molecular structure T. Agag, M. Baqar, J. Maia, H. Ishida, S. Qutubuddin Case Western Reserve University, USA

15:15-15:45 Coffee Break

Chairpersons: H. Ishida and L. Pilato		
15:45	L29	Polycondansates with thermally curable benzoxazine groups B. Kiskan, K. D. Demir, Y. Yagci (Istanbul technical University, Turkey)
16:15	L30	Development of Wood Composite from Eastern Redcedar Particles Reinforced with Benzoxazine Resin/Cashew Nut Shell Liquid Copolymer P. Kasemsiri, S. Hiziroglu, S. Rimdusit (Chulalongkorn University, Thailand)
16:30	L31	Pt-free fuel cell catalysts prepared from mixtures of phenolic resin and Fe phtalocyanine M. Kakimoto, Y. Nabae, L. Wu, S. Miyata (Tokyo Institute of Technology, Japan)
16:45	L32	Nano-phase structures and mechanical properties of epoxy polymer alloys modified with self-assembling acrylic block copolymers H. Kishi (University of Hyogo, Japan)
17:15	L33	Life cycle monitoring of FRP matrix resin by infrared light transmitting optical fiber sensor N. Kabe, M. Kubouchi, S. Aoki, T. Tomiyama, T. Sakai (Tokyo Institute of Technology, Japan)
17:30	L34	Toray's Advanced Materials T. Nishimura (Toray Industries, Inc., Japan)
18:00	L35	Recycling of Carbon Fiber Reinforced Plastic with Supercritical Alcohol I. Okajima, K. Watanabe, Y. Shimamaura, T. Awauya, T. Sako (Shizuoka University, Japan)

18:30 Symmposium Dinner
All Things Bakelaite
Hugh Karraker

Development of Wood Composite from Eastern Redcedar Particles Reinforced with Benzoxazine Resin/Cashew Nut Shell Liquid Copolymer

Pornnapa Kasemsiri [1], Salim Hiziroglu [2], Sarawut Rimdusit [1*]

[1] *Department of Chemical Engineering, Faculty of Engineering, Chulalongkorn University, Pathumwon, Bangkok 10330, Thailand*
[2] *Department of Natural Resource Ecology and Management, Oklahoma State University, 303-G Agricultural Hall, Stillwater, OK 74078, USA*
*E-mail address: sarawut.r@chula.ac.th

Adhesive cost in wood composite manufacture is the main parameter controlling overall production cost. One alternative approach to achieve reduce overall product cost would be maximizing fiber amount without changing adhesive content in the matrix. Interestingly, phenolic resins based on benzoxazine structures have a low a-stage viscosity that allows an addition of greater amount of filler [1]. Furthermore, benzoxazine resins have been reported to provide some outstanding characteristics such as having excellent thermal properties and flame retardance, molecular design flexibility, low moisture absorption and near zero shrinkage upon polymerization [2]. In this study some of the properties of experimentally manufactured wood plastic composite reinforced with benzoxazine resin (BA-a) and cashew nut shell liquid (CNSL) copolymer were investigated. Specimens having 50-75% eastern redcedar (*Juniperus virginiana L.*) particles mixed with matrix material BA-a/CNSL were manufactured for the experiments. Based on the findings in this work, wood particles decreased the curing temperature (T_{cured}) of BA-a/CNSL matrix (as shown in Fig. 1). Dynamic mechanical characteristics of the specimens increased with increasing amount of wood particles. Good compatibility between wood particles and BA-a/CNSL matrix was found and such compatibility resulted in enhanced the glass transition temperature (T_g) value of the specimens (as shown in Fig. 2). It appears that BA-a blended with CNSL can be used as attractive value-added product to be used for certain application where their high performances are desired.

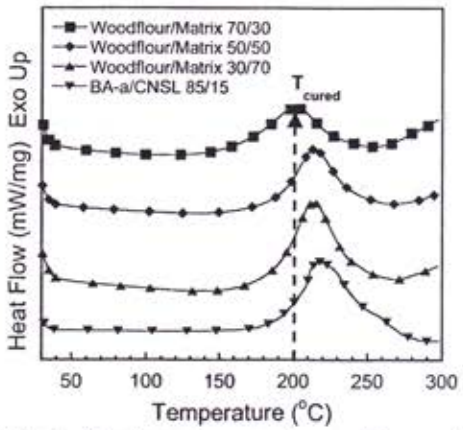

Fig 1. Curing temperature of samples with various filler contents

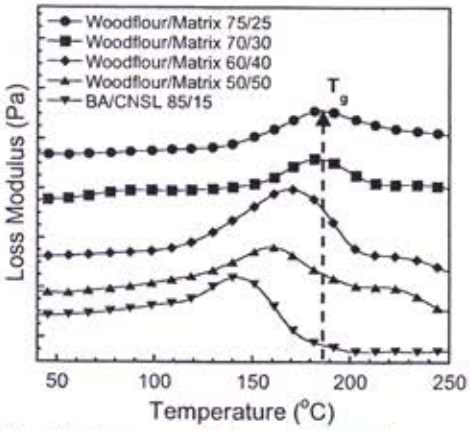

Fig 2. Loss modulus of samples at various filler contents

References

[1]. S. Rimdusit, H. Ishida, Polymer, 41(22), 7941(2000).
[2]. S. Rimdusit, W. Tanthapanichakoon, C. Jubsilp, J Appl Polym Sci, 99(3), 1240(2006).

1st Polymer Conference of Thailand

October 7-8, 2010
Convention Center, Chulabhorn Research Institute, Bangkok

PROCEEDINGS

Organized by :

Sponsored by :

ptt CHEM

NSTDA MTEC NANOTEC SCG CHEMICALS

ptt PHENOL TPC

Session	POLYMERS FOR SUSTAINABILITY (1)
Date/Time/Room	October 8, 2010 / 09:40-10:20 / Meeting Room 5
Session Chair	Rangrong Yoksan
PS-OP-01 (09:40-10:00)	**Effect of NR and ENR on Physical Properties of Poly(butylenes adipate-co-terephthalate)** ***Nuda Pisutthian***, *Pasaree Laokijcharoen and Varaporn Tanrattanakul* Bioplastic Research Unit, Department of Materials Science and Technology, Faculty of Science, Prince of Songkla University
PS-OP-02 (10:00-10:20)	**Effects of Electron Acceptor Content on Efficiency and Morphology of Polymer Solar Cell Based on P3HT** ***Nopparat Keatsirisart***, *Jatuphorn Wootthikanokkhan, Chanchana Thanachayanont and Narumon Seeponkai* Division of Materials Technology, School of Energy Environment and Materials, King Mongkut's University of Technology Thonburi
Session	POLYMERS FOR SUSTAINABILITY (2)
Date/Time/Room	October 8, 2010 / 10:50-12:10 / Meeting Room 5
Session Chair	Suttinun Phongtamrug
PS-OP-03 (10:50-11:10)	**Utilization of Silane-Crosslinked Polymer Waste as Additive for High-Density Polyethylene** ***Phawitporn Chuaythong*** *and Kalyanee Sirisinha* Department of Chemistry, Faculty of Science, Mahidol University
PS-OP-04 (11:10-11:30)	**Fabrication and Mechanical Properties of Non-Woven Thermoplastic Biocomposite of Oil Palm Empty Fruit Bunch Cellulose and Poly(lactic acid) Fibers** ***Sirisart Ouajai***, *Satian Seetawarin and Prichya Kaewklam* Department of Industrial Chemistry, Faculty of Applied Science, King Mongkut's University of Technology North Bangkok
PS-OP-05 (11:30-11:50)	**Thermally Reversible Light Scattering Characteristics of Benzoxazine-Urethane Alloys** ***Pornnapa Kasemsiri***, *Junji Wakita, Shinji Ando and Sarawut Rimdusit* Department of Chemical Engineering, Faculty of Engineering, Chulalongkorn University
PS-OP-06 (11:50-12:10)	**Effect of Hydrogen Bond Network and Chain Mobility on Proton Conductivity in Heterocyclic System for Polymer Electrolyte Membrane Fuel Cell (PEMFC)** ***Chatchai Jarumaneeroj***, *Autchara Pangon and Suwabun Chirachanchai* The Petroleum and Petrochemical College, Chulalongkorn University

Polymers for Sustainability

Thermally Reversible Light Scattering Characteristics of Benzoxazine-Urethane Alloy

Pornnapa Kasemsiri[1], Junji Wakita[2], Shinji Ando[2] and Sarawut Rimdusit[1*]

[1]Department of Chemical Engineering, Faculty of Engineering Chulalongkorn University, Bangkok 10330, Thailand

[2]Department of Chemistry and Materials Science, Tokyo Institute of Technology, Tokyo, Japan

*Corresponding Author E-mail address: sarawut.r@chula.ac.th

Abstract

The transparency of thermally reversible light scattering (TRLS) materials can be switched between opaque and transparent states by varying temperature. TRLS films have potential applications in thermal sensors, optical devices etc. TRLS behavior was observed in the benzoxazine alloyed with urethane prepolymer (BA-a/PU) system. The intensity of transmitted light was evaluated as a function of temperature in successive heating/cooling process. Transparent states were observed during heating in the range of 150-200°C whereas opaque state was investigated upon cooling. In addition, the BA-a/PU system also exhibits enhanced thermal stability i.e. a synergism in glass transition temperature (Tg) was observed for all examined BA-a/PU alloy systems. The Tg value of the copolymer network was found to systematically increase with increasing the PU fraction in the alloys and the highest Tg of the copolymer that could form infinite network was observed at 40 wt% of the PU fraction to be about 241°C.

Keywords: Polybenzoxazine, Urethane prepolymer, Thermally reversible light scattering, Glass transition temperature, Synergism

1. Introduction

Thermally reversible light scattering (TRLS) is material which can be reversibly switched from opaque to transparent states by varying temperature i.e. it can be transparent or opaque depending on whether it is submitted to a cooling or a heating cycle. From this characteristic, TRLS have potential applications in thermal sensors, optical devices, recording media and several other applications. [1-2]

The aim of this research is to investigate the TRLS behavior in benzoxazine (BA-a) resin alloyed with urethane elastomer (PU) i.e. BA-a/PU system. Hence, this system is very attractive for some optical applications besides its outstanding thermal and mechanical characteristics.

The system of BA-a/PU consists of benzoxazine resin and urethane elastomer. The benzoxazine, which is one kind of phenolic resin, has some outstanding properties i.e. low a-stage viscosity, no curing agent required for its polymerization, near zero shrinkage, no curing by-products, as well as high mechanical and thermal properties of the fully cured specimens. Nevertheless, one shortcoming of benzoxazine is high brittleness. In our previous work, it was found that improved toughness of polybenzoxazine by alloying with urethane prepolymer (PU) can be easily achieved. In addition, synergism in glass transition temperature of this alloy was also observed. The Tg of the urethane elastomer and polybenzoxazine were reported to be about -70 to -20°C and 160 to 170°C, respectively. The Tg of BA-a/PU systems were found to increase with the mass fraction of PU. The optimum composition of BA-a/PU alloys in terms of enhanced flexural modulus and maintaining the high flexural modulus of polybenzoxazine were in the range of 90/10 to 70/30 mass ratios whereas those increased toughness, as evidenced by the area under the curves of flexural stress and flexural strain were investigated when the composition of both tougheners was less than 40 wt%. [3]

The purpose of this work is to analyze optical properties of this BA-a/PU system and to observe factors which affect its TRLS phenomenon.

2. Experimental

BA-a monomer used was synthesized from bisphenol A, aniline and formaldehyde at a 1:2:4 molar ratio according to the solventless synthesis technique [1]. The urethane prepolymer was prepared from toluene diisocyanate and polyether polyol (Molecular weight = 2000) at a 2:1 molar ratio. The two reactants were mixed in a distillation flask and the mixture was stirred under a nitrogen stream at 90°C for 2 hours. To accelerate the reaction, 0.4 gram of dibutylin dilurate was used as a catalyst.

To prepare specimens, BA-a monomer was manually blended with PU at a desirable mass fraction. The resin mixture was mixed in aluminum pan and warmed up about 80°C until a homogeneous mixture was obtained. The specimens were cured in an air-circulated oven at 150-200°C for 6 h.

The curing behavior and thermal transition of BA-a and BA-a/PU were measured by a differential scanning calorimeter (DSC) model 2910 from TA Instrument. Each sample was scanned at heating rate of 10 °C/2min from room temperature to 300°C under N_2 purging. The sample was measured at approximately 10 mg.

Fourier transform infrared spectra of all samples under various curing conditions were acquired by using a Spectrum GX FT-IR spectrometer from Perkin Elmer with an ATR accessory. All spectra were taken as a function of time with 32 scans at a resolution of 4 cm^{-1} and a spectral range of 4000-650 cm^{-1}.

The UV-visible optical transmission spectra were recorded on a Hitachi U-3210 spectrophotometer at variable temperature

3. Results

3.1 Curing behavior and thermal transition of BA-a/PU alloys

DSC profiles of the benzoxazine and benzoxazine blended with urethane prepolymer are shown in Figure 1. A single dominant exothermic peak of the curing reaction in each composition was observed. The peak exotherm of BA-a was investigated at 222°C. In the case of BA-a/PU, the peak exotherms were observed to be smaller than that of BA-a. When the amounts of PU in samples increased the positon of the peak exotherm also shifted to higher temperature i.e. 232°C (90/10 BA-a/PU), 243°C (80/20 BA-a/PU), 244°C (70/30 BA-a/PU) and 248°C (60/40 BA-a/PU).

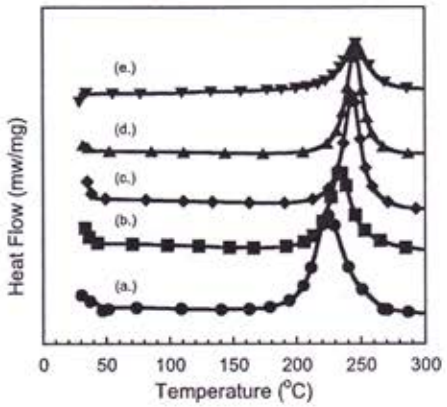

Figure 1. DSC thermograms of curing temperature (a.) 100/0 (BA-a/PU), (b.) 90/10, (c.) 80/20, (d.) 70/30 and (c.) 60/40

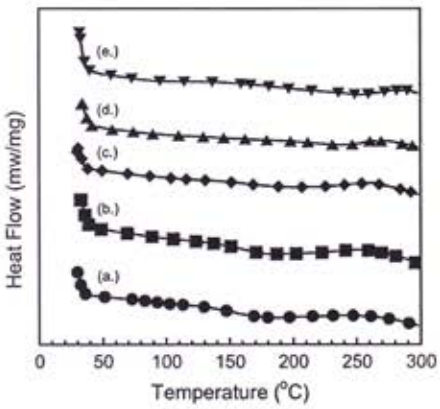

Figure 2. DSC thermograms of glass-transition temperature (a.) 100/0 (BA-a/PU), (b.) 90/10, (c.) 80/20, (d.) 70/30 and (e.) 60/40

Figure 2 illustrates DSC thermograms of BA-a and BA-a/PU at different ratios, after curing process. The exothermic of all compositions disappeared that implied the fully cure stage. The Tg of the fully cured BA-a/PU alloys were observed to be 157°C in BA-a, 162°C in BA-a/PU 90/10, 183°C in BA-a/PU 80/20, 226°C in BA-

a/PU 70/30 and 241°C in BA-a/PU 60/40. This results indicated the synergism in glass transition temperature i.e. the Tgs of all alloys were higher than neat polybenzoxazine (162 °C) and polyurethane (-70 °C). This result is in good agreement with a previous report by Rimdusit et.al. (2005).

3.2 Network Spectroscopic Analysis

The spectra of BA-a monomer, polybenzoxazine and BA-a alloyed were presented in Figure 3. The FT-IR spectra of BA-a monomer (Figure 3a) illustrates the formation of the benzoxazine ring (C-O-C) which was confirmed at 941 and 1230 cm^{-1}. After curing, those absorptions disappeared with the opening of benzoxazine ring (Fig 3b). The characteristic bands of benzoxazine and urethane moieties are presented in Figure 3c. The band at 2242 cm^{-1} was from the NCO group of PU. Figure 3d exhibits the IR spectrum after completion of curing, the absorption at 941, 1230 cm-1(C-O-C) and 2242 cm^{-1} (N-C-O) disappeared, which indicates the formation of BA-a/PU polymer networks.

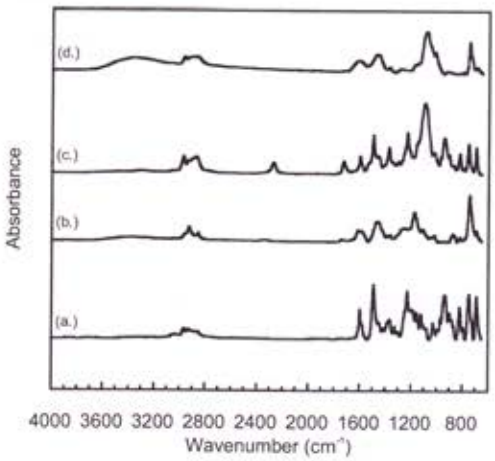

Figure 3. FT-IR spectra of (a) BA-a monomer, (b) polybenzoxazine, (c) 90/10 (BA-a/PU) before curing, (d) 90/10 after curing

The temperature dependence of optical transmission spectra and optical microscope images were exhibited in Figure 4 and 5, respectively. When Ba/PU film at 60/40 mass ratio was heated at 200°C, the specimen became transparent without phase separation. Furthermore, the transmittance at 500-700 nm was significantly higher than the value at room temperature. When the specimen was cooled down to 150°C, the phase separation re-appeared, and gradually became opaque at 100, 50°C and room temperature. Therefore, the phase separation of BA-a/PU alloy was observed at lower temperatures and transformed to a homogenous phase at elevated temperature which led to TRLS phenomenon to BA-a/PU system.

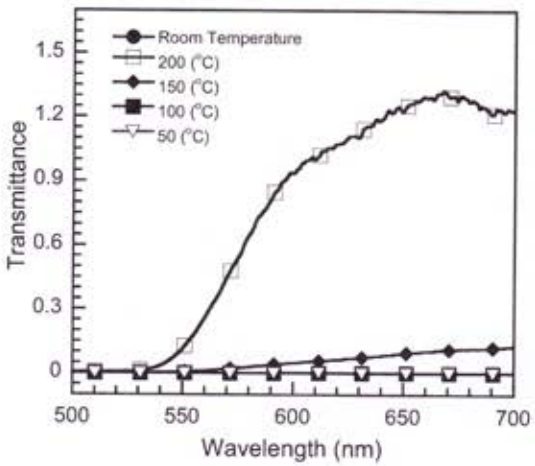

Figure 4. Temperature dependence of optical transmission spectra

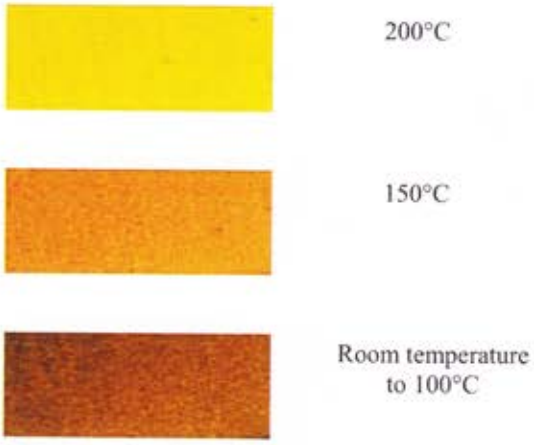

Figure 5. The optical microscope images from 200°C to room temperature of BA-a/PU alloy

3.3 Thermo-optical sensor behavior

The thermo-optical sensor behaviors of 60/40 BA-a/PU at various temperatures were illustrated in Figure 6. The high resolution image covered with this alloy was obtained when temperature increased at 150°C. Furthermore, the image can be repeatedly displayed

or hided controlled by temperature. From, this phenomenon indicated that this alloy would initiate new researches for the preparation and application of "smart materials" such as optical sensor.

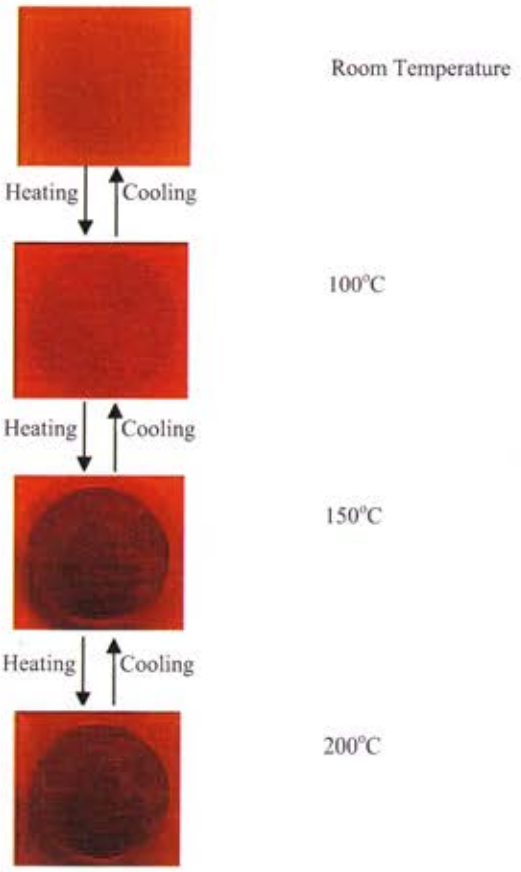

Figure 6. The thermo-optical sensor behaviors of 60/40 BA-a/PU at various temperatures.

4. Conclusions

TRLS behavior was observed in the BA/PU system. The apparent transition from opaque to the transparent state occurred in the range of 150-200°C. When BA/PU film was cooled down to 150°C, the phase separation was observed and gradually became opaque below 100°C. Moreover, the synergistic behavior in Tg were observed at all compositions of BA/PU. Therefore, BA-a/PU is a novel promising material for the future TRLS applications.

Acknowledgements

This research receives financial supports from Chulalongkorn University Dutsadi Phiphat Scholarship, and Thailand Research Fund. Bisphenol A is supported by Thai Polycarbonate Co., Ltd. (TPCC). The authors also would like to acknowledge the Asia-Oceania Top University League on Engineering (AOTULE Scholarship) and Tokyo Institute of Technology University, Tokyo, Japan (Prof. Dr. Shinji Ando)

References

[1] Zucchi, I. A., Resnik, T., Oyanguren, P. A., Galante, M. J., Williams, R. J. J., "Comparison of optical properties of thermally reversible light scattering films consisting in dispersions of polystyrene/naphthalene domains or polystyrene/liquid crystal (EBBA) domains in epoxy matrices" *Polymer Bulletin*, **58:** 145-151 (2007).

[2] Ileana A., Zucchi, M., Galante, J., Roberto, J., Williams, J., "Thermally reversible light scattering films based on the melting/crystallization of organic crystals dispersed in an epoxy matrix", *European Polymer Journal*, **42:** 815–822 (2006).

[3] Rimdusit, S.,Pirstpindvong, S.,Tanthapanichakoon, W., and Damrongsakkul, S., "Toughening of polybenzoxazine by alloying with urethane prepolymer and flexible epoxy: a comparative study", *Polymer Engineering and Science*, **45:** 288-297 (2005).

ASTA 2009

ASTA 2009

Asian Conference on Thermal Analysis and Applications 2009

17-18 December 2009
Bangkok, Thailand

Organized By

MTEC
a member of NSTDA

Supported By

METTLER TOLEDO

10:40 - 11:05	Coffee Break	
	Room: Infinity 2	
11:05 - 11:45	Keynote Lecture 7 Prof. Dr. Takateru Umeda (Sahaviriya Steel Industries Public Co., Ltd., Thailand) Application of Thermal Analysis to Fields of Casting Solidification and Advanced Materials Development	
	Room: Infinity 2	Room: Beta 1
	Session 1: Materials-Organic, Polymers and Petrochemical (Continued)	Session 2: Metal and Composites
11:45 - 12:05	OP-B1-12	OP-B2-05
	B. Ramsiri (Chulalongkorn University), C. Jubsilp (Srinakharinwirot University) and S. Rimdusit (Chulalongkorn University), Thailand	S. Cheanklin, J. Jaroonsaratul (Iron and Steel Institute of Thailand), I. Diewwanit and P. Charunyakorn (Chulalongkorn University), Thailand
	Thermal Properties of Polybenzoxazine Modified with Dianhydrides	A Thermal Modeling of Ladle in Steelmaking Operation
12:05 - 12:25	OP-B1-13	OP-B3-01
	P. Panitanta, B. Hararak, N. Kerddonfag and W. Chinsirikul (MTEC), Thailand	P. Kasemsiri (Chulalongkorn University), S. Hiziroglu (Oklahoma State University), USA and S. Rimdusit (Chulalongkorn University), Thailand
	Investigation of Structural Development of β-Nucleated Polypropylene in Biaxial Orientation Process	Development of Bamboo Fiber-Reinforced with Benzoxazine/Cashew Nut Shell Liquid Oil Alloys
12:25 - 13:35	Lunch	
	Room: Infinity 2	
13:35 - 13:55	Closing Ceremony	
13:55 - 14:45	Departure to MTEC	
14:45 - 16:30	Visit R&D Laboratories at MTEC	
16:30	Departure to Hotel	

Development of Bamboo Fiber-reinforced with Benzoxazine/Cashew Nut Shell Liquid Oil Alloys

Pornnapa Kasemsiri [1], Salim Hiziroglu [2], Sarawut Rimdusit [1]*

[1] Polymer Engineering Laboratory, Department of Chemical Engineering, Faculty of Engineering, Chulalongkorn University, Pathumwon, Bangkok 10330, Thailand

[2] Department of Natural Resource Ecology and Management, Oklahoma State University, 303-G Agricultural Hall, Stillwater, OK 74078, USA

*Corresponding Author E-mail address: sarawut.r@chula.ac.th

Abstract

Mixtures of benzoxazine resin and cashew nut shell liquid (BA-a/CNSL) at various mass ratios reinforced with bamboo fiber (*Dendrocalamus asper*) are investigated as wood composites. In this work, thermal properties of the alloy matrices and those of the bamboo composites are examined using DSC. Flexural properties of the bamboo-filled BA-a/CNSL are also measured using a universal testing machine. The bamboo fiber can be highly filled in the BA-a/CNSL system i.e. with the bamboo fiber content up to 65 % by weight. The curing temperature of the alloy matrices tends to decrease with an addition of the CNSL in benzoxazine resin i.e. CNSL was observed to act as catalyst for benzoxazine curing. Moreover, CNSL can reduce cost of the wood composite matrices as it is the waste from the process to remove the cashew kernel from the nut. The flexural modulus values of the bamboo composites up to 5.97 GPa and flexural strengths up to 66 MPa were obtained when neat polybenzoxazine was used as a bamboo composite matrix. Both flexural modulus and strength of the bamboo composites with CNSL in the matrices slightly reduced with the amount of CNSL. Interestingly, the relationship between flexural stress and strain of the obtained bamboo composites indicated that all alloy matrices modified with CNSL rendered an increase in the flexural strain at break as well as in the areas under the stress-strain curves i.e. an increase in the toughness of the composites or the energy absorption capability. The highest strain at break and toughness were obtained when 30% by weight of CNSL was added in the alloy matrix i.e. with the strain at break value of 1.72% and the area under the stress-strain curve of 0.249 J.

1. Introduction

Natural fibers are well known as renewable and abundantly available materials. Moreover, their cost is less expensive than synthetic fibers which are used as reinforcement in making structural components therefore, natural fibers are suited to common application [1]. The bamboo fibers are often called natural glass fibers due to, their high strength and good mechanical properties. These fibers are an alternative raw material for many types of composite panel production, i.e. furniture units, plywood and flooring [2]. In recent work, wood flour-filled benzoxazine has been investigated as a possible as high performance wood-substitute material. Benzoxazine resins are relatively new members of phenolic resins and have many characteristics of traditional resins such as excellent thermal properties and low melt viscosity. This allowed substantial amounts of woodflour (up to 70% by weight) to be added in the benzoxazine, epoxy, and phenolic novolac resins (BEP resins) system. Relatively high flexural strengths of BEP wood composites up to 70 MPa can also be obtained. The outstanding compatibility between woodflour and the ternary matrices contributed to the modulus and thermal stability enhancement of the wood composites particularly with an increase of the polybenzoxazine fraction in the BEP alloys [3-4].

Recently, a group of bio-composite researchers has investigated the novel cardanol-based benzoxazine

monomer, which contains an oxazine ring in its structure. The ring can react with carbon atoms on benzene ring of cardanol which is the main component of cashew nut shell liquid (CNLS). CNSL was obtained as a by-product during the process of removing the cashew kernel from the nut. Hence, it can be considered a sustainable low cost and largely available natural resource particularly in Thailand [5]. Because of this reason, CNLS is an interesting material for improving the properties of resin and to reduce cost of material. The objective of this work is to evaluate various mechanical and thermal properties of experimental fiberboard samples made from bamboo fiber using benzoxazine resin blended with CNSL as wood adhesive.

2. Experimental

Benzoxazine resin (BA-a) was synthesized from bisphenol-A, Para-formaldehyde and aniline at a 1:2:4 molar ratio following the patented solventless technique [3]. The CNSL was heated at 190 °C for 5 h in order to eliminate volatile organics. The BA-a blended with CNSL as wood composite matrices were prepared at 80 °C. The investigated weight ratios of the BA-a and CNSL in the mixtures were 50/50, 60/40, 70/30, 80/20 and 90/10 respectively. To prepare bamboo composite, bamboo fiber was dried at 100 °C for 24 h. A fixed bamboo fiber content of 65% by weight was compounded with BA-a/CNSL mixture in an aluminum container at 80 °C for at least 30 min and was placed in a preheated $60 \times 25 \times 3$ mm^3 stainless steel mold and compression molded in a hydraulic press using a pressure of 15 MPa, at 100°C for 0.5 h and 170°C for 3.5 h. The cured specimens were left to cool down at room temperature in an open mold before testing.

The curing behavior and thermal transition of specimens were measured by a differential scanning calorimeter (DSC) model from TA Instrument. The heating rate was 10 °C/min from 30 to 300°C and nitrogen gas used for purging.

Densities of bamboo composites were determined by a water replacement method (ASTM D 792-91 Method A.) The bamboo fiber was investigated using a pycnometer (100 ml Sekiya Company).

The flexural modulus and flexural strength of the wood composite specimens were determined according ASTM D790-M93 on a universal testing machine, Instron model 5567. The measurement was performed in a 3-point bending mode with a supporting span of 48 mm and at a crosshead speed of 1.2 mm/min. The dimension of each specimen was $25 \times 60 \times 3$ mm^3.

3. Results

3.1 Curing behavior and thermal transition of BA-a/CNSL matrices

DSC profiles of the benzoxazine and benzoxazine blended with CNSL are shown in Figure 1. The peak exotherm of BA-a was observed at 237°C. In the case of BA-a/CNSL, the peak exotherms were found to be lower than of BA-a. When the amounts of CNSL in samples increased the peak exotherm decrease i.e. 216°C (90/10 BA-a/CNSL), 207°C (80/20 BA-a/CNSL), 203°C (70/30 BA-a/CNSL), 197°C (60/40 BA-a/CNSL) and 186°C (50/50 BA-a/CNSL). This result implied that CNSL acted an acid catalyst for BA-a curing and was thus able to shift the exotherm of the ring-opening reaction of benzoxazine resin to lower temperature [5]. The lowering of exotherms in similar system had also been observed by the acidic protons such as polyamic acid, clay, silica and titania [6]. Figure 2 illustrates DSC thermograms of BA-a and BA-a/CNSL at different ratios, after curing at 170°C for 3.5 h. The degree of conversion of the partially cured samples can be determined according to the following relationship:

$$\%\text{conversion} = \left[1 - \frac{H_{rxn}}{H_0}\right] \times 100 \qquad (1)$$

where H_{rxn} is the heat of reaction of the partially cured specimens, as determined from DSC results, and Ho is the heat of reaction of the uncured resin. The percentage of conversion of each sample is shown in Table 1.

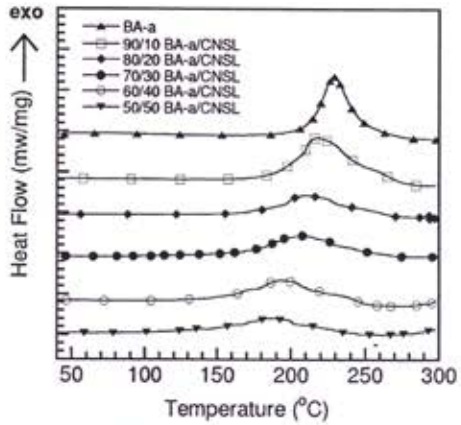

Figure 1. DSC thermograms showing the curing temperature of BA-a/CNSL.

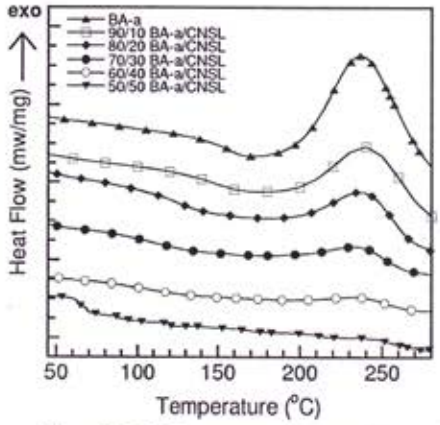

Figure 2. DSC thermograms of BA-a and BA-a/CNSL cured at 170°C for 3.5 h.

Table 1: Degree of conversion of partial cured sample

BA-a/CNSL sample	% conversion of partial cured
100	51.60
90/10	78.80
80/20	90.68
70/30	92.21
60/40	95.56
50/50	97.39

3.2 Flexural properties of bamboo fiber composites

Flexural properties of bamboo fiber filled BA-a/CNSL alloys are exhibited in Figure 3. The average flexural modulus of bamboo fiber composite ranged from 3.86-5.97 GPa. The flexural modulus decreased when amount of CNSL increased, this phenomenon indicated that the addition CNSL into the polybenzoxazine tended to lower the strength or the stiffness of the resulting polybenzoxazine alloys. However, flexural modulus of the bamboo-filled BA-a/CNSL alloys remained significantly higher than those of the reported wood polymer composites, i.e. bamboo reinforced HDPE with 40% by weight bamboo = 3.1 GPa [7], wood flake reinforced HDPE composites with 50% by weight of wood content = 2.7 GPa and 70% by weight of wood content = 3.1 GPa [8]. Furthermore, the flexural modulus of wood composite in present work is higher than typical medium-density fiberboard (MDF) requirement which requires flexural modulus to be in a range of 0.5-3 GPa. Normally, MDF is frequently used as substrate for thin overlays to manufacture furniture units [9].

Figure 4 illustrates the flexural strength of bamboo composites. The average flexural strength value of the bamboo composites ranged from 44.2 to 66.1 MPa. The flexural strength slightly reduced when the amount of CNSL increased from 10 to 50% by weight. However, the bamboo fiber-filled BA-a/CNSL still possessed flexural strength values higher than 40% by weight bamboo reinforced HDPE (21.3 MPa) and commercial wood flake-reinforced HDPE at 50% by weight (31 MPa) and at 70 % by weight (18 MPa) [7-9].

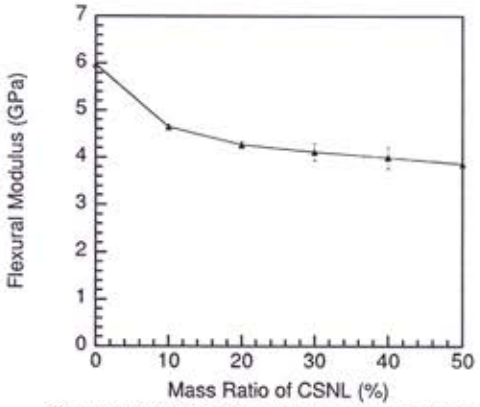

Figure 3. Effect of CNSL content on flexural modulus of wood-BA-a/CNSL composite at various compositions.

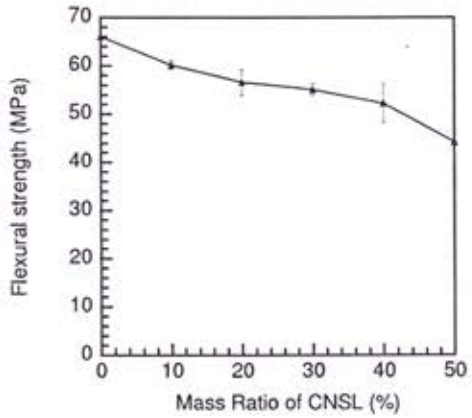

Figure 4. Effect of CNSL content on flexural strength of wood-BA-a/CNSL composite at various compositions.

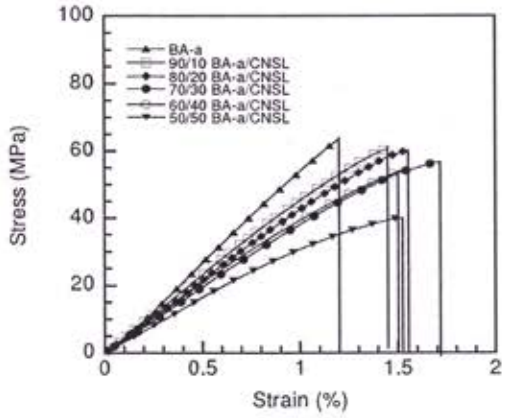

Figure 5. Flexural stress and strain relationship of bamboo-reinforced BA-a/CNSL.

Figure 5 presents the relationship between flexural stress and strain of bamboo reinforced with BA-a/CNSL matrices. Increasing the CNSL content in the composite was observed to cause an optimum in the flexural strain at break of the materials as follows: 1.20% BA-a (100), 1.45% BA-a/CNSL (90/10), 1.55% BA-a/CNSL (80/20), 1.71% BA-a/CNSL (70/30), 1.52% BA-a/CNSL (60/40) and 1.50% BA-a/CNSL (50/50). This phenomenon implied that the BA-a/CNSL matrices at optimum of CNSL could restrain crack growth and absorb and dissipate mechanical energy in the obtained polymer alloys. Furthermore, the area under the flexural stress-strain curve refers to the energy absorption capability of the alloy materials or the toughness of materials. Figure 5 suggested that when the amount of CNSL in alloy contents increased, the area under the curve tended to increase implying higher toughness of the specimens. The highest area under the curve was calculated to be 0.249 J at 70% CNSL content and other relevant values were 0.155 J BA-a/CNSL (80/20), 0.145 J BA-a/CNSL (90/10) and 0.120 J BA-a (100).

3.3 Density of bamboo fiber composite

Theoretical density of the samples was calculated based on density values of polybenzoxazine, bamboo and cashew nut oil which were 1.19 g/cm^3, 0.80 g/cm^3 and 0.94 g/cm^3 ,respectively. Table 2 showed the density of BA-a/CNSL matrices reinforced with bamboo fiber at a fixed weight ratio of 65% (bamboo)/ 35% (matrix). The measured densities of the bamboo composites above 30% by weight of CNSL in the alloys were lower than the theoretical values. This result indicated that the CNSL amount of greater than 30% by weight was in excess to react with benzoxazine resin. Consequently, the excess CNSL might evaporate during the curing process that caused void formation in the composite specimens. The unreacted CNSL might also cause the network defects or incomplete network formation in the alloys which resulted in the lowering of the mechanical and thermal properties of the obtained bamboo composites. The appearances of voids in specimens induced crack growth corresponding to the result in Figure 5, when CNSL adding at 40 and 50% by weight, the value of stress-strain relation ship significantly reduced from the highest value at 30% by weight CNSL in contents.

Table 2: Density of wood-BA-a/CNSL alloy composite at mass ratio of CNSL ratio.

Mass fraction of BA-a/CNSL in composite	Theoretical	Actual
100	1.203	1.121 ± 0.022
90/10	1.194	1.106 ± 0.021
80/20	1.186	1.102 ± 0.017
70/30	1.176	1.029 ± 0.017
60/40	1.169	0.986 ± 0.015
50/50	1.161	0.979 ± 0.009

4. Conclusions

Bamboo fiber can be highly filled in BA-a/CNSL system i.e. with the bamboo fiber content up to 65 % by weight. CNSL was found to act as a curing catalyst to benzoxazine resin by lowering its curing temperature. Both flexural modulus and strength of the bamboo composites with CNSL in the matrices slightly reduced with amount of CNSL. An increase in the flexural strain at break as well as the areas under the stress-strain curves was observed with the presence of the CNSL in benzoxazine matrix.

Acknowledgements

This research receives financial supports from Chulalongkorn University Dutsadi Phiphat Scholarship, Thailand. Bisphenol A is supported by Thai Polycarbonate Co., Ltd. (TPCC), Bamboo fiber is provided by Forest Products Division, Royal Forest Department, Thailand as well as cashew nut shell oil is supported by Maboonkrong Sirichai 25 Ltd. The authors also would like to acknowledge the Asia-Oceania Top University League on Engineering (AOTULE) Scholarship and Tokyo Institute of Technology University, Tokyo, Japan (Prof. Dr. Shinji Ando) for Pyconometer and TGA measurement.

5. References

[1] Seema Jain, Rakesh Kumar. 1992. Mechanical behaviour of bamboo and bamboo composite. 27, 4598-4604.

[2] Fuyuan, D., Jianmin, Z., 1988. Production status of bamboo artificial board in Zhejiang. J. Construct. Mater. New Type. Zhejiang, 11–14.

[3] Ishida, H., 1996. US. Patent 5,543,516.

[4] Jubsilp, C., Takeichi, T., Hiziroglu, S., Rimdusit, S. 2008. High performance wood composites based on benzoxazine-epoxy alloys. Bioresource Technology 99, 8880–8886.

[5] E. T. N. BISANDA, M.P. ANSELL. 1992. Properties of sisal-CNSL composites. Journal of materials Science. 27, 1690-1700.

[6] Tsutomu Takeichi, Takuya Kano, Tarek Agag. 2005. Synthesis and thermal cure of high molecular weight polybenzoxazine precursors and the properties of the thermosets. Polymer 46, 12172–12180.

[7] H. Liu a, Q. Wua, G. Han, F. Yao, Y. Kojima, S. Suzuki. 2008. Compatibilizing and toughening bamboo flour-filled HDPE composites: Mechanical properties and morphologies. Composites: Part A. 39, 1891–190.

[8] Youngquist.1999. Wood-based Composites and Panel Products. Wood Handbook, U.S. Department of Agriculture, Government Printing Office, Madison,WI morphologies. Composites: Part A. 39, 1891–190.

[9] P.W. Balasuriya, L. Ye, and Y.W. Mai. 2001. Mechanical properties of wood flake–polyethylene composites. Part I: effects of processing methods and matrix melt flow behaviour Composite Part A, 32, 619-629.

VITA

Pornnapa Kasemsiri was born on February 12th, 1984 in Khon Kaen, Thailand. She finished high school from Khon Kaen university Demonstration School (Mordindaeng) in 2002, and received the bachelor's degree of Chemical Engineering from Faculty of Engineering, Khon Kaen University in 2006. In 2008, she received the Degree of Master of Engineering in Chemical Engineering at the Department of Chemical Engineering, Chulalongkorn University. After the M.Eng graduation, she immediately pursued her graduate study for a Doctoral Degree in Chemical Engineering at Chulalongkorn University.